

LA-13262-MS

*Summary and Synthesis Report on
Radionuclide Retardation for the Yucca
Mountain Site Characterization Project*

*Yucca Mountain Site Characterization Program
Milestone 3784M*

Los Alamos
NATIONAL LABORATORY

*Los Alamos National Laboratory is operated by the University of California
for the United States Department of Energy under contract W-7405-ENG-36.*

This work was supported by the Yucca Mountain Site Characterization Project Office as part of the Civilian Radioactive Waste Management Program of the U.S. Department of Energy.

An affirmative Action/Equal Opportunity Employer

This report was prepared as an account of work sponsored by an agency of the United States Government. Neither the Regents of the University of California, the United States Government nor any agency thereof, nor any of their employees, makes any warranty, express or implied, or assumes any legal liability or responsibility for the accuracy, completeness, or usefulness of any information, apparatus, product, or process disclosed, or represents that its use would not infringe privately owned rights. Reference herein to any specific commercial product, process, or service by trade name, trademark, manufacturer, or otherwise, does not necessarily constitute or imply its endorsement, recommendation, or favoring by the Regents of the University of California, the United States Government, or any agency thereof. The views and opinions of authors expressed herein do not necessarily state or reflect those of the Regents of the University of California, the United States Government, or any agency thereof. The Los Alamos National Laboratory strongly supports academic freedom and a researcher's right to publish; therefore, the Laboratory as an institution does not endorse the viewpoint of a publication or guarantee its technical correctness.

*Summary and Synthesis Report on
Radionuclide Retardation for the Yucca
Mountain Site Characterization Project*

*Yucca Mountain Site Characterization Program
Milestone 3784M*

*Inés R. Triay
Arend Meijer*
James L. Conca**
K. Stephen Kung
Robert S. Rundberg
Betty A. Strietelmeier
C. Drew Tait*

edited by Roger C. Eckhardt

**GCX, 3821 Anderson Ave. SE, Albuquerque, NM 87108*

***WSU Tri-Cities, 100 Sprout Road, Richland, WA 99352*

TABLE OF CONTENTS

TABLE OF CONTENTSi

LIST OF FIGURESvii

LIST OF TABLESxi

ABSTRACT1

I. INTRODUCTION

 A. THE POTENTIAL REPOSITORY SITE2

 Regulatory Limits for the Release of Radionuclides3

 Stratigraphy of Yucca Mountain4

 B. AN INTEGRATED APPROACH TO SITE CHARACTERIZATION7

 Modeling of Groundwater Chemistry7

 Radionuclide Solubility Studies7

 Sorption Studies8

 Diffusion Studies9

 Dynamic Transport Studies9

 Quality Approved Detailed Procedures10

 The Reference Information Base11

 C. Yucca Mountain Waters11

 Saturated-zone Groundwater Chemistry11

 J-13 Well construction

 Well UE-25 p#1

 Chemical stability of Well J-13 water15

 Unsaturated-zone Water Chemistry16

 Pore Water versus Saturated Groundwaters16

 Synthetic Groundwaters16

 D. Yucca Mountain Tuffs17

 Mineralogy Variability17

 Tuff sample identification

 Zeolitic tuff

 Vitric tuff

 Devitrified tuff

 Minerals

 Surface area of tuffs and minerals19

 Fracture Minerals19

II. GROUNDWATER CHEMISTRY MODEL

 A. INTRODUCTION23

 Purpose and Scope23

 B. GROUNDWATER CHEMISTRY24

 Sources of Data24

 Precipitation Compositions24

Table of Contents

Soil-zone Processes that Influence Water Compositions	25
Evapotranspiration	
Dissolution/precipitation of solid phases in the soil zone	
Pore-water Compositions above the Potential Repository Horizon	31
Perched-water Compositions below the Potential Repository Horizon	37
C. SUMMARY AND CONCLUSIONS	44
Type-1 Waters	44
Type-2 Waters	44
A Survey Approach	45
III. RADIONUCLIDE SOLUBILITY STUDIES	47
A. SOLUBILITY LIMITS	47
Neptunium	47
Plutonium	47
Americium	48
B. SOLUBILITY-LIMIT VALUES RECOMMENDED FOR PERFORMANCE	
ASSESSMENT	49
Assumptions about Groundwater Chemistry	49
Dependence of Solubility on Temperature	49
Limitations of Empirical Solubility Data	50
Solubility Distributions	51
Americium	
Plutonium	
Uranium	
Thorium	
Radium	
Lead	
Neptunium	
Cesium, iodine, technetium, selenium, carbon, and chlorine	
Protactinium	
Actinium	
Tin	
Nickel	
Strontium	
Samarium	
Zirconium	
Niobium	
IV. SORPTION AND SORPTION MODELING STUDIES	55
A. BATCH-SORPTION DATA	55
Introduction	55
Linear versus nonlinear sorption	
Mechanistic models	
Experimental procedures	
The distribution coefficient	
Niobium, Thorium, Tin, and Zirconium	57

Niobium	
Thorium	
Tin	
Zirconium	
Actinium, Americium, and Samarium	.61
Plutonium	.65
Cesium, Radium, and Strontium	.73
Nickel and Lead	.84
Neptunium, Protactinium, Selenium, and Uranium	.85
Neptunium	
Protactinium	
Selenium	
Uranium	
Carbon, Chlorine, Iodine, and Technetium	.107
B. EFFECTS OF ORGANICS ON ACTINIDES	.108
Introduction	.108
Experimental Procedures	.108
Preparation of tuff and oxide minerals	
Preparation of organics and radionuclides	
Sorption Measurements	.109
DOPA sorption	
Radionuclides sorption	
Results and Discussion	.109
Neptunium	
Plutonium	
Summary	.121
C. MODELS THAT CAN EXPLAIN THE SORPTION DATA	.123
Cation Exchange	.123
Description of the process	
Factors affecting cation exchange	
Experimental methods	
Ion-exchange models	
Description of cation-exchange sites in Yucca Mountain tuff	
State of knowledge of cation exchange with respect to Yucca Mountain tuff	
Surface Complexation	.127
Description of surface-complexation process	
Factors affecting surface complexation	
HSAB (hard-soft acid-base) theory	
Description of surface-complexation sites in Yucca Mountain tuff	
Modeling of Yucca Mountain tuff	
State of knowledge of surface complexation with respect to Yucca Mountain	
D. SORPTION DATA RECOMMENDED FOR PERFORMANCE ASSESSMENT	.134
Americium	.134
Plutonium	.135
Uranium	.135
Thorium	.135

Table of Contents

Radium	135
Lead	135
Neptunium	135
Protactinium	135
Tin	135
Nickel	138
Cesium	138
Strontium	138
Selenium	138
Carbon	138
Actinium, Samarium, Niobium, and Zirconium	138
Iodine, Technetium, and Chlorine	138
V. DYNAMIC TRANSPORT STUDIES	
A. CRUSHED-ROCK COLUMNS	139
Experimental Procedures	140
Groundwaters and solutions	
Crushed-rock column procedure	
Relationship between column and batch experiments	
Results and Discussion	141
Neptunium results	
Neptunium summary	
Plutonium and technetium results	
B. SOLID-ROCK COLUMNS	154
Methodology	154
Retardation	
Hydraulic conductivity	
Results and Discussion for Vitric and Zeolitic Tuff	156
Column breakthrough test results	
Batch test results	
Conclusions	158
C. RADIONUCLIDE TRANSPORT THROUGH FRACTURES	160
Experimental Procedures	160
Groundwaters	
Fractured-tuff samples	
Radionuclide solutions	
Fractured-column procedure	
Batch-sorption experiments	
Results and Discussion	164
D. COLLOID-FACILITATED RADIONUCLIDE TRANSPORT	168
Colloid Transport Calculations	169
Evidence of Colloids and Colloid Transport from Field Studies	170
Natural analog sites	
Test sites and other areas	
Detailed Colloid Analyses of J-13 Water at the Nevada Test Site	173
Particle size distribution in J-13 water	

Potential Sources of Colloids at Yucca Mountain	176
Laboratory Experiments on Colloid Stability	178
Future Direction of Colloid Studies in the Yucca Mountain Site Characterization Project ...	183
Will radioactive waste-derived colloids be present at the potential repository?	
Will radioactive waste-derived colloids be stable in the likely groundwaters?	
Can radioactive waste-derived colloids migrate over field-scale distances without being removed by filtration?	
Conclusions and Summary of Data Needs for Colloid Investigation	186
VI. DIFFUSION STUDIES	
A. ROCK-BEAKER EXPERIMENTS	189
Experimental Procedure	189
Data Analysis	189
Results and Discussion	190
B. DIFFUSION-CELL EXPERIMENTS	195
Experimental Procedures and Data Analysis	195
Results and Discussion	196
C. DIFFUSION THROUGH UNSATURATED TUFF	199
VII. SUMMARY	
A. BIOLOGICAL SORPTION AND TRANSPORT (MILESTONE #3363)	203
B. GROUNDWATER CHEMISTRY (CHAPTER II)	204
C. SOLUBILITY AND SPECIATION (CHAPTER III AND MILESTONE #3792M)	204
D. SORPTION (CHAPTER IV)	205
E. TRANSPORT AND DIFFUSION (CHAPTERS V AND VI)	207
VIII. APPLICABILITY, QUALITY, AND RELIABILITY OF RESULTS	
A. INTRODUCTION	209
B. GROUNDWATER CHEMISTRY MODEL	210
Purpose and Objectives of Studies	210
Introduction and objectives	
Objectives for SCP Activity 8.3.1.3.1.1.1	
Regulatory rationale and justification	
Rationale for Tests	219
Technical rationale and justification	
Test constraints	
C. DISSOLVED SPECIES CONCENTRATION LIMITS AND COLLOID BEHAVIOR	224
Purpose and Objectives of Studies	224
Rationale for Species Concentration Limits and Colloid Behavior Studies	227
Rationale for dissolved-species concentration limits	
Rationale for the study of colloid formation, characterization, and stability (Activity 8.3.1.3.5.2.1)	
D. BATCH-SORPTION AND SORPTION-MODELING STUDIES	244
Objectives and Justification of Study	244
Purpose	
Regulatory rationale and justification	

Table of Contents

Rationale	245
Technical rationale and justification	
Constraints	
E. DYNAMIC TRANSPORT STUDIES	254
Purpose and Objectives of Studies	254
Purpose	
Use of results	
Rationale	255
Approach	
Types of measurements to be made	
Rationale for choosing the types of measurements to be made	
Constraints for the study	
Additional factors for consideration	
F. DIFFUSION STUDIES	259
Purpose and Objectives of Studies	259
Purpose	
Use of results	
Rationale	259
Approach	
Types of measurements to be made	
Rationale for choosing the types of measurements to be made	
Constraints on the study	
Additional factors for consideration	
REFERENCES	263
APPENDIX: DESCRIPTIONS OF MINERALS COATING THE FRACTURES OF YUCCA MOUNTAIN TUFFS	
Zeolites	A-1
Silica	A-2
Clays	A-3
Oxides and Hydroxides	A-3
Managanese oxides	
Iron oxides	
Carbonates	A-5
Halides	A-5

LIST OF FIGURES

Fig. 1. Cross Section of Yucca Mountain	3
Fig. 2. Multiple Natural Geochemical Barriers	5
Fig. 3. Zeolitic Tuffs at Yucca Mountain	6
Fig. 4. Unsaturated-zone Hydrology Model	11
Fig. 5. Well J-13	13
Fig. 6. Chemistry of Two Groundwaters	14
Fig. 7. Stability of the Chemistry of Well J-13 Water	15
Fig. 8. X-ray Diffraction Results	19
Fig. 9. Surface Areas of Tuffs and Minerals	20
Fig. 10. Sulfate versus Chloride in Precipitation	25
Fig. 11. Sulfate versus Chloride in Pore Water	27
Fig. 12. Sulfate versus Chloride in Perched Waters and Groundwaters	28
Fig. 13. Sodium versus Chloride	32
Fig. 14. Silica versus Chloride	34
Fig. 15. Bicarbonate versus Chloride	35
Fig. 16. Calcium versus Chloride	37
Fig. 17. Calico Hills Bicarbonate	39
Fig. 18. Calico Hills Sodium	39
Fig. 19. Calico Hills Calcium	40
Fig. 20. Calico Hills Magnesium	41
Fig. 21. Plutonium Sorption	69
Fig. 22. Plutonium Sorption onto Devitrified Tuff in J-13 Water	70
Fig. 23. Plutonium Sorption onto Devitrified Tuff in Synthetic UE-25 p#1 Water	70
Fig. 24. Plutonium Sorption onto Vitric Tuff in J-13 Water	71
Fig. 25. Plutonium Sorption onto Vitric Tuff in Synthetic UE-25 p#1 Water	71
Fig. 26. Plutonium Sorption onto Zeolitic Tuff in J-13 Water	72
Fig. 27. Plutonium Sorption onto Zeolitic Tuff in Synthetic UE-25 p#1 Water	72
Fig. 28. Plutonium Isotherm for Devitrified Tuff in J-13 Water	74
Fig. 29. Plutonium Isotherm for Devitrified Tuff in Synthetic UE-25 p#1 Water	74
Fig. 30. Plutonium Isotherm for Vitric Tuff in J-13 Water	75
Fig. 31. Plutonium Isotherm for Vitric Tuff in Synthetic UE-25 p#1 Water	75
Fig. 32. Plutonium Isotherm for Zeolitic Tuff in J-13 Water	76
Fig. 33. Plutonium Isotherm for Zeolitic Tuff in Synthetic UE-25 p#1 Water	76
Fig. 34. Plutonium Isotherm for Albite in J-13 Water	77
Fig. 35. Plutonium Isotherm for Albite in Synthetic UE-25 p#1 Water	77
Fig. 36. Plutonium Isotherm for Gibbsite in J-13 Water	78
Fig. 37. Plutonium Isotherm for Gibbsite in Synthetic UE-25 p#1 Water	78
Fig. 38. Plutonium Isotherm for Quartz in J-13 Water	79
Fig. 39. Plutonium Isotherm for Quartz in Synthetic UE-25 p#1 Water	79
Fig. 40. Plutonium Isotherm for Clinoptilolite in J-13 Water	80
Fig. 41. Plutonium Isotherm for Clinoptilolite in Synthetic UE-25 p#1 Water	80
Fig. 42. Plutonium Isotherm for Montmorillonite in J-13 Water	81
Fig. 43. Plutonium Isotherm for Montmorillonite in Synthetic UE-25 p#1 Water	81
Fig. 44. Plutonium Isotherm for Natural Calcite in J-13 Water	82

List of Figures

Fig. 45. Plutonium Isotherm for Natural Calcite in Synthetic UE-25 p#1 Water	82
Fig. 46. Neptunium Sorption onto Clinoptilolite-rich Tuff	88
Fig. 47. Neptunium Sorption onto Clinoptilolite	88
Fig. 48. Neptunium Sorption for Wet- and Dry-sieved Tuffs	90
Fig. 49. Neptunium Sorption for Wet- and Dry-sieved Calcite	90
Fig. 50. Time Dependence of Neptunium Sorption for Tuffs and Clinoptilolite	91
Fig. 51. Time Dependence of Neptunium Sorption for Calcite and Hematite in J-13 Water	92
Fig. 52. Time Dependence of Neptunium Sorption for Calcite and Hematite in Synthetic UE-25 p#1 Water	92
Fig. 53. pH Dependence of Sorption at 10^{-7} M	93
Fig. 54. pH Dependence of Sorption at 10^{-5} M	94
Fig. 55. Neptunium Sorption in UE-25 p#1 Well Water	94
Fig. 56. Neptunium Sorption for Hematite	95
Fig. 57. Neptunium Sorption in J-13 Well Water	95
Fig. 58. Neptunium Sorption and Surface Area	96
Fig. 59. Dependence on Water for Sorption onto Tuffs	97
Fig. 60. Dependence on Water for Sorption onto Minerals	97
Fig. 61. High-concentration Sorption onto Tuffs	98
Fig. 62. High-concentration Sorption onto Minerals	98
Fig. 63. High-concentration Sorption onto Tuffs at pH 7	99
Fig. 64. High-concentration Sorption onto Hematite at pH 7	99
Fig. 65. Uranium Sorption onto Clinoptilolite-rich Tuff	106
Fig. 66. Uranium Sorption onto Clinoptilolite	106
Fig. 67. Neptunium Sorption per Unit Mass on Iron Oxides	110
Fig. 68. Neptunium Sorption per Unit Area on Iron Oxides	110
Fig. 69. pH Dependence of DOPA Sorption on Oxides	111
Fig. 70. Neptunium Sorption on Goethite	112
Fig. 71. Neptunium Sorption on Treated and Untreated Tuff	112
Fig. 72. Sorption with and without DOPA on Treated Tuff	113
Fig. 73. Sorption with and without DOPA on Untreated Tuff	113
Fig. 74. Neptunium Sorption on Oxides and Tuff	114
Fig. 75. Sorption on Goethite with or without DOPA	114
Fig. 76. Sorption on Boehmite with or without DOPA	115
Fig. 77. Sorption on Hematite with or without Organics	115
Fig. 78. Sorption on Ferrihydrite with or without Organics	116
Fig. 79. Sorption on Goethite with or without Organics	116
Fig. 80. Boehmite with or without NAFA	117
Fig. 81. Treated Tuff with or without NAFA	117
Fig. 82. Goethite with or without NAFA	117
Fig. 83. Untreated Tuff with or without NAFA	117
Fig. 84. Plutonium Sorption per Unit Mass on Iron Oxides	118
Fig. 85. Plutonium sorption per Unit Area on Iron Oxides	118
Fig. 86. pH Dependence of Plutonium Sorption on Goethite	119
Fig. 87. Sorption on Ferrihydrite with and without Organics	120
Fig. 88. Sorption with and without Organics	120
Fig. 89. Sorption on Ferrihydrite with and without DOPA	121

Fig. 90. Sorption on Goethite with and without DOPA	121
Fig. 91. Modeling of Neptunium Sorption	127
Fig. 92. Surface Complexation versus Hydrolysis	129
Fig. 93. Neptunium Sorption in J-13 Water	132
Fig. 94. Neptunium Sorption in UE-25 p#1 Water	132
Fig. 95. Uranium Adsorption	133
Fig. 96. Cross Section of Crushed-rock Columns	140
Fig. 97. Flow Chart of Crushed-rock Column Experiment	141
Fig. 98. Column 1: Plutonium through Devitrified Tuff (J-13 water)	144
Fig. 99. Column 2: Plutonium through Devitrified Tuff (J-13 water)	145
Fig. 100. Column 3: Plutonium through Devitrified Tuff (synthetic UE-25 p#1 water)	145
Fig. 101. Column 4: Plutonium through Devitrified Tuff (synthetic UE-25 p#1 water)	146
Fig. 102. Column 5: Plutonium through Vitric Tuff (J-13 water)	146
Fig. 103. Column 6: Plutonium through Vitric Tuff (synthetic UE-25 p#1 water)	147
Fig. 104. Column 7: Plutonium through Vitric Tuff (synthetic UE-25 p#1 water)	147
Fig. 105. Column 8: Plutonium through Zeolitic Tuff (J-13 water)	148
Fig. 106. Column 9: Plutonium through Zeolitic Tuff (synthetic UE-25 p#1 water)	148
Fig. 107. Column 10: Plutonium through Zeolitic Tuff (synthetic UE-25 p#1 water)	149
Fig. 108. Column 11: Plutonium in Devitrified Tuff at Various Flow Rates (J-13 water)	149
Fig. 109. Column 12: Plutonium in Devitrified Tuff at Various Flow Rates (syn. UE-25 p#1)	150
Fig. 110. Column 13: Technetium in Devitrified Tuff (J-13 water)	150
Fig. 111. Column 14: Technetium in Devitrified Tuff (synthetic UE-25 p#1 water)	151
Fig. 112. Column 15: Technetium in Vitric Tuff (J-13 water)	151
Fig. 113. Column 16: Technetium in Vitric Tuff (synthetic UE-25 p#1 water)	152
Fig. 114. Column 17: Technetium in Zeolitic Tuff (J-13 water)	152
Fig. 115. Column 18: Technetium in Zeolitic Tuff (synthetic UE-25 p#1 water)	153
Fig. 116. The UFA Method	155
Fig. 117. Breakthrough Curves	157
Fig. 118. Unsaturated Hydraulic Conductivity	158
Fig. 119. Fractured-column Setup	162
Fig. 120. Neptunium in Fractured Tuff (and synthetic J-13 water)	165
Fig. 121. Neptunium in Fractured Tuff (and synthetic UE-25 p#1 water)	165
Fig. 122. Neptunium and Technetium in Fractured Tuff	167
Fig. 123. Technetium in Fractured Tuff	167
Fig. 124. Colloid Sampling	175
Fig. 125. Aggregate Growth for Silica Particles	181
Fig. 126. Aggregate Growth for Kaolinite Clay Particles	181
Fig. 127. Stability Curves	182
Fig. 128. Rock Beaker	189
Fig. 129. Diffusion Data	191
Fig. 130. Diffusion Data Curve Fits	191
Fig. 131. Calculated Diffusion Curves	193
Fig. 132. Comparison of Calculated and Actual Diffusion Data	193
Fig. 133. Tritium, Plutonium, and Uranium Diffusion through Devitrified Tuff	196
Fig. 134. Technetium and Neptunium Diffusion through Devitrified Tuff	197
Fig. 135. Tritium, Plutonium, and Uranium Diffusion through Zeolitic Tuff	197

LIST OF TABLES

Table 1. Important Radionuclides and the Reduction Factor Required to Meet Maximum Allowed Releases	4
Table 2. Los Alamos Yucca Mountain Project Detailed Procedures	10
Table 3. Chemistry of Waters from Wells J-13 and UE-25 p#1 and the Unsaturated Zone (UZ) at the Yucca Mountain Site	12
Table 4. Stratigraphy versus Rock Type	17
Table 5. Minerals in Matrices of Yucca Mountain Rocks	18
Table 6. Minerals Coating Fracture Walls in Yucca Mountain Tuffs	21
Table 7. Average Integrated Precipitation Composition at Kawich Range Sites	24
Table 8. Calculated Calcite Saturation Indices	36
Table 9. Solubility of Neptunium (in M) in J-13 Waters	47
Table 10. Solubility of Plutonium (in M) in J-13 Waters	48
Table 11. Solubility of Americium (in M) in J-13 Waters	48
Table 12. Solubilities used in TSPA-1993	51
Table 13. Plutonium Sorption Distribution Coefficients (under atmospheric conditions)	73
Table 14. Solubility and Speciation of Neptunium in Groundwaters at 25°C	85
Table 15. Neptunium Sorption in J-13 Water under Oxidizing Conditions	87
Table 16. Prediction of Neptunium Sorption on Clinoptilolite-rich G4-1510 Tuff in J-13 Water	89
Table 17. Neptunium Sorption onto Clinoptilolite-rich Tuffs in J-13 Water	89
Table 18. Uranium Sorption in J-13 Water under Oxidizing Conditions	105
Table 19. Prediction of Uranium Sorption on Clinoptilolite-rich G4-1510 Tuff in J-13 Water	105
Table 20. Minerals in Yucca Mountain Tuff with High Cation-exchange Capacities	126
Table 21. Intrinsic Constants for Metal Oxides	129
Table 22. Equations and Parameters Used to Model Neptunium Adsorption onto Zeolitic Tuff	130
Table 23. Groundwater Compositions Used for Neptunium Sorption Modeling	131
Table 24. Additional Equations and Parameters Used to Model Uranium Adsorption onto Devitrified Tuff	133
Table 25. Sorption-coefficient Distributions for Unsaturated-zone Units	136
Table 26. Sorption-coefficient Distributions for Saturated-zone Units	137
Table 27. Comparison of Neptunium K_d Values from Batch and Column Measurements	143
Table 28. Selenium Batch Adsorption on Nonwelded Zeolitic Tuff	158
Table 29. Minerals Coating Fracture Walls in Yucca Mountain Tuffs	161
Table 30. Characteristics of Fractured Devitrified-tuff Columns	163
Table 31. Batch-sorption Results for ^{237}Np in J-13 Well Water	164
Table 32. Concentration and Characteristics of Colloids in J-13 Well Water	176
Table 33. Rock-beaker Diffusion Results for Nonsorbing Radioisotopes	192
Table 34. Batch-sorption Diffusion Coefficients	192
Table 35. Dimensions of Diffusion Cells	195
Table 36. Yucca Mountain Site Characterization Plan (SCP) Studies Relevant to This Report	209
Table 37. Precision as a Function of Counting Time and Solution Concentration	230
Table 38. Environmental Conditions for Solubility Modeling	235

SUMMARY AND SYNTHESIS REPORT ON RADIONUCLIDE RETARDATION FOR THE YUCCA MOUNTAIN SITE CHARACTERIZATION PROJECT

Yucca Mountain Site Characterization Program Milestone 3784M

by

Inés R. Triay, Arend Meijer, James L. Conca, Stephen Kung,
Robert S. Rundberg, Elizabeth A. Strietelmeier, and C. Drew Tait

edited by Roger C. Eckhardt

ABSTRACT

This report is a detailed summary of laboratory and modeling studies performed by or for Los Alamos National Laboratory in support of the Yucca Mountain Site Characterization Project on the mechanisms by which radionuclide transport from the proposed repository for high-level nuclear waste at Yucca Mountain, Nevada, is retarded or enhanced by sorption, diffusion, solubility limits, and colloid transport. As direct input into these studies, the report also includes a summary of what has been accomplished in the development of a model for groundwater chemistry at Yucca Mountain. Chapter I introduces background material, including discussions of the site of the potential repository, the overall approach to this aspect of site characterization, the chemical nature of the on-site waters, and the types and variability of minerals in the rock matrix and on fracture surfaces. Chapter II discusses the groundwater chemistry of the saturated and unsaturated zones and the different types of processes that influence that chemistry. The first line of defense against radionuclide transport, the limits on solubilities, is discussed in Chp. III. The second line of defense, the sorption of radionuclides onto the surrounding tuffs, is discussed in Chp. IV. A summary of what is known for the sorption of all the key radionuclides and a presentation of extensive batch-sorption measurements for uranium, plutonium, and neptunium are included. The effect that organic coatings on mineral surfaces has on the sorption of actinides is also covered. Cation-exchange and surface-complexation models that can explain the sorption data are discussed. Chapter V covers dynamic-transport studies that complement and extend the batch-sorption work. These studies include experiments with crushed-rock columns, solid-rock columns, and fractured columns, as well as work on colloid-facilitated transport of radionuclides. Chapter VI summarizes both the work using rock beakers and diffusion cells to study diffusion in saturated tuff and the work using centrifuge-induced flow to study diffusion through unsaturated tuff. The main conclusions of all of this work are presented in Chp. VII, which also includes a summary of research performed as part of the Biological Sorption and Transport Task on how microorganisms affect radionuclide transport at Yucca Mountain.

I. INTRODUCTION

A. THE POTENTIAL REPOSITORY SITE

Yucca Mountain, in southern Nevada, is the potential site for a repository for high-level radioactive waste from commercial power and nuclear defense industries. Yucca Mountain is composed of a thick (greater than 1.5 km) sequence of ash-flow tuff units and subordinate lavas (Fig. 1). Most units retained enough heat after deposition to develop densely welded, devitrified interiors in which the original glass particles consolidated and crystallized to a high-temperature assemblage of feldspars and silica minerals (Levy 1992). Levy reports that the upper and lower margins of the units remain vitric; thinner, bedded tuffs between the main ash flows are also vitric and nonwelded. In the middle and lower units, most glassy tuffs have diagenetically altered to hydrous assemblages dominated by zeolites.

The location of the proposed repository is approximately 300 m below the surface of the mountain and 200 to 400 m above the static water level (Levy 1992). The presence of the thick zeolitic tuffs in continuous zones throughout the region was a major consideration for choosing Yucca Mountain as a potential repository site (Johnstone and Wolfsberg 1980); the zeolites could sorb important radionuclides from groundwaters and thus retard the movement of radioactivity from the repository site. The potential repository at Yucca Mountain would be located within the densely welded devitrified tuff of the Topopah Spring Member of Paintbrush Tuff with a vitrophyre underlying this location.

Because the proposed location is in the unsaturated zone, conditions are oxidizing. The Yucca Mountain region is in the shadow of the Sierra Nevada range and receives little rainfall. Estimates of groundwater flux are extremely low, and the site is remote, located at the western edge of the Nevada Test Site, approximately 100 miles northwest of Las Vegas, Nevada.

One major aspect of characterizing the site and assessing its suitability as a repository is to determine the extent to which the natural geochemical barriers will prevent the release of radionuclides from the underground repository. The retardation of radionuclides by sorption onto tuffs is of major importance, and one of the main goals of our research at the Los Alamos National Laboratory is to obtain data and to develop models for the sorption behavior of key radionuclides under the physical and chemical conditions anticipated at the proposed repository. Such work involves detailed investigation and modeling of the interactions between solid-rock materials and radionuclides in aqueous solutions.

Several related studies support and complement the main sorption research. The characterization and modeling of the chemistry of Yucca Mountain groundwaters is vital. Other studies include the role of diffusion in Yucca Mountain tuff, the limits imposed by the solubilities of the radionuclides, the potential transport of radionuclides by colloids, the effects of organic compounds on sorption, and radionuclide transport through fractures in the tuff. The validation of the results of static batch-sorption studies with dynamic transport studies is also extremely important.

This report summarizes the laboratory and modeling studies carried out or directed by scientists at Los Alamos for this effort. Specifically, we report on investigations of the mechanisms by which radionuclide transport is retarded or enhanced by sorption, diffusion, solubility limits, and colloid transport.

The role of microbial activity on the transport of radionuclides is described in a Los Alamos report on Yucca Mountain Site Characterization Program milestone 3663 (Hersman 1996).

An assessment of the potential for radionuclide retardation at Yucca Mountain must be based on an understanding of the petrology and mineralogy of

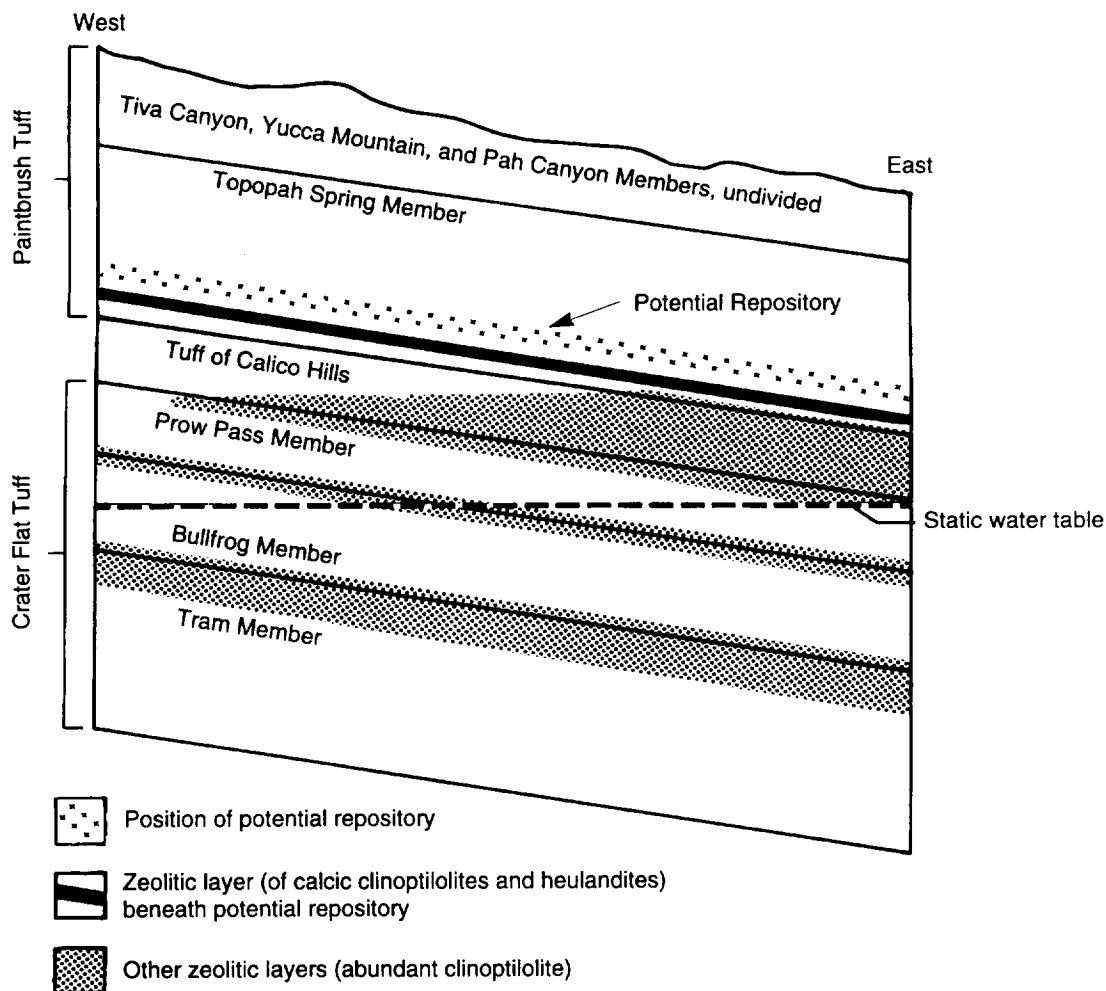


Figure 1. Cross Section of Yucca Mountain. This schematic of an east-west cross section of Yucca Mountain shows the vertical position of the potential repository in relation to the static water table and the principal layers of zeolitic tuffs (from Broxton 1986).

the proposed repository horizon and the underlying strata. This work is summarized in a series of Yucca Mountain Site Characterization milestone reports (Bish et al. 1996a; Levy et al. 1996; Carey et al. 1996).

Regulatory Limits for the Release of Radionuclides

The types of radioactive waste that may be emplaced in the proposed high-level nuclear waste repository include spent fuel, high-level (reprocessing) waste, and high-level defense waste.

Oversby (1987) has evaluated compositions and likely inventories of spent fuel and has provided lists of those radionuclides for which the performance of a geological repository site will be critical with respect to meeting the regulatory release limits. Oversby compared the maximum annual release rates from an engineered-barrier system allowed by the Nuclear Regulatory Commission (NRC) regulations of 10 CFR 60 (NRC 1980) with integrated release limits to the accessible environment allowed by the Environmental Protection Agency (EPA) regulations of 40 CFR 191 (EPA 1982). In effect, Oversby assumed the boundary to

I. Introduction

the accessible environment and the boundary to the engineered barrier to be one and the same. The "important radionuclides" were identified as those for which the allowed NRC annual release rates from the engineered barrier system resulted in integrated release rates to the accessible environment that exceeded the EPA release limits.

Table 1 lists the "important radionuclides" resulting from this evaluation in order of the degree to which they exceed the EPA release limits. Note that this listing is independent of the characteristics of the engineered-barrier system and of the site—it is a direct result of the composition of any quantity of the emplaced waste and the combined NRC and EPA regulations.

Unless the engineered-barrier system itself is designed to provide compliance with the EPA regulations, site characteristics between the boundary of the engineered barrier and the boundary of the accessible environment must be called on for such compliance. The site characteristics that could ultimately determine the rate at which radionuclides are released to the environment (Fig. 2) include: 1) the solubilities of compounds of the important radionuclides that are stable in groundwaters located between the repository horizon and the accessible environment, 2) the rate and volume of water and air movement through the repository to the accessible environment, 3) the dispersion rates for radionuclides in the groundwater and air-flow systems associated with the site, 4) the sorption of radionuclides to immobile and mobile (for example, colloidal) surfaces present in the groundwater and air-flow systems associated with the site, and 5) the decay of the radionuclides during transport.

Stratigraphy of Yucca Mountain

Figure 1 gives the names of the main layers of Yucca Mountain tuff and shows their relationship to the static water table and the intervals of zeolites. Figure 3 is a more detailed, scaled view of Yucca Mountain that also shows the positions of the drill holes used to develop the stratigraphic pic-

Table 1. Important Radionuclides and the Reduction Factor Required to Meet Maximum Allowed Releases

Element	Reduction factor*
Americium	18,300
Plutonium	12,300
Thorium	457
Uranium	52
Curium	46
Carbon	46
Neptunium	46
Radium	38
Nickel	13
Iodine	9
Cesium	5
Tin	5
Selenium	5
Zirconium	5
Niobium	5
Technetium	3
Palladium	3

*Assuming each radionuclide accounts for not more than 0.035 of total U.S. EPA limit and assuming no precipitation.

ture. Samples from the cores of a number of these drill holes were used throughout the research reported on here.

The stratigraphic units in Yucca Mountain include partially-welded to densely-welded devitrified tuff, moderately-welded to densely-welded vitrophyre, and nonwelded vitric tuff that in places has been extensively altered to zeolite minerals (Scott et al. 1983; Carr et al. 1986). As we've pointed out, the potential repository is located in a layer of densely-welded devitrified tuff. Between the repository and the water table, several stratigraphic intervals containing zeolitic tuffs (containing primarily the zeolites clinoptilolite and mordenite) provide probable barriers to downward radionuclide migration in the unsaturated zone. Additional zeolitic tuffs below the water table provide potential barriers to lateral

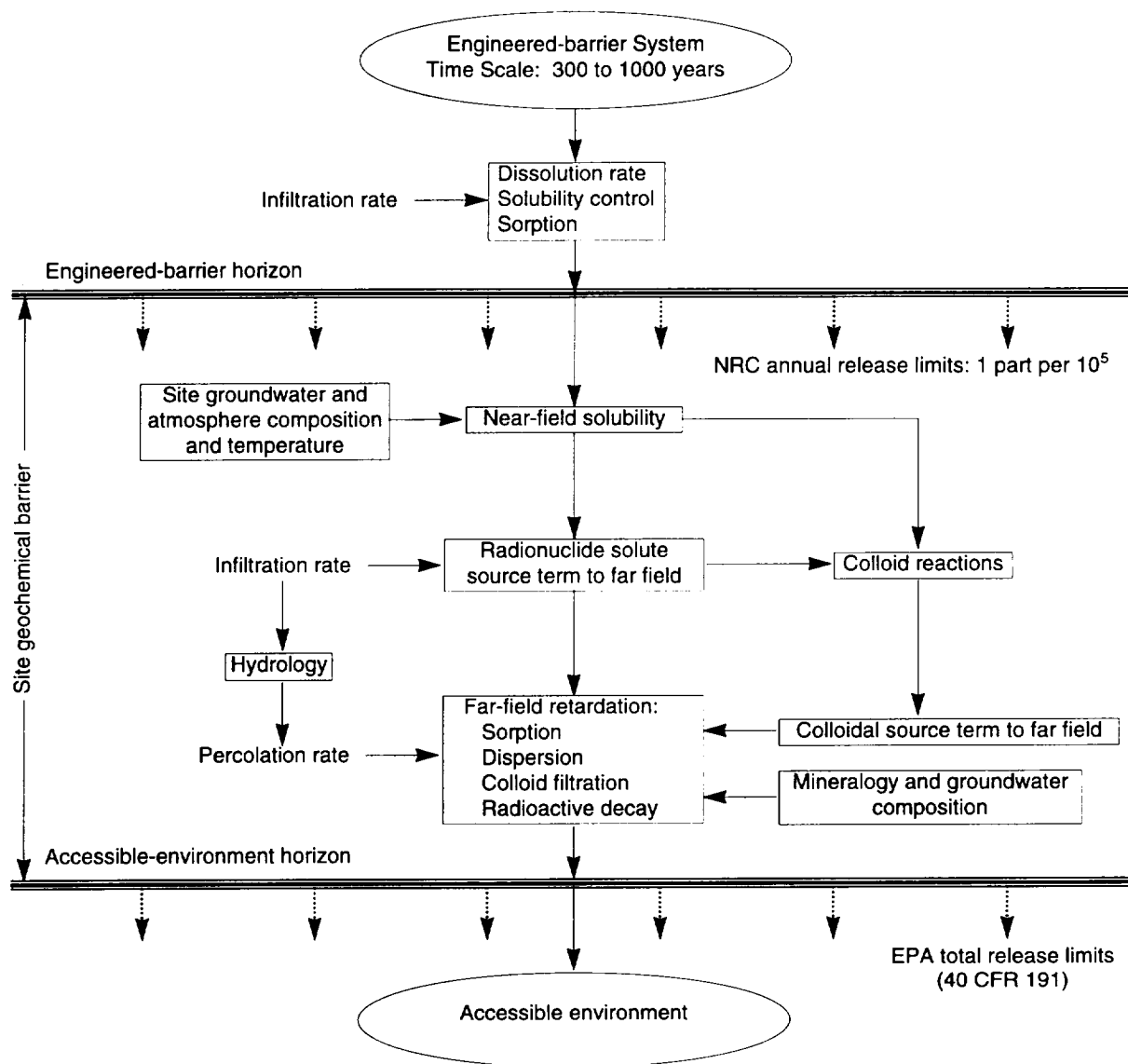


Figure 2. Multiple Natural Geochemical Barriers. This schematic diagram of the potential nuclear-waste repository system illustrates the processes important to retardation of radionuclides between the horizon of the engineered-barrier system, where the release limits are stipulated by the NRC, and the horizon of the accessible environment, where release limits are governed by the EPA. For our purposes, the engineered-barrier system is considered independent of the natural site surrounding that system. Taking the NRC limits as the upper bound for releases across the horizon into the natural site, the various processes (sorption, dispersion, colloid reactions, and so forth) are then examined to see if retardation is adequate to meet the EPA release limits to the accessible environment.

I. Introduction

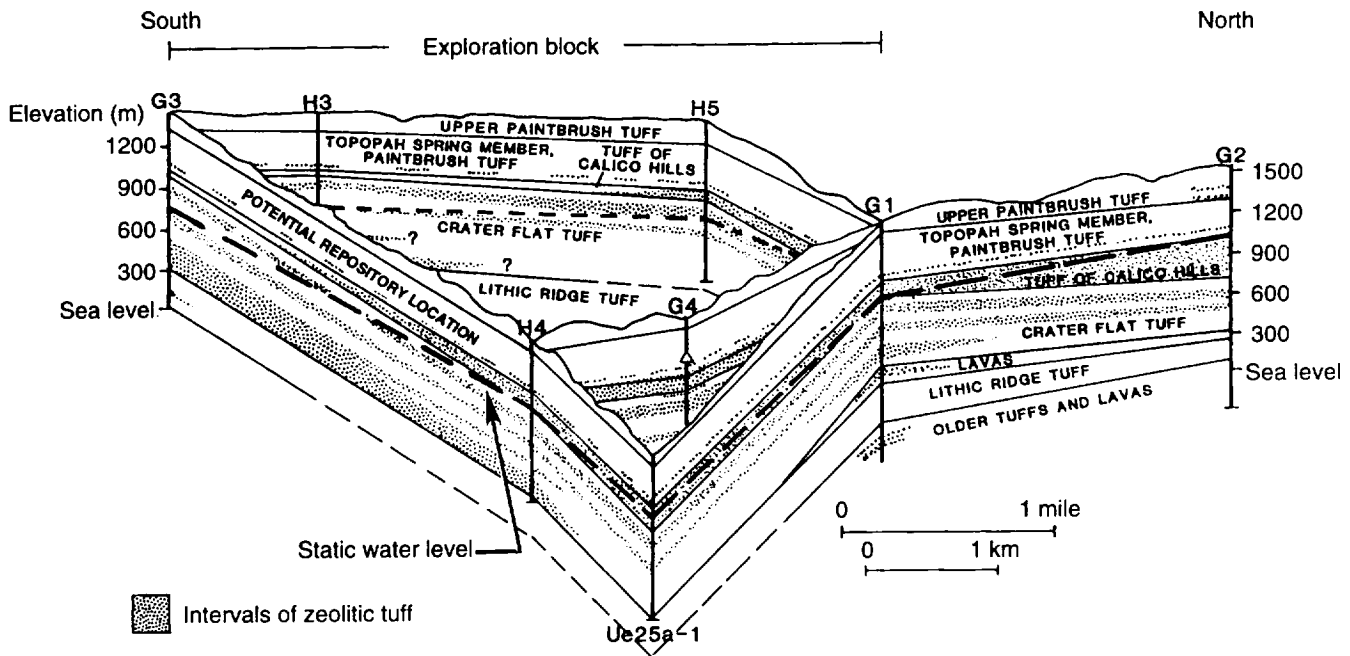


Figure 3. Zeolitic Tuffs at Yucca Mountain. The above fence diagram of the stratigraphy at Yucca Mountain shows the distribution of the principal zeolitic tuffs (tuff containing more than 10% clinoptilolite and mordenite) as shaded areas. The potential repository location is in the lower half of the Topopah Spring member of Paintbrush Tuff. Each “fence post” (for example, G3) represents a USW drill hole. Most of the tuff samples used in the research described in this report were portions of core taken from USW drill holes G-1, G-2, G-4, and GU-3 (located at the G3 site). The figure was taken from Broxton et al. (1986); stratigraphic contacts were from Spengler et al. (1979, 1981), Maldonado and Koether (1983), and Scott and Castellanos (1984); preliminary stratigraphic contacts for drill holes USW H-3, H-4, H-5, and G-4 were provided by R. W. Spengler (personal communication, 1983); and static water-level data were from the USGS Nuclear Hydrology Group.

radionuclide migration through the saturated zone.

The suite of minerals found in the deeper-lying host rock for the potential site includes all four categories of sorptive minerals described by Kent et al. (1988) in the context of a surface-complexation model for radionuclide sorption. These categories are 1) oxide minerals (including iron oxides and silica minerals), 2) multiple-site-type minerals (including the feldspars), 3) fixed-charge minerals (including micas, clays, manganese oxides, and zeolites), and 4) salt-type minerals (including calcite). Chemical speciation and water chemistry may strongly affect the interaction between selected

radionuclides and each of these mineral categories, but the mineral variability and presence of all four mineralogic categories of Kent et al. suggest mineralogic robustness for sorption at Yucca Mountain.

Beneath the potential host rock, the stratified layers of devitrified (mostly quartz plus feldspar) and nonwelded (mostly glass or zeolite) tuffs provide significant mineral variability along both unsaturated and saturated transport pathways. The effectiveness of the individual mineral types in sorbing will depend on the geometry, accessibility, fluid environment, duration of contact, and cumulative abundance along the transport pathway.

B. AN INTEGRATED APPROACH TO SITE CHARACTERIZATION

The natural system at Yucca Mountain defines the site-specific conditions under which we must determine to what extent the natural geochemical barrier will prevent the migration of radionuclides away from the repository. The mineralogy, petrology, and water chemistry at Yucca Mountain define the conditions a radionuclide will encounter if the waste package corrodes and dissolved radionuclides are released across the horizon of the engineered-barrier system into the site environment. There may be many scenarios that could affect the near-field environment, creating chemical conditions more aggressive than conditions presented by the unperturbed system (such as pH changes beyond the range of 6.9 to 8.9 or significant changes in the ionic strength of near-field waters). Without clear near-field-condition bounds at this time, we assume that at some distance away from the waste package, conditions are dominated by the large rock-mass buffer. In the far field, the near-neutral, oxidizing, low-ionic-strength conditions of the normal site environment control the radionuclide solubility limits and the sorption capacity of the tuff.

Our testing strategy (Canepa et al. 1994) thus shows the need for characterization of the natural system, which defines the experimental conditions for solubility and sorption determination. Such characterization requires data on groundwater composition, including natural colloids, on the mineralogy and petrology of the rock, and on mineral stability. Modeling of the groundwater chemistry is designed to lead to an understanding of solubility and speciation of the important radionuclides as well as the possible formation of radio-colloids. Laboratory experiments attempt to characterize sorption and diffusion of the radionuclides in light of this information. Finally, validation of chemical processes in a dynamic system is crucial before laboratory data are applied to the field tests or natural analogs. In this report, we focus on summarizing the research that has been accomplished in the areas described below.

Modeling of Groundwater Chemistry

The purpose of the groundwater-chemistry modeling task is to develop models that describe compositional variations in groundwaters in the unsaturated and saturated zones beneath Yucca Mountain. These models are used to establish bounds on the water compositions to be expected in the ambient Yucca Mountain flow system. They are also used to bound the composition of waters in the far field of the potential repository at Yucca Mountain in the post-closure period.

We can also derive estimates of the possible range of water compositions to be expected in the Yucca Mountain flow system on the basis of the compositional variations observed in present-day groundwaters in volcanic units over a large area such as the Nevada Test Site. The programs to measure transport parameters, such as sorption coefficients and solubilities, incorporate the compositions of these waters as part of the experimental design.

Radionuclide Solubility Studies

The potentially limited solubility of radionuclides in groundwater can be thought of as the geochemical first line of defense against migration. Evaluation of this effect first requires a knowledge of the groundwater chemistry at the site and the expected spatial and temporal ranges of its variability. Second, quantitative determinations of radionuclide solubility in groundwater within this range of chemistry must be made. Speciation and molecular complexation must be ascertained to interpret and apply solubility results. The solubilities thus determined can be used to assess the effectiveness of solubility in limiting radionuclide migration. We can also use these solubilities to evaluate the effectiveness of other retardation processes expected to operate once any dissolution and migration begin.

The short-term goals of the radionuclide solubility task have been to provide solubilities from bulk experiments that attempt to bracket our current estimate of groundwater conditions that might

I. Introduction

exist. Intermediate goals have been to develop the thermodynamic database for solution speciation and solid-state determination as a prerequisite to modeling the results. Once the model is self-consistent and performs well against known solubilities, our long-term goal is to use the model over a continuous, weighted distribution range of potential groundwaters to generate a weighted distribution of solubilities that could be used for performance assessment of the site.

Sorption Studies

A geochemical second line of defense against groundwater transport of radionuclides is "sorption," which comprises several physicochemical processes, including ion exchange, adsorption, and chemisorption. Determining whether sorption will occur requires knowledge of the likely flow paths of the groundwater and the spatial and temporal distribution of sorbing minerals along these paths. Evaluating the retardation effectiveness of sorption for repository design and licensing requires theoretical and quantitative understanding of sorption.

Batch-sorption experiments are useful for bounding more detailed and mechanistic sorption studies. We determined batch-sorption distribution coefficients, defined as

$$K_d = \frac{\text{moles of radionuclide per g of solid phase}}{\text{moles of radionuclide per ml of solution}}, \quad (1)$$

as a function of variables representing conditions expected beyond the region disturbed by waste emplacement. The variables included mineralogy, groundwater chemistry, sorbing element concentration, atmospheric conditions, and temperature.

Batch-sorption results are very sample specific and, therefore, difficult to generalize and apply throughout the mountain. Deconvolution of sorption isotherms provides much greater detail about sorption sites (kind, number, specificity, and so forth). Such information can be correlated with crystallographic data and related to specific sorption sites in the crystal structure. All sites are not

equally selective for all sorbing species. Examining the sorption behavior of individual pure minerals, such as the zeolites and manganese or iron oxyhydroxides found in Yucca Mountain tuffs, could help predict sorption coefficients along flow paths of known mineral content.

One factor that can have an effect on the sorption of radionuclides is organic materials. Naturally occurring organic compounds generated during the transformation of plant and animal debris over time and as a result of the synthetic activities of microorganisms are ubiquitous in surface and subsurface environments. Sorption of organic material onto mineral surfaces can affect the properties of those surfaces, such as charge and hydrophobicity, thereby altering the reactivity of the mineral toward metal ions. A clear understanding of the effects of the organics that frequently coat mineral surfaces in natural environments will lead to improvements in the sorption models used to predict the mobility of radionuclides in natural aquatic environments.

A better understanding of the sorption of radionuclides onto tuff will be possible if we can relate the data to mechanistic models. Two general mechanisms are important: ion-exchange reactions that are primarily electrostatic in nature and surface complexation in which a relatively covalent chemical bond forms with the mineral surface. Ion exchange does not have the same degree of selectivity between aqueous ions of like charge as does surface complexation. The adsorption of metal ions via cation exchange will only occur on surfaces of opposite charge and so is affected by such common components of groundwater as sodium. Surface complexation, on the other hand, can occur even when the mineral surface charge is the same as the aqueous ion. Both of these processes can, in principle, be modeled using a triple-layer surface-complexation model. However, there are significant differences between the cation exchange in zeolites and clays and the formation of surface complexes on metal oxides, so we have treated cation exchange and surface complexation separately.

Physiochemical processes that might accelerate radionuclide migration relative to groundwater flow rates, such as anion exclusion, must also be quantified. These depend largely on the molecular complexation or speciation that occurs in solution. Accordingly, detailed assessment of this possibility is needed to fully evaluate the potential for transport retardation by geochemical processes.

Diffusion Studies

Additional geochemical lines of defense beyond solubility limits and sorption are possible. The lateral diffusion of radionuclide species in porous media may retard longitudinal migration by bringing dissolved radionuclides into contact with sorbing minerals. Also, when the fluid flow is through fractures in highly impermeable rock and there is an absence of sorbing minerals on the fracture surfaces, diffusion may be the only effective retardation mechanism. Most rock (even dense rock such as granite) has small fissures between the crystals that interconnect the pore system containing water. Small molecules of radioactive materials can diffuse in and out of this pore system. The inner surfaces in the rock matrix are much larger than the surfaces in the fractures on which the water flows, and the volume of water in the microfissures is much larger than the volume in fractures. Therefore, over a long time scale, diffusion can play an important role in radionuclide retardation.

Diffusion experiments can provide diffusion information on nonsorbing neutral molecules and anions and on sorbing radionuclides. And because diffusion experiments measure the uptake of radionuclides by tuff as a function of time, information is gained on the kinetics of sorption. The work described here is of two types. In rock-beaker experiments, we placed a radionuclide solution inside the rock beaker and measured the decrease in radionuclide concentration as a function of time. In diffusion-cell experiments, a slab of tuff separates two chambers of groundwater, and we measured the concentration of radionuclide diffusing across the slab from one chamber to the other as a function of time.

Dynamic Transport Studies

Sorption results also must be interpretable and applicable to dynamic and heterogeneous systems, so we developed diffusion and dynamic transport experiments to complement and extend the batch-sorption results to such systems. Three types of dynamic transport experiments were conducted: crushed-rock column experiments, whole-rock column experiments, and transport through fractures.

We used crushed-rock experiments to study kinetic phenomena affecting sorption, including ionic and molecular diffusion. Whole-rock experiments additionally illustrate advective dispersion effects. Fractured-rock experiments represent the closest laboratory approach to the actual environment in which fluid flow and radionuclide migration might occur in an unanticipated scenario.

Studies are also necessary to determine the transport of radionuclides along fractures passing through the site. In the candidate host rock, the fractures contain a complex development of cristobalite, zeolites (mostly clinoptilolite and mordenite), manganese minerals, and calcite (Kent et al. 1988). This composition is in marked contrast to the rock matrix, composed predominantly of feldspars and silica minerals (quartz, cristobalite, and tridymite). Thus, different mechanisms are likely for retardation of radionuclides in flow along fractures and flow through bulk rock, and we have studied these mechanisms using fractured-rock columns.

The fracture-column studies also afforded us an opportunity to investigate colloidal radionuclide migration. Colloidal species may escape sorption and be too large to diffuse, that is, simple filtration may operate to retard movement. On the other hand, fracture flow may afford an easy transport path for colloids to the accessible environment. The dynamic transport experiment is a difficult but powerful method for elucidating separate and coupled processes affecting radionuclide migration.

We also evaluated the likelihood of particle or col-

I. Introduction

loid formation by analyzing a typical Yucca Mountain groundwater for the presence of natural colloids and by conducting laboratory experiments to determine the possibility of radiocolloid formation. We estimated the rate of particle aggregation for various colloids using autocorrelation photon spectroscopy.

The use of batch-sorption experiments to identify sorption mechanisms and to obtain sorption distribution coefficients is fast, easy, and inexpensive compared to other types of sorption experiments. However, measurements made under flowing conditions must be carried out to verify the results of the static batch-sorption experiments. We performed such verification using crushed-tuff and solid-rock column experiments in which mass-transfer kinetics were investigated by measuring radionuclide migration as a function of water velocity. The differences between the column and the batch-sorption experiments should be sensitive to multiple-species formation, colloid formation, and other geochemical reactions not adequately described by batch-sorption coefficients.

Quality Approved Detailed Procedures

All work performed to collect data and test, analyze, model, or describe the natural system under study has been done under the Yucca Mountain Project Quality Assurance program at Los Alamos. In particular, all experimental procedures were carried out in conformance with quality-approved procedures that are described in the *Yucca Mountain Project Detailed Procedures* at Los Alamos. The various procedures for each experimental area and the corresponding reference for the current version of that procedure are listed in Table 2.

The Reference Information Base

The stratigraphy referenced in this report is consistent with the Yucca Mountain Project Reference Information Base Section 1.12(a), "Stratigraphy: Geologic/Lithologic Stratigraphy" and with the Prototype Three-Dimensional Framework Model of September, 1995.

Table 2. Los Alamos Yucca Mountain Project Detailed Procedures

Research area	Procedure	Reference number
General	pH measurement	LANL-CST-DP-35
	Rock sample preparation (crushing and sieving)	LANL-CST-DP-63
	Neptunium, plutonium, and americium solution preparation	LANL-CST-DP-78
	Liquid-scintillation counting	LANL-CST-DP-79
	Eh measurement	LANL-CST-DP-102
Diffusion	Saturated diffusion-cell experiments	LANL-CST-DP-66
	Rock beaker experiments	LANL-CST-DP-67
Sorption	Batch sorption under atmospheric conditions	LANL-CST-DP-86
	Batch sorption within controlled atmosphere of a glove box	LANL-CST-DP-100
Colloids	Particle size distribution (autocorrelation photon spectroscopy)	LANL-CST-DP-75
	Colloid sampling	LANL-CST-DP-101
Dynamic transport	Crushed-rock column studies	LANL-INC-DP-15
	Solid-rock column experiments	LANL-INC-DP-61
	Fracture core experiments	LANL-INC-DP-68

C. YUCCA MOUNTAIN WATERS

A strategy for determining the retardation of radionuclides must be compatible with the hydrology of the site. A generalized conceptual model of unsaturated-zone water flow in Yucca Mountain is shown in Fig. 4 (Montazer and Wilson 1984). According to Montazer and Wilson, water in the unsaturated portion of this system will flow dominantly in the matrix and intermittently in the fractures. Given the low infiltration rate at Yucca Mountain, the rate of water movement in the matrix should be slow (Sinnock et al. 1984), but according to the modeling efforts of Nitao and Buscheck (1989), the rate of water movement in the fractures may actually be fairly rapid. The question of whether or not there will be significant water flow in the fractures beneath the potential repository horizon after waste has been stored

there is unresolved at the present time.

Saturated-zone Groundwater Chemistry

The chemical compositions of groundwaters in the present and future groundwater flow systems are important parameters with regard to the sorption behavior of important radionuclides in this system. Our chemistry and transport studies used water from the Yucca Mountain region, particularly from Well J-13, which accesses the water table several miles east of Yucca Mountain. The uplifted block of tuff units that make up Yucca Mountain dips to the east, and at the J-13 location, the water table and the Topopah Spring Member intersect. Water from Well J-13, although not exactly representative of Yucca Mountain unsaturated pore water, has been in contact with the same unit proposed for the repository and can be used as a reference water.

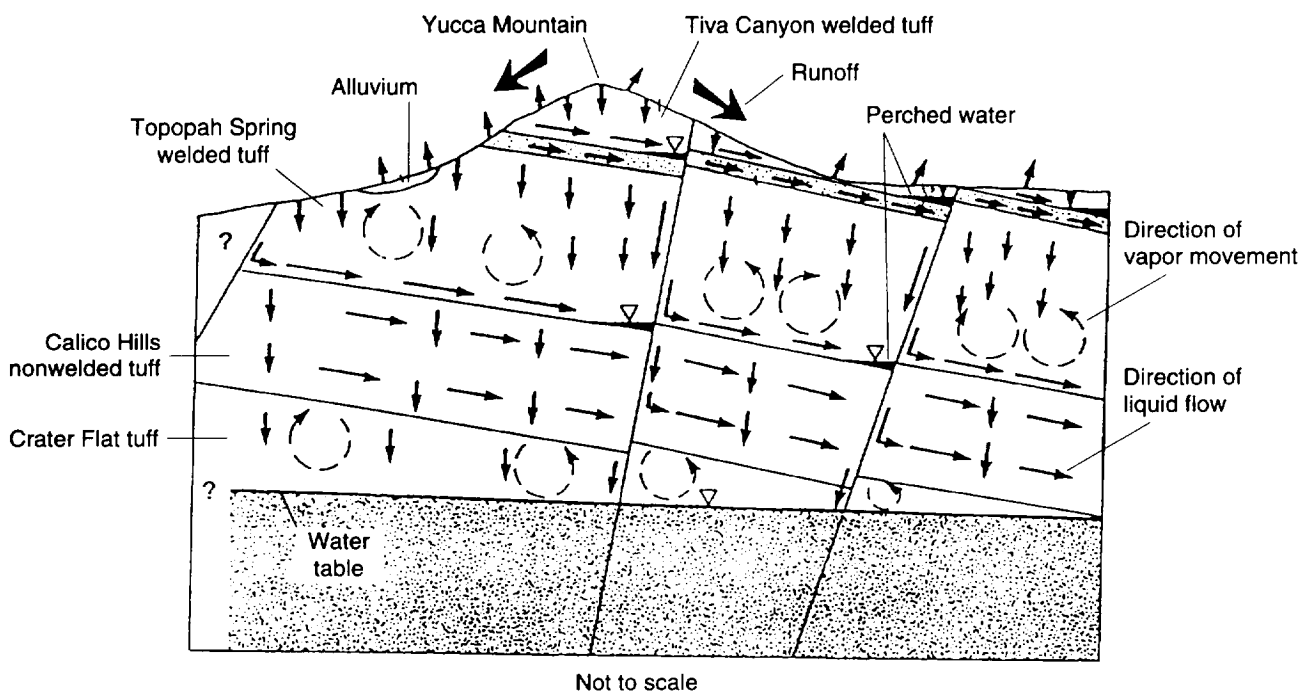


Figure 4. Unsaturated-zone Hydrology Model. This generalized east-west section across Yucca Mountain shows the flow regime under baseline conditions. Dashed arrows indicate movement of water vapor; solid arrows indicate movement of liquid water; and the lengths of the arrows indicate relative magnitude of the fluxes (from Montazer and Wilson 1984).

J-13 Well construction

Details of the construction and penetration levels of Well J-13, located in Fortymile Wash, are presented in Fig. 5. The total depth of the well is 3,500 feet, and it has been producing since its completion in 1963. Inspection of the construction diagram reveals perforations from a long section below the Topopah Spring Member starting at 2,690 feet. However, because of a discrepancy in the records concerning the well configuration (Harrar et al. 1990), it is not clear whether the entire length of the 5.5-inch liner below 1,499 feet is slotted or whether only the interval shown in the figure below 2,690 ft. is open. Resolving this discrepancy is not very important because there is no cement behind the liner, thus providing access to the well to any fluids entering the borehole below about 1,550 feet. However, hydraulic tests performed on the well yielded transmissivities that indicated that only about 20% of the flow may come from other formations, such as the tuffaceous beds of Tuff of Calico Hills, the three Crater Flat Tuff members, and Tuff of Lithic Ridge.

Well UE-25 p#1

Another well, Well UE-25 p#1, is located roughly midway between Yucca Mountain and Well J-13 at a ground-level elevation about 100 meters higher than Well J-13. Water from this well is drawn from the deep paleocarbonates underlying the tuff sequences. It has been the only other water available from the Yucca Mountain region with a chemistry different from J-13 water.

The data available in 1984 on the chemistry of saturated-zone groundwaters were reviewed by Ogard and Kerrisk (1984). In the volcanic units, the groundwaters are basically dilute sodium-bicarbonate waters (Table 3). Listed in order of decreasing concentration in J-13 water, the other major cations are calcium, potassium, and magnesium and the other anions are sulfate, nitrate, chloride, and fluoride. The only other major constituent is silica. The water from the Paleozoic aquifer (Well UE-25 p#1) has higher concentrations of almost all these constituents. Thus, the ionic strength of Well

UE-25 p#1 water is higher than that of J-13 water, although both are relatively low in ionic strength.

The chemistry of groundwaters from Wells J-13 and UE-25 p#1 seems to bound that of the Yucca Mountain groundwaters (Meijer 1992), and thus, these two groundwaters serve as standards for the experimental work. However, certain changes (Fig. 6) take place in the chemistry of the waters between their removal at the well and their use in the laboratory. The J-13 and UE-25 p#1 reference data plotted in Fig. 6 was obtained on site by Ogard and Kerrisk (1984). This on-site chemistry is compared with the chemistry of aliquots of J-13 and UE-25 p#1 waters that were collected at later dates, sent to Los Alamos, and filtered. On site, the pH of the two groundwaters is ~7. However, at Los Alamos, the waters equilibrate in the higher-elevation atmosphere with subsequent evolution of carbon dioxide, which causes the pH of J-13 water to increase to 8.5 and the pH of UE-25 p#1 water to increase to ~9. The data of Fig. 6 indicate that

Table 3. Chemistry of Waters from Wells J-13 and UE-25 p#1 and the Unsaturated Zone (UZ) at the Yucca Mountain Site

Element	J-13* (mg/l)	UZ** (mg/l)	UE-25 p#1* (mg/l)
Sodium	45	26–70	171
Bicarbonate	143	—	698
Calcium	11.5	27–127	87.8
Potassium	5.3	5–16	13.4
Magnesium	1.8	5–21	31.9
Sulfate	18.1	39–174	129
Nitrate	10.1	—	< 01
Chloride	6.4	34–106	37.0
Fluoride	2.1	—	3.5
Silicon	30.0	72–100	30.0
pH	6.9	6.5–7.5	6.7
Eh (mV)	340	—	360

*Ogard and Kerrisk 1984; **Yang et al. 1990.

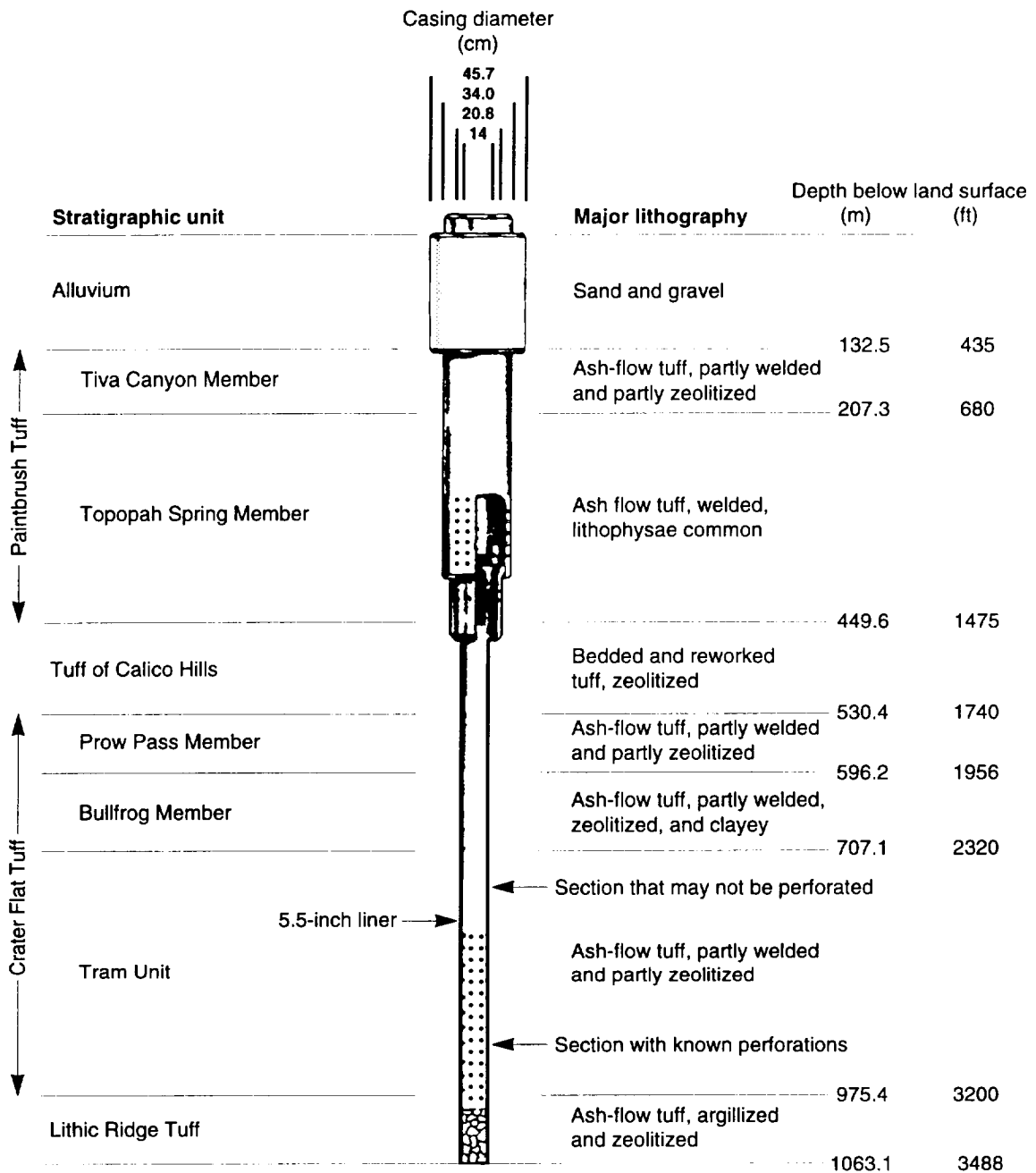


Figure 5. Well J-13. The construction diagram and lithologic units penetrated for Well J-13 (from Harrar et al. 1990) are shown above. Hydraulic tests performed on the well indicate that about 80% of the water flow may come from the Topopah Spring Member of Paintbrush Tuff, which is the same stratigraphic unit as the one proposed for the repository, and only about 20% may come from other formations.

I. Introduction

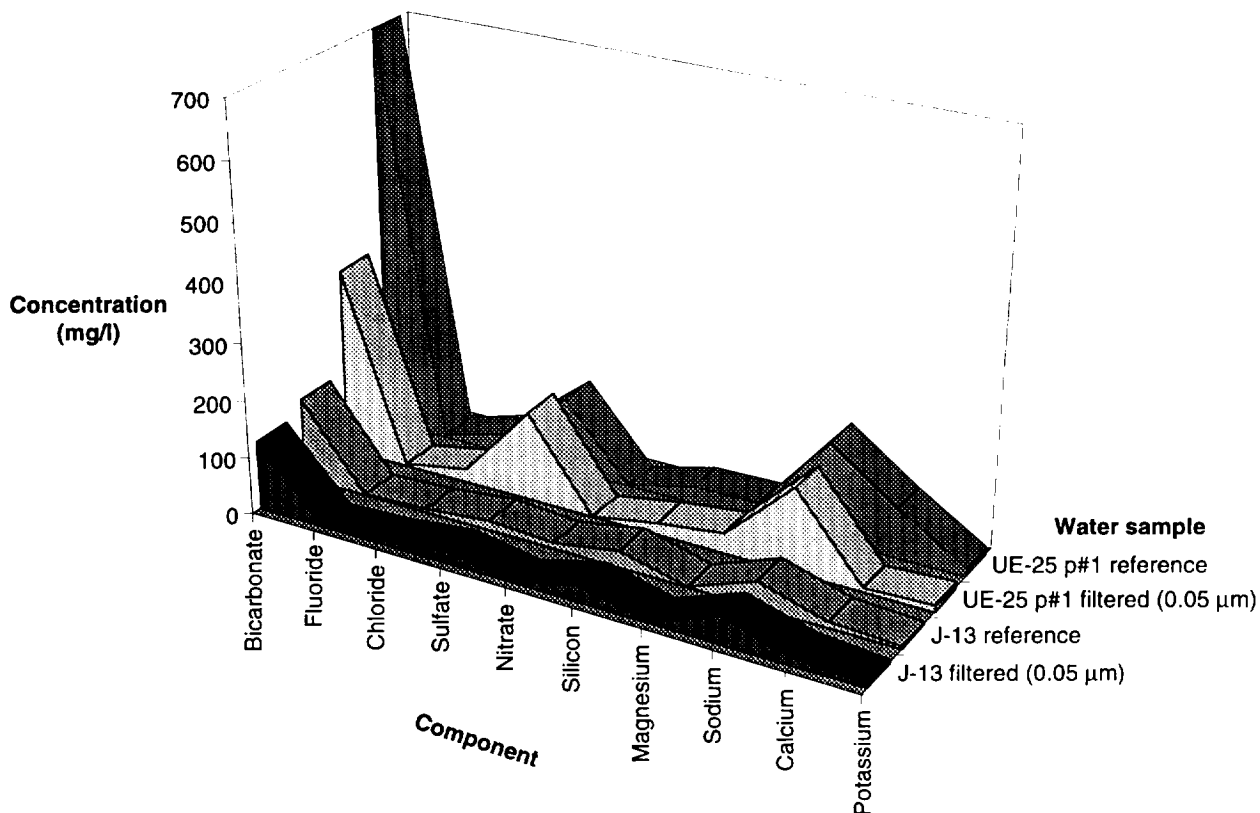


Figure 6. Chemistry of Two Groundwaters. The two reference samples above are water analyzed on-site in Nevada at the J-13 and UE-25 p#1 well sites (Ogard and Kerrisk 1984). The filtered samples are water analyzed at Los Alamos, NM, after being passed through a 0.05- μm filter (data recorded in binder TWS-INC-11-93-32, pages E24–E25, for J-13 water and in binder TWS-INC-03-93-02, page C8, for UE-25 p#1 water). The figure demonstrates the higher ionic strength of UE-25 p#1 water, the stability of J-13 water, and the apparent calcite precipitation in UE-25 p#1 water caused by CO_2 evolution.

carbon-dioxide evolution and filtration does not otherwise change the chemistry of J-13 water but causes calcite precipitation in UE-25 p#1 water. Consequently, the concentrations of bicarbonate and calcium in any UE-25 p#1 water used in the sorption experiments were lower than that of on-site UE-25 p#1 water. Because both waters are oxidizing, all the sorption experiments were performed under oxidizing conditions.

Chemical stability of Well J-13 water

Figure 7 shows a chemical analysis of water from Well J-13 from 1963 to 1993. The front curve represents the average of the chemical analysis of 19 water samples collected between 1963 and 1987 by

five different organizations (Los Alamos National Laboratory, U.S. Geological Survey, Lawrence Livermore National Laboratory, Argonne National Laboratory, and Westinghouse-Hanford Company). Analysis of these results led Harrar et al. (1990) to conclude that the water chemistry of Well J-13 did not change between 1963 and 1987. Comparison of the results of Harrar for that period with similar analyses of water collected in 1992 and 1993 (the other curves shown in Fig. 7) indicates that the chemistry of the water in Well J-13 has been stable for thirty years.

We analyzed aliquots of both groundwaters before and after filtration (Figs. 6 and 7). Comparison of

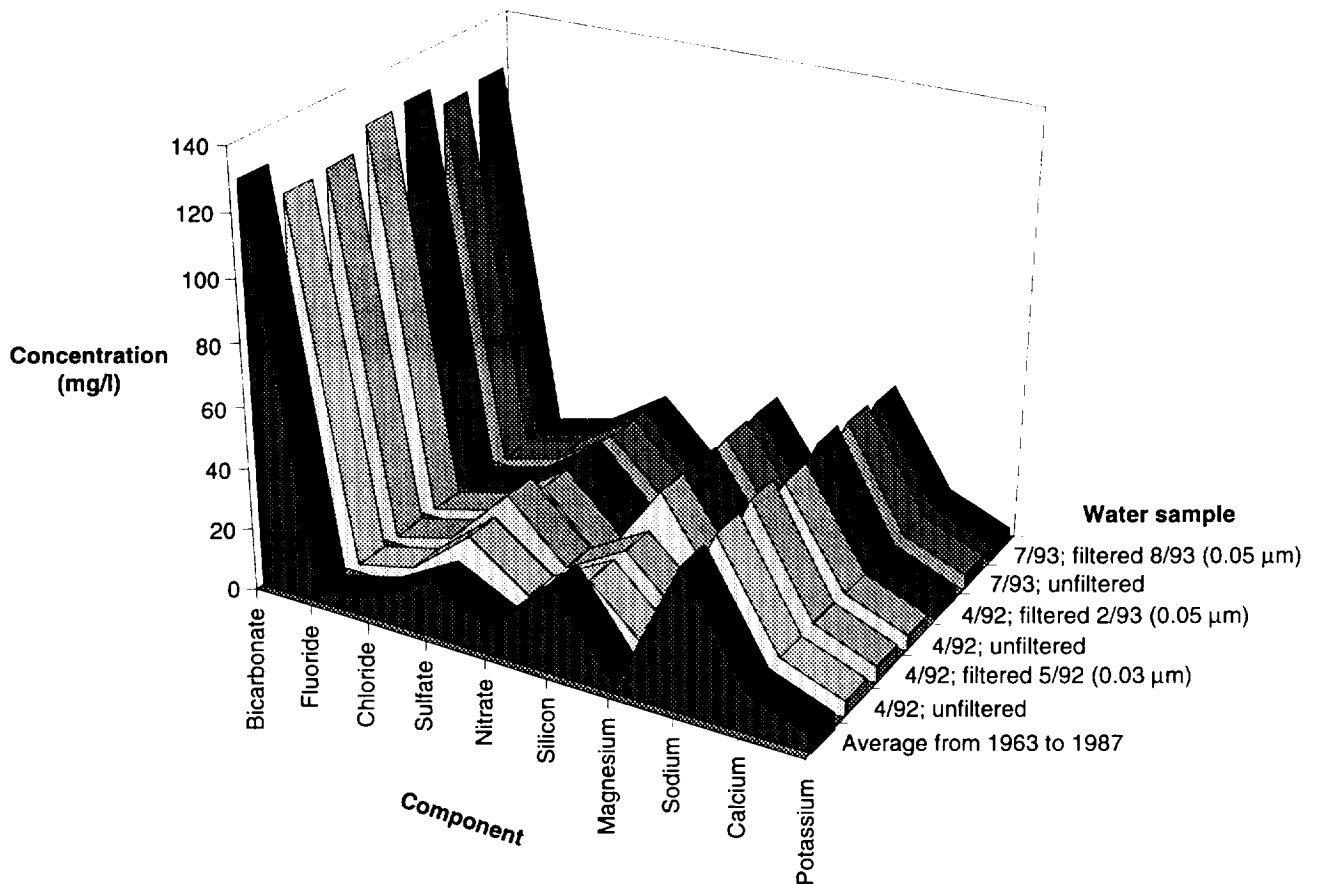


Figure 7. Stability of the Chemistry of Well J-13 Water. The curves above show minimal compositional changes as a function of collection date, filtering, and filter size, indicating that the chemistry of the water in Well J-13 has been stable for 30 years.

these results indicates that filtration does not cause compositional changes (except for the previously noted calcite precipitation in the UE-25 p#1 water that is caused by pH changes).

Unsaturated-zone Water Chemistry

The compositions of waters from the unsaturated zone are not well known. Yang et al. (1990) have reported partial analyses of unsaturated-zone waters from Wells UZ-4 and UZ-5 obtained by triaxial compression and centrifugation methods. Core samples of the wells from which waters were obtained came from the nonwelded portion of the Yucca Mountain and Pah Canyon members of

Paintbrush Tuff. The major cation and anion concentrations in these waters are intermediate between the saturated-zone tuffaceous waters and waters from the carbonate aquifer (Table 3). Water samples from UZ-4 cores tend to be closer in composition to the tuffaceous waters, whereas waters from UZ-5 cores appear to be closer in composition to water from the carbonate aquifer, although this statement is not intended to imply genetic associations of the waters with these aquifers.

The pH and the oxidizing potential, Eh, of the groundwaters in Yucca Mountain are particularly important with respect to the solubilities and sorption behavior of a number of the important ele-

I. Introduction

ments (such as, actinides and technetium). The available data suggest that most of the waters within Yucca Mountain site are oxidizing (for example, Ogard and Kerrisk 1984). Because the spatial and temporal variability in the Eh parameter will be difficult to quantify, the conservative approach would be to assume all the groundwaters between the potential repository and the accessible environment are in equilibrium with atmospheric oxygen. This assumption is conservative because all the important (radionuclide) elements have either higher or equal solubilities in oxidizing waters compared with reducing waters. Available data on the pH of waters in Yucca Mountain show a range from 6.5 to 9.4 (Ogard and Kerrisk 1984; Yang et al. 1990). In this case, no single value can be chosen as being conservative.

The future compositional variations of groundwaters in Yucca Mountain must also be considered in the development of a sorption strategy. To a first approximation, the variations are likely to be similar to the present-day variations as a result of buffering reactions by the country rock.

Pore Water versus Saturated Groundwaters

We must recognize that there are likely more than one type of water in the Yucca Mountain area. Differences in chemistry may exist between waters in saturated zones (at or below the true water table), waters in tuff pores in the hydrologic units of the unsaturated zone, and perched waters, that is, groundwater separated from the underlying water table by an unsaturated zone.

Unsaturated-zone waters may be strongly influenced by soil-zone processes, including evapotranspiration and the precipitation of pedogenic minerals such as calcite, gypsum, and silica. Chemical properties, such as ionic strength, may be a function of the time interval between infiltration events. Other properties, such as pH and oxidation potential, will depend on the partial pressures in the unsaturated zone of such gases as carbon dioxide and oxygen. Whether or not a particular unit of

rock is closed or open to the gas phases of the unsaturated zone is thus important. Also, the various waters may be influenced by hydrolysis reactions, for instance, with aluminosilicates, or by ion-exchange reactions with zeolites.

Evaluation of the database on water compositions in volcanic units at the Nevada Test Site indicates that the variability in major constituents is well-bounded by waters from Wells J-13 and UE-25 p#1. The main parameters not bounded by these water compositions are pH, Eh, and chloride concentration. Our experimental programs to measure transport parameters, such as sorption coefficients and solubilities, have incorporated these water compositions as part of the experimental design, and we have carried out the experiments as a function of pH. Therefore, the primary uncertainties are in the effects of variations in Eh and chloride concentrations.

Synthetic Groundwaters

We used both groundwaters (filtered by a 0.05- μm filter) in the batch-sorption experiments, but in the column-transport and the diffusion experiments, we used filtered J-13 water and, because of the unavailability of water at that time from Well UE-25 p#1, a sodium-bicarbonate buffer that simulated this groundwater. In the fracture studies, filtered J-13 water and sodium-bicarbonate waters simulating both J-13 and UE-25 p#1 waters were used. One reason for using synthetic waters for the fracture studies was the prevention of microbial activity in the fracture columns.

Synthetic UE-25 p#1 water was prepared by dissolving 0.39 g of Na_2CO_3 and 8.90 g of NaHCO_3 in 10 liters of deionized water, which duplicates the larger amount of bicarbonate in reference, or on-site, UE-25 p#1 water. Synthetic J-13 water was prepared by dissolving 0.03 g of Na_2CO_3 and 1.92 g of NaHCO_3 in 10 liters of deionized water.

D. YUCCA MOUNTAIN TUFFS

The stratigraphy of Yucca Mountain considered from the repository horizon to the accessible environment (and including the repository containers themselves) is outlined in Table 4, which shows the rock type for each of the various strata. We have assumed that, for the purposes of sorption measurements, all strata of the same rock type can be grouped. This assumption reduces the number of sorption coefficient distributions needed to four per radionuclide: iron oxides, devitrified tuff, vitric tuff, and zeolitic tuff. The basis for this grouping is the fact that sorption of radionuclides is the result of a chemical reaction between the radionuclide in the groundwater and the minerals in the tuff. The mineralogy of the different strata of the same type of rock is very similar. Thus, the sorption coefficients can be grouped in terms of these rock types (Thomas 1987).

The repository containers are included on the list because the corrosion by-products of the massive multipurpose containers could become a substrate for sorption. In particular, actinides are sorbed

Table 4. Stratigraphy versus Rock Type

Stratum name	Rock type
Repository Container	Iron oxides
Repository: Topopah Spring (welded)	Devitrified
Vitrophyre below repository: Topopah Spring (welded, vitrophyre)	Vitric
Calico Hills (nonwelded, vitrophyre)	Vitric
Calico Hills (nonwelded, zeolitized)	Zeolitic
Prow Pass (welded)	Devitrified
Bullfrog (nonwelded)	Zeolitic
Bullfrog (welded)	Devitrified

strongly by iron oxides, so iron oxides are given as one of the four "rock" types.

Mineralogy Variability

The mineralogy and textures of Yucca Mountain tuffs are important to the sorption behavior of the important radionuclides because they determine 1) the types (that is, structure and composition) of mineral surfaces available in the tuffs and 2) the areas of the different mineral surfaces (internal and external) available for sorption of radionuclides.

The mineral species that have been identified in the matrix of Yucca Mountain tuffs are listed in Table 5 in order of overall abundance. Feldspar and quartz are by far the most common matrix minerals (Bish and Vaniman 1985). They are most abundant in the devitrified tuffs, such as those found in the Topopah Spring Member of Paintbrush Tuff, Prow Pass and Tram Members of Crater Flat Tuff, and the older tuffs.

The zeolites clinoptilolite and mordenite are abundant in parts of some nonwelded units (for example, Calico Hills) but are limited to sparse fracture-lining minerals in most of the devitrified tuffs (see below). In the nonwelded units, the zeolitic zones are thickest in the northern and eastern portions of Yucca Mountain but thin out to the south and west (Bish and Vaniman 1985).

Clays are locally abundant in the matrix of some tuffs (for example, in some parts of the vitrophyres in drill hole G2 and in the bottom of drill hole G1) but are a minor component (1–3%) in most of the tuffs beneath the potential repository (Chipera and Bish 1989).

Calcite is generally a minor component in the tuffs with a bimodal distribution. In most holes, it is a minor-to-abundant constituent at depths less than 300 m and at depths greater than 900 m but is sparse or absent at intermediate depths. Hematite is widely distributed as a trace mineral, particularly in the matrix of the devitrified units.

Tuff sample identification

The tuff samples we used in the batch-sorption and column-transport experiments were obtained from drill holes at Yucca Mountain and labeled with the drill-hole code and drill depth in feet. For example, G4-270 refers to a tuff sample taken from drill hole USW G-4 at a depth of 270 feet. The locations of the drill holes has previously been reported by Bish and Chipera (1989).

The mineralogy of the tuffs that we used in the sorption, diffusion, and transport experiments was determined by x-ray-diffraction (XRD) analysis (Fig. 8), the details of which were previously reported (Bish and Chipera 1989; Chipera and Bish 1989, 1994). Prior to their use in the sorption and the crushed-rock-column experiments, all tuff samples were crushed and wet-sieved (with the groundwater being used in the experiment) to obtain particle sizes ranging from 75 to 500 μm . As previously discussed by Triay et al. (1996a), such crushing and sieving does not cause significant differences in the mineralogy of the tuff samples. In several cases, it appears that sieving to eliminate particles smaller than 75 μm reduces the smectite content. Because smectite is a good sor-

ber for most radionuclides, the sieved tuff samples should yield conservative results for the sorption measurements.

For our experiments, we always used several examples of each of three major rock types for tuff: zeolitic, vitric, and devitrified. Each of these are now briefly described.

Zeolitic tuff

The zeolitic tuffs are represented in Fig. 8 by samples G4-1508 and G4-1510. The major component of these tuffs is clinoptilolite. Other components usually include opal-CT, quartz, and feldspar.

Vitric tuff

The vitric tuffs are represented in Fig. 8 by samples GU3-1405 and GU3-1407. The major component of the vitric tuffs is glass. Another component is usually feldspar. Sample G2-723 is another vitric tuff, but this sample also has a significant component of calcite.

Devitrified tuff

The devitrified tuffs are represented in Fig. 8 by samples G4-268 and G4-270. The major component of the devitrified tuffs is alkali feldspar. Another component of the devitrified tuffs is usually tridymite.

Table 5. Minerals in Matrices of Yucca Mountain Rocks

Major phases	Minor and trace phases
Quartz	Hematite
Alkali feldspar	Dolomite
Clinoptilolite	Chlorite
Cristobalite	Illite
Plagioclase	Fluorite
Tridymite	Hornblende
Opal-CT	Pyroxene
Smectite	Fe-Ti Oxides
Mica	Ilmenite
Mordenite	Zircon
Analcime	Allanite
Calcite	Sphene
(Glass)	Rutile

Minerals

In some of the sorption experiments, we used natural and synthetic minerals. The intent was to identify those minerals responsible for dominating radionuclide sorption onto tuff by measuring sorption with single mineral phases. The natural minerals we used were calcite, montmorillonite, bentonite, clinoptilolite (purified with sodium exchange), quartz, and albite. The synthetic minerals we used were calcite and hematite, which were commercially available CaCO_3 and Fe_2O_3 , respectively.

Surface area of tuffs and minerals

Originally, the available data on total surface area of tuff samples from Yucca Mountain were rather

limited. Wolfsberg et al. (1979) reported surface areas (via the BET method using nitrogen as the adsorbate) for three samples with a range of values from 2.6 to 10.0 m²/g. Data on the specific surface areas of the various mineral phases in Yucca Mountain tuffs were not available. Wolfsberg and Vaniman (1984) presented a summary of "cation-exchange capacities" for Yucca Mountain tuffs. The zeolite and the clay-rich tuffs had cation-exchange capacities in the range from 10 to 175 meq/100 g, and the capacities of devitrified and vitric tuffs were in the range from 0.1 to 10 meq/100 g.

We performed further surface-area measurements on the tuff samples and the minerals using the

BET analysis method. Typical values are shown in Fig. 9.

Fracture Minerals

The Yucca Mountain region has undergone significant deformation due to tectonic and volcanic activity. As a result, many faults and fractures were produced within the tuffaceous units as well as the entire region. In addition, volcanic tuffs are often fractured as a result of cooling. The numerous fractures present at Yucca Mountain potentially represent a breach in the natural barrier by providing a fast pathway for contaminant migration.

Radionuclide transport calculations often assume

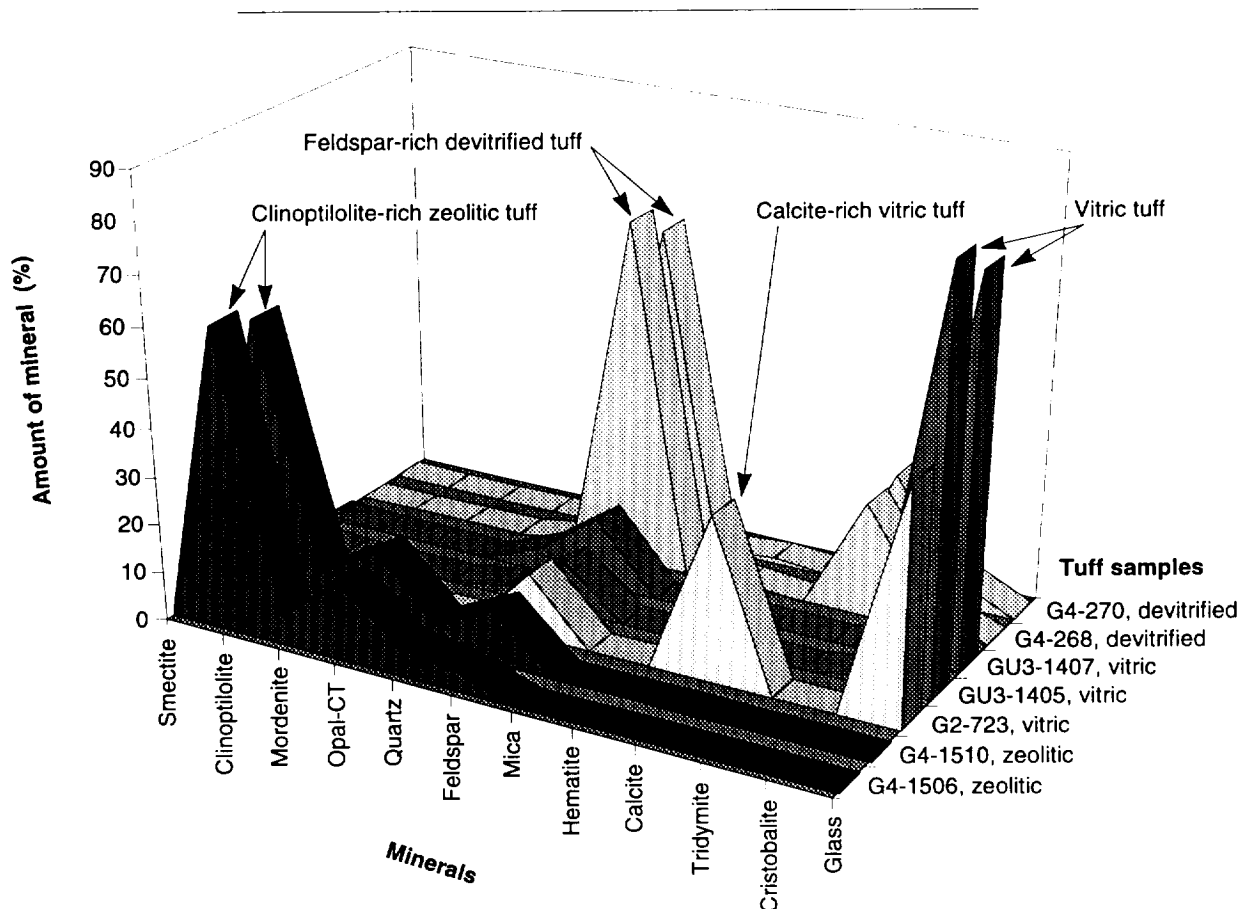


Figure 8. X-ray Diffraction Results. Mineral percentages determined by x-ray diffraction for tuffs used in the experiments are shown. Each tuff, except GU3-1405, was wet-sieved with J-13 well water to particle sizes ranging from 75 to 500 μm.

that radionuclides can travel through fractures unimpeded. This assumption is too simplistic and leads to overconservative predictions of radionuclide releases to the accessible environment. The assumption ignores two of the main retardation mechanisms: diffusion of the radionuclides from the fractures into the rock matrix and sorption of radionuclides onto the minerals coating those fractures.

Minerals coating the fracture walls are generally different from the host-rock mineralogy due to a variety of factors, such as precipitation of hydrothermal waters or alteration of the pre-existing minerals. The minerals lining the fractures found at the Yucca Mountain site (Carlos 1985, 1987, 1989, 1990, 1994; Carlos et al. 1993) are given in Table 6.

Although a relatively large number of fracture minerals have been identified, the overall abundance of these minerals is very small. Manganese minerals are found in fractures throughout most of the holes for which data are available, except in one drill hole where they are restricted to the upper few hundred feet. In most of the holes for which data

are available, calcite is common in fractures within a few hundred feet from the surface, is minor or absent in the middle sections of the holes, and is again common in fractures in the lower parts of the holes, which is consistent with the abundance variations of calcite in the matrix. Clays and zeolites generally increase in abundance in fractures with depth and are the dominant secondary minerals in the lower parts of some holes. Silica and iron-oxide/oxyhydroxide phases are somewhat unevenly distributed in fractures but are nonetheless important fracture-lining phases.

Data on the concentrations of elements on surface sites on minerals in Yucca Mountain tuffs are very limited at present. The minerals for which the greatest number of data are available are the zeolites and clays. This emphasis exists because measurement of the bulk cation abundances (that is, calcium, magnesium, sodium, and potassium) in these minerals reflects the cation populations on intracrystalline exchange sites accessible to aqueous species.

Broxton et. al. (1986) have tabulated chemical data for zeolites and clays from various volcanic units

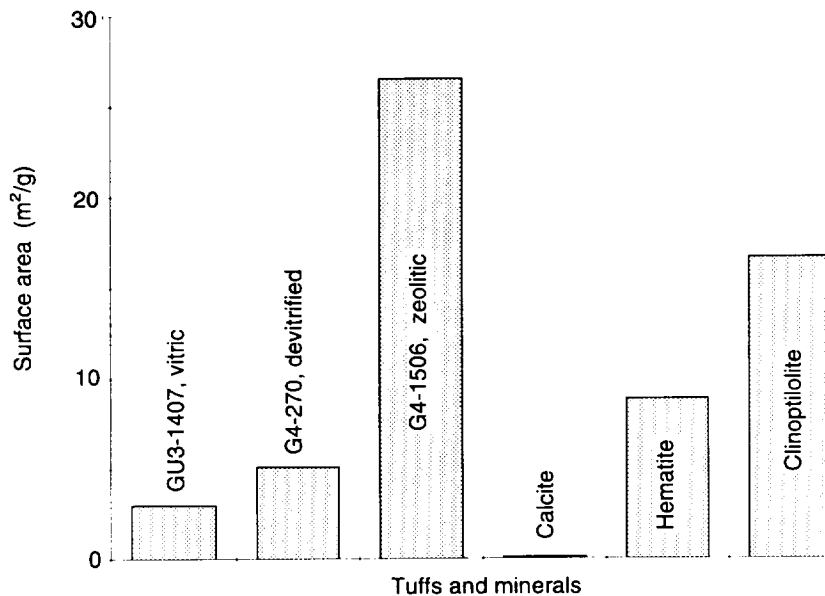


Figure 9. Surface Areas of Tuffs and Minerals. BET analysis was used to determine the surface areas of the tuffs and minerals used in the sorption experiments. The tuffs and the calcite (natural) were wet-sieved with J-13 well water to obtain particle sizes ranging from 75 to 500 μm . The hematite (synthetic) and clinoptilolite were not sieved.

Table 6. Minerals Coating Fracture Walls in Yucca Mountain Tuffs

Zeolites	
Heulandite	Chabazite
Clinoptilolite	Phillipsite
Mordenite	Erionite
Analcime	Stellerite
Silica	
Quartz	Feldspars
Tridymite	Plagioclase-albite
Cristobalite	K-feldspar-sanidine
Opal	
Clays	
Smectites	Sepiolite
Montmorillonite	Palygorskite
Saponite	Illite
Manganese-oxides/hydroxides	
Aurorite	Rancietite
Cryptomelane	Romanechite
Hollandite	Todorokite
Coronadite	Pyrolusite
Lithiophorite	
Iron-oxides/hydroxides	
Hematite	Magnetite
Carbonates and Halides	
Calcite	Fluorite

in Yucca Mountain. In general, samples from the west side of the potential repository block are sodium and potassium rich, whereas the eastern samples are enriched in calcium and magnesium (Broxton et al. 1986; Fig. 1). Carlos (1985, 1989) and Carlos et al. (1990) have provided chemical data on zeolites and clays found in fractures. In general, the zeolites found there are similar in composition to zeolites present in the matrix adjacent to a given fracture sample, although exceptions have been noted. Analytical data on the surface compositions of most of the other mineral phases listed in Table 6 are essentially nonexistent. The actual surface structures (for example, defects and pits) of minerals in Yucca Mountain tuffs are also essentially unknown.

II. GROUNDWATER CHEMISTRY MODEL

A. INTRODUCTION

Variations in the chemistry of groundwater can have a significant impact on the transport behavior of radionuclides. For example, the solubility and sorption behavior of the various radionuclides of interest are a function of groundwater chemistry. To derive bounds on transport parameter values pertaining to the post-closure period of the potential repository, experiments must be carried out as a function of groundwater chemistry.

A groundwater chemistry "model" has been developed that can be used to bound the potential variations in groundwater chemistry to be expected in the post-closure period. This model consists of a set of conceptual submodels that describe the chemical processes that control the chemical evolution of pore waters, perched waters, and groundwaters in Yucca Mountain.

Experiments are used to quantify the submodels, and the results of the experiments can be used to link the submodels using variations in water chemistry observed in the site-characterization phase of this project to calibrate the resulting linked models. Unfortunately, the experimentation phase of the project was not carried to completion as a result of budget constraints. As a result, the linking of the conceptual models remains incomplete.

Purpose and Scope

The purpose of the Groundwater Chemistry Modeling Task is to develop models that describe compositional variations in groundwaters in the unsaturated and saturated zones beneath Yucca Mountain. These models will be used to establish bounds on the water compositions to be expected in the ambient Yucca Mountain flow system. They will also be used to bound the composition of waters in the far field of the potential repository at Yucca Mountain in the post-closure period. This

information will be used by various other tasks in the project.

In this chapter, we will review the currently available data on the chemistry of waters in Yucca Mountain and develop and discuss models that explain the observed variations. We will combine 1) analytical data for precipitation (rain and snow), for pore waters and perched waters from the unsaturated zone at Yucca Mountain, and for groundwaters from the saturated zone at Yucca Mountain, 2) experimental and theoretical data and models for soil-water and rock-water interactions, and 3) computer modeling to identify both the controls on unsaturated-zone and saturated-zone water compositions in Yucca Mountain and the ranges in chemical compositions to be expected in these waters over the lifetime of the proposed repository.

Computer modeling with the code EQ3/6 was used as a tool to formulate and test conceptual models. However, its use in the prediction of future variations in water compositions is severely restricted because appropriate data on the identity of secondary (alteration) phases and data on the kinetics of formation of these phases (nucleation and crystallization) are lacking. For this reason, only preliminary work has been accomplished, and our discussion in this report does not include extensive reference to EQ3/6 modeling results.

B. GROUNDWATER CHEMISTRY

Sources of Data

The main sources of data for this chapter are the publications on precipitation compositions by McKinley and Oliver (1994, 1995) and publications on groundwater chemistry by Ogard and Kerrisk (1984) and Yang et al. (1988, 1996). It is important to state that the groundwater chemistry data of Ogard and Kerrisk and of Yang et al. represent samples from a very limited number of sites and may not be fully representative of waters in the overall Yucca Mountain flow system.

Precipitation Compositions

Precipitation compositions are important for modeling the compositions of waters at Yucca Mountain because they represent the starting point in the evolution of groundwater chemistry. Precipitation compositions are commonly separated into wet-fall and dry-fall. The composition of wet-fall reflects those solutes in falling rain or snow. The composition of dry-fall reflects the dust composition deposited on the land surface. The composition of wet-fall varies with geographic position due to numerous factors, such as the distance of the sampling site from the ocean (Wagner and Steele 1989). An approximation of wet-fall compositions at a given site can best be obtained by sampling while rain or snow is falling. Dry-fall compositions can be obtained by sampling dust.

A common approach to measuring precipitation compositions is to sample rain gauges and rain collectors either on a regular basis or after significant precipitation events. The precipitation compositions obtained with this approach reflect wet-fall, soluble dry-fall, and evaporation that occurred prior to removal of the sample from the collector. These compositions will here be called integrated precipitation compositions, or simply, precipitation compositions.

Dust (dry-fall) compositions were reported for southern Nevada and the Yucca Mountain area by

Reheis et al. (1995). Separate analyses of wet-fall are not available for the Yucca Mountain area, and only a limited number of analyses of integrated precipitation samples is available (Stezenbach 1992). Fortunately, an excellent database of integrated precipitation compositions for the Nevada Test Site area has been provided by a sampling network established by the U. S. Geological Survey in the Kawich Range just north of the Nevada Test Site (McKinley and Oliver 1994, 1995). This database will be used extensively in this report.

Average concentrations for the major constituents in integrated precipitation samples from the Kawich Range site are given in Table 7.

As an example of the variability in precipitation compositions, data for sulfate and chloride concentrations in integrated precipitation samples from the Kawich Range sites are plotted in Fig. 10. The observed scatter reflects variations in wet- and dry-fall compositions between sampling events, variations in the relative contributions from wet-fall and dry-fall in any given sample, evaporation, and ana-

Table 7. Average Integrated Precipitation Composition at Kawich Range Sites*

Component	Concentration (mg/l)
SiO ₂	0.17
Calcium	0.96
Magnesium	0.11
Sodium	0.64
Potassium	0.24
Manganese	0.0084
Strontium	0.0058
Chloride	0.55
Fluoride	0.02
Sulfate	1.18
Nitrate	0.42
Alkalinity	2.7
pH	6.1

*from McKinley and Oliver (1994, 1995)

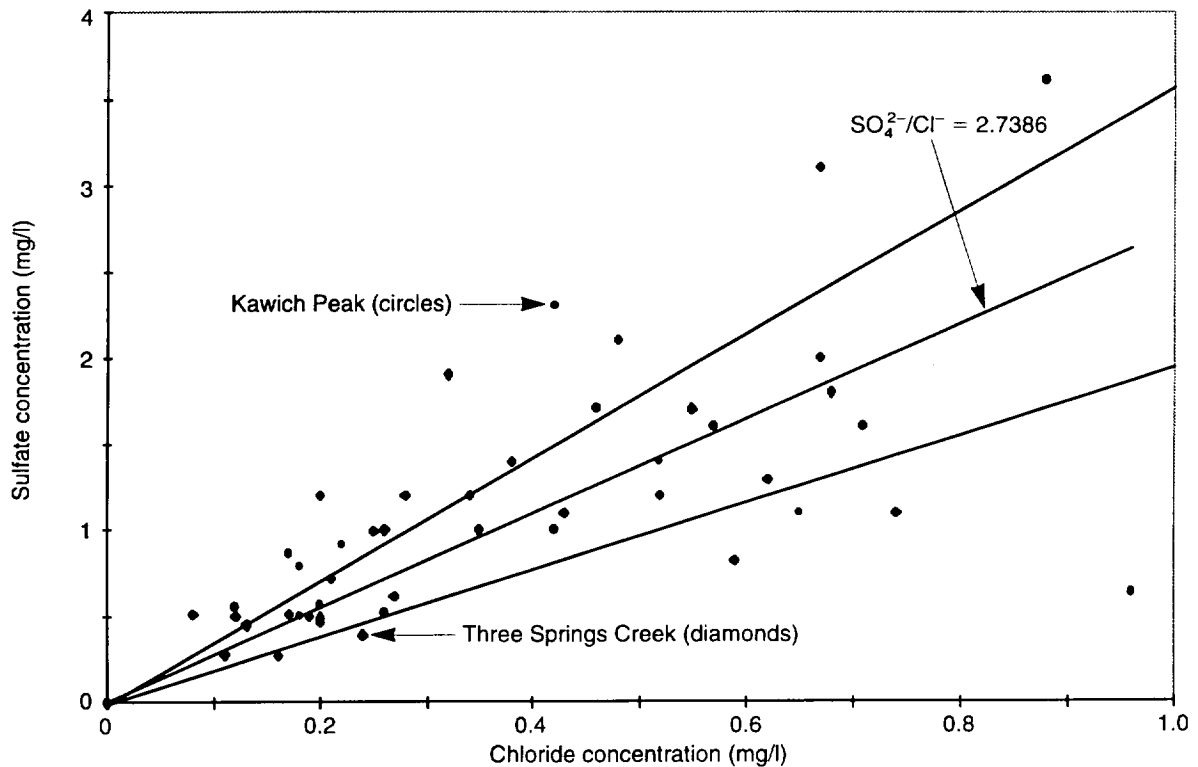


Figure 10. Sulfate versus Chloride in Precipitation. Concentrations of sulfate are plotted against concentrations of chloride for integrated precipitation samples from the Kawich Range sites (from McKinley and Oliver 1994, 1995). The slope of the inner line (a regression fit) gives the SO_4^{2-}/Cl^- ratio of the points plotted. The two outer lines represent a standard deviation of one sigma from the regression line.

lytical errors. Only samples with less than 1.0 mg/l were plotted. Samples with higher chloride concentrations showed significantly greater variability in chloride-to-sulfate ratios, suggestive of unusually high dust inputs. Many of the diagrams in this chapter will show a regression line representing a least-squares fit to the precipitation data and error lines reflecting the variability in the data.

Soil-zone Processes that Influence Water Compositions

In arid regions, such as southern Nevada, the average net infiltration rate is generally very low (Flint and Flint 1994). As a result, dust (dry-fall) and solids dissolved in precipitation (wet-fall) accumulate in the near-surface environment. Over time,

this accumulation process can result in the formation of pedogenic horizons enriched in clays, calcite, silica, gypsum, and, in some cases, highly soluble salts (Watson 1992). The formation of these accumulations or horizons can have major impacts on the chemistry of waters that percolate into the unsaturated zone in these environments.

Recharge water to the unsaturated zone within Yucca Mountain passes through the upper surfaces of the mountain, whereas waters in the saturated zone beneath the mountain appear to represent recharge that infiltrated through soils located at higher elevations within and north of the area of Pahute Mesa that are hydrologically upgradient of Yucca Mountain (Winograd and Thordarson 1975). The soils on Yucca Mountain and Pahute Mesa are

II. Groundwater Chemistry Model

not the same. Soils on Yucca Mountain locally contain abundant caliche and silica horizons (Taylor 1986) and support only limited vegetation. Pahute Mesa soils have little or no caliche and support a greater abundance and variety of vegetation (Spaulding 1985). Soil processes in both of these areas need to be considered in terms of potential impacts on groundwater chemistry. The two soil-zone processes that appear to have the greatest influence on the composition of infiltrating waters are evapotranspiration and dissolution/precipitation of solid phases in the soil.

Evapotranspiration

The term evapotranspiration refers to the loss of water from the soil zone as a result of simple evaporation and transpiration by plants (Freeze and Cherry 1980). Evapotranspiration causes the dissolved-solids content of soil waters to increase. A convenient measure of the amount of evapotranspiration and, by inference, the net infiltration rate associated with a given water sample is its chloride-ion concentration (Scalon 1991). Chloride salts of the major cations have high solubilities, and because Yucca Mountain bedrock is not a significant source of chloride to present-day groundwaters (Fabryka-Martin et al. 1996), the concentration of chloride in these waters can be used to estimate net infiltration rates. The following equation is used to derive this estimate.

$$R = \frac{[\text{Cl}^-]_{\text{precip}}}{[\text{Cl}^-]_{\text{water}}} P, \quad (2)$$

where R is the infiltration rate, $[\text{Cl}^-]_{\text{precip}}$ is the average chloride concentration in precipitation, $[\text{Cl}^-]_{\text{water}}$ is the chloride concentration in the water samples, and P is the rate of precipitation.

According to Hevesi et al. (1992), the average annual precipitation rate at Yucca Mountain is currently 170 mm/yr. If we assume an average chloride concentration in precipitation of 0.55 mg/l (Table 7), the concentration of chloride in water samples from Yucca Mountain can be used to calculate net infiltration rates.

The highest measured chloride concentration (245

mg/l) occurs in one of the shallowest and presumably youngest pore-water samples from the Yucca Mountain Member of Paintbrush Tuff (Fig. 11). The infiltration rate calculated for this sample is 0.4 mm/yr. Pore waters from other Paintbrush Tuff nonwelded units have significantly lower chloride concentrations (30–100 mg/l) and are associated with net infiltration rates of 0.9 to 3 mm/yr. The chloride concentrations in pore-water samples from the Topopah Spring nonwelded units are at the high end of the range observed in the nonwelded vitric units of Paintbrush Tuff. This suggests net infiltration rates were lower when the Topopah Spring pore waters were infiltrated compared to the waters in the overlying Paintbrush Tuff, excluding the Yucca Mountain Member. Presumably, this reflects a drier climate at the time the Topopah Spring pore waters were infiltrated.

The Calico Hills pore-water samples show a range in chloride concentrations from 15 to 82 mg/l. This range overlaps with the Paintbrush Tuff pore-water samples (excluding the Yucca Mountain Member sample) but is lower than the Topopah Spring pore waters. This result could reflect higher net infiltration rates for the Tuff of Calico Hills samples compared to the Topopah Spring samples, or it could simply reflect dilution as discussed further below. Water samples from Prow Pass Member are interesting in that *groundwaters* at the 528-m level have low chloride concentrations whereas *pore waters* from this level are at the high end of the distribution of chloride concentrations found in Tuff of Calico Hills pore waters. This observation indicates that equilibration of saturated-zone groundwaters with pore waters must be a very slow process.

Measured chloride concentrations in perched waters are similar to concentrations observed in saturated-zone groundwaters (Fig. 12). The calculated infiltration rates for these samples range from 2.5 mm/yr for UE-25 p#1 groundwater to 22.8 mm/yr for perched water from SD-7. Clearly, perched waters and saturated-zone groundwaters reflect much higher infiltration rates than do the

unsaturated-zone pore waters. Whether the higher infiltration rates for perched waters reflect a previous wet climate at Yucca Mountain or simply unusually wet years in the modern-day climate cannot be discerned from the water-composition data alone. However, the large difference (factor of 10) in chloride concentrations between pore waters and perched waters in samples from the same depth (for example, UZ-16 at 528 m) support a young age for the perched waters, as diffusion processes would tend to equalize these concentrations over time. It is interesting that similar differences in chloride concentrations between pore waters and fracture waters have been observed at Rainier Mesa (White et al. 1980).

It must be emphasized that the calculated infiltra-

tion rates cited in this section are only as good as the assumptions on which they are based. These assumptions include a constancy of the annual precipitation rate, a constancy of chloride concentrations in precipitation, the representativeness of the average chloride concentration in precipitation used in the calculations, and the lack of chloride leaching from rocks in contact with the water. The fact that the calculated infiltration rates are in the same range as those based on field measurements, as reported by Flint and Flint (1994), does lend support to this approach.

Dissolution/precipitation of solid phases in the soil zone

If concentration (that is, enrichment) of dissolved constituents by evapotranspiration were the only

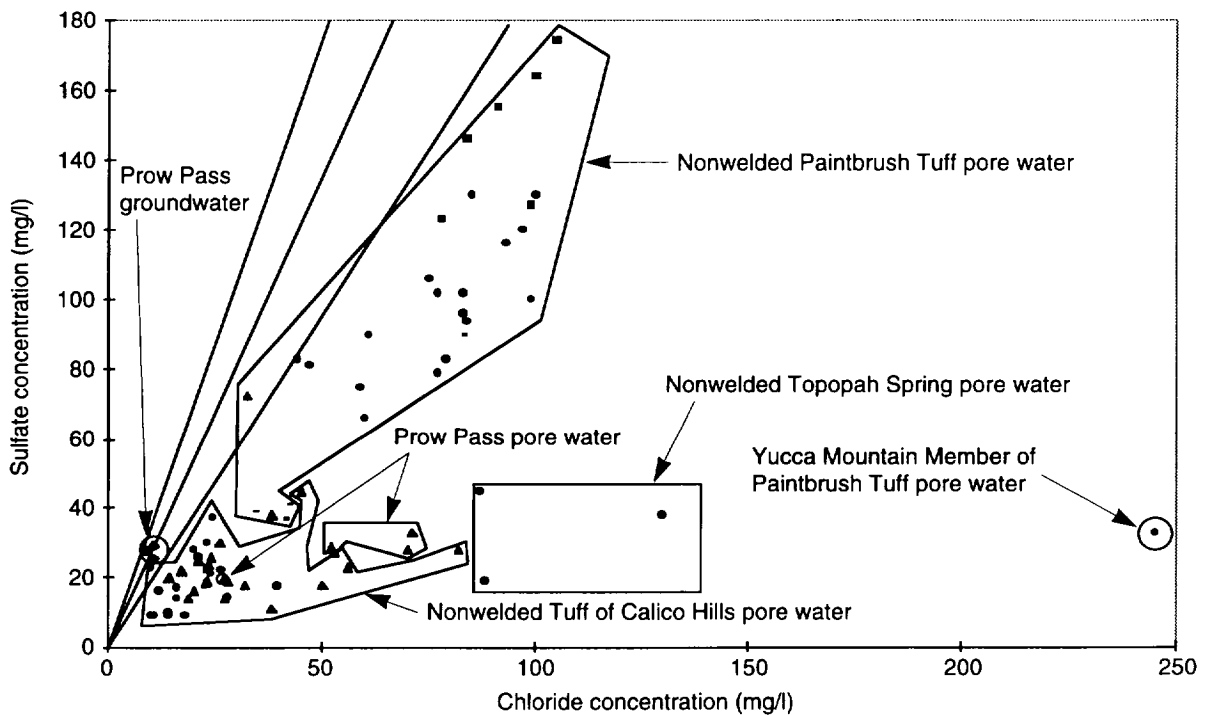


Figure 11. Sulfate versus Chloride in Pore Water. This plot shows sulfate versus chloride concentrations for unsaturated-zone pore-water samples and for three saturated-zone groundwater samples from Prow Pass (all data from Yang et al. 1988, 1996). The central line represents the best-fit line through composition data for precipitation at the Kawich Range sites (see Fig. 10), and the two outer lines reflect one-sigma variability in those precipitation compositions. (Drill-hole designations for the unsaturated-zone data points: circles: UZ-14; triangles: UZ-16; squares: UZ-4; and horizontal bars: UZ-5.)

II. Groundwater Chemistry Model

soil-zone process to impact the composition of infiltrating waters, the concentrations of other major constituents in these waters could be obtained from the net infiltration rate (that is, the chloride concentration) and the ratio of the concentration of the constituent of interest relative to the concentration of chloride in precipitation. However, the presence of soil horizons on Yucca Mountain that are enriched in calcite, silica, and other components (Taylor 1986) suggests the situation is more complicated. These soil horizons indicate that pedogenic processes involving precipitation and dissolution of these phases have occurred in the soils over time. An important question is: "To what extent did these precipitation/dissolution processes influence the unsaturated-zone water compositions analyzed by Yang et al. (1988, 1996), and to what extent are they likely to influence unsaturated-zone water compositions in the future?"

Because age dates obtained for the calcite-rich and silica-rich soil horizons tend to be much older (Paces et al. 1995) than those obtained for pore waters, perched waters, and groundwaters at Yucca Mountain (Yang et al. 1996; Waddell et al. 1984), the relationship between the compositions of these horizons and the compositions of various waters presently in Yucca Mountain is uncertain. To establish a connection, evidence for chemical reactions that are unique to the soil zone must be identified in the unsaturated-zone water compositions.

Sulfate and chloride ions are generally conservative constituents in dilute oxidizing waters such as the unsaturated-zone pore waters in Yucca Mountain. Therefore, we would expect a plot of sulfate and chloride concentrations to show sulfate to chloride ratios similar to those observed in precipitation. However, as shown in Fig. 11, unsatu-

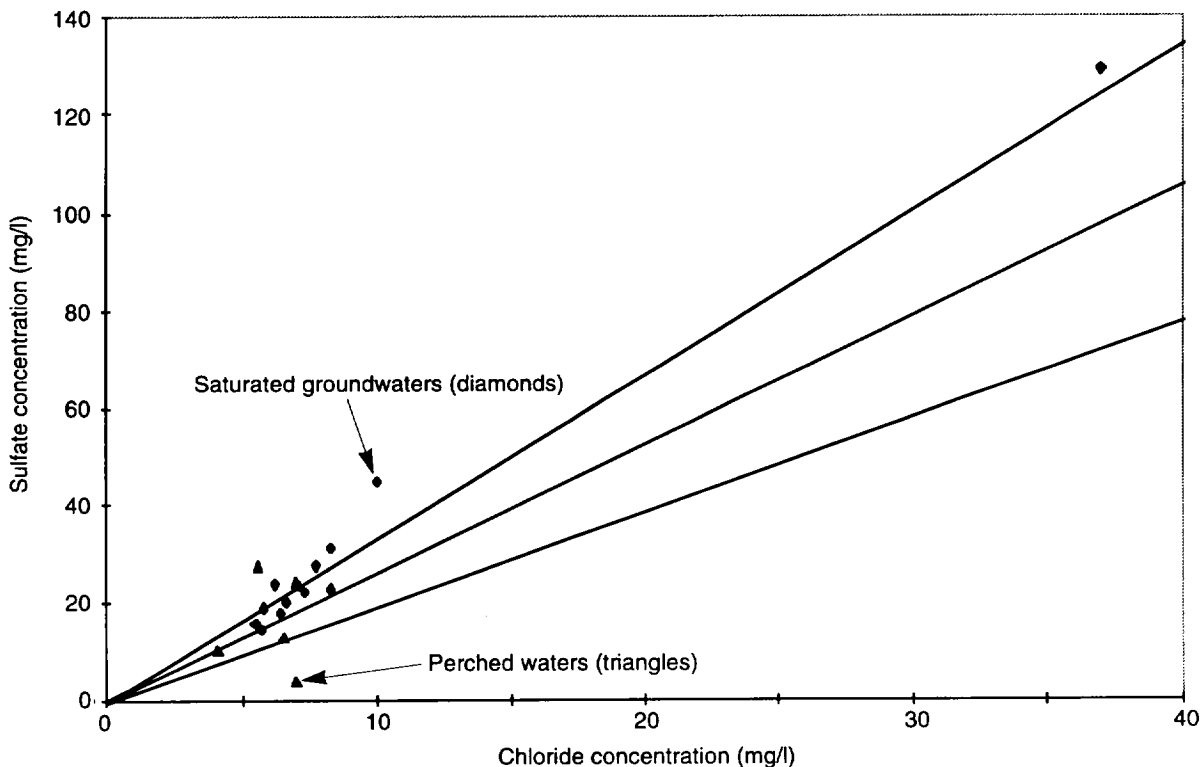


Figure 12. Sulfate versus Chloride in Perched Waters and Groundwaters. This plot shows sulfate versus chloride concentrations for perched waters and saturated-zone groundwaters. The lines are the same precipitation and variation lines as those plotted in Fig. 11.

rated-zone pore waters analyzed by Yang et al. (1988, 1996) show sulfate-to-chloride ratios consistently lower than the ratios observed in recent precipitation. Because all the unsaturated-zone pore-water analyses are grossly undersaturated with chloride phases and with gypsum and other possible sulfate phases involving the major cations, it is unlikely that solid chloride or sulfate phases are precipitated in the unsaturated zone.

Drever and Smith (1978) presented a model that offers one potential explanation for the low sulfate-to-chloride ratios in the unsaturated-zone pore waters. Their model involves drying and wetting cycles in the soil zone. During the drying phase, the concentrations of dissolved solutes are increased in the soil waters by evapotranspiration to the degree that phases such as calcite, gypsum, silica, and the more soluble salts precipitate. During "occasional heavy rains," the phases precipitated during the drying phase are partially redissolved. Because the dissolution rates for highly soluble salts, such as sodium chloride, are higher than the rates for less soluble salts, such as calcite, gypsum, and silica, a portion of the less soluble salts may remain undissolved after the "occasional heavy rains" infiltrate through the soil zone. In terms of sulfate and chloride concentrations, this process could lead to soil waters with lower sulfate-to-chloride ratios than those observed in precipitation. The actual concentrations of sulfate and chloride in these waters would depend on the details of the processes involved, including the dissolution kinetics of the sulfate and chloride phases, the residence time of the waters in the soil zone, and the original masses of sulfate and chloride in the soil zone.

Although differences in the dissolution kinetics of sulfate and chloride salts may be part of the explanation for the low sulfate-to-chloride ratios in pore waters from the unsaturated zone at Yucca Mountain, these differences are likely augmented, and perhaps even dominated, by crystallization-sequence effects. For example, it is possible that minerals, such as calcite and gypsum, that precipi-

tate from evaporating pore waters early in a crystallization sequence are partially or completely sequestered by minerals that precipitate later in the sequence (such as being coated by opal-A and halite). Alternatively, early-crystallized phases may completely fill smaller pores in the rocks and, therefore, be less accessible to infiltrating waters than minerals crystallized later in the sequence in larger pores (for example, Chadwick et al. 1987). During subsequent infiltration events, the latest-formed phases in pores accessible to infiltrating waters would preferentially dissolve, leading to soil solutions enriched in the more soluble salts relative to the less soluble salts.

When viewed from the perspective of this model, chloride and sulfate concentrations for the pore-water sample from the Yucca Mountain Member tuff (Fig. 11) suggest this sample reflects an infiltration event that followed an extended "dry" period of lower than average precipitation. In fact, the chloride concentration of this sample would represent approximately 450 liters of precipitation (rain and snow), assuming an average chloride concentration of 0.55 mg/l for precipitation (Table 7). During the "dry" period, the sulfate concentration in the soil water must have increased to the point where sulfate minerals such as gypsum crystallized from the soil solution. Chloride minerals may also have crystallized at this time. For some extended period, net infiltration into the soil zone was insufficient to wash these pedogenic minerals out of the zone. During this time, these minerals may have been repeatedly dissolved and recrystallized. Eventually, a large precipitation event caused sufficient water to infiltrate the soil zone so that water percolated out of that zone into the unsaturated zone, carrying most of the accumulated chloride and lesser amounts of the accumulated sulfate.

We can estimate the amounts of gypsum and calcite precipitated from the Yucca Mountain Member sample by 1) assuming that soil-zone waters originally had the composition of recent precipitation, 2) assuming that sufficient soil water evaporated so that the chloride concentration in the remaining liq-

II. Groundwater Chemistry Model

uid equals that measured in the Yucca Mountain Member sample, 3) calculating the amount of precipitated gypsum as the difference in the measured sulfate concentration and that inferred from the evaporated precipitation, 4) subtracting enough calcium from the evaporated precipitation to produce the gypsum, 5) assuming that enough calcite precipitated with the remaining calcium so that the concentration measured in the sample is the remainder, and 6) assuming that chloride minerals were totally dissolved by the large infiltration event. The resulting calculated amounts are approximately 700 mg of gypsum and 200 mg of calcite per liter of the Yucca Mountain Member sample.

Pore waters from Paintbrush Tuff, Topopah Spring, Prow Pass, and Tuff of Calico Hills have lower chloride concentrations and lower sulfate-to-chloride ratios than the Yucca Mountain Member sample. According to the model, these would reflect infiltration events that followed shorter "dry" periods. However, there is an additional complication in the sulfate and chloride data for these waters—there is a range of sulfate-to-chloride ratios at a given chloride concentration. If the precipitation of sulfate in the soil zone is the explanation for the deviation of these compositions from evapotranspired precipitation, it is disconcerting that this process appears to produce such a large range of sulfate-to-chloride ratios.

One possible explanation is that the range simply reflects the variability in the infiltration process. For example, if the pore sizes in the sulfate-mineral accumulation horizon are much smaller in one location than another, infiltrating waters may be denied access to a large fraction of the pores in the former case as a result of plugging by early-formed phases (Taylor 1986; Levy 1984). Alternatively, a mixing process could be involved. The rather narrow range of sulfate concentrations (10–40 mg/l) observed for the Calico Hills, Topopah Spring, and Prow Pass samples and the fact that this range includes most perched and saturated-zone samples is suggestive of such a process. The mixing could

involve perched or saturated-zone waters with low sulfate and chloride concentrations and pore waters with low sulfate and high chloride concentrations, such as the Yucca Mountain Member sample. Unfortunately, the lack of certainty in the explanation for the variations in sulfate-to-chloride ratios precludes the development of a quantitative model for this process. More information on the detailed hydrology of Yucca Mountain soils is required.

The conceptual model and the calculations described above imply that sulfate minerals will accumulate in the soil zone on Yucca Mountain. However, analyses of Yucca Mountain soils only occasionally show significant amounts of gypsum, although small amounts (1–2%) are routinely detected (Taylor 1986; Vaniman et al. 1995). The fact that gypsum is not more common in Yucca Mountain soils could be due to a variety of factors including 1) sulfate minerals were not accumulated in soil profiles prior to the last few thousand years as the climate became drier (Spaulding 1985), 2) sulfate minerals occur deeper in the soil profile than the depths covered by the analyses, 3) sulfate minerals were more abundant in soil profiles previously but were leached out during extended wet periods, or 4) some other process such as microbial reduction of sulfate is causing the decrease in sulfate concentrations.

The last factor is unlikely given the oxidizing nature of the unsaturated-zone pore waters. The third factor is a possibility but is difficult to evaluate with existing data. If this factor was responsible, unsaturated-zone waters would have had sulfate-to-chloride ratios in excess of precipitation for some period of time. There is no clear evidence for this process in analyses of the unsaturated zone (Fig. 11), although it is possible that waters of this type were present in the system but were flushed through to the saturated zone. Factor two is unlikely because significant amounts of gypsum were, in fact, found in some of the profiles described by Taylor (1986). The interpretation favored in this report is that sulfate minerals were more abundant in soil profiles in earlier times but

were subsequently leached out, and the amounts found in soils at the present time only reflect the most recent (“dry”) climatic regime.

Another important constituent in soil waters is silica. Silica is important because it is by far the most abundant constituent in the volcanic rocks of Yucca Mountain and its concentration in solution has a major impact on the ability of the solution to dissolve additional mineral components. Silica-rich horizons are often interbedded with calcite-rich horizons on Yucca Mountain (Taylor 1986). A model for the origin of silica-rich horizons in soils derived from volcanic rocks was developed by Chadwick et al. (1987). This model involves the reversible adsorption of silica onto surfaces of other soil constituents (for example, clays, sesquioxides, and weathered primary minerals) and the formation of opaline silica sols and coatings as soils dry out. Silica in these types of soils is apparently quite easily solubilized. Chadwick et al. (1987) found that up to 152 mg/l of monomeric silica could be extracted from the soils in 16 hours. These results are consistent with other reports (for example, Gifford and Frugoli 1964) and suggest that waters percolating from the soil zone into the unsaturated zone at Yucca Mountain will be close to saturation with amorphous silica.

The soil zone is also important to carbon-dioxide partial pressures in the unsaturated zone. The partial pressure of CO₂ in soil atmospheres is commonly elevated over the partial pressure of CO₂ in the earth’s atmosphere (Greenland and Hayes 1978). Measurements of the partial pressure of CO₂ at a depth of 10 feet in the unsaturated-zone drill hole UZ-1 in Yucca Mountain indicate that it is approximately four times the atmospheric value (Yang et al. 1996). This fact suggests that soil-zone processes at the surface of Yucca Mountain could influence the partial pressure of CO₂ in the unsaturated zone. However, the fact that CO₂ partial pressures are quite variable with depth in drill hole UZ-1 suggests there may be additional sources of CO₂ in the unsaturated zone. Interestingly, the isotopic composition of CO₂ in various

wells on Yucca Mountain suggests it has been strongly influenced by biologic activity (Thorstenson et al. 1989; Yang et al. 1996).

Pore-water Compositions above the Potential Repository Horizon

The types of chemical reactions that could affect unsaturated-zone water compositions include 1) dissolution/precipitation reactions, 2) ion-exchange reactions, and 3) gas-phase reactions (Meijer 1995). Because the absolute abundance of ion-exchanging minerals is generally low in units above the zeolitized Tuff of Calico Hills (Bish and Chipera 1989), dissolution/precipitation reactions and gas-phase reactions are likely dominant in this zone and will, therefore, be the focus of this section.

Sulfate-to-chloride ratios in waters from the unsaturated zone suggest there are at least two types of waters in the unsaturated zone above Tuff of Calico Hills (Figs. 11 and 12). These are relatively dilute perched waters and higher-ionic-strength pore waters. Because perched-water compositions are very similar to saturated-zone water compositions (Fig. 12), they will be discussed in the next section (“Perched-water compositions below the potential repository horizon”).

As discussed in Meijer (1995), dissolution reactions in devitrified and vitric silicic tuffs will involve the hydrolysis of feldspar and glass, respectively. These hydrolysis reactions generally leach sodium (± calcium, magnesium, and potassium) in exchange for hydrogen ions (White et al. 1980). Therefore, relative to a conservative solute such as chloride, sodium concentrations should increase in the pore waters relative to the original precipitation compositions if hydrolysis reactions are of importance. As shown in Fig. 13, this is contrary to what is observed. In the pore waters from units above Calico Hills (that is, Yucca Mountain Member, nonwelded Paintbrush Tuff, and nonwelded Topopah Spring), sodium-to-chloride ratios are generally lower than those observed in modern-day precipitation. This

II. Groundwater Chemistry Model

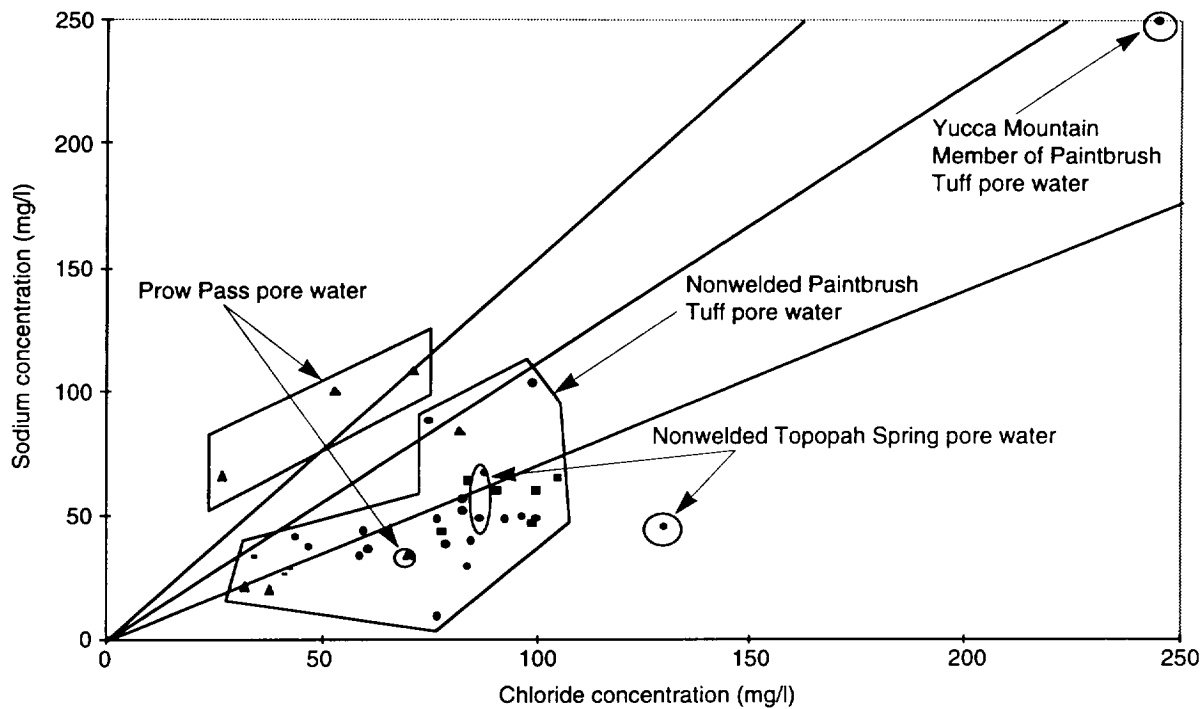


Figure 13. Sodium versus Chloride. This plot shows the sodium (rather than sulfate) concentration versus the chloride concentration of unsaturated-zone pore-water samples from Yucca Mountain. Here, the central line represents a regression fit of sodium-versus-chloride precipitation data, and the outer lines represent one standard deviation for the scatter of those data. (Drill-hole designations for data points: circles: UZ-14; triangles: UZ-16; squares: UZ-4; and horizontal bars: UZ-5.)

observation implies that hydrolysis reactions have not significantly impacted the chemistry of these waters.

Why sodium-to-chloride ratios in these pore waters are lower than those observed in recent precipitation is not entirely clear. Potential explanations include the possibility that nonchloride sodium salts (for example, sodium sulfate) crystallized in the soil zone prior to chloride-salt crystallization and were sequestered, that precipitation (wet-fall plus dry-fall) had lower sodium-to-chloride ratios in the past, or that ion-exchange reactions (for example, with clays) removed sodium ions from solution. The latter explanation appears unlikely given that clay analyses from units at this level are enriched in calcium and magnesium, not sodium (Levy 1984). Resolution of this question will

require additional investigations of the soil-zone processes at Yucca Mountain.

The lack of evidence in the sodium-versus-chloride concentration data for hydrolysis reactions in units above Calico Hills is not unexpected and is, in fact, corroborated by other observations. These observations include the persistence of abundant 10-to-12-million-year-old volcanic glass in the unsaturated zone within Yucca Mountain and the fact that, with some exceptions, only limited amounts of secondary minerals are found in the glassy and devitrified tuffs (Bish and Chipera 1989). The exceptions are the localized clay-rich horizons in parts of the nonwelded Paintbrush Tuff. The origin of these horizons is uncertain at the present time. They may reflect alteration of glass in high-flow (water) zones (Levy 1984), or they may have

formed during weathering reactions that occurred while the tuffs were exposed at the surface.

The lack of evidence for hydrolysis reactions in the sodium-versus-chloride concentration data for pore waters in units above Calico Hills likely reflects the fact that concentration of cations (for example, sodium) by evapotranspiration combined with the saturation of infiltrating waters with amorphous silica in the soil zone has lowered the reactivity of these waters with respect to dissolution of the aluminosilicate solids (such as feldspar and glass). For feldspars, this can be quantified by calculating the saturation state of the pore waters with respect to feldspar minerals. Aluminum and potassium concentrations were not reported for pore waters by Yang et al. (1988, 1996), precluding direct calculation of feldspar saturation states. However, the high sodium and silica concentrations in the pore waters ensure that they will be saturated with albite when in contact with a solid source of aluminum (such as feldspar or glass). This effect implies that the feldspars in the devitrified tuffs will not be significantly altered by the waters percolating out of the soil zone. The observed lack of secondary minerals in the devitrified zones (Bish and Chipera 1989) corroborates this conclusion.

In the case of volcanic glass, the situation is less straightforward because glass is thermodynamically unstable with respect to secondary minerals at ambient temperatures and pressures. In fact, many studies have been carried out in recent years to gain an understanding of glass alteration behavior, mainly to provide a basis for predictions of the alteration behavior of nuclear waste glasses. An important result of these studies is that the glass dissolution rate has been shown to be quite sensitive to the silica concentration in solution. As this concentration reaches saturation with amorphous silica, the dissolution reaction slows down dramatically (Grambow 1992). Apparently, for glass alteration to proceed, the "gel reaction zone" that forms on the glass surface needs to dissolve. If the solution phase is saturated with amorphous silica, the dissolution of this material is inhibited because the

affinity of the dissolution reaction is low.

Conceivably, other silica polymorphs with lower solubilities (for example, opal C-T, cristobalite, and quartz) could nucleate and crystallize, thereby causing the silica concentration in solution to be maintained at a lower level. This effect, in turn, could enhance the glass dissolution rate. However, the nucleation rates of these other polymorphs appear to be inhibited for some reason that remains to be determined.

The concentrations of silica in unsaturated-zone pore waters are generally high (Fig. 14). Although essentially all of the pore-water samples analyzed by Yang et al. (1988, 1996) are saturated with α -cristobalite, many are saturated with opal-CT and some are even saturated with opal-A at 25°C (Fig. 14). The concentrations tend to be higher in pore-water samples from Paintbrush Tuff and Tuffs of Calico Hills compared to samples from Topopah Spring and Prow Pass. Temperature does not appear to be a controlling parameter. Also, there do not appear to be consistent trends in silica concentration with depth in a given unit. The high silica concentrations in the Paintbrush Tuff pore waters presumably reflect the presence of abundant glass in this unit. The slightly lower silica concentrations in Tuff of Calico Hills pore waters may reflect the fact that the mineralogy of the host rock consists of zeolites and opal-CT (Bish et al. 1996b). The mineralogy of the Topopah Spring and Prow Pass tuff samples in drill holes UZ-14 and UZ-16 was not available at the time this report was being written.

Part of the scatter in the silica data plotted in Fig. 14 may reflect analytical techniques. The pore-water samples were not filtered prior to analysis, and the analyses were carried out by inductively coupled plasma-emission spectroscopy, which does not discriminate monomeric silica from other forms of silica in solution. This is likely the explanation for the high silica concentrations (> 80 mg/l) measured in some of the Calico Hills pore-water samples. The analyses of these samples also showed some relatively high alumina concentra-

II. Groundwater Chemistry Model

tions, which are an indication of the presence of particulate matter (for example, colloids), as aluminum is very insoluble in near-neutral solutions. At this point, it is difficult to quantify the controls on pore-water silica concentrations at ambient temperatures other than to say that as long as volcanic glass remains in the unsaturated zone, these concentrations will be in a range between saturation with α -cristobalite and saturation with opal-A.

The concentration of bicarbonate in Yucca Mountain waters is an important parameter with respect to the solubility and sorption of many of the radionuclides in high-level radioactive waste (GCX 1994). The data presented by Yang et al. (1996) show that pore waters in the units above Tuff of Calico Hills tend to have bicarbonate-to-chloride ratios that are equal to or below the aver-

age observed in recent precipitation (Fig. 15). This trend likely reflects the crystallization of calcite in the soil zone prior to percolation of the waters into the unsaturated zone. If hydrolysis reactions were important in the evolution of these waters, bicarbonate-to-chloride ratios would exceed those observed in precipitation. This result is, in fact, observed in the analyses of perched waters, saturated-zone groundwaters, and pore waters from Tuff of Calico Hills, as discussed in more detail in the next section on perched-water compositions.

Calcite dissolution and precipitation is also likely to exert a major influence on the calcium concentration in pore waters in units above the zeolitized tuff in Calico Hills. Unfortunately, quantitative modeling of calcite dissolution/precipitation behavior in the unsaturated zone at Yucca Moun-

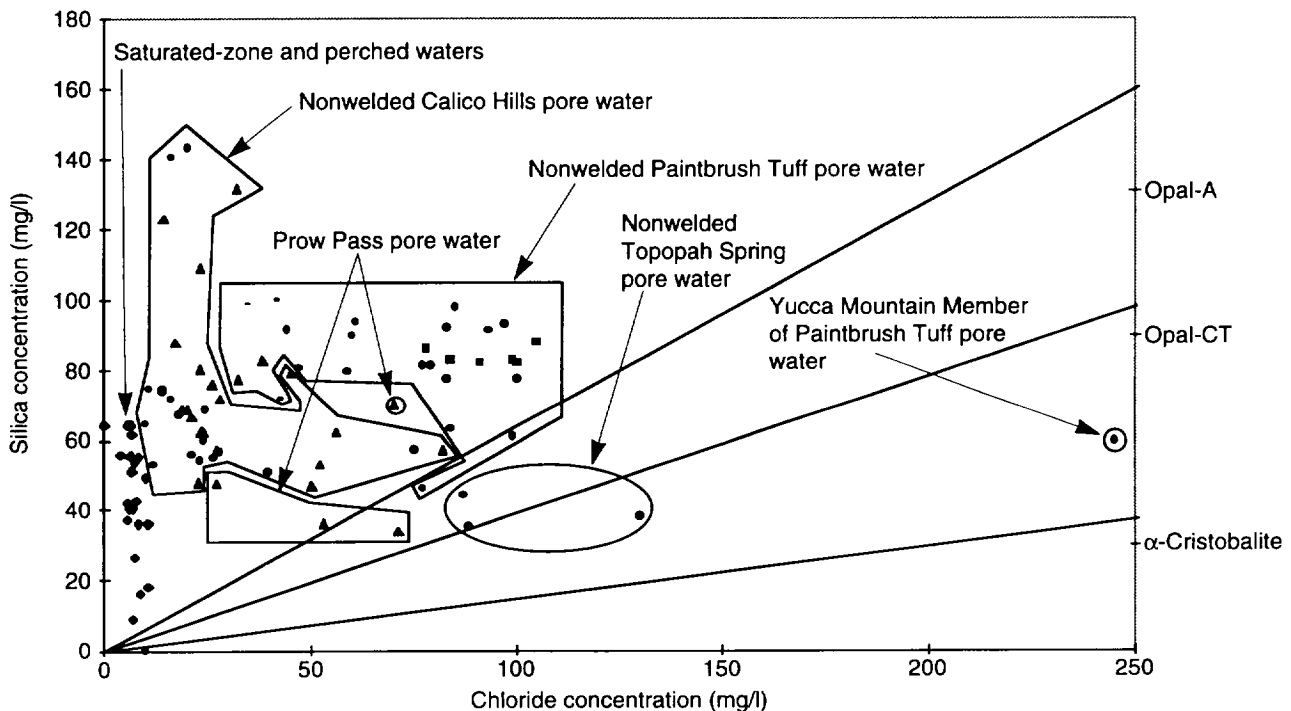


Figure 14. Silica versus Chloride. This plot shows silica versus chloride concentrations in pore waters, perched waters, and saturated-zone groundwaters (perched and saturated-zone data are not differentiated). The silica concentrations at which the waters would be saturated with opal-A, opal-CT and α -cristobalite at 25°C are given on the right. The straight lines are the regression fit to silica-versus-chloride concentrations in precipitation and the one-sigma deviations. (Drill-hole designations: circles: UZ-14; triangles: UZ-16; squares: UZ-4; horizontal bars: UZ-5; and diamonds: perched and saturated-zone waters.)

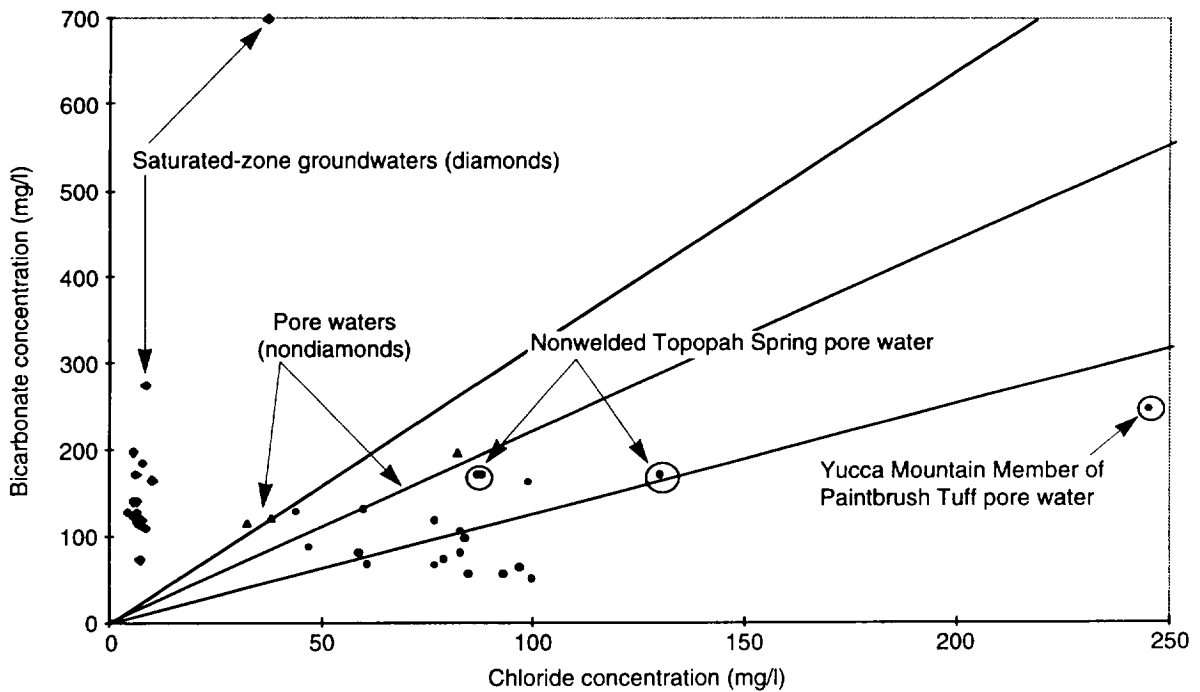


Figure 15. Bicarbonate versus Chloride. This plot shows bicarbonate versus chloride concentrations in pore waters from units above Tuff of Calico Hills and in saturated-zone groundwaters. The central line shows bicarbonate versus chloride concentrations in precipitation; the outer lines are the one-sigma deviations. (Drill-hole designations: circles: UZ-14; triangles: UZ-16; diamonds: saturated-zone waters.)

tain is complicated by the fact that the partial pressure of carbon dioxide in the gas phase present in the unsaturated zone appears to be quite variable (Yang et al. 1996). Detailed gas-composition data have been collected from borehole UZ-1 for over ten years. These data show that, for some as yet undetermined reason, that the partial pressure of carbon dioxide in the unsaturated zone exceeds the atmospheric value (0.00032 atmospheres) at nearly all depths sampled. The pressure is approximately 0.01 atmospheres in the alluvium and decreases to approximately 0.0003 atmospheres in the middle tuff of Topopah Spring. Below this depth, it increases to values in excess of 0.003 atmospheres in the lower portion of Topopah Spring where the borehole bottoms out. Data for the partial pressure of carbon dioxide in the gas phase in units below the lower tuff of Topopah Spring are not available.

By combining pore-water compositions from borehole UZ-14 with carbon-dioxide partial pressures reported for borehole UZ-1 (Yang et al. 1996), located in close proximity to UZ-14, the saturation state of calcite in the pore waters can be calculated (Table 8). The values of the calcite saturation index presented in that table reflect the degree to which the water is saturated with calcite. Positive numbers reflect oversaturation and negative numbers reflect undersaturation. It is of interest that only the sample from the Yucca Mountain Member (UZ14-45, which is from borehole UZ-14 at 45 feet) shows a positive value. The sample at 135 feet is close to saturation, whereas the other samples are undersaturated and, therefore, could dissolve calcite if it were present. Because data on the partial pressure of carbon dioxide are not available for pore-water samples from other boreholes, calcite saturation cannot be realistically evaluated for these.

Table 8. Calculated Calcite Saturation Indices

Sample ID	Saturation Index*
UZ14-45	0.0153
UZ14-85	-0.1835
UZ14-91	-0.2485
UZ14-95	-0.5756
UZ14-96	-0.5503
UZ14-100	-0.6820
UZ14-114	-0.7885
UZ14-135	-0.0158
UZ14-144	-0.2219
UZ14-147	-0.6269
UZ14-177	-0.8767
UZ14-178	-0.1829
UZ14-215	-0.8890
UZ14-225	-0.7191
UZ14-235	-0.4746
UZ14-240	-0.4952
UZ14-245	-0.7692
UZ14-1258	-0.0389

* $\log(IAP/K_T)$, where $IAP = [Ca^{2+}][CO_3^{2-}]$ is the measured ion association product for the water and K_T is the equilibrium product for the solubility of calcite at the temperature of interest.

The fact that most of the UZ-14 pore-water samples are undersaturated with calcite is not surprising given the spotty distribution of calcite in Yucca Mountain (Vaniman and Chipera 1996). Calcite is more likely to be precipitated in fractures for which the partial pressure of carbon dioxide is lower as a result of more direct access to the atmosphere. Because the total amount of calcite in fractures is small relative to the total mass of solute in pore waters, precipitation/dissolution reactions involving fracture calcite are unlikely to control pore-water calcium concentrations.

The elevated partial pressure of carbon dioxide will tend to keep the pH in the pore waters in the range from 7 to 8. If carbon-dioxide partial pressures in the unsaturated-zone gas phase decrease with time due to venting associated with operations at the potential repository, the pH of pore waters could

increase to values above 8, depending on the extent of degassing. Because the total volume of the excavations are small relative to the total volume of the rock mass surrounding the potential repository, it is unlikely this effect will be very significant overall.

The concentrations of the major cations in pore waters are of interest with respect to the solubility and sorption behavior of the radionuclides in high-level radioactive waste. As noted above, the generally low abundances of ion-exchanging minerals in the units above the zeolitized Tuff of Calico Hills suggest that cation proportions in pore waters from this portion of Yucca Mountain will reflect primarily soil-zone precipitation/dissolution processes. As shown in Fig. 16, the calcium-to-chloride ratios in pore waters from units above Tuff of Calico Hills are either on the precipitation line or below it. Sodium-to-chloride ratios in these samples also plot below the precipitation line (Fig. 13). If ion-exchange reactions were controlling the relative concentrations of calcium and sodium, there would be an antithetic relationship in their concentrations. This relationship is not evident in the data, which suggests that ion-exchange reactions are of secondary importance relative to other reactions that involve these elements, such as the precipitation of calcite, gypsum, and other salts in the soil zone.

The oxidation-reduction potential (Eh) of waters in the unsaturated zone should reflect the fact that the gas phase in the unsaturated zone has an oxygen partial pressure equal to that in the atmosphere (Thorstenson et al. 1989; Yang et al. 1996). This condition will cause the Eh to be in the range from 400 to 600 mV.

The pH of pore waters in the unsaturated zone will reflect the partial pressure of carbon dioxide in the gas phase. Because this partial pressure is variable with depth (Yang et al. 1996) and above atmospheric levels, the pH of the pore waters will vary in a range from approximately 7 to 8.

Bounds on future variations in the composition of

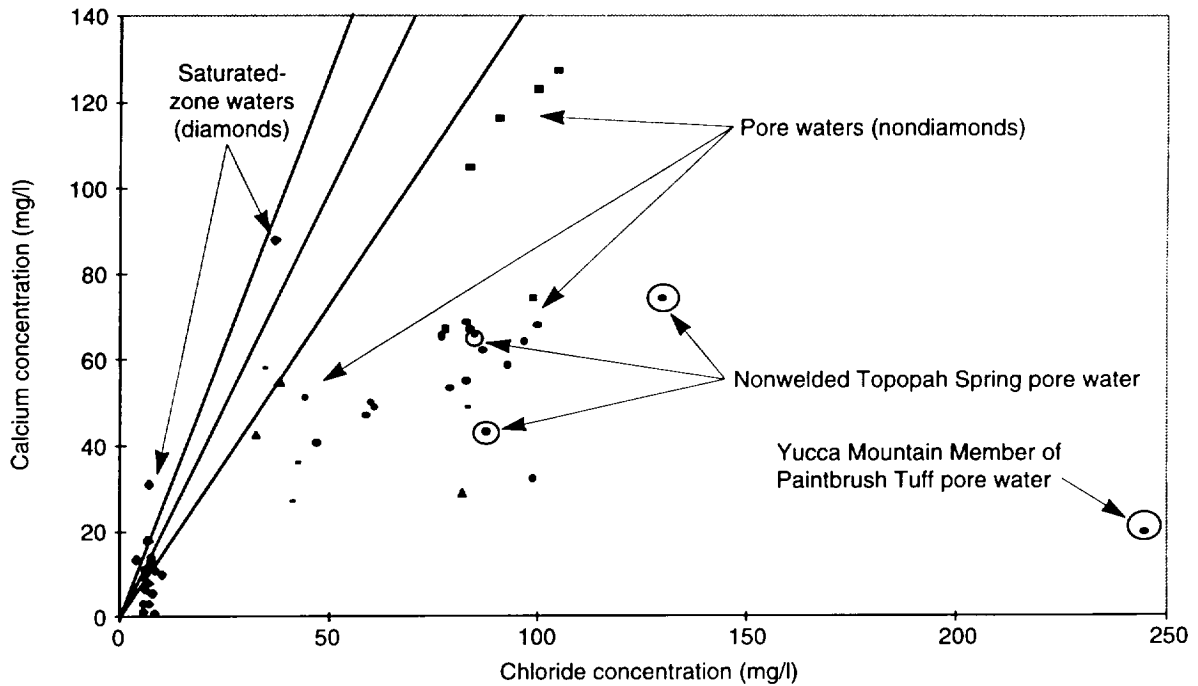


Figure 16. Calcium versus Chloride. This plot shows calcium versus chloride concentrations of unsaturated-zone pore waters from units above Tuff of Calico Hills and of saturated-zone groundwaters. The straight lines are the regression fit of precipitation data for calcium versus chloride and the one-sigma deviations from that fit. (Drill-hole designations: circles: UZ-14; triangles: UZ-16; squares: UZ-4; horizontal bars: UZ-5; diamonds: saturated-zone waters.)

pore waters in units above and within the repository horizon are difficult to determine solely on the basis of chemical arguments. The main controls on these compositions are the amount of evapotranspiration that occurs in the soil zone and precipitation reactions in the soil zone. High amounts of evapotranspiration will lead to pore waters with high ionic strength. Such waters will tend to precipitate calcite, gypsum, silica, and possible other soluble salts. Fortunately, the higher the evapotranspiration, the less infiltration there will be. In other words, high-ionic-strength pore waters will be of limited volume and may not percolate to the level of the potential repository over its useful lifetime. Because the detailed soil hydrology can have a significant impact on the chemical evolution of soil waters, a coupled flow-chemistry model is required to properly model the evolution of these waters.

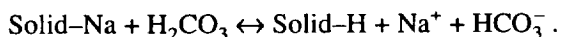
Perched-water Compositions below the Potential Repository Horizon

Sulfate-to-chloride ratios in perched and saturated-zone waters show little evidence of soil-zone precipitation reactions involving gypsum and other soluble sulfate salts. In fact, they show sulfate-to-chloride ratios that are somewhat higher than those observed in precipitation (Fig. 12). This result may reflect somewhat higher sulfate-to-chloride ratios in the precipitation when these waters were infiltrated, or the waters may be dissolving small amounts of sulfate as they infiltrate through the soil zone and the unsaturated zone.

An important characteristic of perched waters, saturated-zone groundwaters, and many of the pore waters in Tuff of Calico Hills is that these waters all have elevated bicarbonate-to-chloride and sodi-

II. Groundwater Chemistry Model

um-to-chloride ratios relative to the ratios observed in recent precipitation (Figs. 17 and 18). This observation suggests that these waters have been subject to hydrolysis reactions (White et al. 1980). In these reactions, hydrogen ions resulting from the dissociation of carbonic acid exchange with cations in the solid phase. An example of such a reaction involving sodium is



Elevated bicarbonate-to-chloride ratios provide the most definitive evidence of hydrolysis reactions because elevated sodium-to-chloride ratios could also reflect ion-exchange processes.

The fact that pore waters in the Topopah Spring Member overlying Tuff of Calico Hills do not show evidence of significant hydrolysis reactions suggests that either hydrolysis reactions are currently operative in Tuff of Calico Hills or that the Calico Hills pore waters contain water from another source. Pore waters from Prow Pass Member, which underlies Tuff of Calico Hills, have bicarbonate-to-chloride ratios similar to those observed in tuff from Topopah Spring Member. Therefore, the high bicarbonate-to-chloride ratios in pore waters from Calico Hills are sandwiched between units with low bicarbonate-to-chloride pore waters. Interestingly, *groundwater* pumped from Prow Pass Member in borehole UZ-16 has bicarbonate-to-chloride ratios that are much higher than those observed in recent precipitation and that are similar to those observed in the pore waters of Calico Hills. This fact suggests that the higher bicarbonate-to-chloride ratios in the pore waters of Calico Hills are not simply the result of in-situ hydrolysis reactions. If they were, similar bicarbonate-to-chloride ratios would be observed in Prow Pass pore waters. The important point is that pore waters in Tuff of Calico Hills and groundwaters from below the water table have compositions that are distinct from the compositions of pore waters in the units above and below Tuff of Calico Hills.

The relative importance of hydrolysis and ion-

exchange reactions in these waters can be approximated as follows. Assume that the "excess" bicarbonate (the amount in excess of that indicated by the precipitation ratio at the given chloride concentration) in these waters reflects only hydrolysis reactions and also that the amount of sodium released to solution during the reaction is approximately 0.6 equivalents of sodium per equivalent of bicarbonate (White et al. 1980). The amount of sodium in the water analysis in excess of that originally in the water (from the sodium-to-chloride ratio in precipitation) plus the sodium released through hydrolysis reactions is assumed to be the amount contributed to the solution by ion-exchange reactions. This calculation suggests that up to 95% of the "excess" sodium in solution (relative to precipitation) appears to be contributed by hydrolysis reactions. The relatively small proportions that appear to be contributed by ion-exchange reactions in pore waters from Tuff of Calico Hills are more or less consistent with the amounts of calcium and magnesium lost from these waters (relative to precipitation) (Figs. 19 and 20).

The Calico Hills pore waters are interesting in that in addition to showing evidence of hydrolysis reactions in their bicarbonate-to-chloride and sodium-to-chloride ratios (Figs. 17 and 18), they also show evidence of soil-zone processes in their sulfate-to-chloride ratios (Fig. 11). That is, these latter ratios are well below those observed in recent precipitation. As discussed above, the sulfate-to-chloride ratios in these pore waters could reflect mixing of perched or saturated-zone waters with pore waters percolating into Tuff of Calico Hills from Topopah Spring Member. If this is true, the high bicarbonate-to-chloride ratios in these pore waters would also be a result of the mixing of these waters. The proportions of perched/saturated-zone water and Topopah Spring pore water in the hypothetical mixtures can be estimated on the basis of chloride concentration of the Topopah Spring samples and the perched/saturated-zone samples at a given bicarbonate concentration. These estimates fall in the range of from 60 to 90% perched/saturated-zone water and from 10 to 40% pore water.

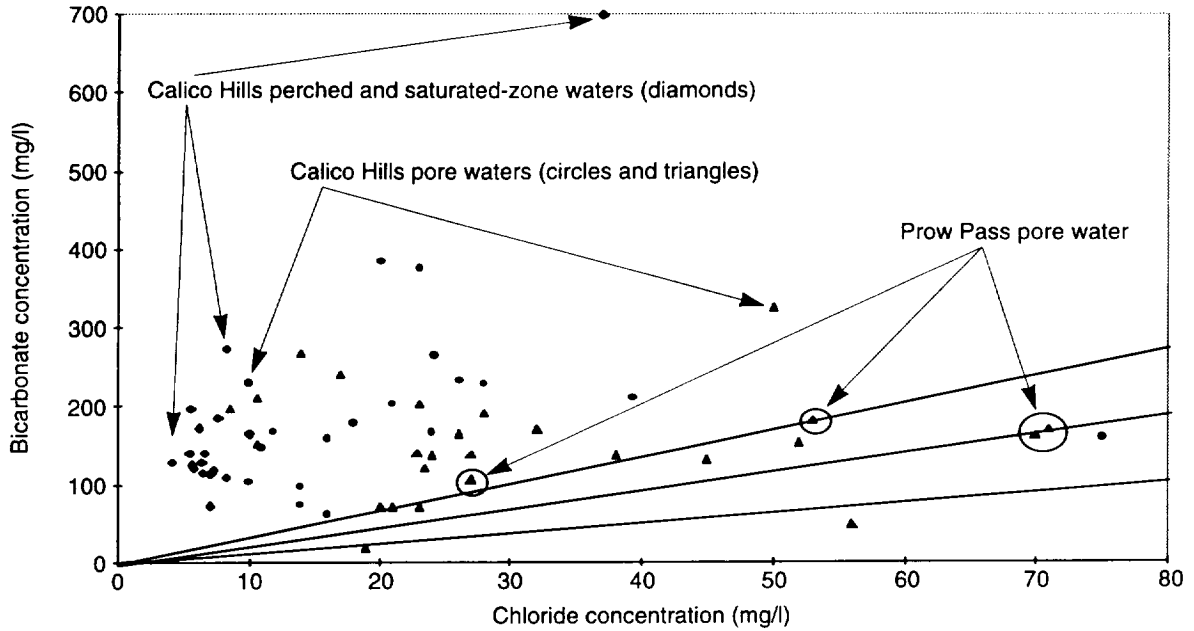


Figure 17. Calico Hills Bicarbonate. This plot shows bicarbonate versus chloride concentrations in Calico Hills pore waters, perched waters, and saturated-zone groundwaters. The straight lines are the regression fit of precipitation data for bicarbonate versus chloride and the one-sigma deviations from that fit. (Drill-hole designations: circles: UZ-14; triangles: UZ-16; diamonds: saturated-zone waters.)

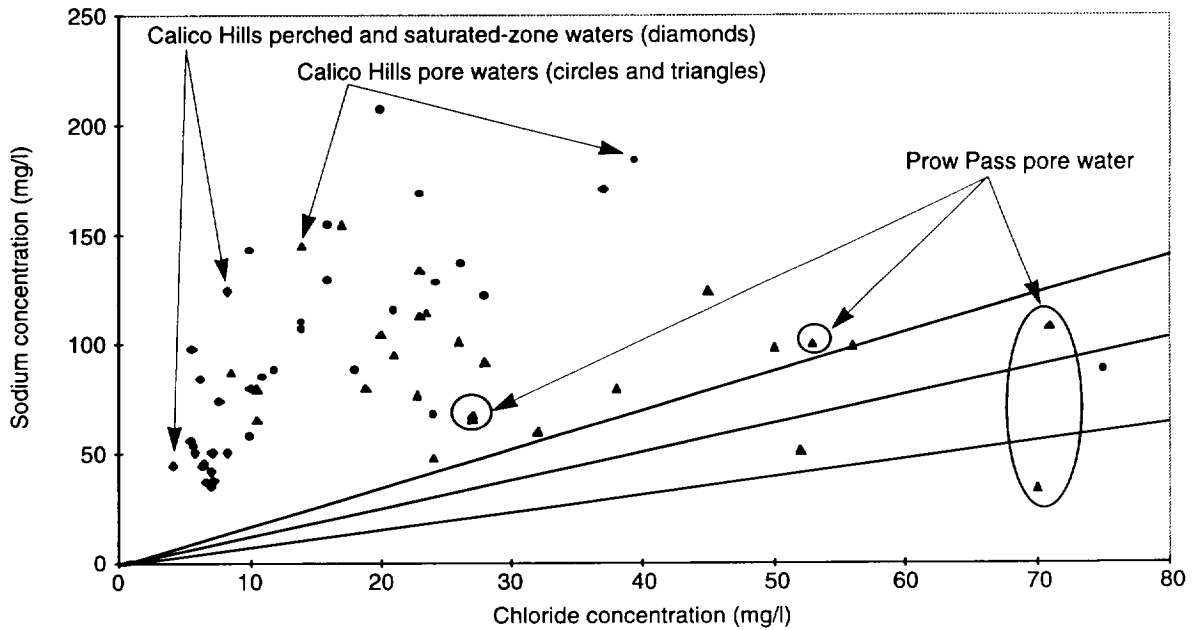


Figure 18. Calico Hills Sodium. This plot shows sodium versus chloride concentrations in Tuff of Calico Hills pore waters, perched waters, and saturated-zone groundwaters. The straight lines are the regression fit and one-sigma deviations for sodium-versus-chloride precipitation data. (Drill-hole designations: circles: UZ-14; triangles: UZ-16; diamonds: saturated-zone waters.)

II. Groundwater Chemistry Model

Whether or not these estimates are representative of waters in Tuff of Calico Hills in other parts of Yucca Mountain cannot be established without additional sampling and detailed flow modeling. The fact that Calico Hills pore waters from depths as much as 100 m above the water table show evidence of hydrolysis reactions does suggest that perched waters are likely the dilute component.

Establishing bounds on the present and future compositions of perched waters and saturated-zone waters requires bounding the impact of the ion-exchange and hydrolysis reactions. Because zeolites in Yucca Mountain have relatively large selectivity coefficients for calcium and magnesium (Pabalan 1994; Viani and Bruto 1992), waters that percolate thru the zeolitized Tuff of Calico Hills will lose nearly all their calcium and magnesium before they reach the water table. This loss is evi-

dent in pore-water samples obtained from the lower part of Tuff of Calico Hills in drill holes UZ-14 and UZ-16 (Figs. 19 and 20).

As noted above, hydrolysis reactions that involve feldspar are limited by reaction affinity. That is, as the solution reaches saturation with a particular feldspar, the affinity for further reaction is progressively reduced until the solution is saturated with the feldspar, at which point the affinity for dissolution is zero. Therefore, the composition of waters in the devitrified units (such as the potential repository horizon) will be primarily constrained by saturation with feldspar and α -cristobalite. Pore waters percolating into the devitrified zones from non-welded units will already be supersaturated with feldspar and α -cristobalite as a result of glass dissolution reactions. Therefore, little additional dissolution is anticipated in the devitrified zones over-

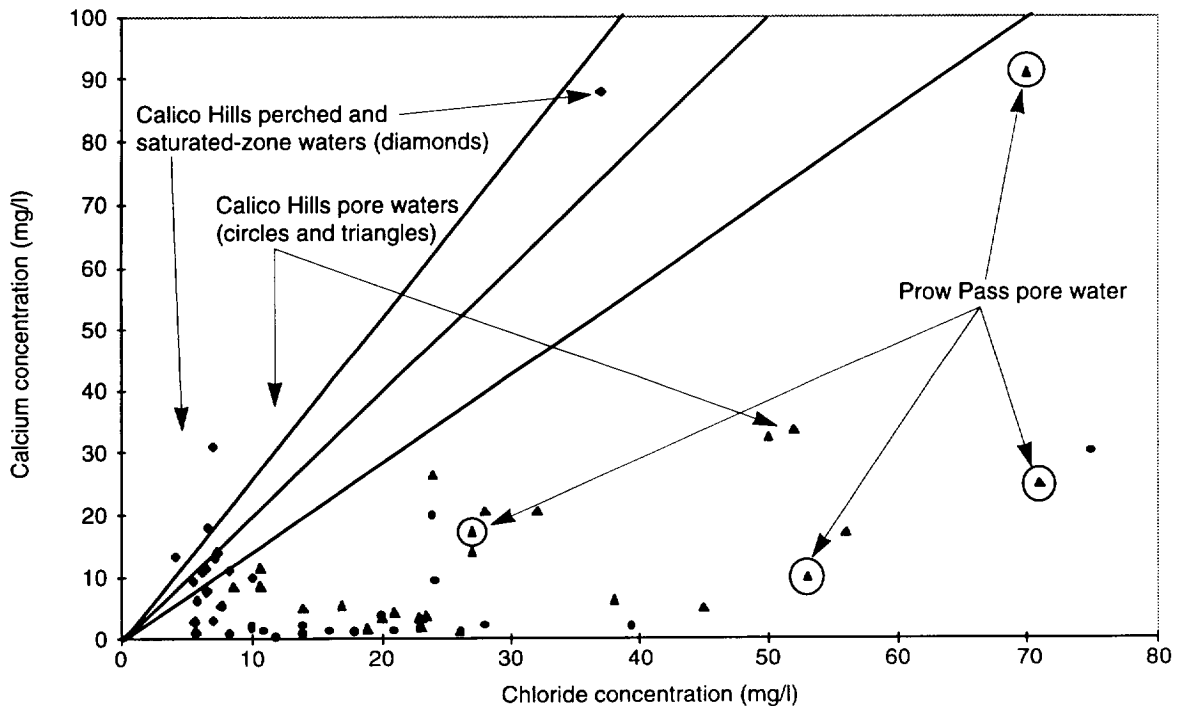


Figure 19. Calico Hills Calcium. The plot shows calcium versus chloride concentrations in Calico Hills pore waters, perched waters, and saturated-zone groundwaters. The straight lines are the regression fit and one-sigma deviations for calcium-versus-chloride precipitation data. (Drill-hole designations: circles: UZ-14; triangles: UZ-16; diamonds: saturated-zone waters.)

lain by nonwelded tuffs. In fact, soluble silica in pore waters from the nonwelded units may be crystallized onto existing α -cristobalite grains in the upper portion of the devitrified units, leading to reductions in porosity.

For vitric units, the situation is less straightforward because volcanic glasses cannot achieve thermodynamic equilibrium with an aqueous solution at ambient temperatures and pressures. That is, all volcanic glass would crystallize if it were not for the slow kinetics of nucleation and crystallization of the secondary phases that can form at ambient temperatures and pressures. Although the recrystallization of volcanic glass may be kinetically inhibited, glasses do dissolve at appreciable rates at ambient temperature and pressure when the dissolving waters are far from equilibrium with potential secondary phases. Many studies have been

carried out in recent years to gain an understanding of glass-alteration behavior, mainly to provide a basis for predictions of the alteration behavior of nuclear waste glasses. An important result of these short-term experimental studies is the finding that the glass dissolution rate is quite sensitive to the silica concentration in solution. As the silica concentration in solution approaches saturation with amorphous silica, the dissolution reaction slows down dramatically (Grambow 1992). Apparently, in order for glass alteration to proceed, the "gel reaction zone" that forms on the glass surface needs to dissolve. If the solution phase is near saturation with amorphous silica, the dissolution of this material is inhibited, presumably because the affinity of the dissolution reaction is low.

High silica activities in solution cannot be maintained very long (days to months) in the presence

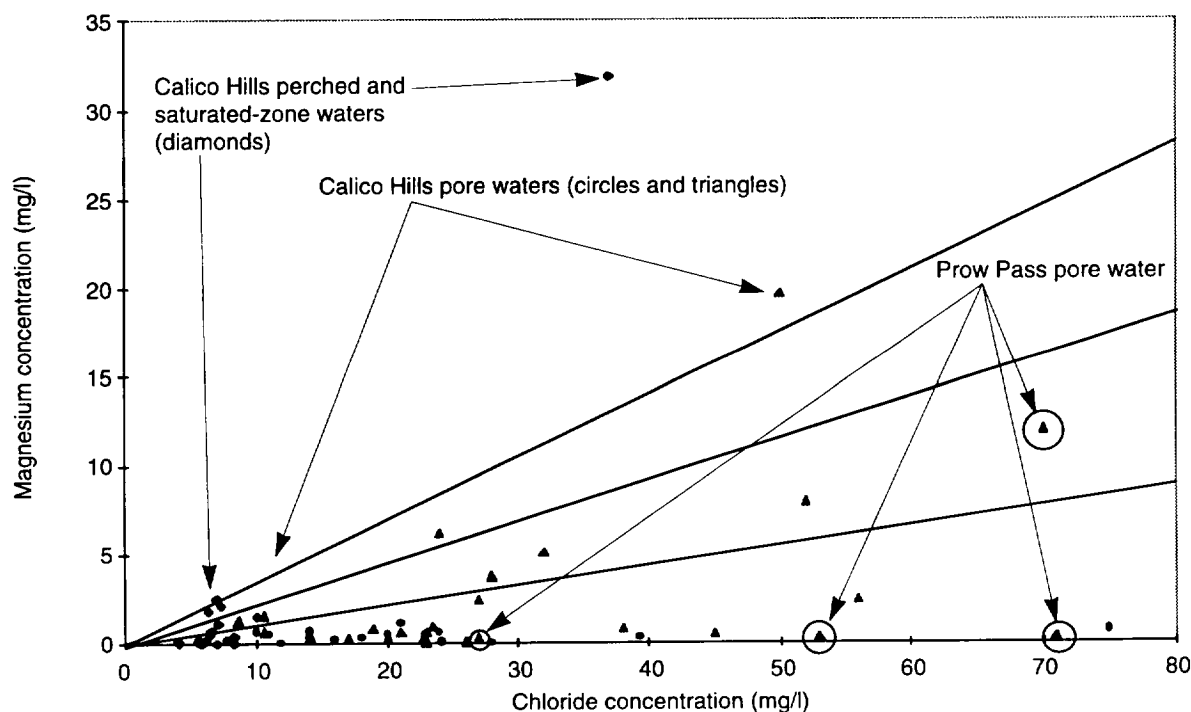


Figure 20. Calico Hills Magnesium. The plot shows magnesium versus chloride concentrations in Calico Hills pore waters, perched waters, and saturated-zone groundwaters. The straight lines are the regression fit and one-sigma deviations for magnesium-versus-chloride precipitation data. (Drill-hole designations: circles: UZ-14; triangles: UZ-16; diamonds: saturated-zone waters.)

II. Groundwater Chemistry Model

of seed crystals of α -cristobalite and quartz (Rimstidt and Barnes 1980). This fact implies that Yucca Mountain waters with high silica activities lack sufficient surface areas of α -cristobalite or quartz seed crystals, in the units from which these waters were obtained, to control silica activities. This situation appears to be the case in nonwelded units within Yucca Mountain (Bish and Chipera 1989). The lack of adequate seed-crystal surface area most likely reflects the slow nucleation kinetics of these minerals at ambient temperature and pressure conditions (Nielsen 1964).

An important point is that most Yucca Mountain waters do not appear to be saturated with amorphous silica at ambient temperatures (Fig. 14). This observation suggests amorphous silica could not nucleate spontaneously, even in waters that contact volcanic glass. Interestingly, this does not mean that amorphous silica is not present in glassy samples. Iler (1973) has shown that the adsorption of ions such as Al^{3+} and Mg^{2+} onto the surface of amorphous silica greatly reduces the "equilibrium" solubility of this phase. Thus, amorphous silica could be a metastable phase in the vitric units, even though the silica concentrations measured in the waters of these units are below saturation levels with regard to amorphous silica. If adsorption of aluminum onto amorphous silica can lower the silica activity in solution, perhaps hydration and hydrolysis of (amorphous) silicic volcanic glass may produce the same result. The volcanic glass in the tuffs is initially 75 to 80 weight per cent SiO_2 and 12 to 13 weight per cent Al_2O_3 (Broxton et al. 1986). After hydration and hydrolysis ($\text{Na}^+ \leftrightarrow \text{H}^+$), the glass composition and structure likely approximate those of amorphous silica combined with some alumina and minor amounts of cations.

Whether or not such amorphous aluminosilicate material could maintain (metastable) equilibrium with an aqueous solution over time in the same manner that amorphous silica can is uncertain. The fact that volcanic glass remains abundant in many of the vitric units of Yucca Mountain (Bish et al. 1996b) after 11 to 13 million years in a hydrous

environment suggests that it can. However, this conclusion must be tempered by the observation that clay minerals are found in many, if not most, of these vitric units. The problem is that these clay minerals could have formed almost anytime in the 11-to-13-million-year interval since these units were deposited. Further, because the distribution of clays is not homogeneous in any given vitric unit, their origin must involve more than simply in-situ alteration in a hydrous environment; otherwise, all glasses in a given unit would show similar evidence of alteration. Open-system alteration may be a determinant of whether or not clays are formed (Gislason and Eugster 1987). For example, clays may be preferentially formed along pathways with higher than average water fluxes (Levy 1984). To model the long-term alteration behavior of silicic volcanic glass, particularly as a function of temperature, data on the kinetics of conversion of the glass to an amorphous aluminosilicate or clay would be required. Such data are unavailable at the present time.

However, data are available on the dissolution rates of silicic volcanic glasses. White et al. (1980) have presented rate constants for the dissolution of vitric silicic tuffs in distilled water at various pH values. The dissolution rate constants for individual elements indicate that the dissolution reactions are incongruent; that is, the dissolution rates of the individual elements were not directly a function of the concentration of the elements in the original glass. This fact suggests that an alteration layer was formed on the glass surface, which was enriched in silica, alumina, and potash relative to the original glass. This layer would presumably control the chemistry of waters in contact with it. It could be an amorphous aluminosilicate or an incipient clay. An important question is what would happen to this layer if temperatures were raised in the glassy units.

Knauss et al. (1986) reacted volcanic glass with J-13 water at 90°C for more than 2 months and found that no secondary minerals were produced and only minor etching was observed. This result suggests

the rate at which the water reacts with glass is very slow, even at somewhat elevated temperatures.

Unfortunately, without additional data on the nucleation and crystallization kinetics of the glass surface layer produced during alteration, reliable predictions of glass alteration behavior and the effect of glass alteration on water chemistry cannot be derived.

Hydrolysis reactions can have significant impacts on the pH of waters. The pH of waters in contact with the gas phase in pores in the unsaturated zone in Yucca Mountain will be buffered in the range from 6.8 to 8.0 depending on the actual partial pressure of carbon dioxide. The pH of groundwaters that become isolated from the carbon-dioxide reservoir in the unsaturated zone may increase as hydrolysis reactions consume hydrogen ions. The extent of such increases will be limited if the partial pressure of carbon dioxide in the saturated zone is buffered by some reservoir (for example, diffusion of gas from Paleozoic units). In any case, the potential increases in pH will be limited to values around 10, at which point silicic acid starts to dissociate, buffering the pH.

The oxidation-reduction potential, or Eh, of waters in contact with the unsaturated-zone gas phase will be oxidizing because this gas phase contains the same concentration of oxygen as the atmosphere (Yang et al. 1996). The range of Eh values to be expected in waters in the saturated zone is difficult to define because the identity of the dominant oxidation-reduction reaction is unknown at the present time. It could be reducing or oxidizing depending on the degree to which the waters have access to atmospheric oxygen or to reducing agents (for example, methane). The measurements reported by Ogard and Kerrisk (1984) suggest that reducing conditions exist at depth in some wells in the Yucca Mountain area. Why conditions are reducing in these wells is uncertain. Perhaps the wells access a volume of rock that is isolated from contact with the atmosphere and that contains sulfides or reduced organic compounds. Further measurements are required to develop a more complete understanding of oxidation-reduction potentials in

the saturated zone at Yucca Mountain.

In the absence of adequate glass-alteration models, some estimates of upper bounds on the concentrations of cations and bicarbonate species in perched waters, saturated-zone groundwaters, and Calico Hills pore waters can also be derived on the basis of data currently available for analyzed waters from aquifers in a variety of volcanic rock types at the Nevada Test Site (Ogard and Kerrisk 1984; Yang et al. 1988, 1996; McKinley et al. 1991). On the basis of the compilation by McKinley et al., the concentrations of major cationic constituents and bicarbonate in groundwater from Well UE-25 p#1 are at the high end of the range of concentrations reported for all waters (60 in all) sampled from volcanic units at the Nevada Test Site. In terms of the other anions, water from Well UE-25 p#1 is also at the high end of the range of chloride and fluoride concentrations. Sulfate, nitrate, and silica are exceptions. Sulfate is higher (449 mg/l) than UE-25 p#1 water only in Well J-11 in Jackass Flats. The elevated sulfate in this well may reflect the oxidation of sulfide minerals in the Wahmonie area to the east of the well. Nitrate is higher (up to 12 mg/l) in a number of wells, and silica is higher (up to 81 mg/l) in various wells. Well J-13 has nitrate and silica concentrations at the high end of the range of Nevada Test Site waters. In general, waters from Wells J-13 and UE-25 p#1 bound the range in concentrations of most of the major constituents found in waters from volcanic units over the entire Nevada Test Site.

Importantly, the Eh and pH of J-13 and UE-25p#1 waters do not bound the ranges for these parameters observed in waters from the Nevada Test Site. Both waters have a relatively oxidizing Eh (360–450 mV) and low pH (6.7–7.2). The pH values observed in Nevada Test Site waters from volcanic units range from 6.7 to 9.0 (McKinley et al. 1991). The range of Eh values in these waters is unknown as values for this parameter were not reported by McKinley et al. (1991). Ogard and Kerrisk (1984) report a range of –143 to +402 mV for groundwaters from the Yucca Mountain area.

C. SUMMARY AND CONCLUSIONS

The available data on the chemistry of pore waters, perched waters, and saturated-zone groundwaters at Yucca Mountain suggest there are essentially two types of waters at Yucca Mountain. Type-1 waters are found as pore water above Tuff of Calico Hills and from portions of Prow Pass member. Type-2 waters are found as perched water and saturated-zone groundwaters. The pore waters in Tuff of Calico Hills appear to be mixtures of these two water types.

Type-1 Waters

The chemistry of type-1 waters (mainly pore waters above Tuff of Calico Hills) will be controlled primarily by soil-zone processes, including evapotranspiration and the precipitation/dissolution of pedogenic minerals such as calcite, gypsum, and amorphous silica. The primary constraints on these processes are largely nonchemical and include evapotranspiration and the detailed soil-zone hydrology. These waters are generally saturated with opal-CT and do not appear to be influenced by hydrolysis reactions involving aluminosilicates.

Evapotranspiration is important in concentrating solutes in the soil zone that were originally in precipitation as wet-fall and dry-fall. Soil-zone hydrology controls the ionic strength and the chemical composition of waters infiltrating the unsaturated zone. Both the ionic-strength control and the compositional control reflect the flux and residence time of infiltrating waters in the soil zone prior to percolation into the unsaturated zone. The soil hydrology also impacts the water compositions through the crystallization sequence in which small pores are filled with early-formed phases, whereas the later-crystallizing phases preferentially form in the space available in the larger pores.

Because our understanding of soil-zone hydrology at Yucca Mountain is not fully developed, the impact of hydrology on the composition of unsatu-

rated-zone pore waters can best be bounded by analyses of unsaturated-zone pore waters. Fortunately, there is a trade-off between ionic strength and water volume. That is, the higher the ionic strength of the water (for example, more corrosive), the less of it there will be.

The pH and Eh of type-1 unsaturated-zone pore waters will be regulated by the composition of the gas phase in the pores. The Eh will be oxidizing (400–600 mV) because this gas phase has an oxygen partial pressure equal to that observed in the atmosphere (Thorstenson et al. 1989; Yang et al. 1996). The pH should remain in the range of 7 to 8 supported by carbon-dioxide partial pressures that are greater than atmospheric.

Type-2 Waters

The compositions of type-2 waters (perched and saturated-zone waters) are dominated by hydrolysis reactions. These reactions involve the exchange of cations (dominantly sodium) with hydrogen ions on the surfaces of aluminosilicate phases in the rocks (such as feldspar and volcanic glass). Hydrogen ions are supplied by the dissociation of carbonic acid. Therefore, the partial pressure of carbon dioxide is a critical parameter that controls hydrolysis reactions. It also has a major influence on the pH of the waters.

As we stated for type-1 waters, in systems open to the unsaturated-zone gas phase, the pH of the water will remain in the range of 7 to 8. Systems that become closed for some reason may have lower or higher pH values, depending on whether or not there are additional sources of carbon dioxide in the system. The upper bound on pH is approximately 10, the value at which silicic acid dissociation buffers the pH.

The Eh of type-2 water ranges from oxidizing to reducing, depending on whether the waters have access to atmospheric oxygen or to reducing agents, respectively.

Prediction of the future compositional variations in type-2 perched and saturated-zone groundwaters requires that the hydrolysis reactions be modeled. Such modeling requires knowledge of the secondary phases involved in the reactions.

For devitrified tuffs, these phases are likely dominated by alkali feldspar and α -cristobalite. Therefore, the future variations in the composition of waters in devitrified tuffs can be modeled by assuming saturation with alkali feldspar and α -cristobalite. The main unknowns in such modeling would be the pH and Eh of the system. The carbon-dioxide partial pressure must be known to calculate pH. Field measurements are required to constrain the Eh.

For glassy units, the modeling is more difficult because the identity of the secondary phases are not known with certainty. More importantly, the rates at which these phases form are unknown. There is information available on the rate of dissolution of silicic glasses. This information allows one to derive the initial chemistry of waters in vitric units, but it does not provide a basis for predictions of the long-term variations in water chemistry.

A Survey Approach

As a surrogate for the modeling approach, a survey of water chemistries in silicic volcanic rocks can be used to estimate bounds on the future variations of water chemistry in Yucca Mountain. A survey of water compositions from volcanic units indicates that waters from Wells J-13 and UE-25 p#1 have compositions that bound the observed range of variability for most major constituents. The main exceptions are pH, Eh, and chloride concentrations. Laboratory experiments designed to derive transport parameters, such as sorption coefficients and solubilities, have used these two water compositions and a range of pH values.

The variability in chloride concentrations is not a serious issue for the derivation of these parameters because chloride is not a strong complexing agent

for most radionuclides of interest. However, chloride concentrations in unsaturated-zone waters are important to the longevity of the waste package, as high chloride concentrations enhance corrosion rates.

Measurements of Eh in the saturated zone beneath Yucca Mountain suggest that reducing conditions exist locally. If redox conditions are generally reducing at depth in the saturated zone, the migration potential of radionuclides of elements such as neptunium and technetium would be greatly diminished. Additional field measurements at the site are required to test the variability in Eh and the redox state of saturated-zone groundwaters.

III. RADIONUCLIDE SOLUBILITY STUDIES

A. SOLUBILITY LIMITS

Radionuclide migration would be mitigated by several barriers in a potential repository. One of the initial barriers is the solubility of the radionuclides in any water that infiltrates the potential repository. The solubility of neptunium, plutonium, and americium will depend on solution speciation (especially with OH^- and CO_3^{2-} ligands) and on the solubility-limiting actinide-bearing solid. Bulk solubility experiments can provide empirical data directly, but since they are long-term experiments, only a limited amount of data can be collected over a limited range of conditions. To determine solubility for general conditions, the system must be modeled thermodynamically. The model can be tested against the solubility found from the bulk experiments prior to being used in the general cases for performance assessment. Therefore, our short-term goal has been to provide solubilities from bulk experiments that attempt to bracket our current estimate of groundwater conditions that might exist. Intermediate goals have been to develop the thermodynamic data for solution speciation and solid-state determination as a prerequisite for modeling the results using the chemical-equilibrium code EQ3/6. Once this model is self-consistent and tests well against known solubilities, the long-term goal will be to use the model over a continuous, weighted-distribution range of potential groundwaters to generate a weighted distribution of solubilities that could be used in the performance assessment. This distribution would have a clear, documented path (using quality-assured protocol) for acquiring solubility numbers for the total-system performance assessment (TSPA) that does not resort to "expert elicitation."

Neptunium

Recent measurements (Efurd et al. 1996) have shown that the bulk solubility of neptunium in J-13 water ranges from 6×10^{-6} to 10^{-3} M (top values in Table 9). This study strived to minimize the ionic strength that, in a previous study (lower val-

ues in brackets in Table 9), was induced by controlling pH (Nitsche et al. 1993a). The reduced ionic strength resulted in solubilities up to an order of magnitude lower. Furthermore, the solubility-limiting solid was predominately (but not exclusively) Np_2O_5 rather than the double-carbonate salt $\text{NaNpO}_2\text{CO}_3 \cdot x\text{H}_2\text{O}$. For water conditions expected at Yucca Mountain, the data for Np(V) solutions (Tait 1996) is consistent, and modeling with the EQ3/6 computer code suggests the dominate species to be a combination of NpO_2^+ and $\text{NpO}_2\text{CO}_3^-$ (Janecky et al. 1994, 1995). The current state of modeling is to decide on which set of Np(IV) data to use (especially the solid-state formation constants). Recent modeling work at Los Alamos indicates Np(IV) solids may form in Yucca Mountain waters (Janecky et al. 1994, 1995), depending on which solid-state numbers are used. The importance of this observation is that Np(IV) solids may be much less soluble than the Np(V) solids currently considered in the performance-assessment calculations (Efurd et al. 1996).

Plutonium

The same study (Efurd et al. 1996) showed that the

Table 9. Solubility of Neptunium (in M) in J-13 Waters

Top values from Efurd et al. (1996).
Lower values (brackets) from Nitsche et al. (1993a).

T(°C)	pH = 5.9	pH = 7.0	pH = 8.5
25	6.5×10^{-4} [5.3×10^{-3}]	3.1×10^{-5} 1.3×10^{-4}	1.5×10^{-5} 4.4×10^{-5}
60	9.4×10^{-4} [6.4×10^{-3}]	1.6×10^{-5} 9.8×10^{-4}	1.7×10^{-5} 1.0×10^{-4}
90	0.9×10^{-3} [1.2×10^{-3}]	7.9×10^{-6} 1.5×10^{-4}	5.5×10^{-6} 8.9×10^{-5}

bulk solubility of plutonium in J-13 water extends over a relatively narrow range from 4×10^{-9} to 5×10^{-8} M (top values in Table 10). The values are again generally lower than those reported previously by Nitsche et al. (1993a). Both studies agree that the predominate solubility-limiting solid is a Pu(IV) oxide polymer at 25°C that ages to the more crystalline PuO₂(s) at 90°C. Controversies involving solution speciation have been noted (Tait 1996), and because of the uncertainties about the solution thermodynamic constants, modeling work is still in the preliminary stages (Janecky et al. 1994, 1995). The model calculates that plutonium speciation is dominated by Pu(OH)₅⁻ in J-13 water and the solids PuO₂(s) and Pu(OH)₄(s) are super-saturated to saturated (Janecky et al. 1994). Some of the current sets of data, such as the alternate composite data set (data0.alt.R1b) provided by Lawrence Livermore National Laboratory, can be dismissed from this early modeling work.

Americium

Because of americium's low solubility (Table 11) and high sorption coefficients (Meijer 1992), less emphasis has been placed on this radionuclide in the Yucca Mountain Project. The bulk solubility experiment of Nitsche et al. (1993a) is summarized in Table 11, and the solubility is observed to range from 3×10^{-10} to 4×10^{-6} , with the latter value possibly a bad datum point as judged by its neighboring values in the table. Note that the 25 and 90°C experiments were carried out with a mixture of Nd³⁺ and ²⁴¹Am, whereas the 60°C experiment was carried out both with the mixture and with pure ²⁴³Am (both gave comparable results). The use of Nd³⁺ as a surrogate and carrier for the americium stems from the belief that only Am(III) (and no other oxidation state) is important in solutions (Nitsche et al. 1993a), although such an assumption was challenged in the higher-temperature bulk-solubility study of americium from undersaturation in UE-25 p#1 water by Hobart and co-workers (Becraft et al. 1994). The solubility-limiting solid was reported to be a mixture of hexagonal and orthorhombic forms of AmOHCO₃

Table 10. Solubility of Plutonium (in M) in J-13 Waters

Top values from Efurud et al. (1996).
Lower values (brackets) from Nitsche et al. (1993a).

T(°C)	pH = 5.9	pH = 7.0	pH = 8.5
25	4.7×10^{-8} [1.1×10^{-6}]	2.4×10^{-8} 2.3×10^{-7}	0.9×10^{-8} 2.9×10^{-7}
60	0.9×10^{-8} [2.7×10^{-8}]	0.8×10^{-8} 3.8×10^{-8}	0.6×10^{-8} 1.2×10^{-7}
90	4.3×10^{-9} [6.2×10^{-9}]	3.6×10^{-9} 8.8×10^{-9}	4.2×10^{-9} 7.3×10^{-9}

(Nitsche et al. 1993a), but this assertion is controversial, and more work needs to be done to confirm or reject this statement. Only preliminary modeling of americium has been done in which the predominate solution species was calculated to be AmCO₃⁺ in J-13 water except at 90°C and a pH of 8, in which case the dominant species was calculated to be Am(CO₃)₂⁻ (Janecky et al. 1994). Furthermore, the hydroxo solids Am(OH)₃ and amorphous Am(OH)₃ were calculated to be significantly below saturation throughout the experimental conditions for the bulk solubility study (Janecky et al. 1994). The only solid to approach saturation in these calculations was AmOHCO₃.

Table 11. Solubility of Americium (in M) in J-13 Waters

All values from Nitsche et al. (1993a).

T(°C)	pH = 5.9	pH = 7.0	pH = 8.5
25	1.8×10^{-9}	1.2×10^{-9}	2.4×10^{-9}
60	3.6×10^{-6}	5.5×10^{-9}	1.6×10^{-8}
90	1.7×10^{-9}	3.1×10^{-10}	3.4×10^{-10}

B. SOLUBILITY-LIMIT VALUES RECOMMENDED FOR PERFORMANCE ASSESSMENT

Assumptions about Groundwater Chemistry

Solubility is a function of groundwater chemistry. The water chemistry at Yucca Mountain is summarized in section I.C. "Yucca Mountain Groundwaters" (for example, Table 2) and was reviewed by Meijer (1992). The concentration of the major cations and anions in unsaturated-zone groundwaters appears to be intermediate between the saturated-zone tuffaceous waters (Well J-13) and waters from the carbonate Paleozoic aquifer (Well UE-25 p#1). Consequently, the first assumption made to recommend values for the performance assessment was that the water from these two wells be taken to bound the chemistry of the groundwaters at Yucca Mountain.

Most of the waters at Yucca Mountain are oxidizing. Two basic container types are being considered for the potential repository: a thin stainless-steel or alloy container and a large container with a thick iron shroud over a thin stainless-steel or alloy liner ("a robust container"). The large amounts of iron in the robust container would result in a reducing environment, although it is not clear how long that reducing environment would last. The conservative approach is to assume that groundwaters that move from the repository to the accessible environment are oxidizing because radionuclides (such as the actinides and technetium) have higher solubilities in oxidizing than in reducing waters. Consequently, the second assumption was to consider solubility under oxidizing conditions only.

The third assumption was that the solubilities would be best determined by the far-field environment. The increased temperature from the repository may cause more aggressive groundwater chemistries and increased solubilities for radionuclides in the near field; however, when the solute is transported out of the near field, the potentially lower solubilities in the far field would cause pre-

cipitation and, thus, would be the limiting factor. This assumption is due primarily to the dirt of information about the near-field water chemistry, which made accurate predictions of solubility impossible for this region. It must be noted that the high thermal loads being considered for the potential repository (for example, 114 kilowatts per acre) may cause near-field conditions to extend throughout the unsaturated zone.

Dependence of Solubility on Temperature

The functional dependence of solubility with temperature can be expressed with thermodynamic rigor. However, this approach requires knowing the thermodynamic solubility products (K_{sp}°) of the dominating dissolution reactions. The thermodynamic treatment to obtain the functional dependence of an equilibrium constant (such as K_{sp}°) with temperature, which follows, is only valid when considering the same chemical reaction attaining equilibrium at different temperatures.

The symbols used in this derivation are:

K_{sp}° = solubility product,

G = Gibbs free energy,

$$\Delta G = \sum_{\text{products}} G_i - \sum_{\text{reactants}} G_i \quad ,$$

$^{\circ}$ refers to reactants and products in their standard state (1 atm, zero ionic strength),

H = enthalpy,

S = entropy,

R = gas constant,

T = temperature,

C_p = heat capacity at constant pressure, and

a, b, c are constants.

First, at constant T , the laws of thermodynamics give

$$\Delta G = \Delta H - T\Delta S \quad . \quad (3)$$

The functional dependence of the heat capacity of a substance with temperature is described by

III. Radionuclide Solubility Studies

$$C_p = a + bT + cT^{-2} . \quad (4)$$

Thus, the functional dependence of ΔC_p with temperature, where ΔC_p is the sum of the heat capacities of the products minus the corresponding sum for the reactants (that is, the net change in heat capacity resulting from the reaction), is given by

$$\Delta C_p = \Delta a + \Delta bT + \Delta cT^{-2} . \quad (5)$$

Next, Kirchoff's formula is

$$\Delta C_p = \left[\frac{\partial(\Delta H)}{\partial T} \right]_p . \quad (6)$$

Substituting Eqn. 5 for ΔC_p in Eqn. 6 and then integrating yields

$$\Delta H = \Delta H_i + \Delta aT + \frac{1}{2}\Delta bT^2 - \Delta cT^{-1} , \quad (7)$$

where ΔH_i is an integration constant. We can now take the partial derivative of Eqn. 3 with respect to temperature at constant pressure to get

$$\left[\frac{\partial(\Delta G/T)}{\partial T} \right]_p = -\frac{\Delta H}{T^2} , \text{ or}$$

$$\left[\frac{\partial(\Delta G/T)}{\partial(1/T)} \right]_p = \Delta H . \quad (8)$$

Substituting for ΔH using Eqn. 7 and integrating either form of Eqn. 8 yields

$$\Delta G = \Delta H_i - \Delta aT \ln T - \frac{1}{2}\Delta bT^2 - \frac{1}{2}\Delta cT^{-1} + iT \quad (9)$$

where i is another integration constant.

The solubility product is related to Gibbs free energy by

$$\Delta G^\circ = -RT \ln K_{sp}^\circ . \quad (10)$$

Substituting Eqn. 9 for ΔG° in this equation yields, after algebraic rearrangement,

$$-R \ln K_{sp}^\circ =$$

$$\frac{\Delta H_i^\circ}{T} - \Delta a \ln T - \frac{1}{2}\Delta bT - \frac{1}{2}\Delta cT^{-2} + i , \quad (11)$$

an equation that describes the functional depen-

dence of the solubility product with respect to temperature.

Limitations of Empirical Solubility Data

With regard to the Laboratory's empirical solubility data for actinides (Nitsche et al. 1993a), it is important to make the following observations:

1) Nitsche et al. only report solubility data obtained from oversaturation, 2) the solid phases reported at 25°C and 60°C for neptunium do not match the solid phases found at 90°C, 3) information on the solid phases of plutonium formed is not available, and 4) it is not clear that equilibrium is obtained in the time scale of the experiments. These observations are important for the following reasons:

1) Deriving a K_{sp} from the data of Nitsche et al. requires knowing the dissolution reaction and knowing that the same reaction takes place across the desired temperature range. It is not clear that this is the case for either neptunium or plutonium. 2) If equilibrium is not attained during the solubility experiments, the variability of the solubility data with temperature could be a result of kinetic effects. In particular, the apparent solubility as measured by Nitsche et al. could increase with temperature as a result of faster dissolution rates at higher temperatures. 3) To define a K_{sp} , equilibrium has to be attained from oversaturation and from undersaturation. The same solubility for americium, neptunium, and plutonium must be measured (regardless of whether the experimenter starts from an oversaturated solution or from an undersaturated solution using the solid phases formed during the oversaturation experiments). Data from undersaturation are not available yet, although experiments are in progress (Nitsche et al. 1993a, 1993b). Consequently, the members of the Radionuclide Solubility Working Group (SolWOG) of the Yucca Mountain Site Characterization Project (David Morris, Mike Ebinger, Heino Nitsche, Robert Silva, James Johnson, David Clark, and Drew Tait) decided not to apply a rigorous thermodynamic treatment to extrapolate the empirical solubilities reported by Nitsche et al. (1993a, 1993b) as a function of temperature.

Two potentially important issues were ignored in the solubility data used: the impact of future climate changes as they relate to potential changes in the water chemistry at Yucca Mountain and the impact of colloid formation in facilitating radionuclide transport at Yucca Mountain. A strategy was developed by the Yucca Mountain Site Characterization Project to address the latter issue (Triay et al. 1995b). The results of the work delineated by Triay et al. will be used in the next total-system performance-assessment (TSPA) calculation.

Table 12 shows the parameters for the solubility models that were presented to the members of SolWOG. After reviewing the actinide solubilities, they suggested only two changes: 1) the minimum value for the solubility of neptunium should be 5×10^{-6} M (rather than 10^{-8}) and 2) the minimum value for the solubility of plutonium should be 10^{-8} M (rather than 10^{-10}).

Solubility Distributions

Americium

The minimum and maximum values for the americium solubility distribution in Table 12 are based on the empirical solubility data reported by Nitsche et al. (1993a, 1993b). The SolWOG members thought that any value within the range would be equally likely (a uniform distribution). A uniform distribution over the range implies that approximately 90% of samples from this distribution would lie between 10^{-7} and 10^{-6} M, whereas approximately 0.1% of the samples would lie between 10^{-10} and 10^{-9} M.

Plutonium

Plutonium is more soluble than americium (as the SolWOG members pointed out) based on the data of Nitsche et al. (1993a, 1993b). These experts chose a distribution for plutonium solubility identical to the one chosen for americium. As has been already pointed out, a uniform distribution over the

Table 12. Solubilities used in TSPA-1993

Element*	Minimum Value (M)	Maximum Value (M)	Expected Value (M)	Coefficient of Variation	Distribution
Americium	10^{-10}	10^{-6}			uniform
Plutonium	10^{-10} (10^{-8})**	10^{-6}			uniform
Uranium	10^{-8}	10^{-2}	$10^{-4.5}$	0.20	log beta
Thorium	10^{-10}	10^{-7}			log uniform
Radium	10^{-9}	10^{-5}	10^{-7}	0.10	log beta
Lead	10^{-8}	10^{-5}	$10^{-6.5}$	0.08	log beta
Neptunium	10^{-8} ($10^{-5.3}$)**	10^{-2}	10^{-4}	0.20	log beta
Protactinium	10^{-10}	10^{-5}			log uniform
Actinium	10^{-10}	10^{-6}			uniform
Tin	10^{-11}	10^{-7}			uniform
Nickel	10^{-6}	10^{-1}	$10^{-2.75}$	0.25	log beta
Strontium	10^{-6}	10^{-3}	10^{-4}	0.12	log beta
Samarium	10^{-10}	10^{-6}			uniform
Zirconium	10^{-12}	10^{-7}			log uniform
Niobium	10^{-9}	10^{-7}			log uniform

* Cesium, iodine, technetium, selenium, carbon, and chlorine are very soluble. **Values in parentheses recommended by SolWOG.

III. Radionuclide Solubility Studies

range in Table 12 implies that most of the samples from this distribution would lie between 10^{-8} and 10^{-6} M. Kerrisk (1984a) used the computer program EQ3/6 to calculate the solubility of plutonium in Yucca Mountain groundwaters and obtained a value of 1.8×10^{-6} M. The SolWOG members agree that the empirical data were more reliable for the TSPA calculations.

Uranium

No empirical data have been collected by the Yucca Mountain Site Characterization Project for uranium because its high solubility is not expected to be the limiting factor for the uranium source term. The possible solubilities for uranium occur over a wide range, but the data support a central tendency between 10^{-4} and 10^{-5} M with an approximate one-order-of-magnitude spread (Wanner and Forest 1992). The SolWOG members thought that uranium solubility should be represented in terms of logarithmic space; the resulting distribution is skewed log-normal.

Thorium

Thorium is extremely insoluble (less soluble than americium and plutonium). Such low solubilities make this element generally unimportant. As with americium, the SolWOG members believed that the range of values was well defined but that the distribution should favor selection of lower solubilities. They decided on a log-uniform distribution believing that it was equally likely to select the log of any value within the prescribed range.

Radium

Radium solubility is similar to barium solubility. The distribution chosen is based on Kerrisk's calculation with EQ3/6 (Kerrisk 1984a). The solubility of radium depends on the presence of sulfates. The SolWOG members chose a small relative standard deviation for radium solubility because this element forms only one cation and is relatively insensitive to groundwater chemistry.

Lead

The lead solubility distribution is based on the

range published by Andersson (1988) and Pei-Lin et al. (1985). This element's solubility depends on the amount of carbonate in the groundwater so that variations in carbonate concentration in the groundwaters cause variations in lead solubility.

Neptunium

The neptunium solubility distributions were based on Nitsche's data (1993a, 1993b). The SolWOG members believed that the data supported a central tendency on log space with a spread of less than an order of magnitude. The neptunium solubilities used in TSPA-1991 (Barnard et al. 1992) were very low (approximately five orders of magnitude below those suggested by the SolWOG members). The TSPA-1991 solubilities were derived from spent fuel tests (conducted by Wilson 1990a, 1990b). The results from the spent-fuel test are not necessarily representative of neptunium solubilities in the groundwaters.

Cesium, iodine, technetium, selenium, carbon, and chlorine

All these elements are very soluble. The source term needs to be determined by leaching tests. A source term of 1 M is a reasonable approximation.

Protactinium

The range for protactinium solubilities was derived from the results of the Swedish Nuclear Power Inspectorate (SKI) (Andersson 1988). The solubility distribution for protactinium is expected to have a large variance, skewed towards smaller values. The SolWOG members believed that this radionuclide was less soluble than the range published by Andersson suggests. Therefore, a log-uniform distribution was chosen for protactinium.

Actinium

The solubility distribution chosen for actinium is identical to the americium solubility distribution.

Tin

Tin is very insoluble. The distribution range was obtained from the results published by SKI (Andersson 1988); any value within this range was

equally probable. A uniform solubility distribution was chosen.

Nickel

Nickel solubility is a function of pH. The SolWOG members chose the same range as the one published by the SKI (Andersson 1988). The mean and standard deviation of the solubility distribution were approximated from data gathered in support of the caisson experiment conducted at Los Alamos (Siegel et al. 1993).

Strontium

The solubility distribution for strontium is based on the results of SKI (Andersson 1988) and those published by Siegel et al. (1993).

Samarium

The solubility distribution chosen for samarium is identical to that for americium

Zirconium

Zirconium is very insoluble. The chosen distribution was based on the SKI results (Andersson 1988). A log-uniform solubility distribution was chosen for this element because the SolWOG members expected to see many values for zirconium solubility in the lower range.

Niobium

The niobium solubility distribution is based on SKI results (Andersson 1988).

IV. SORPTION AND SORPTION MODELING STUDIES

A. BATCH-SORPTION DATA

Introduction

The solubility limits of radionuclides can act as an initial barrier to radionuclide migration from the potential repository at Yucca Mountain. However, once radionuclides have dissolved in water infiltrating the site, sorption of these radionuclides onto the surrounding tuffs becomes a potentially important second barrier. Thus, the study of the retardation of actinides and other key radionuclides is of major importance in assessing the performance of the potential repository.

Sorption actually comprises several physicochemical processes, including ion exchange, adsorption, and chemisorption. Determining whether sorption will occur requires knowledge of the likely flow paths of the groundwater and the spatial and temporal distribution of sorbing minerals along these paths. Evaluating the retardation effectiveness of sorption for repository design and licensing requires theoretical and quantitative understanding of sorption. We thus combined experimental measurements of sorption with modeling of the data in an attempt to identify key sorption mechanisms.

The use of batch-sorption experiments to obtain sorption distribution coefficients and to identify sorption mechanisms is fast, easy, and inexpensive compared to other types of sorption experiments. A disadvantage is the fact that such experiments are static in nature, whereas transport of radionuclides through the site is, obviously, a dynamic process. However, batch-sorption experiments are useful for bounding more detailed and mechanistic sorption studies, and a major part of our experimental effort was devoted to such measurements.

In our experiments, we determined batch-sorption distribution coefficients as a function of variables representing conditions expected beyond the region disturbed by waste emplacement. The variables

included mineralogy, groundwater chemistry, sorbing element concentration, atmospheric conditions, and temperature. Batch-sorption results are very sample specific and, therefore, difficult to generalize and apply throughout the mountain. Deconvolution of sorption isotherms provides much greater detail about sorption sites (kind, number, specificity, and so forth), and we did this analysis for a number of the actinides. Such information is correlated with crystallographic data and related to specific sorption sites in the crystal structure. All sites are not equally selective for all sorbing species.

We also examined the sorption behavior of individual pure minerals, such as the zeolites and manganese or iron oxyhydroxides found in Yucca Mountain tuffs. This approach can help predict sorption coefficients along flow paths of known mineral content.

Linear versus nonlinear sorption

The sorption distribution coefficient, K_d , for the species being sorbed, is the ratio of its concentration in the solid phase, F , to its concentration in the solution phase, C , which implies a linear relationship between the concentrations:

$$F = K_d C \quad (12)$$

Besides linearity, the valid use of sorption distribution coefficients in transport calculations also requires the sorption to be instantaneous and reversible, conditions that may or may not be met for the sorption of radionuclides onto Yucca Mountain tuffs.

Nonlinear adsorption isotherms have been reviewed by de Marsily (1986, p. 258). A useful nonlinear relationship, Freundlich's isotherm, is given by the equation

$$F = KC^{1/n} \quad (13)$$

where K and n are positive constants (with $n \geq 1$). Another nonlinear relationship is Langmuir's

IV. Sorption and Sorption Modeling Studies

isotherm, given by

$$F = \frac{K_1 C}{1 + K_2 C}, \quad (14)$$

where K_1 and K_2 are positive constants. Part of our research was an attempt to assess the validity of using the linear distribution coefficients as opposed to other isotherm functional forms to describe retardation by sorption in transport calculations.

Mechanistic models

A better understanding of the sorption of radionuclides onto tuff is possible if we can relate the data to mechanistic models. Two general mechanisms are important: ion-exchange reactions that are primarily electrostatic in nature and surface complexation in which a relatively covalent chemical bond forms with the mineral surface. Ion exchange does not have the same degree of selectivity between aqueous ions of like charge as does surface complexation. The adsorption of metal ions via cation exchange will only occur on surfaces of opposite charge and so is affected by such common components of groundwater as sodium. Surface complexation, on the other hand, can occur even when the mineral surface charge is the same as the aqueous ion. Both of these processes can, in principle, be modeled using a triple-layer surface-complexation model. However, there are significant differences between the cation exchange in zeolites and clays and the formation of surface complexes on metal oxides, so we have treated cation exchange and surface complexation separately.

Physiochemical processes that might accelerate radionuclide migration relative to groundwater flow rates must also be quantified. For example, mineral surfaces in rock pores are predominantly negatively charged, so anions are typically repelled and can actually migrate through the rock faster even than the water. Such acceleration processes depend largely on the molecular complexation or speciation that occurs in solution. Accordingly, detailed assessment of this possibility is needed to fully evaluate the potential for transport retardation by geochemical processes.

Experimental procedures

All batch-sorption experiments were performed at room temperature. The procedure first involved pretreating the solid phase with the groundwater being studied (J-13 or UE-25 p#1 well water or a synthetic bicarbonate groundwater) in the ratio of 1 g of solid to 20 ml of solution. The pretreated solid phase was then separated from the groundwater by centrifugation and equilibrated with 20 ml of a radionuclide solution (in the groundwater being studied). After sorption, the phases were again separated by centrifugation.

The amount of radionuclide in solution initially and then after sorption was either determined with a liquid-scintillation counter (such as for neptunium and plutonium) or with inductively coupled plasma mass spectrometry (such as for uranium). The amount of radionuclide in the solid phase was determined by difference.

The liquid-scintillation counting technique we used can discriminate alpha activity from beta activity. Consequently, no interference from beta emitters (such as ^{233}Pa , the daughter of ^{237}Np) is expected. Because the efficiency of this liquid-scintillation counter is approximately 100%, the counts per minute (cpm) measured are approximately equivalent to disintegrations per minute.

As controls, we used container tubes without solid phases in them to monitor radionuclide precipitation and sorption onto the container walls during the sorption experiment. The difference in the concentration of the radionuclide in the initial solution and in the solution in the control tube generally was only a few percent, and then in either a plus or a minus direction.

Results for the plutonium solution did show a small amount of sorption onto the container walls. Even here, the difference in concentration between the initial plutonium solution and the plutonium solution in the control tube never exceeded 7% for the experiments reported. Nevertheless, in the case of plutonium, we calculated the amount of radionu-

clide sorbed in the solid phase by taking the difference of the final plutonium solution concentration both with the initial solution concentration and with the solution concentration in the control tube. The latter approach is conservative because plutonium may sorb to container walls only in the absence of the geologic material.

We performed batch-sorption experiments under atmospheric conditions and inside glove boxes with a carbon-dioxide overpressure. The pH of the J-13 and UE-25 p#1 waters under atmospheric conditions was approximately 8.5 and 9, respectively, and inside the glove boxes was 7 (the carbon-dioxide overpressure was adjusted to bring the pH of both waters down to 7). Details of the experimental setup and the analytical techniques that we used in the sorption experiments are given in the *Yucca Mountain Project Detailed Procedures* (Table 2).

The distribution coefficient

The batch-sorption distribution coefficient, K_d , was calculated using

$$K_d = \frac{F}{C} = \frac{\text{moles of radionuclide per g of solid phase}}{\text{moles of radionuclide per ml of solution}} \quad (15)$$

K_d thus has units of ml/g.

Determination of very small or very large batch-sorption distribution coefficients results in large uncertainties in the K_d values calculated. When very little sorption occurs, calculations can yield negative K_d values; the error results from subtracting two large numbers (the initial radionuclide concentration in solution and the radionuclide concentration after sorption) to obtain a small number (the amount of radionuclide left in the solid phase). Therefore, small K_d values (in the range of ± 1) are not significant. On the other hand, when a great deal of sorption occurs, calculations can yield large uncertainties associated with measuring the small amount of radioactivity left in solution after sorption. Because of these uncertainties, most K_d values are only reported to one significant figure.

Niobium, Thorium, Tin, and Zirconium

The radionuclides of concern represented by these elements have several characteristics in common. First, in groundwater-rock systems of concern in this report, these elements have stable oxidation states. Niobium is present in a +5 oxidation state, whereas the others are typically in +4 oxidation states (Brookins 1988). Second, in aqueous solutions with compositions typical of groundwaters, these elements tend to occur as sparingly soluble oxides or silicates (Brookins 1988). They may also form solid solutions with other, more common, sparingly soluble oxides, such as titania (TiO_2). Third, the dominant solution species associated with these oxides are hydrolysis products (Baes and Mesmer 1976). Fourth, the hydrolyzed solution species tend to have high affinities for adsorption onto oxide surfaces as discussed further below. The radionuclides represented by these elements are in the "strongly-sorbing" group discussed by Meijer (1992).

Niobium

Behavior in solutions representative of Yucca Mountain groundwaters.

According to Baes and Mesmer (1976), at a dissolved niobium concentration of 10^{-6} M, the dominant solution species in pure water are the neutral species $\text{Nb}(\text{OH})_5$ and the anionic species $\text{Nb}(\text{OH})_6^-$. The anionic species predominates at values of pH above 7, and the neutral species is stable below a pH of 7. At surficial temperatures and pressures, evidence for significant complexation of niobium by nonhydroxide ligands in natural aqueous solutions is lacking. As discussed below, carbonate complexation may occur at higher temperatures and pressures.

The concentrations of niobium in surficial aqueous solutions are extremely low, presumably due to the low solubility of the pentavalent oxide (Baes and Mesmer 1976) and to sorption onto mineral surfaces. In geologic systems, niobium may substitute as a trace element in the more abundant oxide phases such as micas, titanium oxides (for exam-

ple, rutile), and clays (Goldschmidt 1958). This effect also leads to low solution concentrations.

Qualitative evidence for behavior in the surficial environment.

The geologic literature contains numerous papers that qualitatively discuss the mobility, or more accurately, the immobility of niobium in rocks during alteration processes (for example, Cann 1970). In various studies of soils or altered, weathered, or metamorphosed rocks, geological, geochemical, and statistical evidence has been presented that supports the conclusion that niobium is essentially immobile in the surficial environment. Although some of these studies deal with rocks that have been altered under conditions of low fluid-to-rock ratios, the general lack of evidence for niobium mobility suggests that this element would also be immobile in systems with higher water-rock ratios, such as the Yucca Mountain flow system. For example, Brookins (1983) notes that 100 per cent of the niobium produced by fission at the natural reactor at Oklo, Gabon, has been retained by the host pitchblende even though the reactor was active in water-bearing sandstones that were subjected to elevated temperatures during and after the critical (that is, nuclear) stage of the reactor.

Grimaldi and Berger (1961) studied the concentrations of niobium in twenty lateritic soils from West Africa and concluded that silica is depleted more rapidly from these soils than is niobium and niobium more rapidly than aluminum. Further, these workers note that there is a strong association of niobium with the clay-sized fraction and also with titanium. They propose that the association of niobium with the clay fraction may be due to the presence of niobium-rich authigenic rutile in the clays. The observation that niobium was mobilized more readily than aluminum in this environment does not necessarily imply niobium was transported out of the system as a dissolved solution species. The tendency of elements such as niobium, titanium, tin, and so forth to form very fine-grained precipitates is well known. Such colloidal-sized particles can be transported by soil solutions and surface waters.

Evidence for niobium mobility during greenschist metamorphism of mafic rocks has been presented by Murphy and Hynes (1986). These workers suggest that carbonate-rich metamorphic solutions can mobilize and transport niobium (as well as titanium, zirconium, phosphorus, and yttrium).

Presumably, carbonate can form mobile complexes with niobium under conditions of elevated temperature and pressure. No references were found that address the ability of carbonate to complex niobium under low temperatures and near atmospheric pressures.

Conclusions regarding sorption behavior with respect to expected variations in groundwaters.

On the basis of the geological evidence and because niobium forms primarily hydrolyzed species in groundwaters of the type associated with Yucca Mountain, niobium should be very insoluble in Yucca Mountain groundwaters and strongly sorbed onto mineral phases present in Yucca Mountain tuffs from the whole range of groundwater compositions expected at the site.

Thorium

Behavior in solutions representative of Yucca Mountain groundwaters.

Langmuir and Herman (1980) have compiled and critically reviewed thermodynamic data for thirty-two dissolved thorium species and nine thorium-bearing solid phases. In the groundwater compositions expected within Yucca Mountain, thorium will be fully hydrolyzed ($\text{Th}(\text{OH})_4$), and thorium complexing with other inorganic ligands will be insignificant based on the data presented in Langmuir and Herman (1980). Thorium compounds are among the most insoluble in the group of elements considered in this report. Solubilities in the range of 10^{-50} M are common for thorium compounds (for example, thorianite (ThO_2) and thorite (ThSiO_4)). Nevertheless, concentrations well above this range have been found in various natural waters and appear to reflect complexation with organic ligands in organic-rich waters. Such waters are not expected at Yucca Mountain.

Qualitative evidence for behavior in the surficial environment.

Thorium is one of the elements considered to be immobile in most surficial environments (Rose et al. 1979). Studies of the isotopic disequilibrium in the uranium and thorium decay series found in natural aquifers suggest that thorium isotopes are strongly retarded in these flow systems relative to other members of the decay series (Krishnaswami et al. 1982). Studies of the migration of thorium away from thorium ore bodies also indicate that it is "extraordinarily immobile" in these environments (Eisenbud et al. 1984). Brookins (1983) found that thorium was immobile in the Oklo reactor environment. Studies of thorium concentration gradients with depth in seawater also point to high sorption affinities for this element on oceanic particulate matter (Moore and Hunter 1985).

Data from laboratory sorption experiments.

Hunter et al. (1988) carried out thorium sorption experiments on MnO_2 and FeOOH in artificial seawater and in a simple NaCl solution. The primary objective was to determine the effects of major ions (for example, Mg^{2+} and SO_4^{2-}) on the adsorption of thorium by goethite (FeOOH) and MnO_2 relative to sorption in a pure NaCl electrolyte system. The effects of magnesium and calcium ions on thorium adsorption were very small (probably within the margin of experimental error), but the presence of sulfate at seawater concentrations (0.028 M) increased the adsorption edge on FeOOH by one-half of a pH unit. Because the adsorption edge is in the range of pH values from 3 to 5 in all the experiments, this effect is not considered important for thorium sorption behavior at the Yucca Mountain site.

LaFlamme and Murray (1987) evaluated the effects of carbonate on the adsorption characteristics of thorium on goethite. They found that carbonate alkalinity could decrease thorium sorption onto goethite at alkalinity values greater than 100 meq/l. Because the alkalinity values expected in the Yucca Mountain flow system are orders of magnitude lower than this value, carbonate alkalinity

is not expected to affect thorium adsorption behavior in this system.

According to Langmuir and Herman (1980), the adsorption of thorium onto clays, oxides, and organic material increases with pH and approaches 100 per cent completion by a pH of about 6.5. As the thorium ion is largely hydrolyzed above a pH of about 3.2, it follows that hydroxy complexes of thorium are primarily involved in adsorption processes (in carbonate-poor systems). Using a mixed quartz-illite soil as a sorbent, Rancon (1973) measured a K_d value of 5 ml/g at a pH of 2, which increased to 5×10^5 ml/g at a pH of 6. With a quartz-illite-calcite-organic-matter soil, Rancon found that the K_d decreased from 10^6 ml/g at a pH of 8 to 100 ml/g at a pH of 10. This change was attributed to the dissolution of soil humic acids and the formation of thorium-organic complexes at this high pH.

Lieser and Hill (1991) reported thorium sorption coefficients for rock-water systems associated with the Gorleben site in Germany. They found that thorium was strongly sorbed in such systems ($K_d = 10^3$ – 10^5 ml/g). However, they also found that colloidal transport may be of potential significance to the migration of thorium in the surficial environment.

Thorium sorption experiments on Yucca Mountain rock samples in J-13 groundwater were reported by Rundberg et al. (1985) and Thomas (1988). The sorption coefficients obtained in these experiments ranged from 140 to 23,800 ml/g. No correlations were noted between the values obtained for the sorption coefficient and rock type or pH (5.3–7.5). Part of the reason for the large range in sorption coefficients obtained in these experiments may lie in the presence of fine colloidal particles in the solution phase used to obtain the sorption coefficients (for example, Lieser and Hill 1991).

Conclusions regarding sorption behavior with respect to expected variations in groundwaters.

The dominance of hydrolysis reactions in solution,

IV. Sorption and Sorption Modeling Studies

the low solubility of thorium oxides and silicates, the large values measured for thorium sorption coefficients in different water compositions, including seawater, combined with the general lack of evidence for mobility of thorium in the surficial environment suggest that the sorption coefficients for thorium will be large (> 100 mg/l) in all hydrochemical environments associated with Yucca Mountain in the present day or in the future.

Tin

Behavior in solutions representative of Yucca Mountain groundwaters.

The dominant tin solution species in surficial waters appears to be $\text{Sn}(\text{OH})_4$. The concentrations of tin in natural groundwaters are extremely low due to the low solubility of the tetravalent oxides (about 10^{-9} M in pure water; Baes and Mesmer 1976). Cassiterite (SnO_2) should be the solubility-limiting oxide in most groundwaters. Tin could also coprecipitate with other insoluble oxides or silicates such as niobium pentoxide, zirconium and thorium dioxide, and thorium silicate. In natural waters with high sulfide concentrations, tin sulfide minerals could control tin solubility. However, such water compositions are not expected in association with the proposed repository site at Yucca Mountain.

Qualitative evidence for behavior in the surficial environment.

Tin is one of the elements considered to be immobile in most near-surface geologic environments (Rose et al. 1979). This assignment is based on various types of data, including observations on the mobility of tin in and around tin ore deposits. However, De Laeter et al. (1980) note that some tin has migrated out of the pitchblende at the natural reactor at Oklo, Gabon. The cause for this migration has not been established but may reflect the existence of reducing conditions during some phase of the history of the reactor.

Data from laboratory sorption experiments.

Sorption experiments with tin have been carried out on several whole-rock samples from Yucca

Mountain in contact with J-13 water, UE-25 p#1 water, H-3 water, and several waters separately spiked with sodium sulfate, sodium bicarbonate, and calcium chloride (Knight and Thomas 1987). The measured sorption coefficients ranged from 77 to 35,800 mg/l at pH values in the range of 8.4 to 9.2. Coefficients obtained from desorption experiments were generally larger (300–52,500 mg/l) than those obtained from sorption experiments. The devitrified tuff samples produced the highest sorption and desorption coefficient values (> 2900 mg/l), whereas the vitric and zeolitic tuff samples produced lower values. Sorption coefficients were generally highest in the UE-25 p#1 water and the calcium-chloride-spiked J-13 water. Apparently, high calcium concentrations in the solution phase result in high sorption-coefficient values for tin. Alternatively, high calcium concentrations cause the precipitation of some type of tin-bearing compound. As with thorium, the large range in sorption coefficients observed in the experiments may reflect the presence of colloidal-size particles in the solution phase used to obtain the coefficients.

Conclusions regarding sorption behavior with respect to expected variations in groundwaters.

The dominance of hydrolysis reactions in solution, the low solubility of tin oxides, and the large values measured for tin sorption coefficients in different water compositions combined with the general lack of evidence for mobility of tin in the surficial environment suggest that the sorption coefficients for tin will be large (> 100 mg/l) in all hydrochemical environments associated with Yucca Mountain in the present-day or in the future.

Zirconium

Behavior in solutions representative of Yucca Mountain groundwaters.

In near-neutral solutions, the dominant zirconium solution species appear to be hydrolysis products, such as $\text{Zr}(\text{OH})_4$. The degree to which zirconium forms complexes with other inorganic ligands present in Yucca Mountain groundwaters is insignificant (Sillen and Martell 1964, 1971). The solubility of zirconium in dilute solutions is extremely

small (Sillen and Martell 1964, 1971), although the identity of the solubility-controlling solid is uncertain. The solubility-controlling compounds for zirconium in most natural groundwaters are likely zircon (ZrSiO_4) or baddeleyite (ZrO_2). Zirconium solubilities in surficial environments may also reflect coprecipitation in other sparingly soluble oxides or silicates. The concentrations of zirconium in natural waters may be dominantly controlled by sorption reactions.

Qualitative evidence for behavior in the surficial environment.

Zirconium is one of the elements considered to be immobile in most near-surface geologic environments (Rose et al. 1979). Studies of zirconium concentrations in altered and unaltered or less-altered rocks from the same original geologic unit (Cann 1970) form part of the basis for this conclusion. Other evidence includes the persistence of zircon (ZrSiO_4) in the weathering zone and the low concentrations of zirconium in waters associated with zirconium-rich rocks. Brookins (1983) noted that zirconium was retained within the reactor zones at Oklo, Gabon, although it may have been subject to very local-scale redistribution.

Data from laboratory sorption experiments.

Data on the sorption behavior of zirconium in soil-rock-water systems have been reported by Rhodes (1957), Spitsyn et al. (1956), Prout (1959), Serne and Relyea (1983), and others. Rhodes (1957) has presented data on zirconium sorption coefficients for a soil-water system that show large values ($> 1980 \text{ mg/l}$) up to a pH of 8.0 followed by a decrease to 90 mg/l at a pH of 9.6 and a return to high values at a pH of 12. He attributed the decreased sorption for values of pH from 8 to 12 to the stabilization of colloidal components in solution in this pH range. Spitsyn et al. (1956) observed little movement of zirconium through a sandy soil in a field test under both acidic and alkaline conditions. Serne and Relyea (1983) report large values for zirconium sorption coefficients in all media tested.

Conclusions regarding sorption behavior with respect to expected variations in groundwaters.

The dominance of zirconium hydrolysis reactions in solution suggests that pH will be the dominant groundwater compositional parameter controlling zirconium solubility and sorption behavior. The lack of evidence for zirconium transport in field tests under both acidic and alkaline conditions and the general lack of evidence for mobility of zirconium in the surficial environment combined with the large values of the sorption coefficient reported in the literature for zirconium suggest that in all hydrochemical environments associated with Yucca Mountain in the present-day or in the future this element's sorption coefficients will be large ($> 100 \text{ mg/l}$).

Actinium, Americium, and Samarium

The radionuclides of concern represented by these elements have the following characteristics in common: 1) In groundwater-rock systems of concern in this report, these elements are all present in the +3 oxidation state. 2) In aqueous solutions with compositions typical of groundwaters, the solubility of these elements tends to be controlled by sparingly soluble carbonates, phosphates, fluoride-carbonate complexes, and to a lesser extent, hydroxy-carbonate compounds (Mariano 1989). The elements may also form solid solutions with carbonates, phosphates, fluorides, and oxides of the major cations in groundwaters. 3) The dominant solution species associated with these elements are generally complexes with carbonate, phosphate, and hydroxide ligands (Sillen and Martell 1964, 1971). 4) The solution species tend to have high affinities for adsorption onto oxide surfaces as discussed further below. The radionuclides represented by these elements are all in the "strongly-sorbing" group discussed by Meijer (1992).

Because the chemistry of all three of these elements is similar in aqueous solution and sorption reactions, they will be discussed as a group.

Behavior in solutions representative of Yucca Mountain groundwaters.

The trivalent ions of the rare-earth elements are essentially spherical and form aqueous complexes that are similar to those formed by the alkaline and alkaline-earth elements. Thompson (1979) notes that the partially filled *f* orbital is so effectively shielded from most chemical bonding that the crystal-field effects are about 100 cm^{-1} compared to values of around $30,000 \text{ cm}^{-1}$ for many first-row transition elements. Chemical interactions of the rare-earth elements are almost entirely ionic and the rare-earth elements are not easily polarized owing to their relatively large charge-to-ionic-radius ratio. As noted by Cotton and Wilkinson (1988), the trivalent actinides show many similarities in solution chemistry to the lanthanides. In fact, Nitsche et al. (1994) have used neodymium as a direct analog for americium in solubility studies.

In solution, americium and the rare-earth elements occur as simple (trivalent) cations, carbonate complexes, phosphate complexes, and hydrolysis products (Wood 1990). Complexes with other inorganic ligands (for example, Cl^- , F^- , and SO_4^{2-}) will not be of importance in the water compositions expected in the Yucca Mountain flow system. Therefore, speciation models for the rare-earth elements and trivalent actinides should consider pH, carbonate-ion concentration, and possibly phosphate-ion concentration as key variables. According to Byrne and Kim (1993), phosphate complexes will not be significant unless the ratio of the total phosphate concentration to the total carbonate concentration is greater than 1.3×10^{-3} . This condition makes it unlikely that phosphate rare earths or americium complexes will be important in Yucca Mountain groundwaters. Therefore, carbonate complexes are expected to dominate the solution species for these elements. The solubility-controlling solids in Yucca Mountain groundwaters will likely be carbonates, hydroxycarbonates (Kerrisk 1984b), and possibly phosphates (see the following section).

According to Nitsche et al. (1992, 1994), the solu-

bilities of americium compounds in solutions representative of water compositions expected within Yucca Mountain are approximately 1 to 2×10^{-9} M in J-13 water and 3 to 30×10^{-7} M in UE-25 p#1 water as a function of pH at 25°C . At 60°C , the solubilities of americium compounds were 1×10^{-8} to 2.5×10^{-6} M in J-13 water and 7×10^{-10} to 3×10^{-9} M in UE-25 p#1 water as a function of pH. The solubility-controlling solids were found to be hexagonal and orthorhombic forms of AmOHCO_3 . The speciation of americium in these solutions could not be determined due to the low solubilities of americium in these water compositions relative to the detection limits of the available spectroscopic techniques. Preliminary modeling calculations with the speciation code EQ3 suggest that carbonate complexes dominate in both J-13 and UE-25 p#1 waters at 25° and 60°C (Ogard and Kerrisk 1984).

Qualitative evidence for behavior in the surficial environment.

Although the geological community generally regards the rare-earth elements as immobile during most water-rock alteration processes (Taylor and McLennan 1988), detailed studies of weathering profiles suggest that these elements may be redistributed within these profiles during weathering. Duddy (1980) studied a weathering profile formed on a homogeneous sedimentary rock unit in southeastern Australia. This profile was formed in a cool temperate climate with 200 cm/yr precipitation. The profile contained bleached zones and ferruginous zones in which iron was reduced or oxidized, respectively. The rare-earth elements were up to 7 times enriched in the bleached portions of the profile. Based on the sorption data discussed in the following section, this is somewhat puzzling as one might expect these elements to be coprecipitated or adsorbed to the secondary ferric oxides formed in the profile. In fact, the rare-earth elements appeared to be enriched in vermiculite, an expanding magnesium-ferrous iron trioctahedral clay that formed in the weathering profile as a result of the alteration of biotite. Up to 10 weight per cent of rare-earth elements was reported in ver-

miculites on the basis of electron-probe analyses. The elements originated from the dissolution of apatite ($\text{Ca}_5(\text{PO}_4)_3(\text{F},\text{Cl},\text{OH})$) and other minerals present higher in the profile.

Banfield and Eggleton (1989) studied the rare-earth elements in an Australian weathering profile formed on granite. These authors also noted that these elements were mobile in the profile.

However, they found that (primary) biotite crystals in the granite contained rare-earth-element-rich apatite inclusions or cavities resulting from the dissolution of apatite. The apatite crystals were apparently dissolved during weathering leaving behind fine-grained ($< 10 \mu\text{m}$) rare-earth-element phosphate phases including florencite, rhabdophane ($\text{CePO}_4 \cdot \text{H}_2\text{O}$), and an unidentified phosphate-free aluminum-rare-earth-element mineral, possibly a carbonate, hydroxycarbonate, or fluorocarbonate. Vermiculites were also present in this profile, but they were not analyzed for rare-earth-element contents.

These two studies clearly indicate that the rare-earth elements can be mobilized in the surficial environment. However, they also suggest that this mobilization is generally of a local nature resulting in the precipitation of new rare-earth-element phases or the incorporation of these elements in other secondary phases, such as clays. These studies did not address the question of whether adsorption of the rare-earth elements onto the surfaces of other mineral phases is a significant process in controlling the mobility of these elements in surficial environments. Loubet and Allegre (1977) noted that the light rare-earth elements were not mobilized in the reactor zones at Oklo, Gabon.

Data on the behavior of americium in the surficial environment is limited to anthropogenic examples. Americium was found to be very immobile in most of the studies located in the literature (for example, Means et al. 1978; Carpenter et al. 1987). The main uncertainty regarding the surficial behavior of americium appears to be the degree to which it is mobilized through colloidal transport (for

example, Penrose et al. 1990).

Data from laboratory sorption experiments.

Ion-exchange studies involving the sorption of lanthanide ions on montmorillonitic clays have been reported by Frysinger and Thomas (1960), Aagard (1974), Bruque et al. (1980), and Bonnot-Courtois and Jaffiezic-Renault (1982). These studies conclude that essentially all of the exchange capacity of the clays is available to lanthanide ions and that the exchange reactions are rapid (that is, minutes). Frysinger and Thomas noted that the $\text{Cs}^+ - \text{Y}^{3+}$ binary exchange was not dependent on pH over the range from 3 to 7. At low cesium concentrations, such as are likely to occur in the potential repository horizon, the clay showed a slight preference for the lanthanide ions relative to cesium, and this preference increased with temperature (30–75°C).

Bruque et al. (1980) only studied the exchange of lanthanide ions with hydrogen-montmorillonite, which is not of interest in this report. However, Bonnot-Courtois and Jaffiezic-Renault (1982) studied the exchange reactions in potassium-, sodium- and calcium-exchanged clays, which are of interest. In the latter study, the rare-earth elements, at initial solution concentrations of 10^{-2} to 10^{-4} M, showed distribution coefficients greater than 1.0 only when the concentrations of the major cations, in the case of sodium and potassium, were below 0.1 M and, in the case of calcium, were below 0.01 M. The rare-earth elements were apparently, to a large degree, sorbed irreversibly, as they could not be readily desorbed from the clay.

Koeppenkastrop and De Carlo (1992, 1993) have evaluated the sorption of the rare-earth elements by iron oxides, manganese oxides, and apatite from high ionic-strength aqueous solutions (that is, ultraviolet-irradiated natural seawater). One nanomole of each rare-earth-element radiotracer was equilibrated with approximately 10 mg of the solid phase in 1 kg of seawater. The pH of the system was maintained at 7.8 in all the experiments. The percentage of rare-earth element adsorbed on FeOOH and MnO_2 was measured in the presence and

IV. Sorption and Sorption Modeling Studies

absence of carbonate. Carbonate appeared to affect the kinetics of the adsorption reactions but not the extent of adsorption at equilibrium. The sorption reactions equilibrated within tens of minutes. Under the conditions of the experiments, the rare-earth elements are shown to have very high affinities for the oxide and phosphate phases ($K_d \gg 1,000$ ml/g). Koepfenkastro and De Carlo (1993) further state that modeling of sorption data derived from experiments with natural particles indicates that desorption rate constants are much smaller than adsorption rate constants.

The high affinity of the rare-earth elements for iron and manganese-oxide phases suggests that these phases would act as "getters" for these elements in surficial environments. Yet the data reported by Duddy (1980) suggest that the rare-earth elements in the weathering profile he studied were preferentially incorporated in vermiculite in the "bleached" zones and not adsorbed onto ferric oxides in the ferruginous zones. This effect suggests that there were other constituents in the solution phase of the profile investigated by Duddy (1980) that had higher affinities for the oxide surfaces than the rare-earth elements and that they were present in sufficient quantity to saturate the available surface sites. A possible candidate would be the Al^{3+} ion (for example, see Brown et al. 1956).

Stammose and Dolo (1990) reported on batch-sorption experiments with americium (10^{-8} M) on clay as a function of pH and ionic strength. The clay used in the experiments was a mixed-layer clay consisting of kaolinite and smectite. At ionic strengths of 0.01 and 0.1 M ($NaClO_4$), the americium sorption coefficient was greater than 10^3 mg/l over the entire pH range (3–10) addressed by the experiments. In the higher ionic-strength solutions (1 and 3 M), the sorption coefficients were low (10 mg/l) at a pH of 2 but increased to values in the range of 10^4 to 10^5 mg/l for pH values greater than 6.

Overall, the data presented by these authors suggest: 1) the ion-exchange sites on the clay have a

very high selectivity for americium at trace concentrations; 2) sodium ions at sufficiently high concentrations can displace the americium from these sites; 3) americium is also adsorbed in surface-complexation reactions; 4) the surface-complexation reactions define a sorption edge that has minimum values at low pH and reaches a maximum at a pH of approximately 7; 5) americium is adsorbed as an inner-sphere complex, and its adsorption affinity in surface-complexation reactions is therefore not a function of ionic strength; and 6) at trace americium concentrations, carbonate complexation of americium may compete with surface-complexation reactions in the pH range from 8 to 10, leading to a slight decrease in adsorption in this range.

Allard and Beall (1979) have presented americium sorption-coefficient data for a range of mineral types including clays, feldspars, carbonates, phosphates, oxides, oxyhydroxides, and other less common minerals. The sorption coefficients were measured over a range of pH from 4 to 9 in a low ionic-strength (synthetic) groundwater similar in composition to an average Yucca Mountain groundwater. Initial americium solution concentrations were in the range from 1.8 to 5.0×10^{-9} M. Data presented for clay minerals indicate that ion exchange occurred on these minerals in the lower pH range (< 6). Surface recrystallization reactions are evident in the low pH data for apatite (also, see Jonasson et al. 1985) and fluorite. On the remaining silicates and nonsilicates, americium appears to sorb dominantly by surface-complexation reactions. In all cases, the sorption coefficient values are in excess of 10^3 mg/l over the pH range likely to be encountered in the Yucca Mountain groundwaters.

In summary, trivalent actinium, americium, and samarium likely sorb by at least two distinct mechanisms. At pH values less than approximately 6, ion-exchange reactions on clays and other ion-exchanging minerals may dominate the adsorption behavior of these elements in low ionic-strength solutions. These reactions will show dependencies

on ionic strength and ion selectivity. At pH values greater than 6, sorption appears to involve primarily inner-sphere surface-complexation reactions. Although these reactions are independent of ionic strength, they will likely be subject to competition with other sorbing species at sufficiently high sorption densities. In the pH range from 8 to 10, carbonate-complexation reactions in solution may compete with the surface-complexation reactions involving these elements. However, the surface-complexation reactions are expected to dominate over carbonate-complexation reactions in Yucca Mountain groundwaters.

Sorption data obtained on Yucca Mountain samples.

Sorption coefficients for cerium, europium, and americium have been determined for a variety of rock samples from Yucca Mountain and in several groundwater compositions from the site (Thomas 1987; Knight and Thomas 1987). The data are generally consistent with the conclusions stated in the previous section. However, several additional points should be emphasized. First, experiments with rock samples that contained calcite (for example, G1-2901 and G2-723) or groundwater that was saturated with calcite (such as UE-25 p#1) showed very large sorption coefficients for these elements. This result suggests the radionuclides were either coprecipitated with carbonates (for example, calcite) or formed solid solutions on the surfaces of existing carbonates. Because groundwaters in the unsaturated zone at Yucca Mountain are likely near saturation with calcite, this observation suggests the trivalent lanthanides and actinides will not be mobile in the proposed repository horizon. Second, experiments on samples with more than a few percent clay (for example, G1-3658) also showed high sorption coefficients. For these rock types, the ionic strength of the groundwaters may play a role in determining the magnitude of the sorption coefficients for these elements. Third, experiments with groundwaters containing high carbonate concentrations (such as UE-25 p#1) show large sorption coefficients for these elements, suggesting that carbonate complexation in solution

does not lead to significant decreases in the sorption coefficients for these elements in Yucca Mountain groundwaters.

Conclusions regarding sorption behavior with respect to expected variations in groundwaters.

The impact of variations in groundwater compositional parameters within the ranges expected in Yucca Mountain on the sorption behavior of actinium, americium, and samarium should be relatively minor. Over the expected pH range (6–9), the trivalent actinides and lanthanides appear to sorb primarily by inner-sphere surface-complexation mechanisms. These mechanisms are not sensitive to variations in ionic strength. Further, these elements appear to have high affinities for the mineral surfaces typically available in the Yucca Mountain rock units over the entire pH range expected. This result suggests that the trivalent actinide and lanthanide radionuclides will be strongly sorbed ($K_d > 100$ ml/g) over the entire range of expected groundwater compositions.

Plutonium

Behavior in solutions representative of Yucca Mountain groundwaters.

The solution behavior of the element plutonium is the most complicated of all the elements of interest and the least understood, particularly in near-neutral solutions representative of water compositions expected within the Yucca Mountain flow system. Plutonium can have several oxidation states in a given solution, and it can form complexes with a variety of ligands.

According to Nitsche et al. (1992, 1994), plutonium will be present in the +3, +4, +5, and +6 oxidation states in solutions representative of water compositions expected within Yucca Mountain. The +5 and +6 oxidation states should predominate in solution at redox potentials in the range of 230 to 350 mV. In J-13 and UE-25 p#1 waters, the +5 oxidation states should be dominant (60–80%) at 25°C. Most of the remaining plutonium in solution is in the +6 oxidation state in J-13 water and

IV. Sorption and Sorption Modeling Studies

the +4 oxidation state in UE-25 p#1 water.

Experimentally determined solubilities range from 3.0×10^{-7} to 1.0×10^{-6} M at 25°C. The solubility-controlling solids were found to be mixtures of polymeric Pu(IV) and smaller amounts of plutonium carbonates. The solubilities measured at pH values of 6 and 7 are consistent with the data reported by Rai et al. (1980). However, the solubilities measured for a pH of 8.5 exceed those reported by Rai et al. for amorphous Pu(OH)₄ in 0.0015 M CaCl₂. This result suggests that carbonate complexation of plutonium is significant at a pH of 8.5 in the Yucca Mountain groundwaters.

At 60°C, the +6 oxidation state was dominant (> 80%) in the UE-25 p#1 water at all three pH values. In J-13 water, the +5 and +6 oxidation states were present in nearly equal amounts (50%) at a pH of 7, whereas the +5 state dominated (60%) at a pH of 8.5 and the +6 state dominated (70%) at a pH of 6.

Experimentally determined solubilities at 60°C in J-13 water ranged from 2.7×10^{-8} M at a pH of 6 to 1.2×10^{-7} M at a pH of 8.5. For UE-25 p#1 water, the solubilities ranged from 4.5×10^{-7} M at a pH of 7 to 1.0×10^{-6} M at a pH of 8.5. The solubility-controlling solids at 60°C were found to be amorphous Pu(IV) polymer and PuO₂.

The speciation of plutonium in these solutions could not be determined due to the low solubilities of plutonium in these water compositions relative to the detection limits of the available spectroscopic techniques. Modeling calculations with the EQ3 speciation computer code suggest that in J-13 water at 25°C the plutonyl ion and various carbonate complexes are most important at pH values from 6 to 7, whereas carbonate complexes and hydrolysis products are most important at a pH of 8.5 (Nitsche 1991). Speciation in the UE-25 p#1 water has not been modeled.

It is noteworthy that the experimentally determined redox behavior of plutonium in solution was quite

distinct from the behavior predicted on the basis of EQ3 calculations (Nitsche 1991). The causes for the differences in measured and calculated behavior have not been defined. They could involve various types of kinetic effects, including radiolysis effects, as well as the quality of the literature data in the EQ3 database. In any case, the uncertainties in our knowledge of the solution behavior of plutonium will make it difficult to properly interpret the sorption behavior of that element.

Qualitative evidence for behavior in the surficial environment.

Although naturally occurring plutonium has been detected at ultratrace levels in the environment, there is little documentation of the chemical controls on the mobility of this plutonium. However, anthropogenic plutonium has been present in the environment for decades. Data on the environmental behavior of this plutonium provide some indications of the behavior to be anticipated for plutonium emplaced in the proposed repository at Yucca Mountain.

Various papers in the literature discuss the transport of plutonium in the surficial environment around process stream outfalls or burial sites (for example, Means et al. 1978; Price and Ames 1978; Polzer et al. 1983). Unfortunately, the data on plutonium transport discussed in these papers are difficult to apply to the Yucca Mountain site because the waste streams included various types of organic ligands (for example, EDTA) that tend to enhance the transport of plutonium at these sites. In addition, the initial pH of many of these waste streams was in the acid range (2–4). Low pH conditions are not expected in the Yucca Mountain flow system. Organic ligands may be present at trace levels in this flow system, but they are not expected to play a major role in radionuclide transport.

The results of studies of plutonium transport in areas exposed to physical dispersal processes (for example, safety tests of nuclear weapons) are also difficult to interpret because of subsequent disturbances of the surface soils by wind, burrowing ani-

mals, construction activities, and so forth (for example, Essington et al. 1978).

Studies of the fate of global fallout for atmospheric nuclear weapons tests are more appropriate to the prediction of the transport of plutonium from a potential repository at Yucca Mountain. Most of these studies have involved the measurement of plutonium activities in seawater, lake water, and associated sediments (for example, Sholkovitz 1983). In general, these studies find that the bulk of the fallout-derived plutonium is present in the sediments with minor concentrations found in the waters. Interestingly, the plutonium present in the waters is often an oxidized form (that is, +5 or +6), whereas the fraction in the sediment is thought to be a reduced form (Waters 1983). "Distribution coefficients" have been calculated based on the water and sediment plutonium concentrations even though the water and sediment samples may be from areas that are separated by tens of kilometers. This makes it difficult to evaluate the calculated distribution coefficients in relation to sites such as the potential repository in Yucca Mountain.

More pertinent perhaps are the measurement of plutonium concentrations in oceanic sediments and their associated pore waters (Buesseler and Sholkovitz 1987). Such studies invariably yield sorption coefficients for plutonium in the range of 10^3 to 10^5 mg/l with the lower values observed in the more oxidized sediments. Given the high ionic strength of seawater (that is, the pore waters), these data suggest that ionic-strength effects are not an issue in the plutonium sorption behavior in natural systems. However, complexation of plutonium by carbonate can be significant and appears to be the cause for elevated plutonium activities in several high alkalinity (0.3–3.0 M) lakes in the western United States (Sanchez et al. 1985). Because alkalinity values are expected to be orders of magnitude lower within the Yucca Mountain flow system relative to the levels found in these lakes, carbonate complexation in the solution phase should not be an issue at this site.

An important aspect of all the studies on plutonium sorption behavior is the issue of redox disequilibrium. In seawater and many lake waters, the inorganic species of plutonium in solution appears to be dominated by the +5 and +6 oxidation states with the +3 and +4 states present at much lower concentrations (Waters 1983). In the solid phase, the oxidation state is thought to be predominantly +4. This aspect of plutonium solution chemistry has been studied in the laboratory for many years and appears to involve various disproportionation reactions that are not fully understood (for example, Newton et al. 1986).

The question of concern to the present study is how groundwater compositional parameters will effect this redox disequilibrium and, in turn, the sorption behavior of plutonium. In the disproportionation experiments reported by Newton et al. (1986) and in the solubility experiments reported by Nitsche et al. (1992, 1994), plutonium concentrations in the experiments were sufficiently high that radiation effects were evident. An important question is "If plutonium is present at trace levels and not in contact with a 'pure' plutonium compound, are disproportionation reactions still a factor?" If they are not, then the next question would be "What is the stable oxidation state of plutonium when it is present at trace levels in Yucca Mountain groundwaters?" If the +5 or +6 oxidation states of plutonium are the dominant stable states in groundwaters such as those found within Yucca Mountain, as suggested by the experiments of Nitsche et al. (1992, 1994), then plutonium might be as mobile as neptunyl in the far-field of the potential repository, assuming it is present as the plutonyl ion or its complexes. On the other hand, if the +4 or +3 oxidation states are the dominant stable states in these groundwaters, this element would likely behave as other +3 and +4 actinides and be strongly sorbed with minimal migration potential.

Data from laboratory sorption experiments.

Allard (1982) reported results on experiments involving plutonium sorption on quartz, apatite, attapulgite, montmorillonite, and various minerals

IV. Sorption and Sorption Modeling Studies

rich in ferrous iron in a dilute groundwater containing plutonium at 1.8×10^{-11} M. For all the minerals, the sorption coefficients were greater than 10^3 ml/g over a pH range from 4 to 9. Apatite, attapulgite, biotite, and montmorillonite showed sorption coefficients greater than 10^4 ml/g over this pH range. Torstenfelt et al. (1988) presented data for plutonium sorption on feldspars, clays, and granite in contact with J-13 water. The sorption coefficients reported by them are generally between 100 to 200 ml/g in neutral to alkaline solutions. These authors emphasized the importance of proper experimental technique in the determination of sorption coefficient values for plutonium and noted the potential for colloid formation in these types of experiments. Data indicating high affinity of plutonium for ferric oxyhydroxide, manganese oxide, and carbonate mineral surfaces were presented by Means et al. (1978), Keeney-Kennicutt and Morse (1985), and Sanchez et al. (1985). Means et al. noted that manganese oxides sorb plutonium more strongly than ferric oxyhydroxides in natural environments (presumably as a result of redox reactions on the manganese-oxide surface).

Measurements of plutonium sorption coefficients involving Yucca Mountain rock samples and J-13 groundwater were summarized by Thomas (1987). The following observations are considered the most significant. First, the values measured for the plutonium sorption coefficient range from 20 to greater than 4,500 ml/g with most values lying between 100 to 2,000 ml/g at a pH of from 8.2 to 8.8. Second, the coefficients determined during the desorption experiments were occasionally in the range of the sorption coefficient values, but more typically, they were 10 to 20 times larger, reflecting the irreversibility of the sorption reactions. Third, zeolitic samples typically had lower sorption coefficient values than vitric or devitrified samples. It appears that rocks that have essentially no reduction capacity remaining (that is, samples lacking ferrous iron or sulfide) show the lowest sorption coefficients for plutonium. Fourth, samples with calcite or clay showed the largest sorption coefficients ($> 4,500$ ml/g for samples with

30% calcite). Fifth, based on the six to eight experiments for which data are available, there was up to a factor of twelve variation in sorption coefficients as a function of groundwater composition. Water from well UE-25 p#1 was associated with the largest values (240–540 mg/l, sorption-desorption) with waters from wells H-3 and J-13 showing the lowest values (20–230 ml/g). The higher values obtained with UE-25 p#1 water may reflect calcite precipitation. Sixth, there did not appear to be a dependence of the sorption coefficient on pH over the range from 7 to 9, although the available data are limited on this issue. Seventh, there was less than a factor of four dependence of the sorption coefficient on radionuclide concentration over the range from 10^{-9} to 10^{-12} M.

Conclusions that can be drawn from these data include: 1) the plutonium sorption coefficient will be greater than 100 ml/g for most of the groundwater and rock compositions likely to be encountered within Yucca Mountain; 2) calcite and clay promote plutonium sorption/coprecipitation and may retard plutonium migration in fractures; and 3) the redox state of the groundwaters and of the rock units in which they occur may be critical to the sorption behavior of plutonium.

We studied the sorption of plutonium onto the three main types of tuff in J-13 water (under oxidizing conditions) using a carbon-dioxide overpressure (to obtain a pH of 7). To identify the sorbing minerals in the tuffs, we also studied sorption onto the pure minerals hematite, clinoptilolite, albite, and quartz. The results of the batch-sorption experiments for plutonium are summarized in Fig. 21. Because plutonium sorbs onto nongeologic media, the batch-sorption distribution coefficients reported in Fig. 21 are based on the concentration of plutonium in the control solutions. The affinity of tuffs for plutonium at a pH of 7 in decreasing order is zeolitic $>$ vitric $>$ devitrified. The affinity of minerals for plutonium in decreasing order is hematite $>$ clinoptilolite $>$ albite $>$ quartz. Inspection of Fig. 21 indicates that plutonium sorption is nonlinear in the concentration range

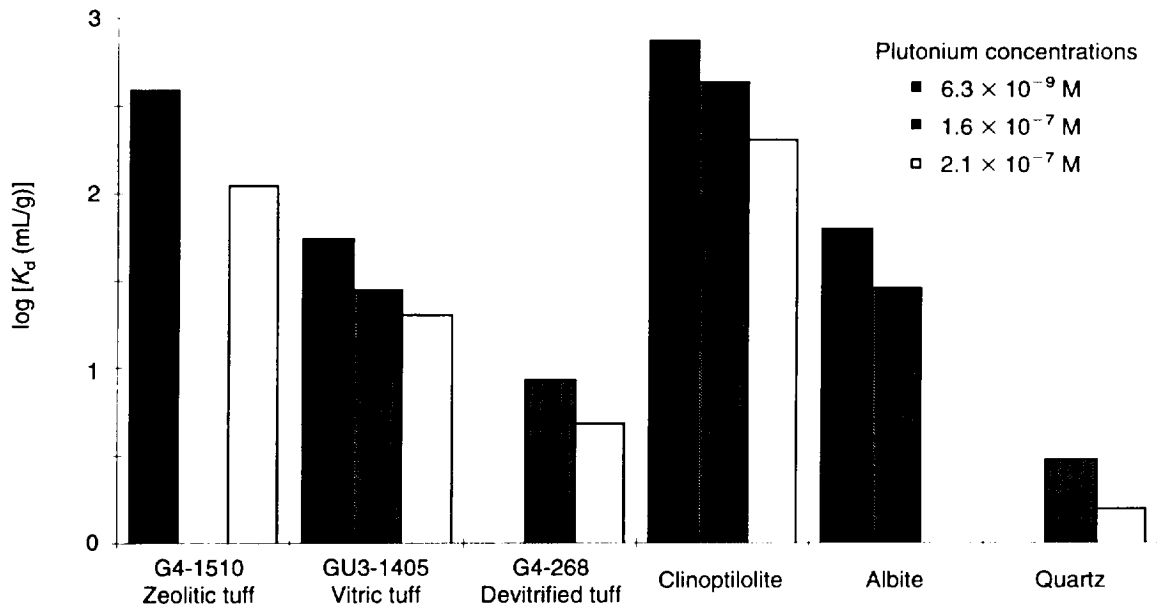


Figure 21. Plutonium Sorption. The logarithm of the batch-sorption distribution coefficient, $\log K_d$, is shown for the sorption of plutonium in J-13 well water at a pH of 7 and the specified initial plutonium concentrations. All solids, except clinoptilolite, were wet sieved to particle sizes ranging from 75 to 500 μm . The periods of pretreatment and sorption were each 3 days.

from 6×10^{-9} to 2×10^{-7} M.

Nitsche et al. (1993a) report that even when a plutonium solution in J-13 or UE-25 p#1 water is prepared starting in the +4 oxidation state, the predominant final oxidation state is +5, or Pu(V). The solution used for our plutonium sorption experiments was prepared from a well-characterized Pu(V) acidic stock in J-13 well water. Consequently, it would be reasonable to assume that the plutonium would have remained predominantly in the +5 oxidation state in the solution used for the sorption studies.

Comparison of the data of Fig. 21 with the results of similar experiments with neptunium and uranium indicates that significant plutonium sorption occurred in tuffs and minerals that exhibit very small sorption of Np(V) and U(VI). This result is very puzzling; if plutonium in J-13 well water is predominantly Pu(V) and Pu(VI), it is expected that its sorption behavior would have been similar

to that observed for Np(V) and U(VI). Several possible explanations of the plutonium sorption results are: 1) Nitsche's data for the oxidation states are incorrect, and the predominant plutonium oxidation state in J-13 well water at a pH of 7 is Pu(IV), not Pu(V) and Pu(VI); 2) the Pu(IV) species is what sorbs from J-13 water but a re-equilibration in the solution phase produces more Pu(IV) to maintain equilibrium (which implies that the kinetics of plutonium speciation in solution are fast); and 3) Pu(V) and Pu(VI) reduce to Pu(IV) at solid surfaces (as a result of changes in the solution redox potential in the presence of the solid phases).

The sorption of plutonium onto tuffs and minerals in J-13 and synthetic UE-25 p#1 water under atmospheric conditions was studied (Figs. 22 to 27) as a function of time and initial plutonium solution concentration. Inspection of these figures indicates that plutonium sorption is extremely slow (possibly due to a redox reaction at the solid surface). Even after 32 days of sorption, equilibration

continued on page 73

IV. Sorption and Sorption Modeling Studies

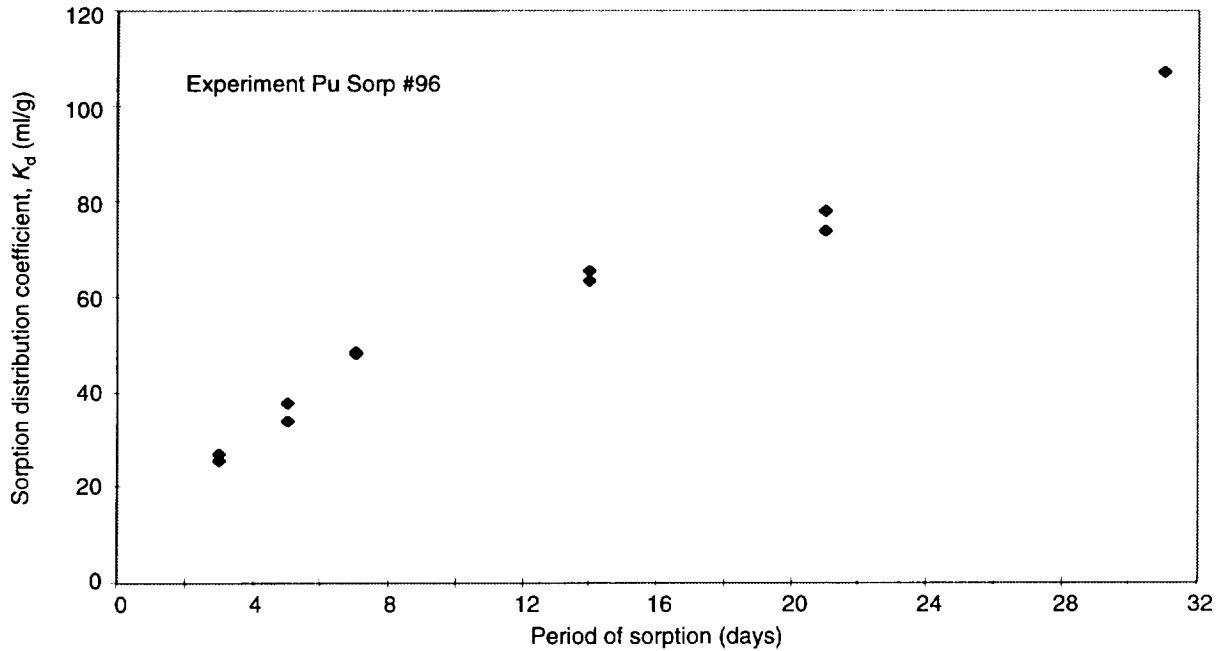


Figure 22. Plutonium Sorption onto Devitrified Tuff in J-13 Water. The plot shows plutonium sorption onto tuff sample G4-272 as a function of time under atmospheric conditions with an original plutonium concentration in J-13 well water of 2.4×10^{-7} M.

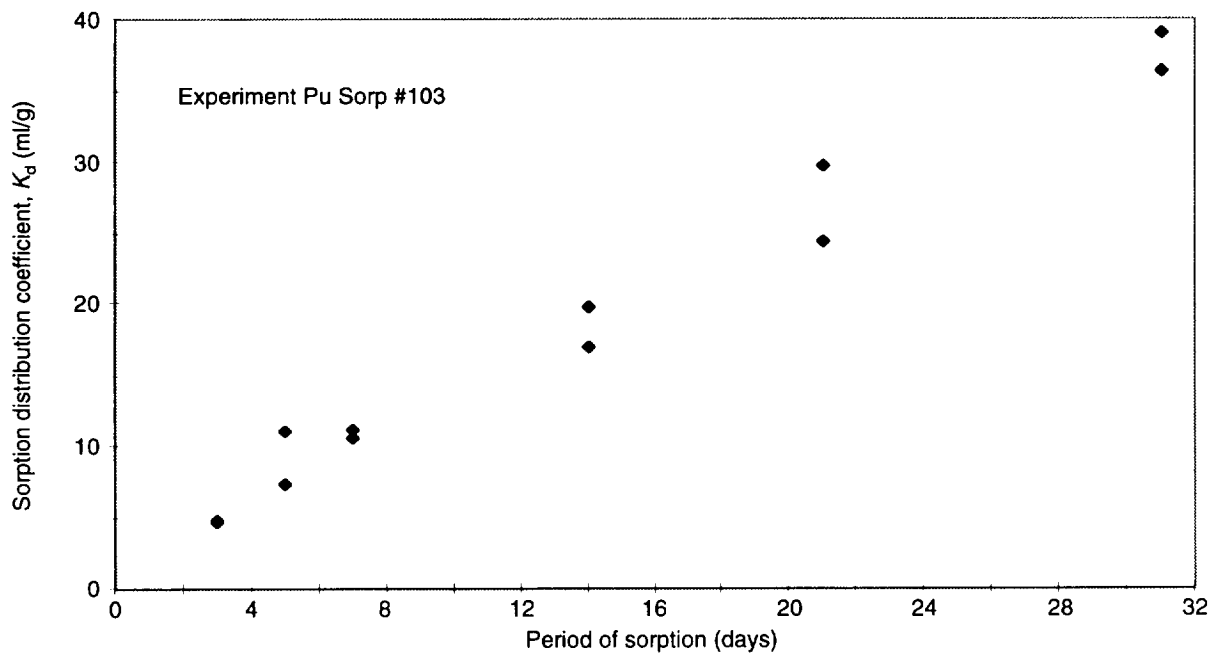


Figure 23. Plutonium Sorption onto Devitrified Tuff in Synthetic UE-25 p#1 Water. The plot shows plutonium sorption onto tuff sample G4-272 as a function of time under atmospheric conditions with an original plutonium concentration in synthetic UE-25 p#1 water of 2.4×10^{-7} M.

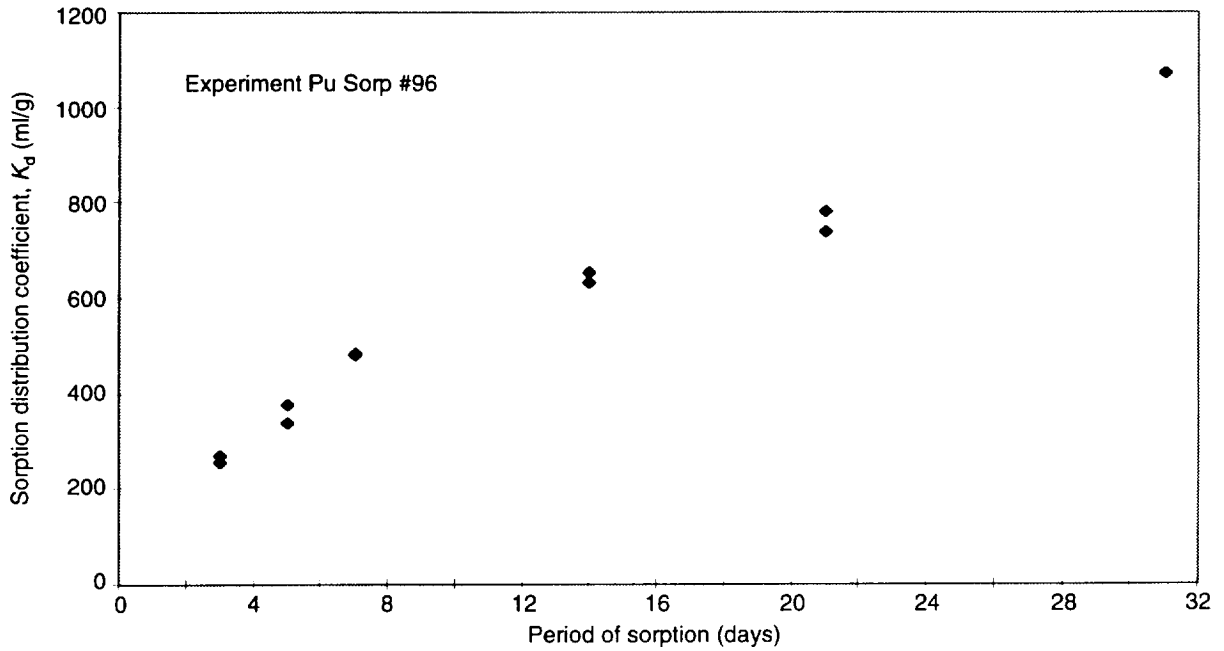


Figure 24. Plutonium Sorption onto Vitric Tuff in J-13 Water. This plot shows plutonium sorption onto tuff sample GU3-1414 as a function of time under atmospheric conditions with an original plutonium concentration in J-13 well water of 2.4×10^{-7} M.

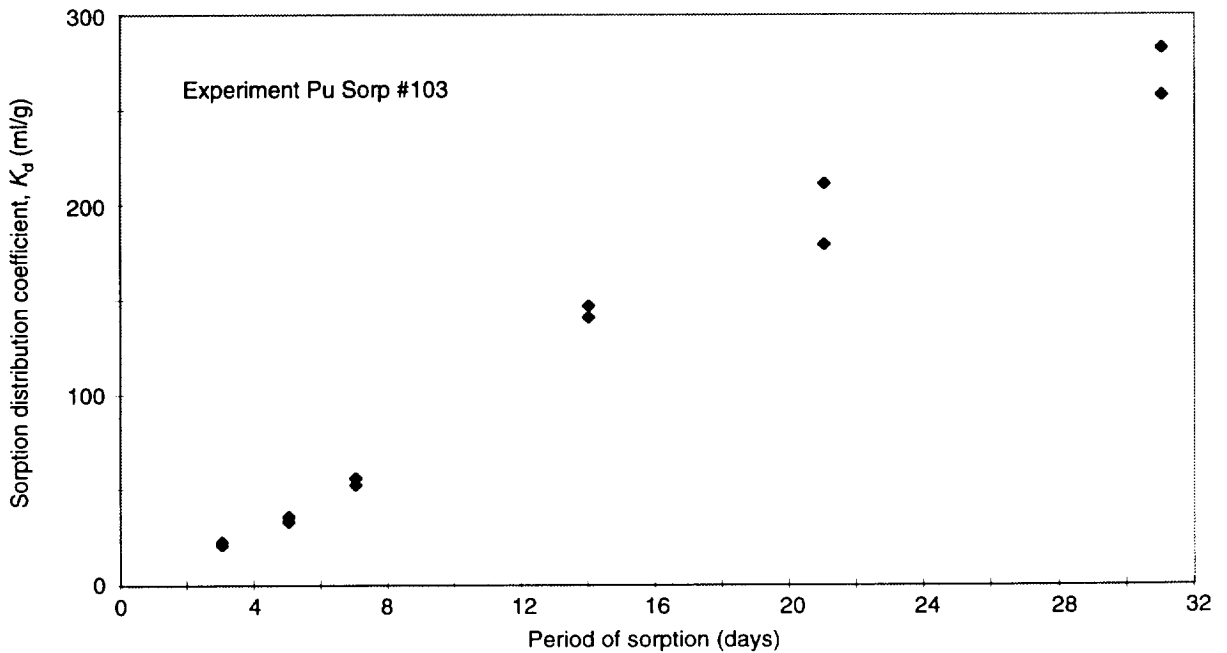


Figure 25. Plutonium Sorption onto Vitric Tuff in Synthetic UE-25 p#1 Water. The plot shows plutonium sorption onto tuff sample GU3-1414 as a function of time under atmospheric conditions with an original plutonium concentration in synthetic UE-25 p#1 water of 2.4×10^{-7} M.

IV. Sorption and Sorption Modeling Studies

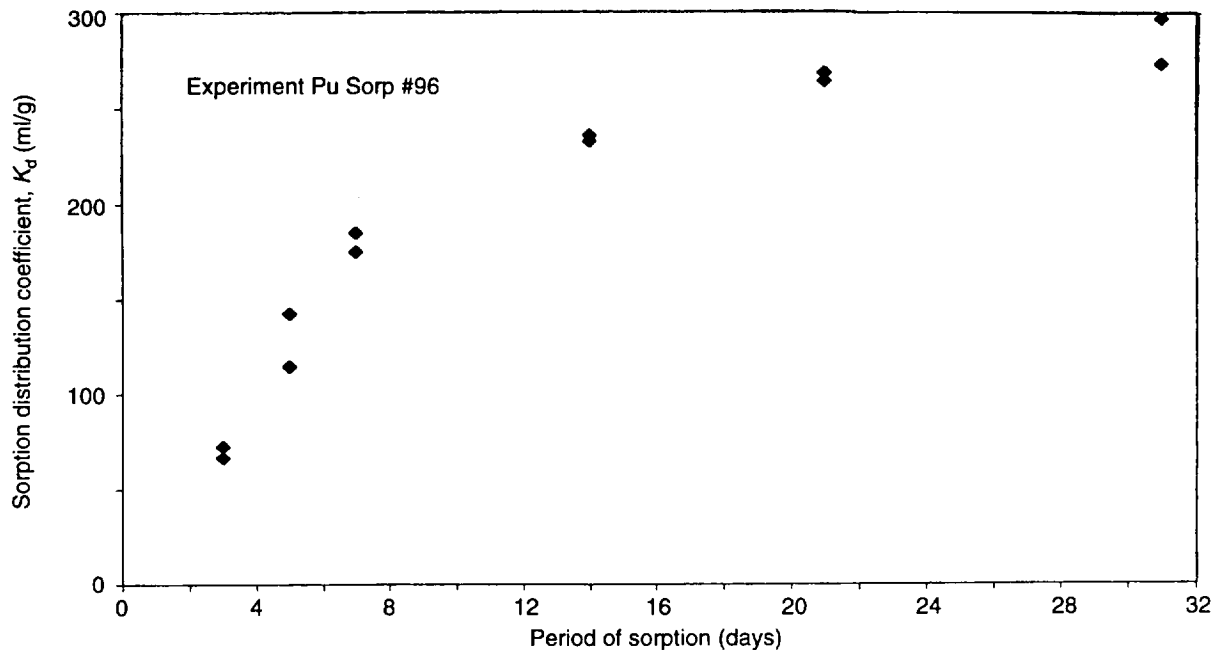


Figure 26. Plutonium Sorption onto Zeolitic Tuff in J-13 Water. This plot shows plutonium sorption onto tuff sample G4-1515 as a function of time under atmospheric conditions with an original plutonium concentration in J-13 well water of 2.4×10^{-7} M.

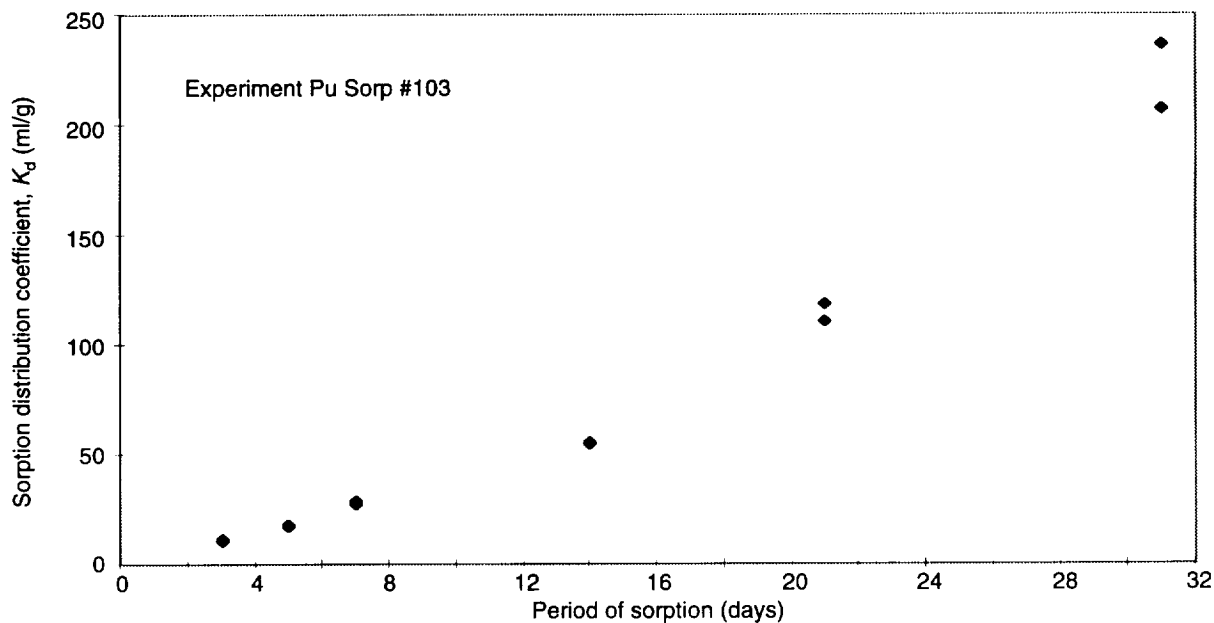


Figure 27. Plutonium Sorption onto Zeolitic Tuff in Synthetic UE-25 p#1 Water. The plot shows plutonium sorption onto tuff sample G4-1515 as a function of time under atmospheric conditions with an original plutonium concentration in synthetic UE-25 p#1 water of 2.4×10^{-7} M.

continued from page 69

had not been achieved. The sorption of plutonium onto the tuffs and minerals is very substantial.

Table 13 summarizes the ranges for sorption distribution coefficients in Yucca Mountain groundwaters for plutonium. The sorption isotherms for plutonium (Figs. 28 to 45) indicate that plutonium sorption as a function of radionuclide concentration cannot be expressed using a K_d ; the isotherms are generally nonlinear. However, given the high affinity of Yucca Mountain tuffs for plutonium and the other observations made in this study, it appears that using a K_d to predict plutonium radionuclide transport in performance-assessment calculations will provide conservative predictions for the release of radionuclides.

Conclusions regarding sorption behavior with respect to expected variations in groundwaters. On the basis of the discussion in the previous sections, it appears the most important groundwater compositional parameter in relation to plutonium sorption is the redox potential. Closely related to this parameter is the abundance of ferrous iron in the rock units. Note that redox potentials in

groundwaters may not reflect equilibrium with the host rock (Lindberg and Runnells 1984). Complexation reactions with inorganic ligands in solution and variations in solution pH appear to have less significant impacts on the sorption behavior of plutonium in Yucca Mountain rock-water systems.

Cesium, Radium, and Strontium

Behavior in solutions representative of Yucca Mountain groundwaters.

These elements show relatively simple solution behavior in typical groundwaters. They are not subject to changes in oxidation state in the groundwater compositions expected in Yucca Mountain. Radium and cesium are invariably present as the simple Ra^{2+} and Cs^+ cations in the expected groundwater compositions (Ogard and Kerrisk 1984). Strontium exists primarily as the Sr^{2+} ion in these waters but may also be present as the neutral aqueous species $SrSO_4$ at concentrations of a few per cent of the total strontium solution concentration (Ogard and Kerrisk 1984).

continued on page 83

Table 13. Plutonium Sorption Distribution Coefficients (under atmospheric conditions)

Solid Phase	K_d Range in J-13 Water (ml/g)	K_d Range in Synthetic UE-25 p#1 Water (ml/g)
Vitric tuff	600 – 2,000	100 – 400
Zeolitic tuff	300 – 500	100 – 400
Devitrified tuff	40 – 100	20 – 70
Synthetic hematite	> 10,000	> 10,000
Montmorillonite	> 10,000	> 10,000
Clinoptilolite	600 – 3,000	2,000 – 5,000
Calcite	200 – 1,000	100 – 800
Gibbsite	0 – 10	10 – 90
Albite	3 – 10	< 10
Quartz	< 10	< 10

IV. Sorption and Sorption Modeling Studies

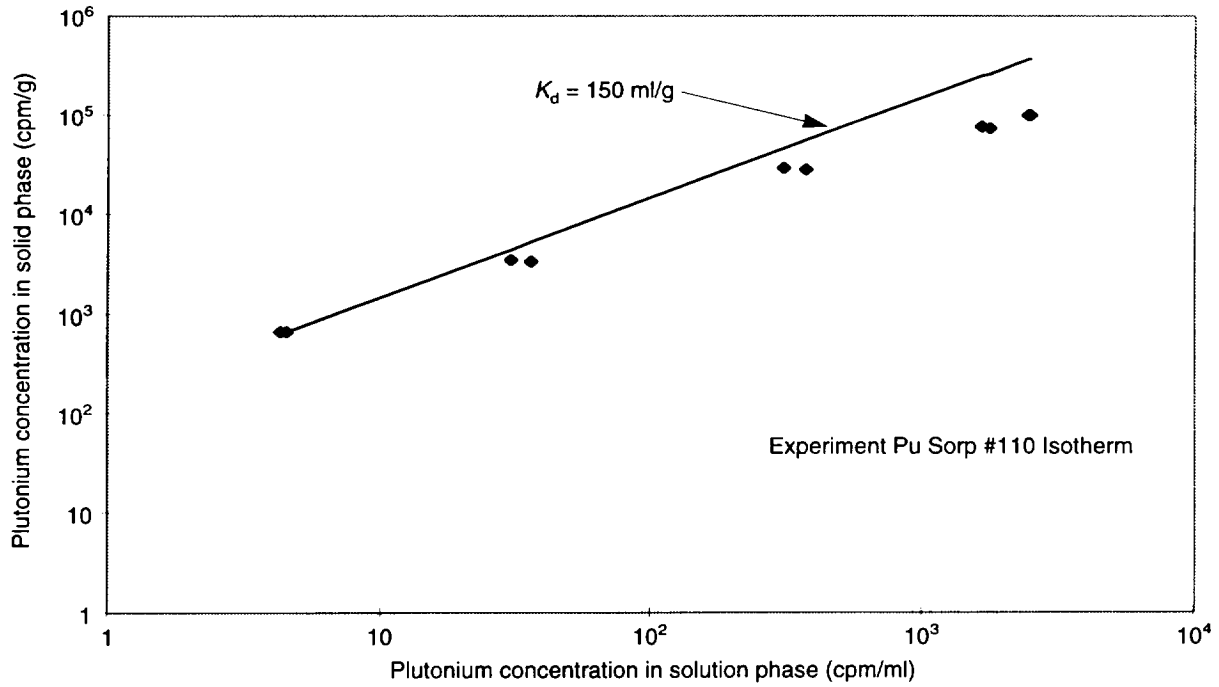


Figure 28. Plutonium Isotherm for Devitrified Tuff in J-13 Water. This plot shows plutonium sorption data (diamonds) and a linear isotherm (line) for sorption onto the tuff sample G4-272 under atmospheric conditions in J-13 well water. The period of sorption was 21 days.

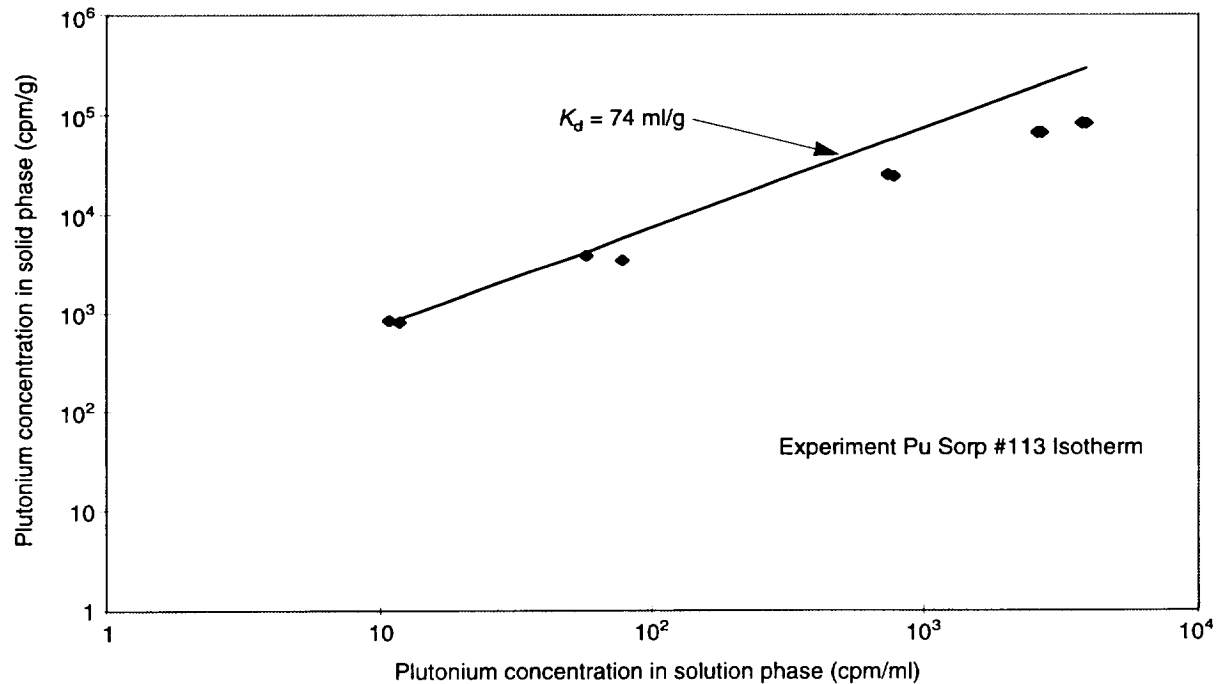


Figure 29. Plutonium Isotherm for Devitrified Tuff in Synthetic UE-25 p#1 Water. This plot shows plutonium sorption data (diamonds) and a linear isotherm (line) for sorption onto the tuff sample G4-272 under atmospheric conditions in synthetic UE-25 p#1 water. The period of sorption was 21 days.

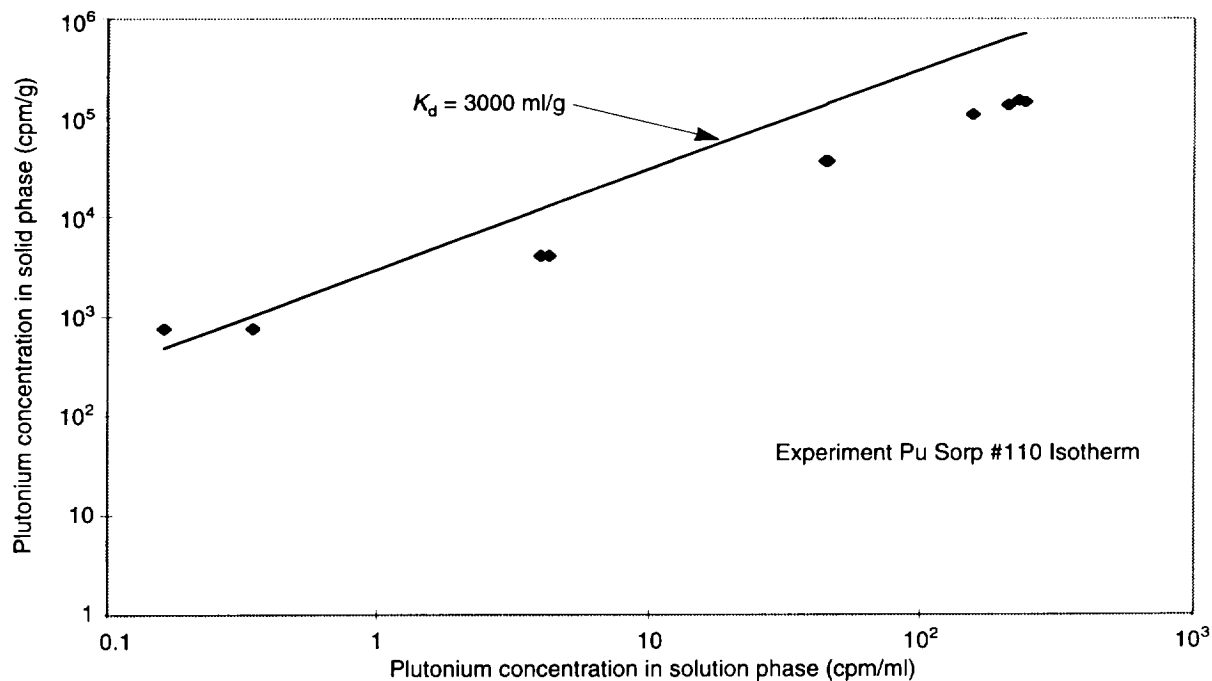


Figure 30. Plutonium Isotherm for Vitric Tuff in J-13 Water. This plot shows plutonium sorption data (diamonds) and a linear isotherm (line) for sorption onto the tuff sample GU3-1414 under atmospheric conditions in J-13 well water. The period of sorption was 21 days.

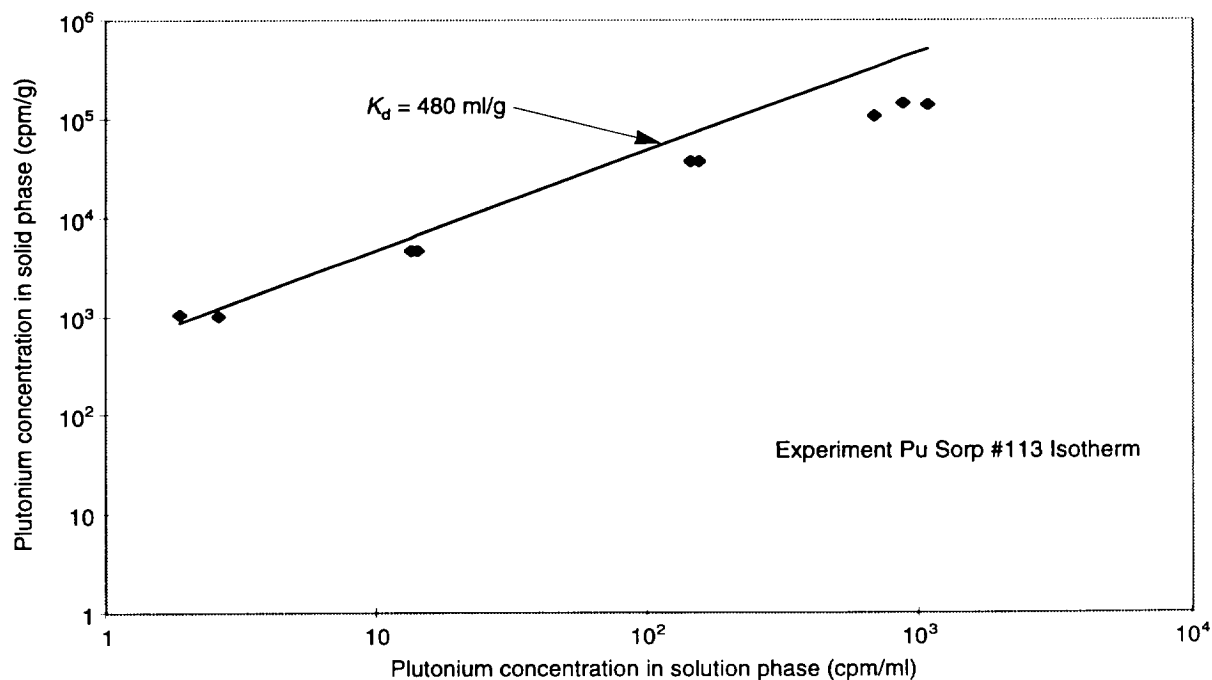


Figure 31. Plutonium Isotherm for Vitric Tuff in Synthetic UE-25 p#1 Water. This plot shows plutonium sorption data (diamonds) and a linear isotherm (line) for sorption onto the tuff sample GU3-1414 under atmospheric conditions in synthetic UE-25 p#1 water. The period of sorption was 21 days.

IV. Sorption and Sorption Modeling Studies

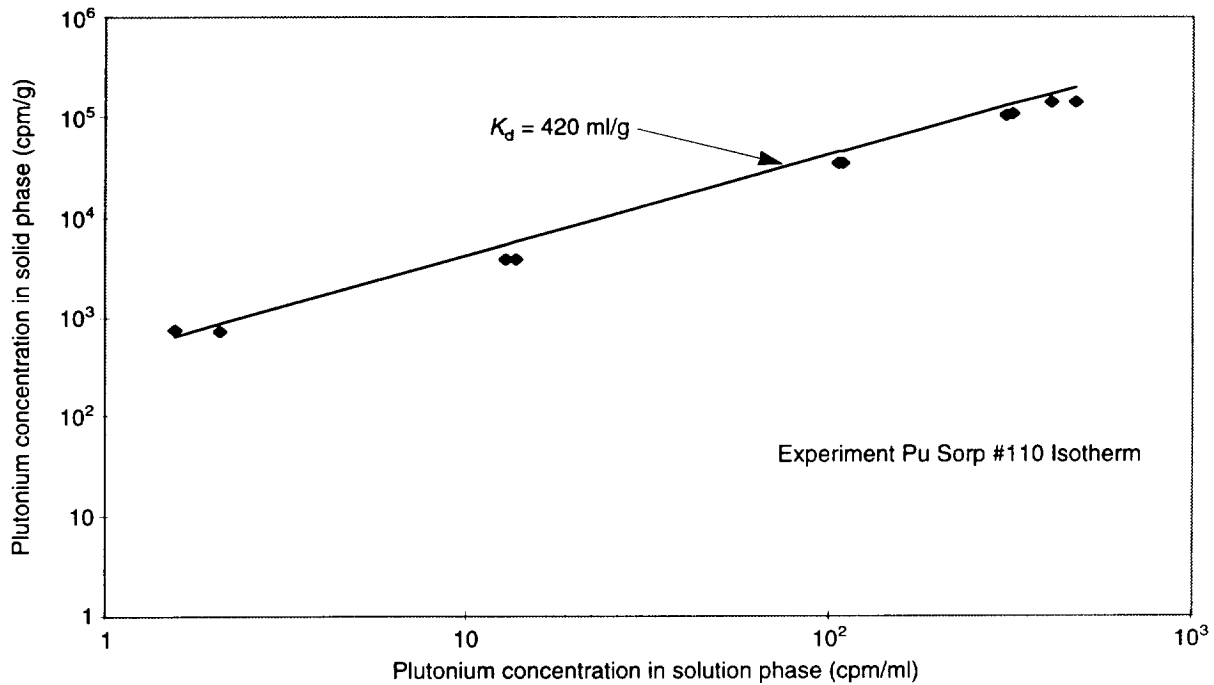


Figure 32. Plutonium Isotherm for Zeolitic Tuff in J-13 Water. This plot shows plutonium sorption data (diamonds) and a linear isotherm (line) for sorption onto the tuff sample G4-1515 under atmospheric conditions in J-13 well water. The period of sorption was 21 days.

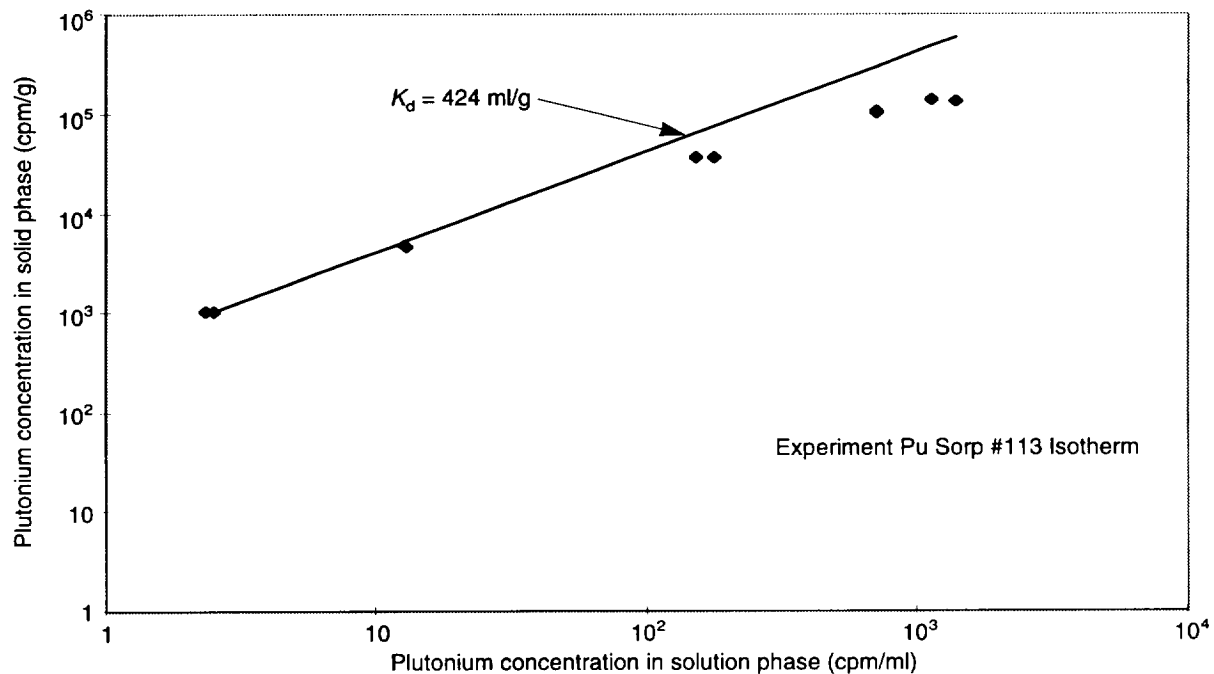


Figure 33. Plutonium Isotherm for Zeolitic Tuff in Synthetic UE-25 p#1 Water. This plot shows plutonium sorption data (diamonds) and a linear isotherm (line) for sorption onto the tuff sample G4-1515 under atmospheric conditions in synthetic UE-25 p#1 water. The period of sorption was 21 days.

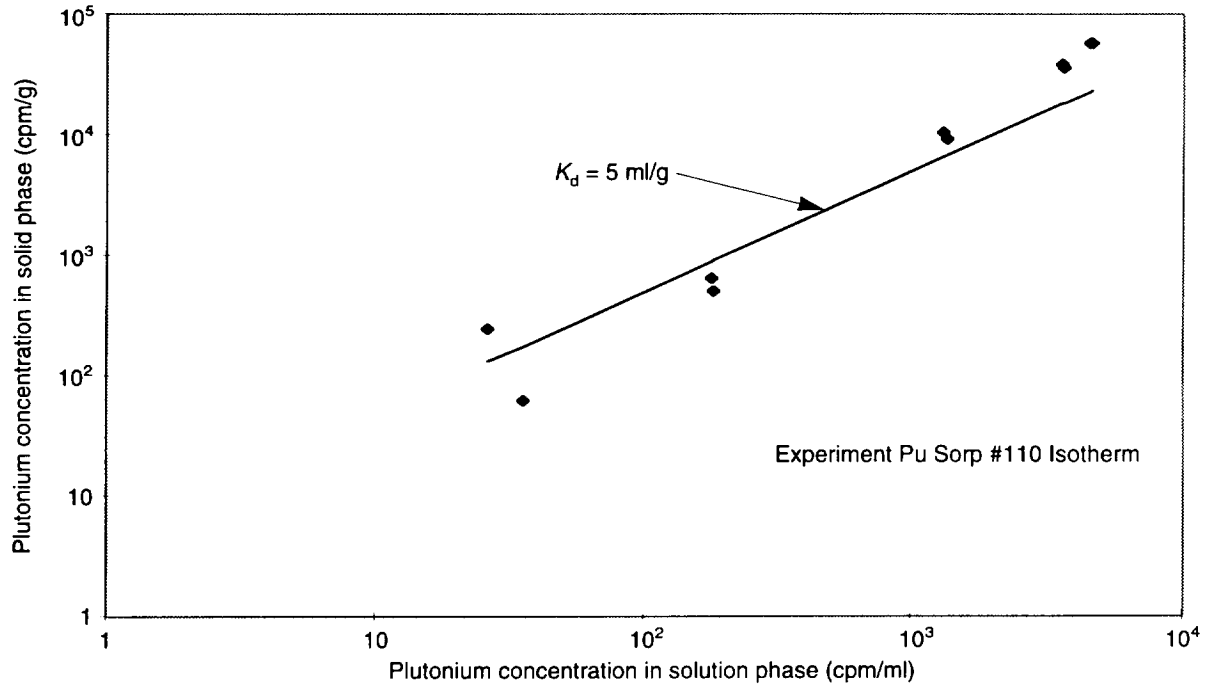


Figure 34. Plutonium Isotherm for Albite in J-13 Water. This plot shows plutonium sorption data (diamonds) and a linear isotherm (line) for sorption onto albite under atmospheric conditions in J-13 well water. The period of sorption was 21 days.

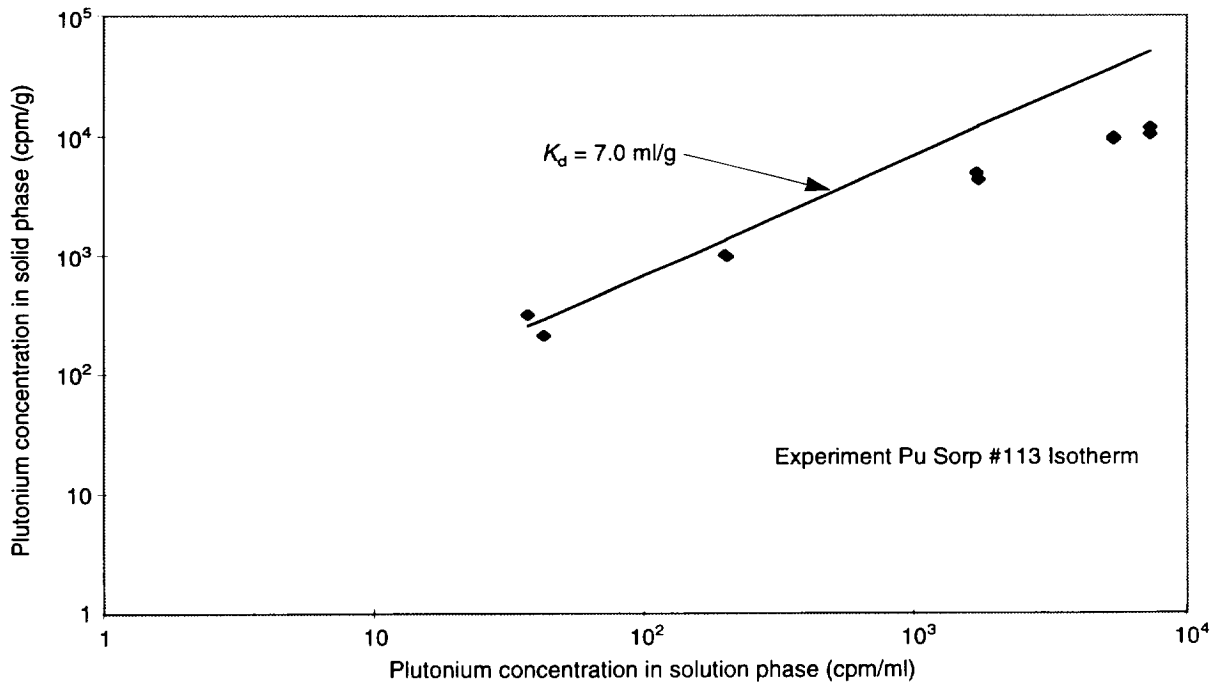


Figure 35. Plutonium Isotherm for Albite in Synthetic UE-25 p#1 Water. This plot shows plutonium sorption data (diamonds) and a linear isotherm (line) for sorption onto albite under atmospheric conditions in synthetic UE-25 p#1 water. The period of sorption was 21 days.

IV. Sorption and Sorption Modeling Studies

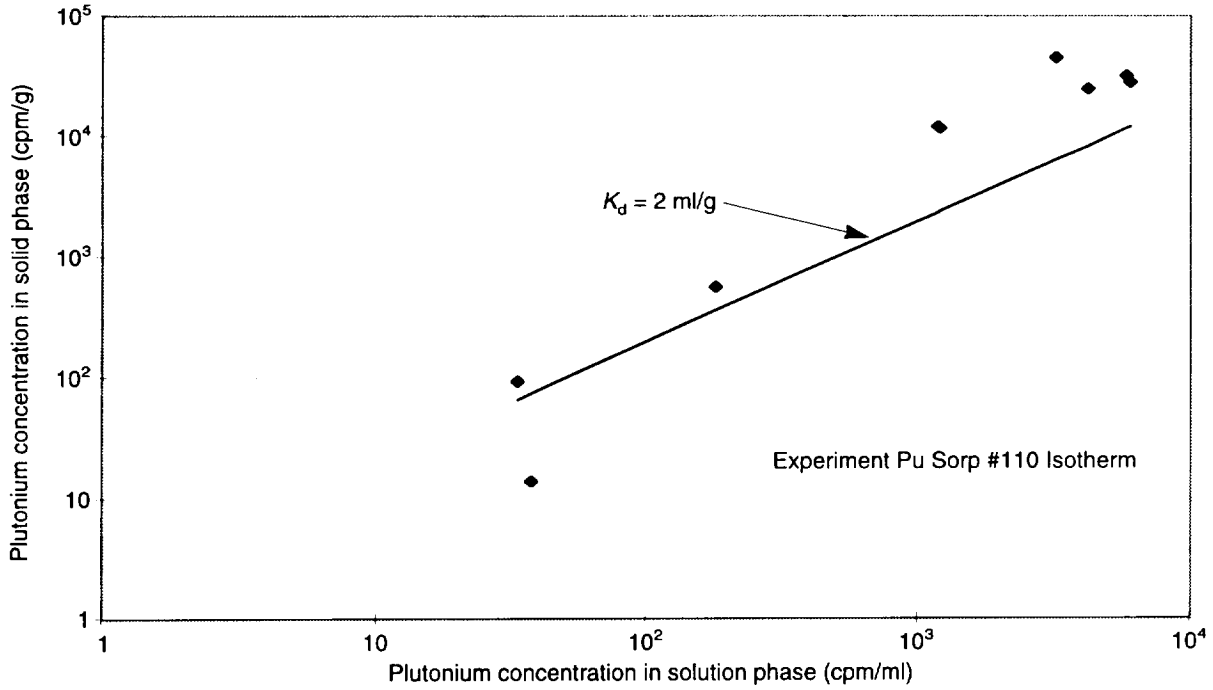


Figure 36. Plutonium Isotherm for Gibbsite in J-13 Water. This plot shows plutonium sorption data (diamonds) and a linear isotherm (line) for sorption onto gibbsite under atmospheric conditions in J-13 well water. The period of sorption was 21 days.

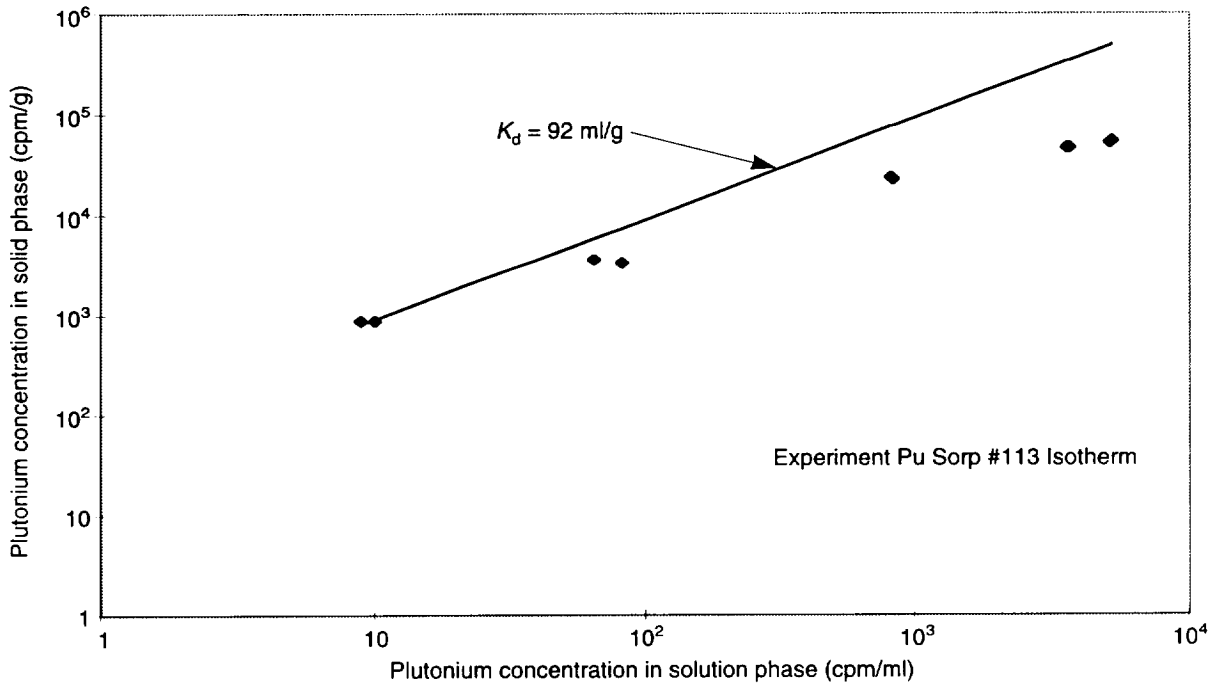


Figure 37. Plutonium Isotherm for Gibbsite in Synthetic UE-25 p#1 Water. This plot shows plutonium sorption data (diamonds) and a linear isotherm (line) for sorption onto gibbsite under atmospheric conditions in synthetic UE-25 p#1 water. The period of sorption was 21 days.

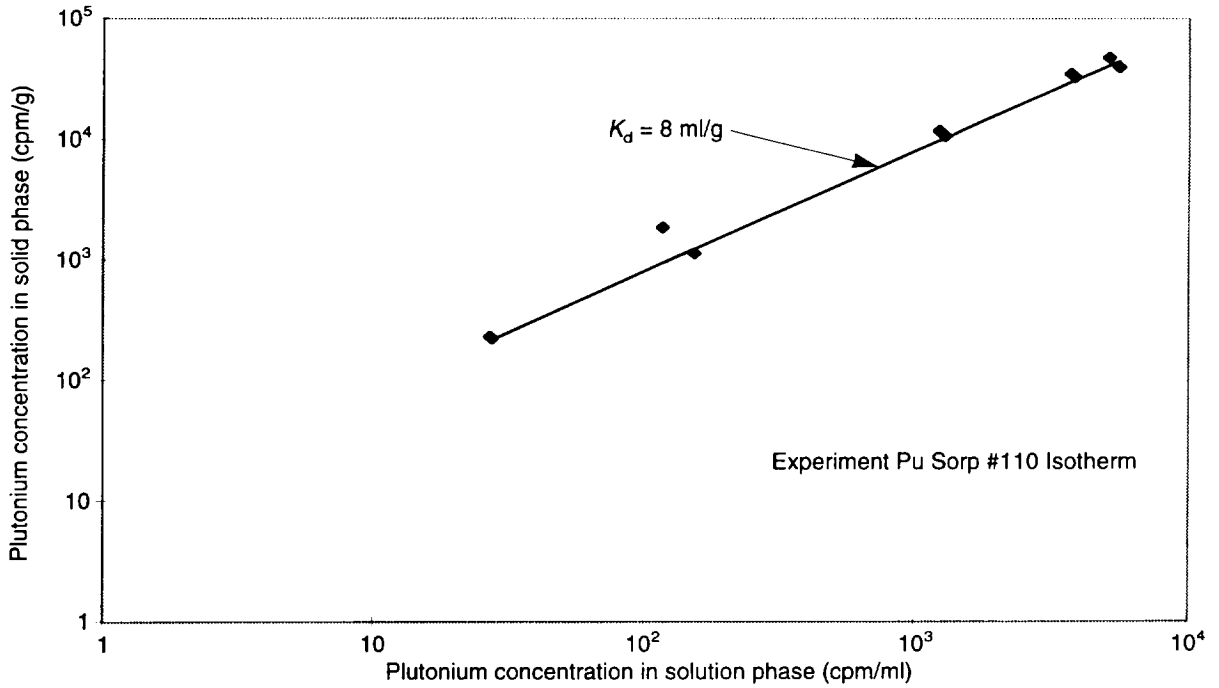


Figure 38. Plutonium Isotherm for Quartz in J-13 Water. This plot shows plutonium sorption data (diamonds) and a linear isotherm (line) for sorption onto quartz under atmospheric conditions in J-13 well water. The period of sorption was 21 days.

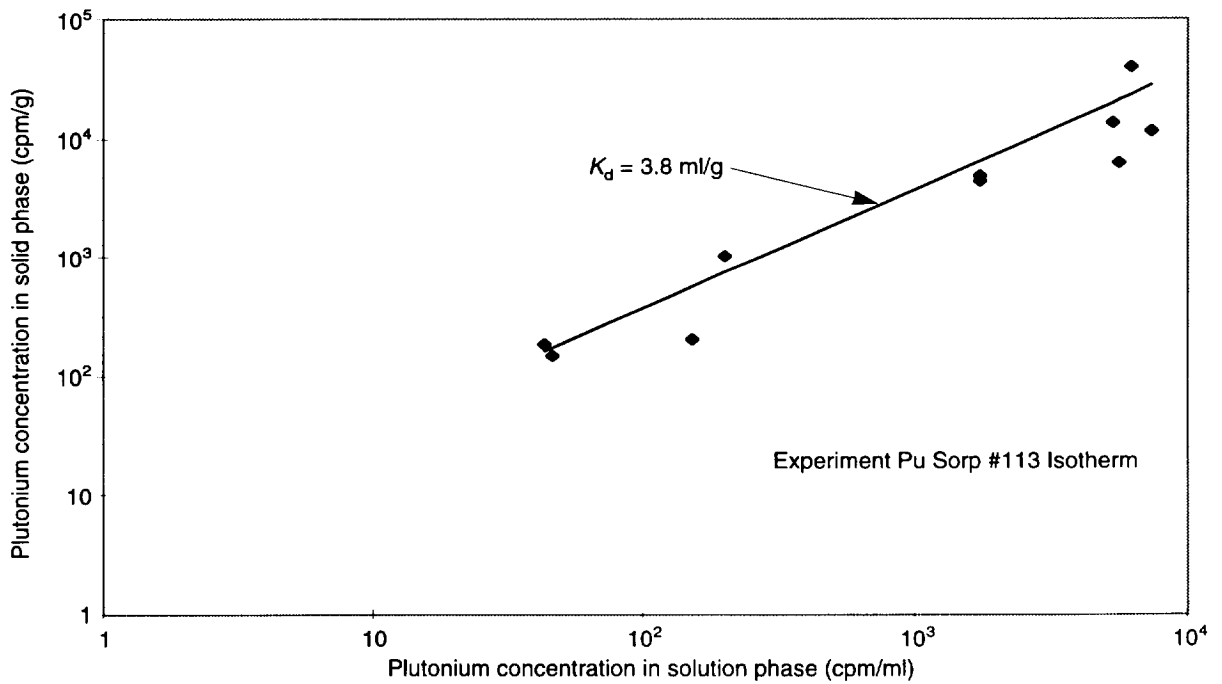


Figure 39. Plutonium Isotherm for Quartz in Synthetic UE-25 p#1 Water. This plot shows plutonium sorption data (diamonds) and a linear isotherm (line) for sorption onto quartz under atmospheric conditions in synthetic UE-25 p#1 water. The period of sorption was 21 days.

IV. Sorption and Sorption Modeling Studies

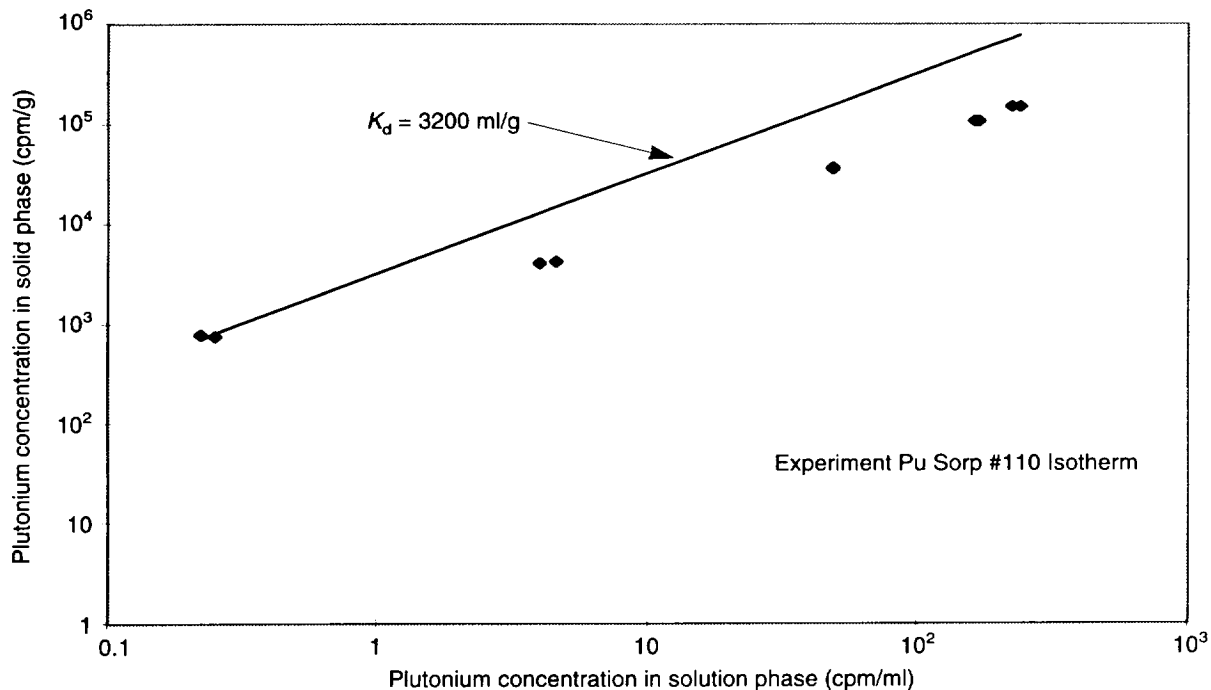


Figure 40. Plutonium Isotherm for Clinoptilolite in J-13 Water. This plot shows plutonium sorption data (diamonds) and a linear isotherm (line) for sorption onto clinoptilolite under atmospheric conditions in J-13 well water. The period of sorption was 21 days.

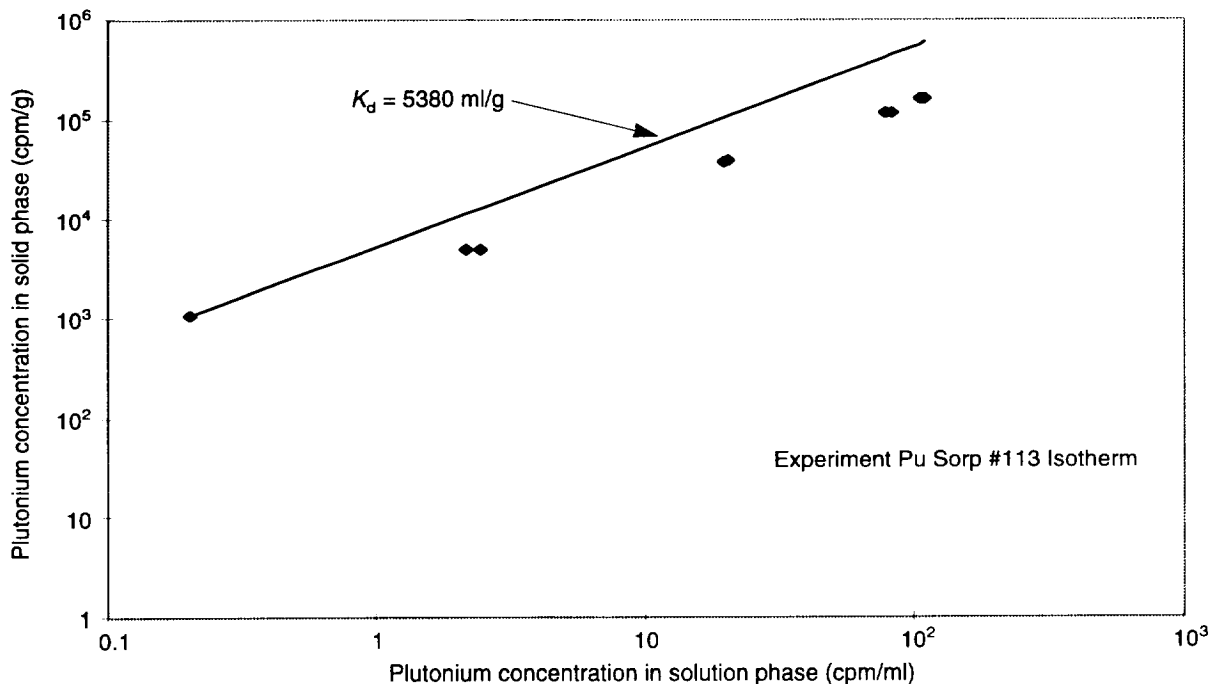


Figure 41. Plutonium Isotherm for Clinoptilolite in Synthetic UE-25 p#1 Water. This plot shows plutonium sorption data (diamonds) and a linear isotherm (line) for sorption onto clinoptilolite under atmospheric conditions in synthetic UE-25 p#1 water. The period of sorption was 21 days.

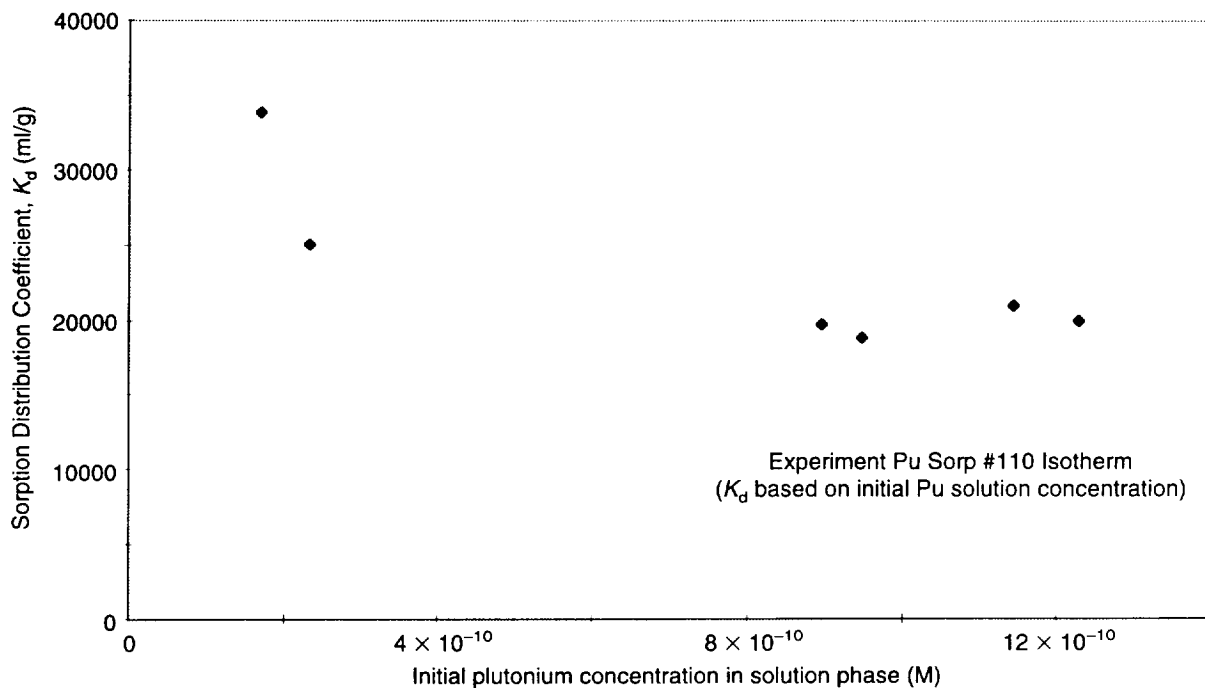


Figure 42. Plutonium Isotherm for Montmorillonite in J-13 Water. This plot shows plutonium sorption distribution coefficients (diamonds) for sorption onto montmorillonite under atmospheric conditions in J-13 well water. The period of sorption was 21 days.

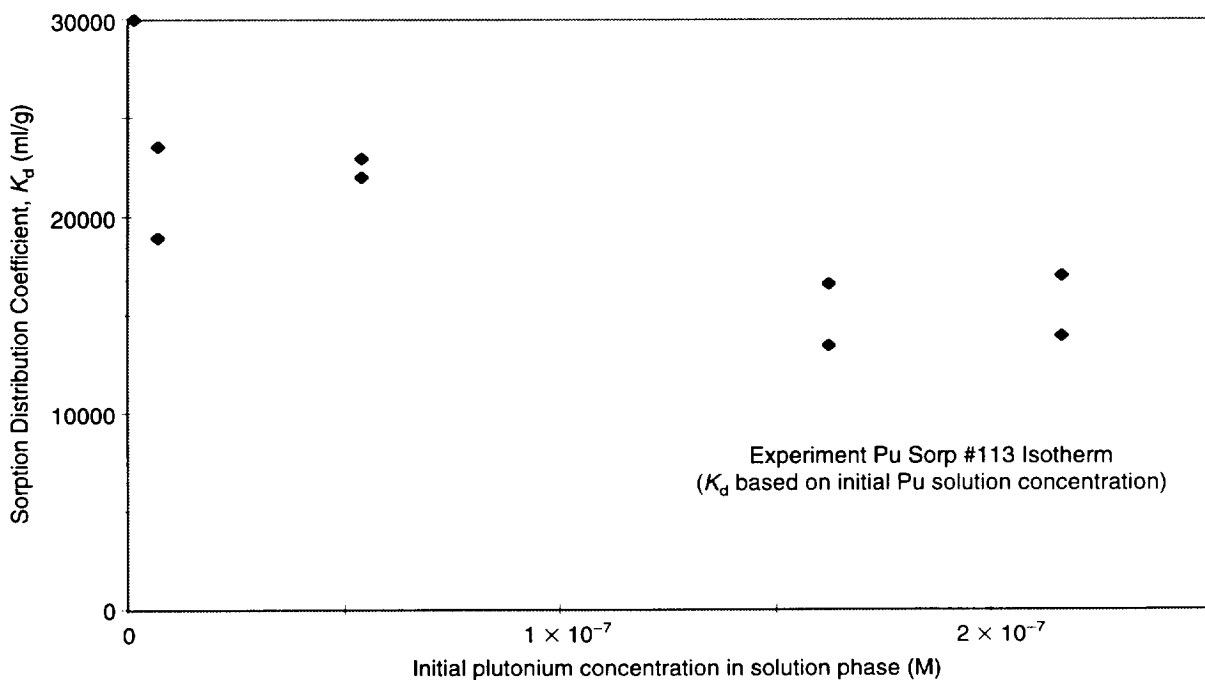


Figure 43. Plutonium Isotherm for Montmorillonite in Synthetic UE-25 p#1 Water. This plot shows plutonium sorption distribution coefficients (diamonds) for sorption onto montmorillonite under atmospheric conditions in synthetic UE-25 p#1 water. The period of sorption was 21 days.

IV. Sorption and Sorption Modeling Studies

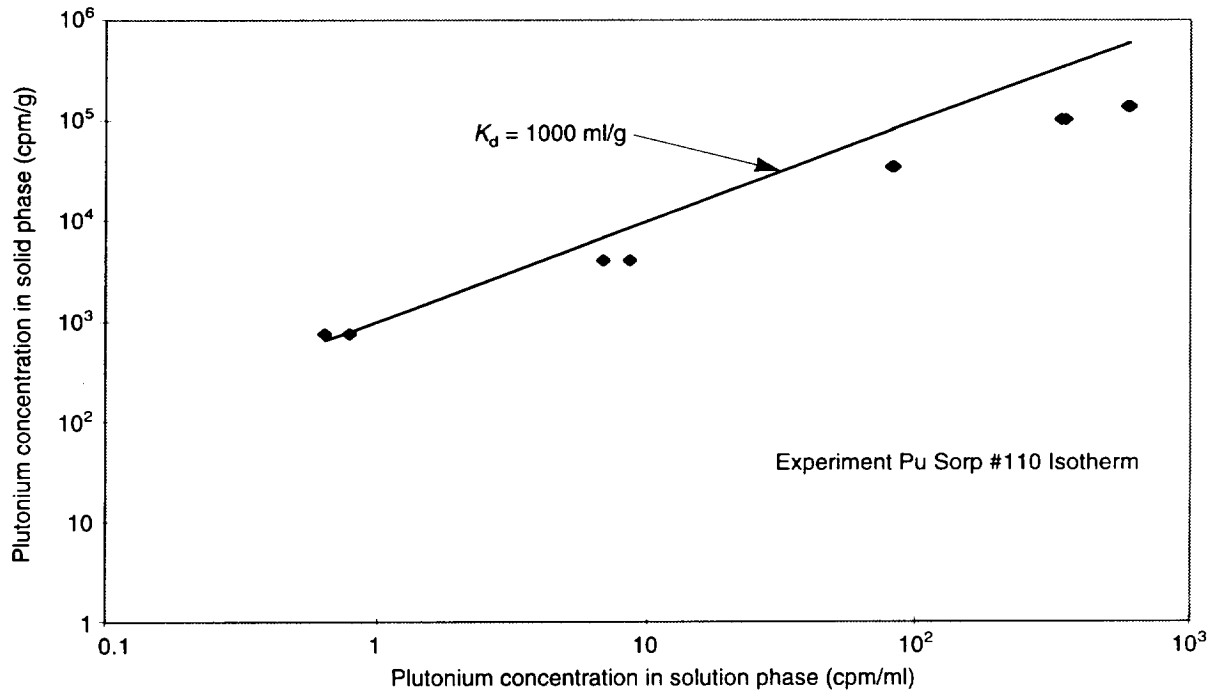


Figure 44. Plutonium Isotherm for Natural Calcite in J-13 Water. This plot shows plutonium sorption data (diamonds) and a linear isotherm (line) for sorption onto natural calcite under atmospheric conditions in J-13 well water. The period of sorption was 21 days.

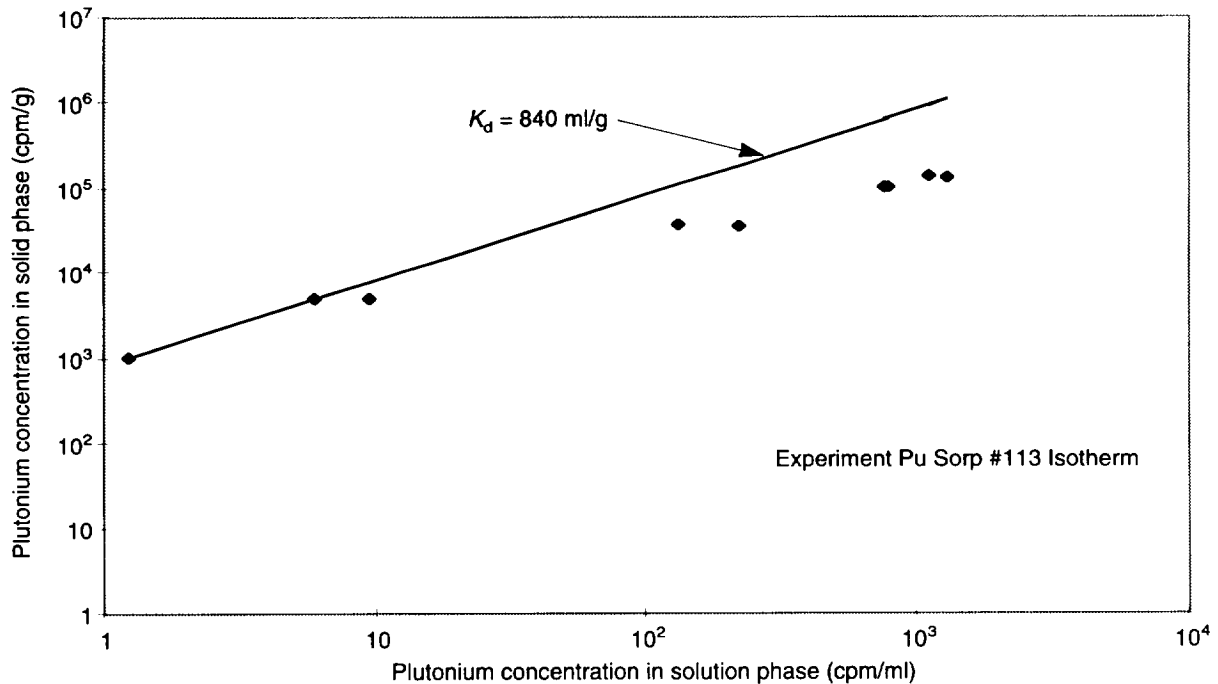


Figure 45. Plutonium Isotherm for Natural Calcite in Synthetic UE-25 p#1 Water. This plot shows plutonium sorption data (diamonds) and a linear isotherm (line) for sorption onto natural calcite under atmospheric conditions in synthetic UE-25 p#1 water. The period of sorption was 21 days.

continued from page 73

Qualitative evidence for behavior in the surficial environment.

The literature on the behavior of cesium, radium, and strontium in the surficial environment is voluminous and will not be reviewed here. Their sorption behavior is fairly well understood and is largely controlled by ion-exchange reactions (Bolt and Bruggenwert 1976), although surface-complexation reactions involving these elements have also been discussed (for example, Balistrieri and Murray 1982). The dominant controls on the ion-exchange reactions are the cation-exchange capacities of the minerals in the system, the abundances of these ion-exchanging minerals, their selectivity coefficients for the various cations in the solution phase, and the concentrations of the competing cations in the solution phase. The selectivity of most clays and zeolites for cesium, radium, and strontium is greater than the selectivities for the major cations in solution. Further, pH does not have a significant effect on the sorption behavior of these elements over the pH range of interest. Because their sorption behavior is fairly well understood and because this behavior depends strongly on local conditions, data from sites other than Yucca Mountain will not be reviewed here.

Data from laboratory sorption experiments.

Sorption coefficients for cesium, radium, and strontium were reviewed by Daniels et al. (1983), Thomas (1987), and Meijer (1990). For cesium at low concentrations (10^{-8} M), sorption coefficients are greater than 100 ml/g for all water-rock combinations tested except UE-25 p#1 water in contact with vitric tuff (Knight and Thomas 1987). Cesium sorption coefficients for the devitrified-tuff/J-13-water system show a clear concentration dependence that has been modeled with a Freundlich isotherm (Polzer and Fuentes 1988). The coefficients for this particular rock-water system are greater than 100 ml/g for cesium solution concentrations below 5×10^{-5} M. For UE-25 p#1 water in contact with this rock type, the coefficient would be 100 ml/g at somewhat lower solution concentrations. In any case, in the higher ionic-strength waters (0.02 eq/l), including unsaturated-

zone waters, the sorption coefficients for cesium on devitrified and vitric samples may be less than 100 ml/g if solution concentrations of cesium exceed 10^{-6} M. For zeolitic tuffs, cesium sorption coefficients are greater than 100 ml/g for all water compositions and cesium concentrations anticipated in the potential repository environment.

Radium appears to have a somewhat higher affinity for sorption onto Yucca Mountain tuffs than cesium. In addition, the solubility of RaSO_4 limits the concentrations in solution to trace levels (10^{-7} – 10^{-8} M; Ogard and Kerrisk 1984). At concentrations below the solubility limit for RaSO_4 , sorption coefficients for radium are greater than 100 ml/g in essentially all rock-water combinations tested, using barium as an analog for radium (Knight and Thomas 1987). This fact suggests that a minimum sorption coefficient of 100 ml/g can be used for radium in all rock-water systems. For zeolitic samples, minimum values of 1,000 ml/g can be used.

Strontium sorption behavior is more sensitive to mineral and water compositions than the other two elements discussed in this section. For devitrified and vitric tuffs, sorption coefficients for the higher ionic-strength waters (such as UE-25 p#1) are in the range of 10 to 30 ml/g (Knight and Thomas 1987). These sorption coefficients will decrease as the solution concentration of strontium is increased above approximately 10^{-5} M (Thomas 1987). However, this concentration is close to the solubility limit for SrCO_3 in these waters so that the 1000 ml/g range is likely appropriate for use in performance-assessment calculations in the devitrified or vitric tuffs. For zeolitic tuffs, a minimum value of 1,000 ml/g would be appropriate (Knight and Thomas 1987).

Conclusions regarding sorption behavior with respect to expected variations in groundwaters.

The existing sorption-coefficient database for cesium, radium, and strontium should be adequate for performance-assessment calculations. The main concern would be the concentration of

IV. Sorption and Sorption Modeling Studies

cesium in the solution phase in contact with devitrified and vitric tuffs. If this concentration is over 10^{-5} M, the appropriate value for the sorption coefficient may be less than the minimum recommended value of 100 ml/g. The sorption coefficients for strontium in devitrified and vitric tuffs will be as low as 10 to 30 ml/g in higher ionic-strength waters. If additional experiments were to be carried out for this group of elements, they should focus on strontium in contact with devitrified and vitric tuffs in the higher ionic-strength waters.

Nickel and Lead

Behavior in solutions representative of Yucca Mountain groundwaters.

The aqueous solution behavior of nickel and lead is relatively simple. Within the range of groundwater compositions expected in the Yucca Mountain flow system, these elements are present in solution primarily as simple divalent cations. Several per cent of the total nickel concentration will be present as the NiSO_4^+ (aq) complex. Similarly, several per cent of the total lead concentration will be present as the PbCl^+ complex.

Qualitative evidence for behavior in the surficial environment.

The behavior of nickel and lead in the surficial environment has been studied in some detail (for example, Snodgrass 1980). These elements are generally quite particle-reactive. The dominant mechanisms that control their sorption behavior are ion exchange on clay minerals (for example, Bowman and O'Connor 1982) and adsorption onto various oxides (for example, Theis and Richter 1980). The selectivities of clay minerals for nickel and lead are large relative to the major cations (such as Mg^{2+}) in typical groundwaters (Decarreau 1985). Solution compositional parameters that can influence this adsorption behavior include pH, ionic strength, concentrations of competing ions, and concentrations of complexing agents (see review by Rai and Zachara 1984).

Data from laboratory sorption experiments.

Data on the sorption behavior of nickel in Yucca Mountain rock-water systems were reported by Knight and Lawrence (1988). Sorption and desorption ratios were determined in several water compositions in the pH range from 8.3 to 9.0 with nickel concentrations in solution of approximately 10^{-8} M. For devitrified and zeolitic samples, sorption coefficients were in the range of 200 to 400 ml/g. Sorption coefficients obtained in the desorption step were generally a factor of two larger than the sorption coefficients. In the only vitric sample analyzed, sorption coefficients ranged from approximately 30 to 70 ml/g. For the desorption step, the coefficients were in the range of 33 to 72 ml/g for this rock type. We were unable to find references to the adsorption behavior of lead on tuffaceous or even granitic rock samples.

Data on sorption of transition metals on synthetic zeolites suggest that Pb^{2+} has a high affinity for ion exchange compared with Sr^{2+} , whereas Ni^{2+} has a lower affinity relative to Sr^{2+} (Barrer and Townsend 1976; Obeng et al. 1981; Blanchard et al. 1984). This suggests the zeolitic zones within Yucca Mountain could be significant barriers to lead migration.

Conclusions regarding sorption behavior with respect to expected variations in groundwaters.

Based on information in the literature, the sorption behavior of these elements will be determined largely by the free-ion activities in solution and the cation-exchange capacity of the host rock (for example, Bowman and O'Connor 1982 and Rai and Zachara 1984). Solution pH and oxide-mineral abundances may be a factor in rocks in which nickel and lead sorb primarily by surface-complexation mechanisms. In any case, lead appears to sorb more strongly than nickel in most surficial environments, and both elements appear to sorb more strongly than strontium (Bowman and O'Connor 1982). The nickel sorption coefficients discussed in the previous section could reasonably be used as default values for lead in performance-assessment calculations. For nickel, a minimum

sorption coefficient of 100 ml/g could be used in the devitrified and zeolitic zones. For the vitric zones, the performance-assessment calculations could be done using random sampling and a normal distribution ranging from 0 to 50 ml/g.

Neptunium, Protactinium, Selenium, and Uranium

The main factor that neptunium, protactinium, selenium, and uranium have in common is that they all tend to show small values for sorption coefficients in the rock-water systems expected within Yucca Mountain under oxidizing conditions. Under more reducing conditions, they would all have much lower solubilities and higher sorption affinities in Yucca Mountain groundwaters. As the solution and sorption behavior is somewhat different for each of these elements, they will be discussed separately.

Neptunium

Behavior in solutions representative of Yucca Mountain groundwaters.

In solutions representative of water compositions expected within the Yucca Mountain flow system, neptunium will be predominantly in a +5 oxidation state. Unlike pentavalent niobium and protactinium, Np(V) compounds are relatively soluble (Nitsche et al. 1994). This result appears to be due to the formation of the oxocation NpO_2^+ in solution. Pentavalent niobium and protactinium apparently do not form analogous oxocations (that is, NbO_2^+ and PaO_2^+) in near-neutral solutions to an appreciable degree. Instead they hydrolyze and form insoluble precipitates. The NpO_2^+ ion appears to be quite stable in aqueous solutions (Cotton and Wilkinson 1988).

Nitsche et al. (1992, 1994) studied the solubilities and speciation of neptunyl compounds in solutions representative of water compositions expected within Yucca Mountain. The results at 25°C and several pH values are summarized in Table 14. The solubility-controlling solids were found to be hydrated sodium neptunyl carbonates, and the pri-

mary species for the water compositions expected at Yucca Mountain were NpO_2^+ and $\text{NpO}_2(\text{CO}_3)^-$. The speciation results of Table 14 for J-13 water are similar, although not identical, to those calculated using the EQ3 speciation code (Nitsche 1991).

At higher temperatures (60° and 90°C), neptunium was less complexed by carbonate at pH values of 6 and 7 but more highly complexed with carbonate at a pH of 8.5. The solubilities at 60°C were similar to those in Table 14, although they were somewhat higher at a pH of 8.5 relative to the 25°C results.

Qualitative evidence for behavior in the surficial environment.

Although ^{237}Np has been detected in the surficial environment (for example, Sakanoue 1987), essentially no information has been found on its transport behavior in this environment.

Data from laboratory sorption experiments.

Laboratory experiments have been carried out on neptunium sorption with a variety of rock and mineral types and solution compositions. The results of neptunium sorption experiments with pure mineral separates have been reported by Allard (1982), Meijer et al. (1989), Triay et al. (1993b), and others. On the basis of these results, it is evident that neptunium has a high affinity for ferric oxides and

Table 14. Solubility and Speciation of Neptunium in Groundwaters at 25°C

Water	pH	Solubility (M)	NpO_2^+	$\text{NpO}_2\text{CO}_3^-$
J-13	6	5×10^{-3}	90%	10%
	7	1×10^{-4}	45%	55%
	8.5	4×10^{-5}	40%	60%
UE-25 p#1	6	3×10^{-3}	100%	0%
	7	5×10^{-4}	60%	40%
	8.5	7×10^{-6}	0%	100%

IV. Sorption and Sorption Modeling Studies

oxyhydroxides, apatite, and attapulgite (a magnesium-rich clay). It has a somewhat lower affinity for carbonates (such as calcite), sulfates (for example, anhydrite) and manganese minerals (for example, cryptomelane). It has a low affinity for most silicate minerals. Neptunium also shows high affinities for minerals that contain ferrous iron (such as pyrite, olivine, augite, magnetite, hornblende, epidote, biotite, and chlorite). This affinity is likely due to the reduction of Np^{5+} to Np^{4+} by Fe^{2+} on the surfaces of these minerals. Although ferrous iron-bearing minerals are, at best, minor species in Yucca Mountain tuffs (Bish and Chipera 1989), they could be of considerable significance to neptunium sorption.

In addition to the nature of the available mineral surfaces, it is also evident that pH is a critical parameter. In general, neptunium sorption increases with increasing pH. This effect is particularly evident in the experiments with iron oxyhydroxides (for example, Combes et al. 1992). However, similar behavior is evident in the sorption experiments with silicate minerals. In the latter case, the sorption edge (as a function of pH) is located at a higher pH (8–9) than the edge associated with the ferric oxyhydroxides (a pH of 6–7). Data reported by Combes et al. (1992) suggest neptunium is sorbed as an inner-layer complex on ferric oxyhydroxide.

Neptunium does not appear to have a high affinity for ion-exchange reactions on clays and zeolites (Allard 1982; Triay et al. 1993b). This phenomenon may be due to the small charge-to-radius ratio and the large size of the neptunyl ion.

The results of neptunium sorption experiments involving Yucca Mountain rock and water samples have been reported by Daniels et al. (1982), Thomas (1987, 1988), Triay et al. (1993b), and others. These experiments indicate that neptunium has a low affinity (for example, K_d values of 0–5 ml/g) for the surfaces in Yucca Mountain tuffs over most of the pH range and water compositions expected in the Yucca Mountain flow system. The sorption mechanisms are apparently not entirely

reversible as coefficients obtained from desorption experiments are commonly larger than those obtained from sorption experiments even though the isotherms are linear in the concentration range covered by these experiments. There is some indication of increased sorption coefficients (5–40 ml/g) at the highest pH values (8.5–9.0). Torstenfelt et al. (1988) suggest that this result reflects increased hydrolysis of the neptunyl ion, resulting in an increase in surface-adsorption reactions. However, in Yucca Mountain rock-water systems, it could also reflect increased potential for calcite precipitation at high pH.

In the pH range from 6.5 to 8.5, the small but consistent affinity of neptunium for the tuffs most likely reflects the existence of a limited number of favorable adsorption sites for neptunium. This number apparently does not involve ion-exchange sites because zeolitic rock samples also show low sorption coefficients. For example, Thomas (1988) describes a case in which a zeolitic tuff sample (G4-1608) with a cation-exchange capacity of approximately 1.5 meq/g appears to have essentially the same affinity for neptunium as a devitrified tuff sample (GU3-433) with an exchange capacity of approximately 0.02 meq/g. These sites are apparently not present in the same abundance on all tuff samples. That is, some zeolitic, vitric, and devitrified tuff samples have almost no affinity for neptunium over the pH range from 6.5 to 8.5, whereas other samples with similar proportions of major minerals show sorption coefficients in the range of 5 to 10 ml/g. This result suggests, but does not prove, that the favorable sites are associated with some minor primary or secondary phase that has variable abundance. Hematite and calcite are candidates for this phase based on pure mineral studies. Because ferric oxides are present at trace levels in most of the rock units within Yucca Mountain, they could be the source of the low but consistent values (0.5–2 ml/g) observed in experiments on devitrified and zeolitic tuffs. Alternatively, neptunium may be sorbed (through reduction to Np^{4+}) by the small amounts of ferrous-iron-bearing minerals present in the rock samples used

in the sorption experiments.

The increased sorption of neptunium on tuffaceous samples known to contain calcite suggests this mineral is of considerable potential significance to neptunium sorption on Yucca Mountain tuffs. If so, prediction of the adsorption behavior of neptunium will depend on knowledge of the surface areas of calcite in the various hydrologic units or on the saturation state of calcite in groundwaters present in these units. Because even small amounts of calcite appear to significantly increase neptunium sorption coefficients, current mineral identification techniques may not be adequate for prediction of neptunium sorption behavior. A more viable approach may be to determine the calcite saturation level in the various groundwater compositions expected within Yucca Mountain. If calcite is saturated or oversaturated in a given groundwater, the upper end of the range of experimentally determined sorption coefficients could be used with the assumption that neptunium will either coprecipitate with calcite or adsorb to calcite surfaces. Alternatively, if calcite is undersaturated in a given water, the lower end of the range could be used under the assumption that neptunium is sorbed on oxides, such as ferric or ferrous oxides. For vitric units lacking iron oxides and calcite, neptunium may not be sorbed at all.

We studied the sorption of Np(V) onto samples of the three types of tuff in J-13 water (under oxidizing conditions) at two pH values (7 and 8.5). However, to identify the sorbing minerals in the tuffs, we also studied sorption onto the pure minerals hematite, clinoptilolite, albite, and quartz. We found that neptunium in J-13 water does not sorb onto devitrified and vitric tuffs, albite, and quartz (Table 15).

The initial neptunium concentrations for the data reported in Table 15 ranged from 1×10^{-7} to 3×10^{-5} M. We used wet-sieved tuffs, albite, and quartz samples with particle sizes in the range from 75 to 500 μm . The pretreatment period lasted 2 to 3 days, and the sorption period, 2 to 4 days. The

Table 15. Neptunium Sorption in J-13 Water under Oxidizing Conditions

Solid phase	pH	K_d (ml/g)*
G4-268, devitrified tuff	7	7×10^{-3}
	8.5	-4×10^{-2}
GU3-1405, vitric tuff	7	2×10^{-1}
	8.5	3×10^{-1}
Quartz	7	-1×10^{-1}
	8.5	-2×10^{-1}
Albite	7	-8×10^{-2}
	8.5	-1×10^{-1}

*The uncertainties in the data are ± 0.5

negative values reported in the table are a result of the analytical error for the case of very little sorption (that is, a small number is obtained as the difference of two large numbers).

For the experimental conditions cited earlier, the sorption of neptunium onto zeolitic tuffs and clinoptilolite appears to be linear in the concentration range from 1×10^{-7} to 3×10^{-5} M and can be fitted using a K_d (Figs. 46 and 47). The sorption of neptunium onto zeolites is higher at a pH of 7 than a pH of 8.5, which might be explained by the larger amount of NpO_2^+ relative to $\text{NpO}_2\text{CO}_3^-$ in J-13 water at a pH value of 7 than at a pH value of 8.5.

One surprise for neptunium is the relatively small amount of sorption (values of K_d ranging from 1.5 to 3 ml/g) compared to the large amount expected for a cation-exchange sorption mechanism in a zeolite with a large cation-exchange capacity (such as clinoptilolite). This result indicates that the sorption mechanism for neptunium onto clinoptilolite is a surface reaction rather than cation exchange within the cages of the zeolite. One possible explanation is steric: the shape and large size of the neptunyl cation prevents cation exchange. This ion likely has a trans-dioxol configuration normal to a puckered equatorial ring containing six bound water molecules.

IV. Sorption and Sorption Modeling Studies

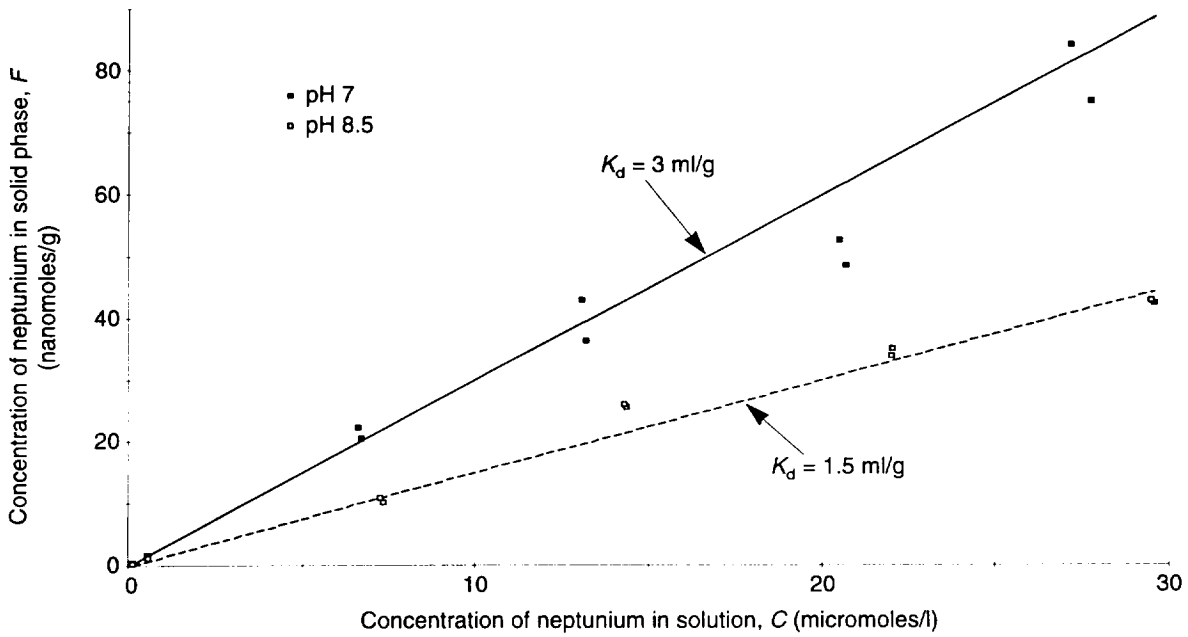


Figure 46. Neptunium Sorption onto Clinoptilolite-rich Tuff. A plot is shown of the concentration, F , of neptunium in the solid phase of the clinoptilolite-rich tuff G4-1510 versus the concentration, C , of neptunium in the solution phase of J-13 well water and linear (K_d) fits to the data for two values of pH.

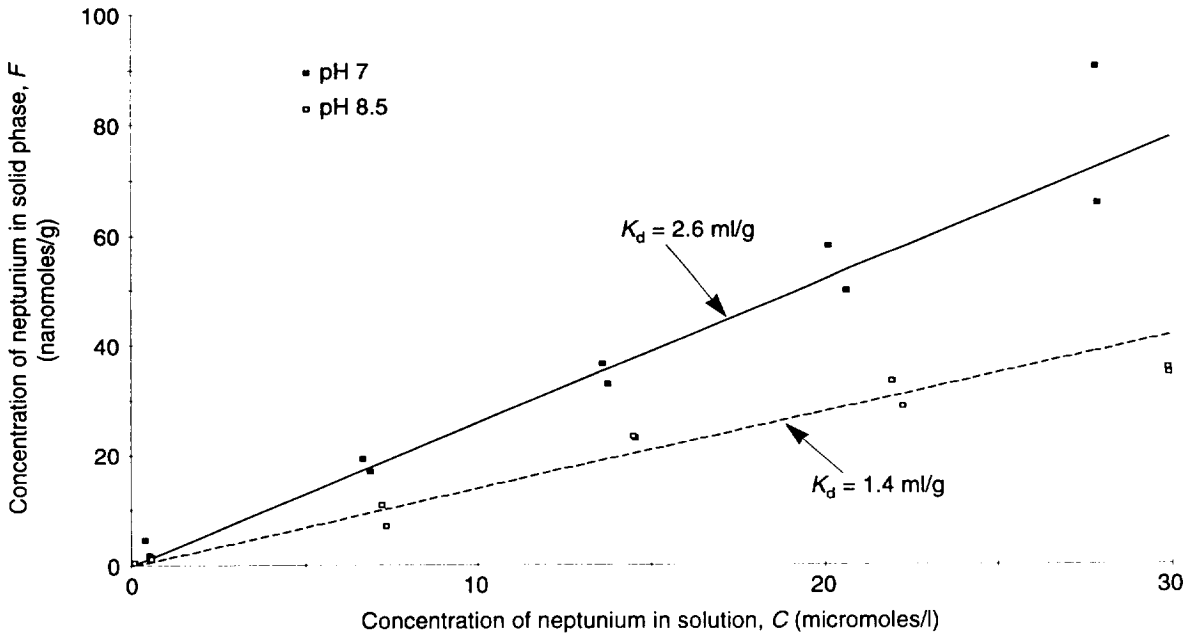


Figure 47. Neptunium Sorption onto Clinoptilolite. A plot is shown of the concentration, F , of neptunium in the solid phase of clinoptilolite versus the concentration, C , of neptunium in the solution phase of J-13 well water and linear (K_d) fits to the data for two values of pH.

The experiments with pure clinoptilolite indicate that sorption increases with decreasing pH for Np(V). Because the major constituent of tuff G4-1510 is clinoptilolite, predictions of the K_a (K_d divided by the solid-phase surface

area) were made for neptunium sorption onto this tuff by assuming that clinoptilolite is the only sorbing phase. Table 16 shows measured and predicted values of K_a for the clinoptilolite-rich tuff G4-1510 at two different pH values. Because sorption is correlated with surface area, we made similar calculations (Table 17) for a series of tuff samples containing various amounts of clinoptilolite for which the surface area had been measured. The values in the two tables indicate that reasonable predictions can be made based on neptunium sorption data for pure clinoptilolite (assuming clinoptilolite is the only sorptive mineral).

Table 16. Prediction of Neptunium Sorption on Clinoptilolite-rich G4-1510 Tuff in J-13 Water

Initial concentration (M)	pH	Measured K_a (m)	Predicted K_a (m)*
1×10^{-7} to 3×10^{-5}	7	1×10^{-7}	9×10^{-8}
	8.5	6×10^{-8}	5×10^{-8}

*Assuming clinoptilolite is the only sorbing mineral in the tuff

The sorption of neptunium onto pure iron oxides is very large (we measured values of K_d for hematite that range from 100 to 2000). Although the sorption onto pure hematite is very large, neptunium sorption onto devitrified tuffs, which appear to have traces of hematite ($1\% \pm 1$), is essentially zero. This result could be due to differences in the surface of pure hematite compared to hematite in tuff. It could also be due to passivation of the hematite surfaces in the tuff by elements (such as the rare earths) that have a higher affinity for hematite than neptunium and, thus, occupy the sorption sites.

Table 17. Neptunium Sorption onto Clinoptilolite-rich Tuffs in J-13 Water*

Tuff sample	Measured K_a (m)	Predicted K_a (m)	Clinoptilolite percentage
G1-1405	1×10^{-7}	1×10^{-7}	68 ± 7
G4-1505	9×10^{-8}	1×10^{-7}	74 ± 7
G4-1506	1×10^{-7}	1×10^{-7}	62 ± 7
G4-1510	8×10^{-8}	1×10^{-7}	59 ± 7
G4-1529	7×10^{-8}	1×10^{-7}	59 ± 8
G4-1625	9×10^{-8}	1×10^{-7}	61 ± 7
G4-1772	1×10^{-7}	1×10^{-7}	63 ± 5
G4-2077	5×10^{-8}	8×10^{-8}	51 ± 8

*Atmospheric conditions; initial neptunium concentrations ranged from 6 to 8×10^{-7} M; tuffs were wet-sieved to particle sizes ranging from 75 to 500 μm ; the pretreatment period was 2 to 14 days; and the sorption period was 3 to 23 days.

We investigated sorption as a function of sieving procedure for devitrified (G4-270) and zeolitic (G4-1506) tuffs in J-13 and UE-25 p#1 well waters. Data presented in Fig. 48 indicate that wet-sieving probably eliminates small particles that cause artificially high K_d values. As previously determined by Rogers and Chipera (1994), the optimal batch-sorption procedure involves wet-sieving the tuff samples to a size of 75 to 500 μm . Figure 49 illustrates the problem that could arise when sorption experiments are performed with pure minerals consisting of very finely divided particles that cannot be wet-sieved. The neptunium batch-sorption coefficients determined vary by more than an order of magnitude between the dry- and the wet-sieved natural calcite. The potential differences in surface area and particle size between a pure mineral and that same mineral in the tuff samples may make predictions of sorption behavior on whole rock impossible when the basis of those predictions is pure mineral work. As illustrated in Fig. 49, the trends in sorption as a func-

IV. Sorption and Sorption Modeling Studies

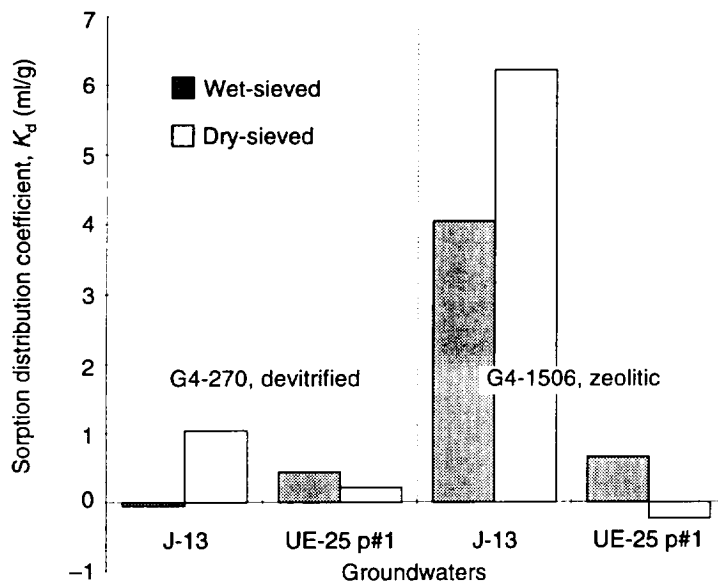


Figure 48. Neptunium Sorption for Wet- and Dry-sieved Tuffs.

Experimental values of the batch-sorption distribution coefficient, K_d , are shown for sorption of neptunium onto tuff (under atmospheric conditions) that allow comparisons of both groundwaters (J-13 and UE-25 p#1), two types of tuff (devitrified and zeolitic), and wet- or dry-sieving to particle sizes ranging from 75 to 500 μm . The initial neptunium concentration was 1×10^{-6} M. The pretreatment period with the two groundwaters was 13 to 15 days; the neptunium sorption period was 21 to 22 days.

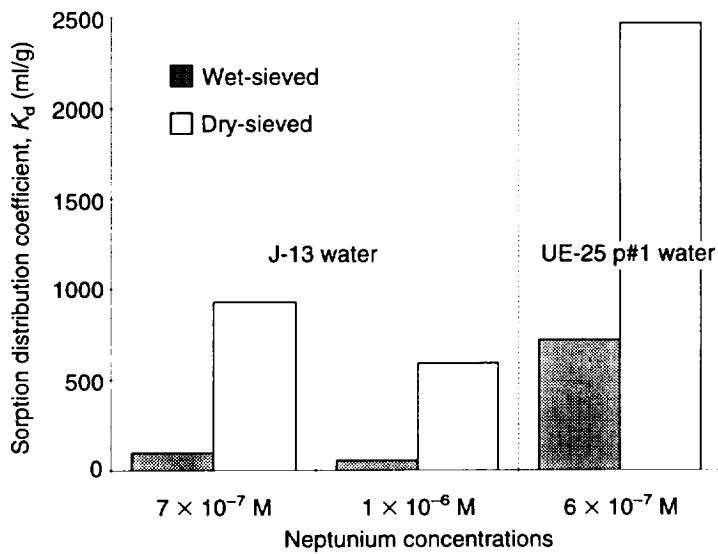


Figure 49. Neptunium Sorption for Wet- and Dry-sieved Calcite.

Experimental values of the batch-sorption distribution coefficient, K_d , are given for sorption of neptunium onto calcite (under atmospheric conditions) that allow comparisons of both groundwaters (J-13 and UE-25 p#1), different initial concentrations of neptunium, and wet- or dry-sieving to particle sizes ranging from 75 to 500 μm . The pretreatment period was 14 to 15 days; the sorption period was 17 to 24 days.

tion of concentration and groundwater chemistry stay the same regardless of whether dry- or wet-sieved calcite is used.

Consequently, the most effective use of pure mineral sorption data is the identification of trends in the sorptive behavior of a mineral. Figures 48 and 49 also illustrate the effect of water chemistry on neptunium sorption; for example, the sorption of neptunium onto zeolitic tuffs decreases consider-

ably with the increasing carbonate content and ionic strength of the UE-25 p#1 water. The reverse trend is observed for calcite samples.

We investigated the kinetics of neptunium sorption onto tuffs and pure minerals and found that the sorption of neptunium onto tuffs and clinoptilolite appears to be fast (Fig. 50). No significant differences are observed in neptunium sorption as a function of time for the tuffs studied and for

clinoptilolite. This is not the case for pure minerals that tend to sorb by means of a coprecipitation mechanism (such as calcite) or by surface complexation (such as hematite). Figures 51 and 52 show the sorption dependence on time for calcite and hematite in waters from the Wells J-13 and UE-25 p#1. The dissolution/precipitation reactions that may accompany the coprecipitation of neptunium with calcite may be slow compared with other sorption mechanisms. Future experiments will address this issue by monitoring the chemistry of the groundwater as it is being equilibrated with these minerals.

Figures 53 and 54 give further data from our investigation of the dependence of neptunium sorption on pH in J-13 water. The figures show that for vitric tuffs (such as samples G2-767 and GU3-1407), pH does not seem to make a significant difference in the amount of neptunium sorption measured. Likewise, the sorption of neptunium onto devitri-

fied tuffs (such as sample G4-270) in J-13 is not affected by pH. Samples G2-1813, G2-1951, G2-2000, and G2-2222 are zeolitic tuffs, but until the XRD analyses of these samples become available, it is difficult to know the relative amounts of clinoptilolite versus mordenite in each. However, tuff samples G4-1510 and G4-1395 consist of 59% and 22% clinoptilolite, respectively, and exhibit the same trend as clinoptilolite itself: an increase in sorption as the pH is decreased from 8.5 to 7, probably because of the increase of neptunyl cation concentration. As discussed earlier, these results seem to indicate that neptunium sorption onto clinoptilolite may follow an ion-exchange mechanism, but the fact that neptunium sorption on pure clinoptilolite is so small favors a surface-complexation reaction, even for this zeolite. Again, the reason may be that the hydrated neptunyl cation is too large to fit in the zeolite cages.

We also studied the sorption of neptunium in

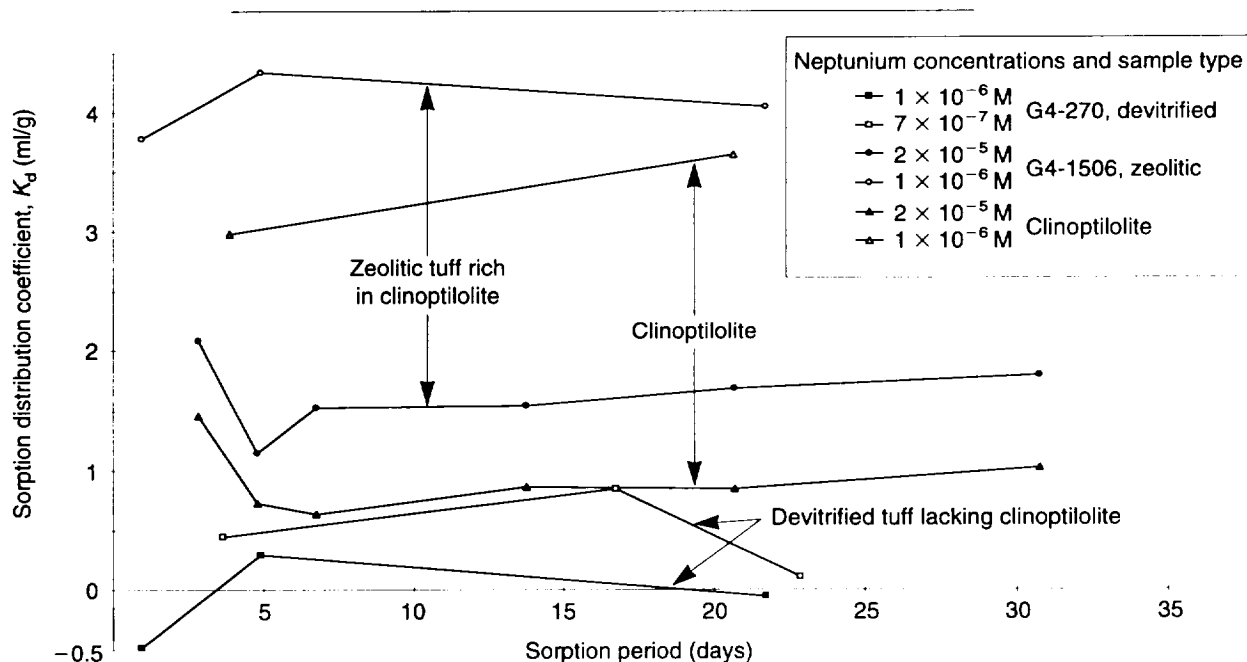


Figure 50. Time Dependence of Neptunium Sorption for Tuffs and Clinoptilolite. Variation with time of K_d for sorption of neptunium onto devitrified tuff (G4-270) lacking clinoptilolite (squares), zeolitic tuff (G4-1506) rich in clinoptilolite (circles), and pure clinoptilolite (triangles) under atmospheric conditions and at the specified initial neptunium concentrations in J-13 well water. Tuffs were wet-sieved to particle sizes from 75 to 500 μm ; the clinoptilolite was not sieved. The pretreatment period was 2 to 14 days.

IV. Sorption and Sorption Modeling Studies

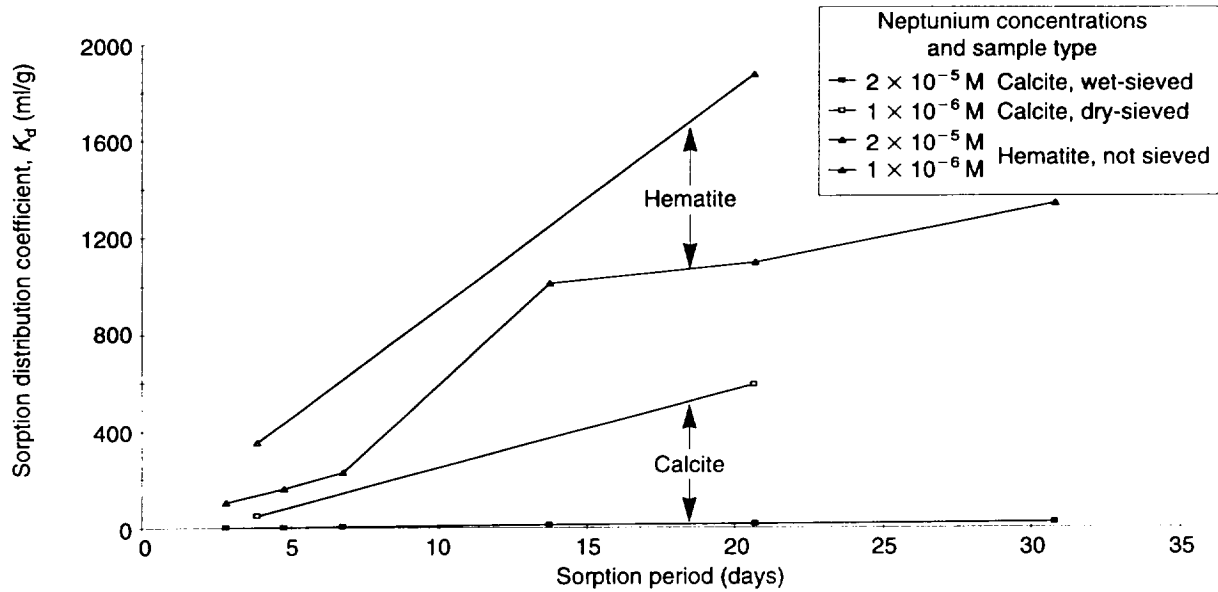


Figure 51. Time Dependence of Neptunium Sorption for Calcite and Hematite in J-13 Water. Variation with time of K_d for sorption of neptunium onto calcite (squares) and hematite (triangles) under atmospheric conditions and at the specified initial neptunium concentrations in J-13 well water. The calcite was either wet- or dry-sieved to particle sizes from 75 to 500 μm ; the synthetic hematite was not sieved. The pretreatment period with J-13 water was 2 to 14 days.

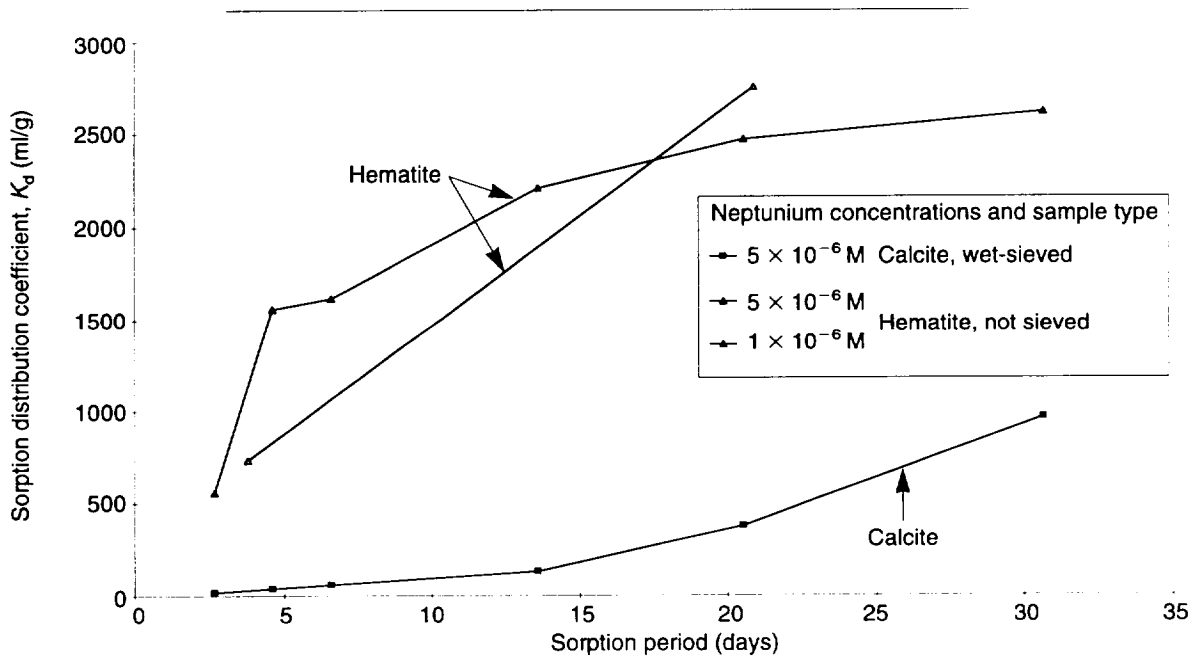


Figure 52. Time Dependence of Neptunium Sorption for Calcite and Hematite in UE-25 p#1 Water. Variation with time of K_d for the sorption of neptunium onto calcite (squares) and hematite (triangles) under atmospheric conditions and at the specified initial neptunium concentrations in UE-25 p#1 well water. The calcite was wet-sieved to particle sizes ranging from 75 to 500 μm ; the synthetic hematite was not sieved. The pretreatment period in UE-25 p#1 water was 2 to 13 days.

UE-25 p#1 water and found that, regardless of the conditions, neptunium sorption onto tuffs and zeolites is negligible ($K_d < 1$ ml/g) in this water (Fig. 55). If clinoptilolite is the only mineral affecting neptunium sorption and if ion exchange at the surface is the dominating mechanism, one might conclude that the reason for the lack of neptunium sorption on clinoptilolite is the formation of the neptunium carbonato complex ($\text{NpO}_2\text{CO}_3^-$) in UE-25 p#1 water to the exclusion of the neptunyl cation. The data reported by Nitsche et al. (1994) do not support this conclusion (Table 14); the relative amount of neptunyl in UE-25 p#1 water is larger than that in J-13 water at a pH of 7. If the data of Nitsche et al. are correct, another possible reason for the lack of neptunium sorption on clinoptilolite in UE-25 p#1 water is competitive effects due to the larger ionic strength of that water compared with J-13 water, which has a smaller ionic strength by nearly an order of magnitude.

As we mentioned earlier, iron oxides have a high affinity for neptunium (Combes et al. 1992). Figure 56 shows further data on the sorption of

neptunium onto hematite, this time in both J-13 and UE-25 p#1 waters as a function of pH. It is important to note that the trends observed in this figure (sorption increasing with increasing pH and larger sorption in UE-25 p#1 water than in J-13 water) are not followed by the neptunium sorption reported for clinoptilolite-rich tuff samples. Also once again, the neptunium sorption in the rest of the tuff samples is so small (even in the samples that contain traces of hematite) that the iron oxides appear to be passivated in the tuffs.

As illustrated in Fig. 57, regardless of the tuff studied, neptunium sorption onto tuffaceous materials is extremely limited. One exception is tuff sample G2-723 (not shown), which contains a large amount of calcite, a good sorber for neptunium. This sample will be discussed later.

Figure 58 is a plot both of neptunium sorption data in J-13 water and of surface area for tuffs for which BET-surface-area and XRD analyses exist. The surface-area data correspond to the surface area for the tuffs sieved in J-13 water with the following

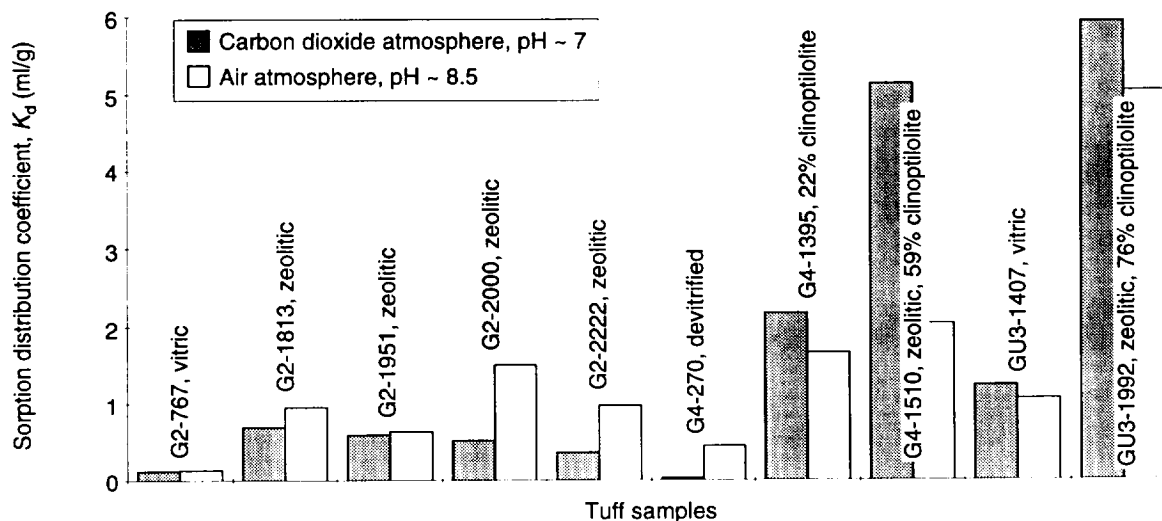


Figure 53. pH Dependence of Sorption at 10^{-7} M. Experimental values of K_d for the sorption of neptunium onto tuffs in J-13 water at initial concentrations of 6 to 7×10^{-7} M are compared for atmospheric conditions (pH ~ 7) and a carbon-dioxide overpressure (pH ~ 8.5). Tuffs were wet-sieved to particle sizes from 75 to 500 μm . The pretreatment period was 2 to 3 days; the sorption period was 3 to 5 days.

IV. Sorption and Sorption Modeling Studies

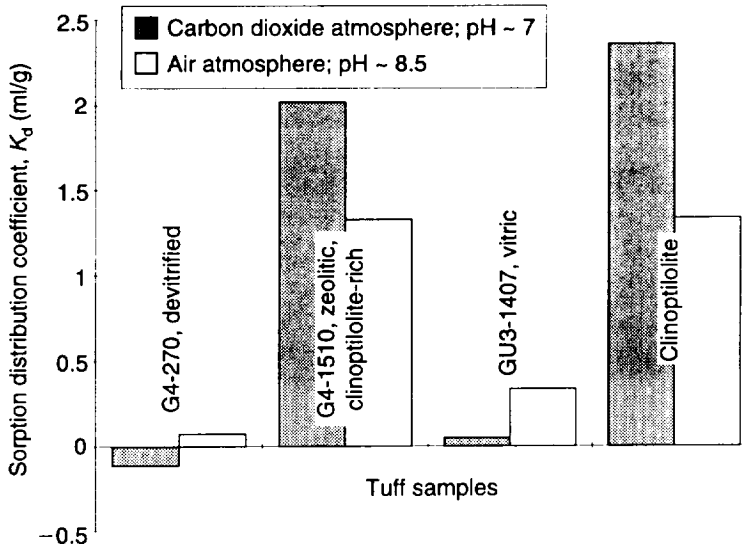


Figure 54. pH Dependence of Sorption at 10^{-5} M. Experimental values of K_d for the sorption of neptunium onto several tufts and clinoptilolite in J-13 well water at an initial neptunium concentration of 3×10^{-5} M are compared for both atmospheric conditions (pH \sim 8.5) and a carbon-dioxide overpressure (pH \sim 7). Tufts were wet-sieved to particle sizes that ranged from 75 to 500 μ m; the clinoptilolite was not sieved. The pretreatment period was 2 to 3 days; the sorption period was 3 to 5 days.

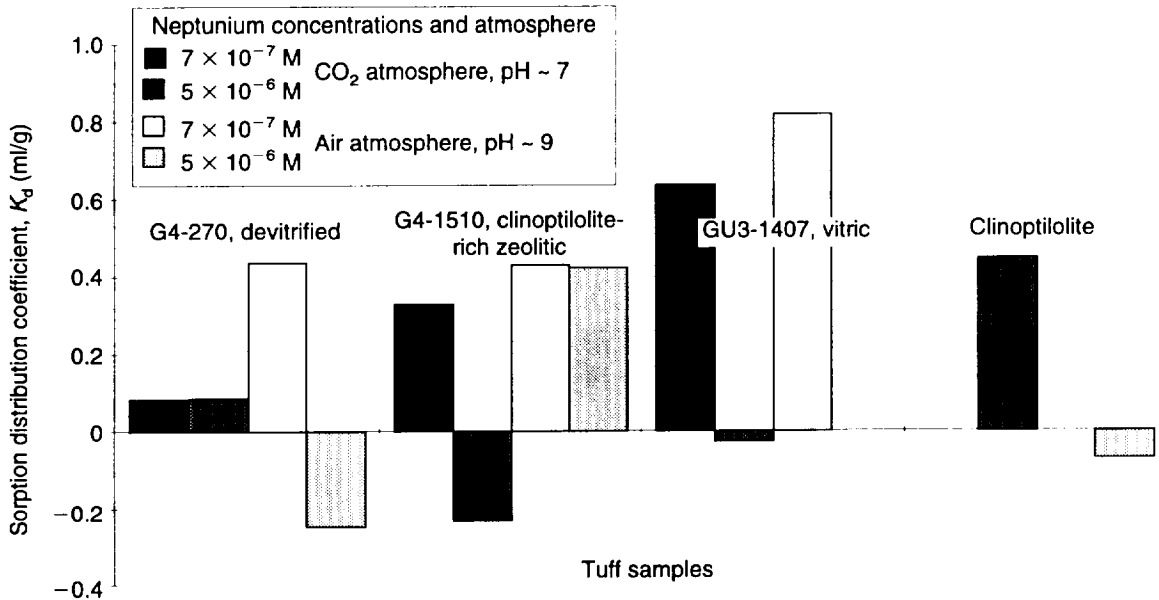


Figure 55. Neptunium Sorption in UE-25 p#1 Well Water. Experimental values of the batch-sorption distribution coefficient, K_d , for neptunium in UE-25 p#1 water show negligible sorption regardless of sample type (devitrified tuff, clinoptilolite-rich zeolitic tuff, vitric tuff, or clinoptilolite), pH (\sim 7 or \sim 9), or initial neptunium concentration (5×10^{-6} or 7×10^{-7}).

exceptions: the surface area used for sample G4-2077 was for dry-sieved tuff; the surface area used for tufts G4-268 and G4-272 was the same as that measured for tuff G4-270; the surface area plotted for tufts G4-1505 and G4-1510 was the

same as that measured for tuff G4-1506; and the surface area plotted for tuff GU3-1405 was the same as that measured for tuff GU3-1407. Figure 58 shows a reasonable correlation between sorption and surface area. The surface areas that are

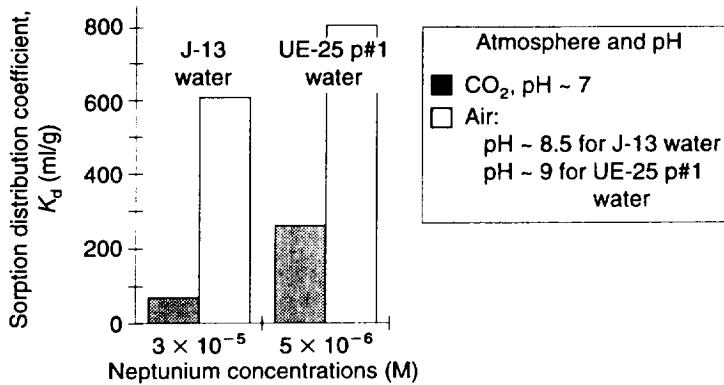


Figure 56. Neptunium Sorption for Hematite. Values of the batch-sorption distribution coefficient, K_d , are given for the sorption of neptunium onto hematite in UE-25 p#1 well water at the specified initial neptunium concentrations and pH values. The pretreatment period was 2 to 3 days, and the sorption period was 3 to 5 days.

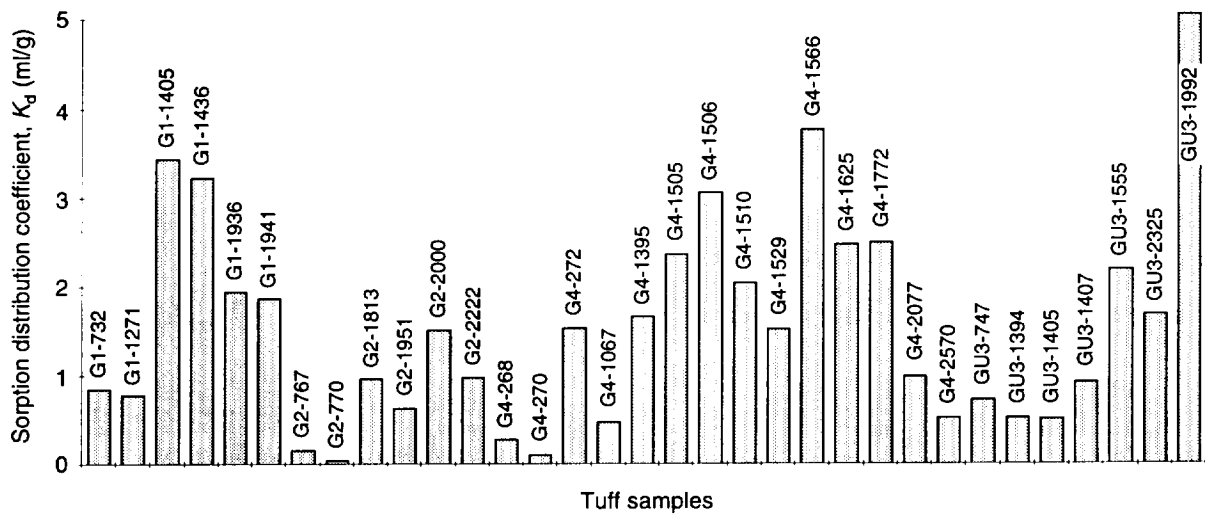


Figure 57. Neptunium Sorption in J-13 Well Water. These values of the batch-sorption distribution coefficient, K_d , illustrate the limited sorption of neptunium onto a large range of Yucca Mountain tuffs in J-13 well water under atmospheric conditions. The initial neptunium concentration ranged from 6 to 8×10^{-7} M. The tuffs were wet-sieved to particle sizes that ranged from 75 to 500 μm . The pretreatment period was 2 to 14 days; the sorption period was 3 to 23 days.

larger than 18 m^2/g correspond to clinoptilolite-rich tuffs.

Figures 59 and 60 summarize the sorption of neptunium under atmospheric conditions for tuffs and minerals as a function of water type. Sorption onto zeolitic tuffs decreases considerably with increasing carbonate content and ionic strength of the water. Figure 60 also shows the calcite-rich tuff G2-723 (34% calcite), which exhibits considerable sorptive capacity for neptunium. Assuming that

the calcite in the tuff sample has the same surface area as the natural calcite used for these experiments (and that calcite is the only sorptive mineral in the tuff), one would predict from neptunium sorption on pure calcite a $\log(K_d)$ for tuff G2-723 of 1.5. This prediction agrees well with the measured K_d (Fig. 60).

As the neptunium concentration is increased towards the solubility limit for neptunium in the J-13 and UE-25 p#1 groundwaters, the observed

IV. Sorption and Sorption Modeling Studies

sorption decreases, but the general trends remain the same (as seen by comparing Figs. 58 and 61). The extremely low neptunium sorption reported for devitrified tuffs in J-13 and UE-25 p#1 waters is supported by the sorption data plotted for albite (Fig. 62), which appears to be a very poor sorber for neptunium (in both waters). The nonlinearity of neptunium sorption in the high-concentration region (approaching the solubility limits for neptunium) is further illustrated in Figs. 63 and 64 (for J-13 and UE-25 p#1 waters under a carbon-dioxide atmosphere at a pH of 7).

Conclusions regarding sorption behavior with respect to expected variations in groundwaters.

The mechanisms by which neptunium appears to sorb onto mineral surfaces in the Yucca Mountain flow system appear to be surface complexation on oxide phases and coprecipitation and surface

adsorption involving carbonate minerals. The surface-complexation mechanism appears to be relatively insensitive to variations in ionic strength, detailed groundwater composition, and pH over the range from 6.5 to 8.5. This mechanism is likely responsible for the 0.5 to 5.0 ml/g range in sorption-coefficient values consistently measured in many different rock samples. The high end of this range may reflect secondary mechanisms, such as the reduction of Np(V) to Np(IV) on mineral surfaces containing ferrous iron. Regardless of the details of the mechanisms, performance-assessment calculations could use a probability distribution for sorption-coefficient values, as was done for the 1993 total-system performance assessment (Wilson et al. 1994).

For hydrologic units in which calcite is known to be present or in which groundwaters are oversatu-

continued on page 100

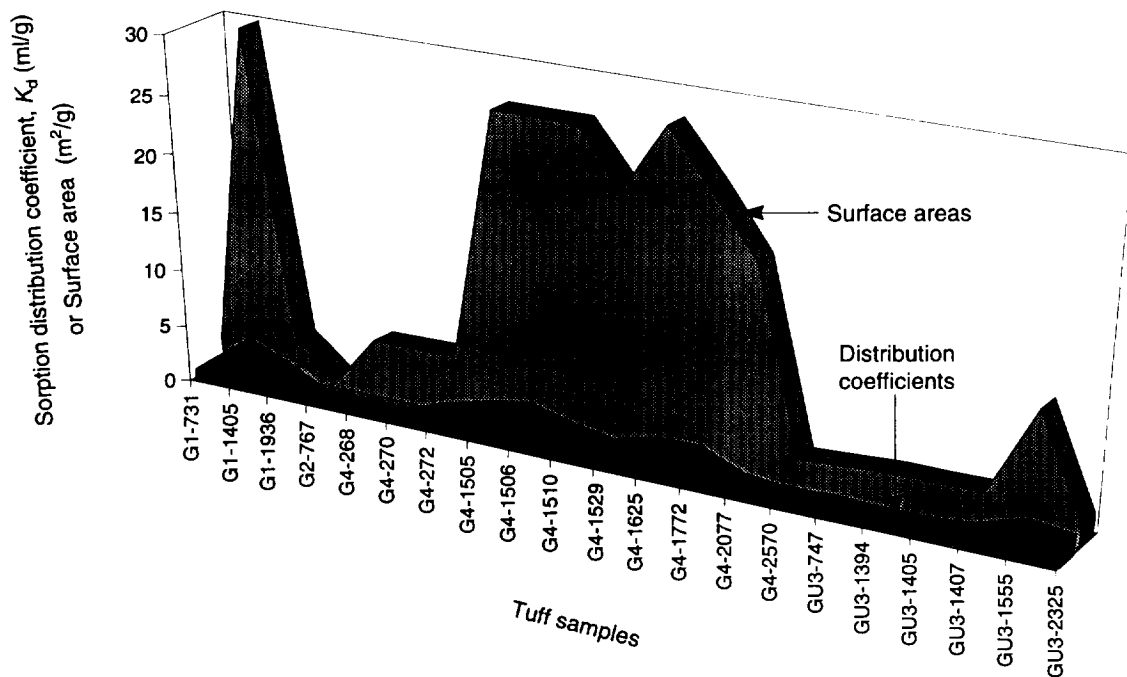


Figure 58. Neptunium Sorption and Surface Area. Values of the batch-sorption distribution coefficient, K_d , for neptunium onto various tuffs are compared to the corresponding surface areas of those tuffs. The sorption is for J-13 well water under atmospheric conditions at an initial neptunium concentration ranging from 6×10^{-7} to 8×10^{-7} M. The tuffs were wet-sieved to particle sizes that ranged from 75 to 500 μm . The pretreatment period was 2 to 14 days; the sorption period was 3 to 23 days.

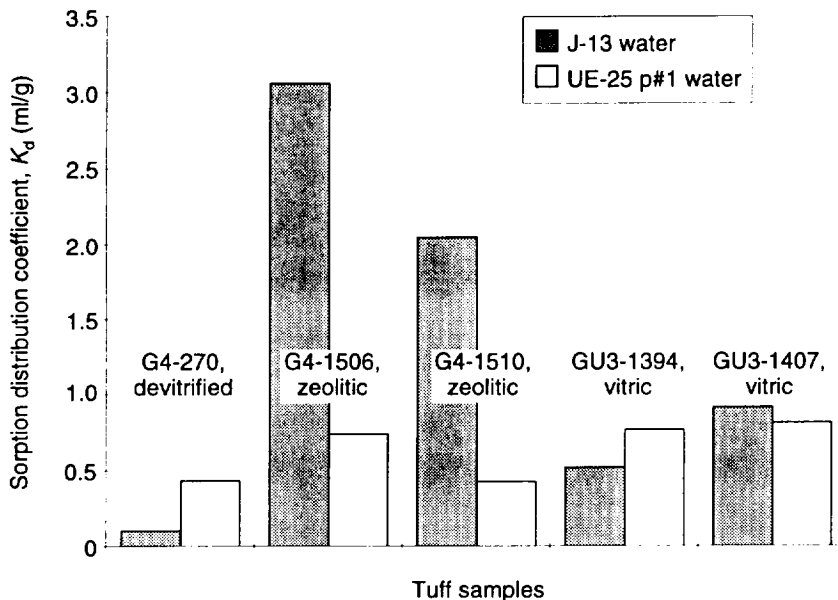


Figure 59. Dependence on Water for Sorption onto Tuffs. Values of K_d for sorption of neptunium onto several tuffs that allow comparison of sorption (under atmospheric conditions) for the two types of groundwaters. The initial neptunium concentration ranged from 6×10^{-7} to 8×10^{-7} M. The tuffs were wet-sieved to particle sizes ranging from 75 to 500 μ m. The pretreatment period was 2 to 14 days, and the sorption period was 3 to 23 days.

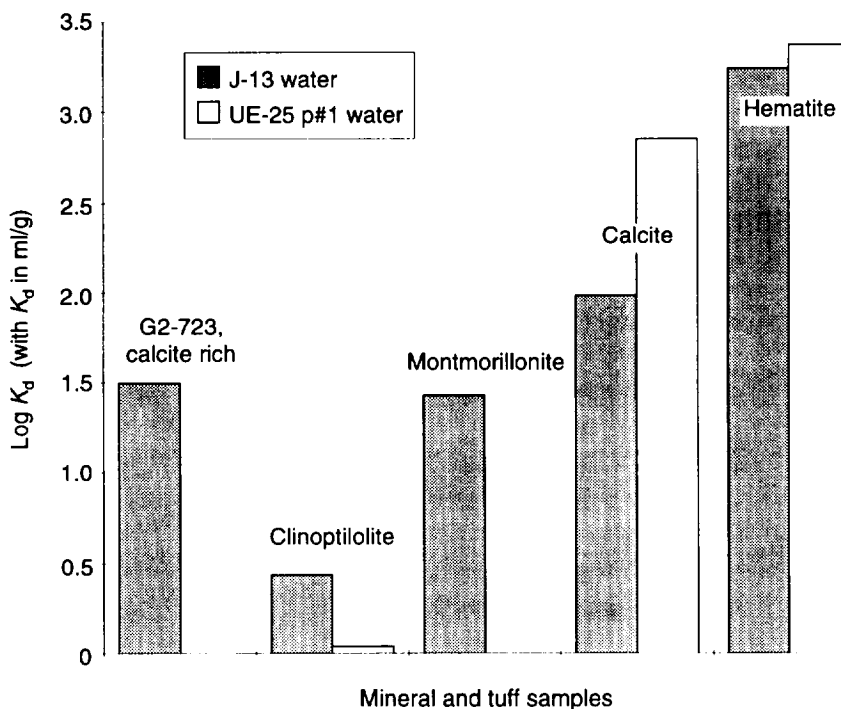


Figure 60. Dependence on Water for Sorption onto Minerals. Values of K_d for neptunium onto several minerals and a calcite-rich tuff that allow comparison of sorption (under atmospheric conditions) for the two groundwaters. The initial neptunium concentration ranged from 6×10^{-7} to 8×10^{-7} M. The tuff and the calcite were wet-sieved to particle sizes ranging from 75 to 500 μ m, the montmorillonite was dry-sieved; the clinoptilolite and hematite were not sieved. The sorption period was 17 to 22 days.

IV. Sorption and Sorption Modeling Studies

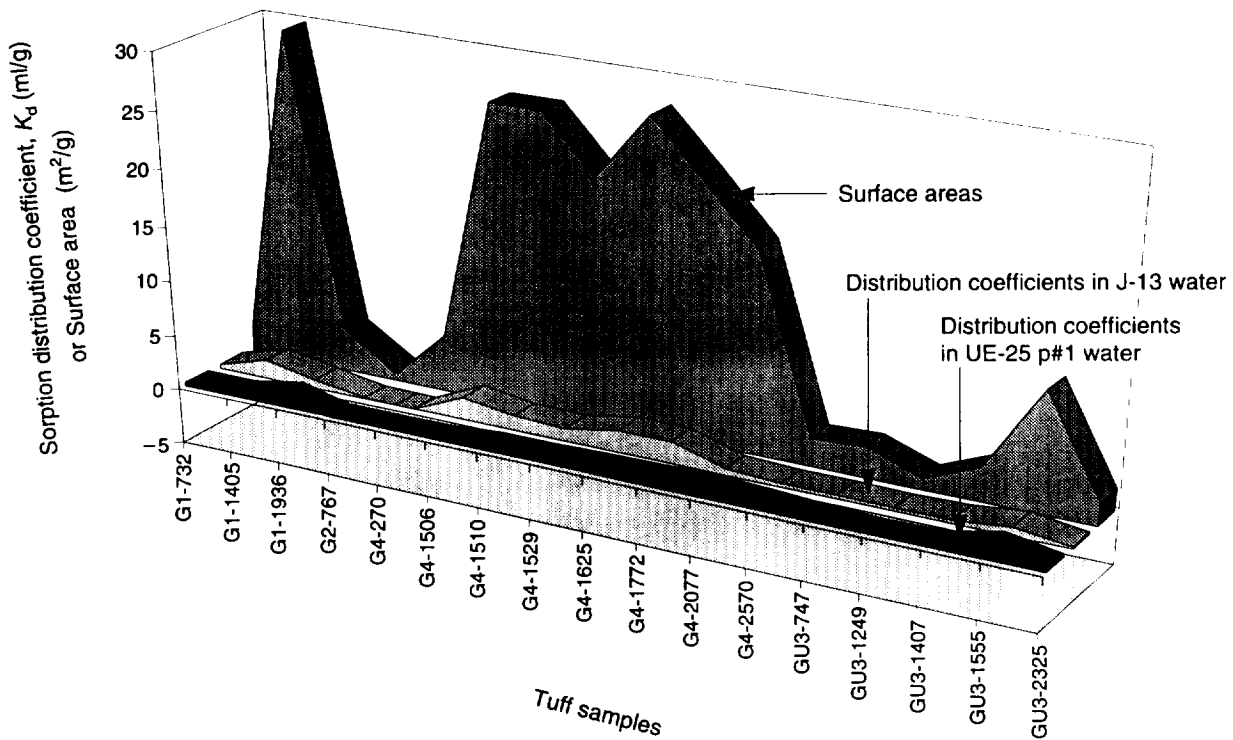


Figure 61. High-concentration Sorption onto Tuffs. Values of K_d for sorption of neptunium onto tuffs under atmospheric conditions and near the solubility limit (initial neptunium concentrations of 2 to 4×10^{-5} M in J-13 water and 5×10^{-6} M in UE-25 p#1 water) are compared with the surface areas of those tuffs. The tuffs were wet-sieved to particle sizes ranging from 75 to 500 μm . The pretreatment period was 2 to 5 days; the sorption period was 2 to 4 days.

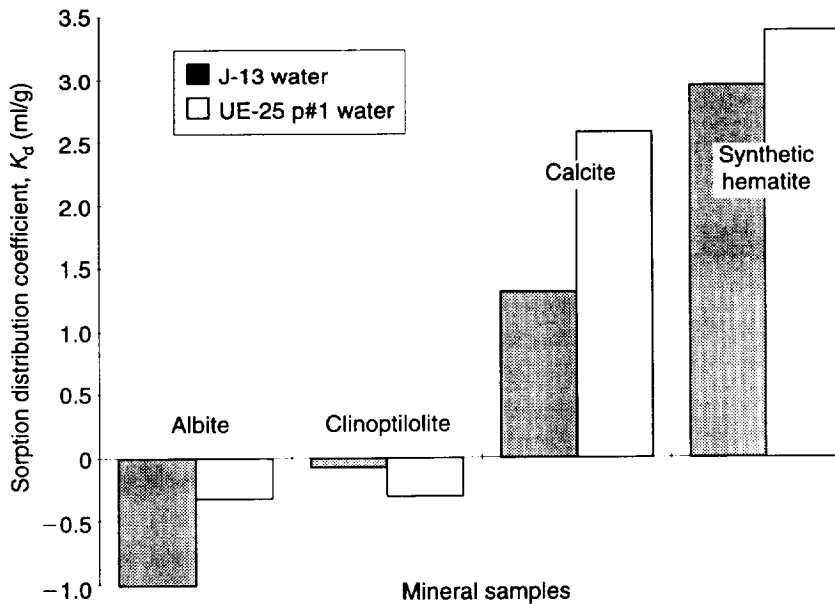


Figure 62. High-concentration Sorption onto Minerals. Values of K_d for sorption of neptunium onto minerals under atmospheric conditions for neptunium concentrations near the solubility limit (initially, 2 to 4×10^{-5} M in J-13 water and 5×10^{-6} M in UE-25 p#1 water). The calcite was wet-sieved to particle sizes ranging from 75 to 500 μm ; the others were not sieved. The pretreatment period was 2 to 31 days; the sorption period was 21 days.

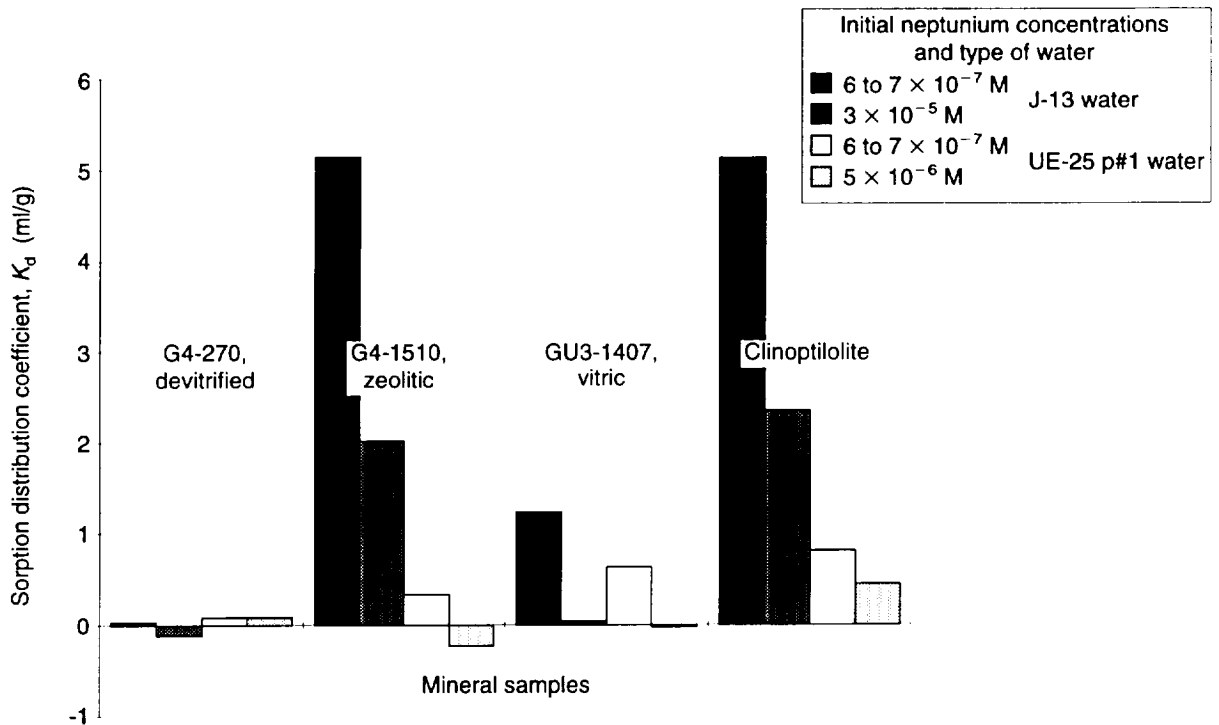


Figure 63. High-concentration Sorption onto Tufts at pH 7. Values of K_d for sorption of neptunium onto several tufts and clinoptilolite under a carbon-dioxide overpressure (to obtain a pH of approximately 7) are shown. The tufts were wet-sieved to particle sizes ranging from 75 to 500 μm ; the clinoptilolite was not sieved. The pretreatment period was 2 to 3 days; the sorption period was 3 to 4 days.

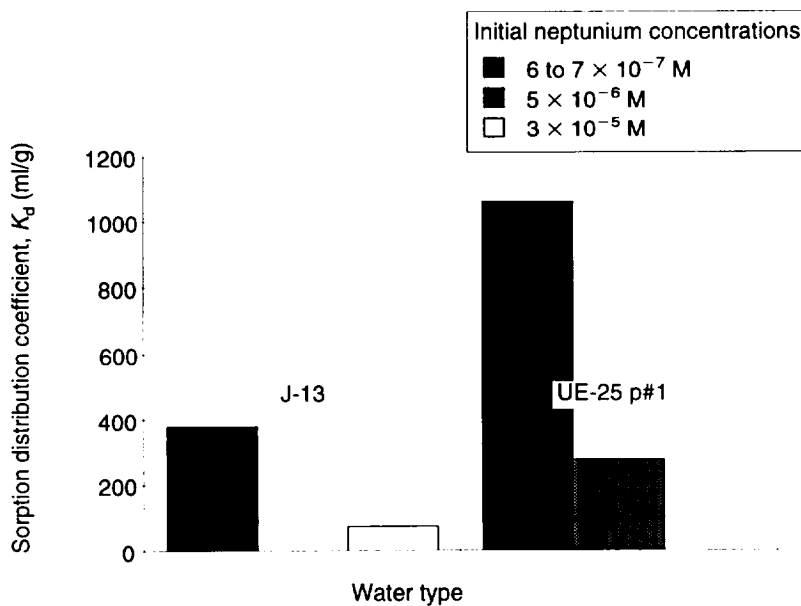


Figure 64. High-concentration Sorption onto Hematite at pH 7. Values of the batch-sorption distribution coefficient, K_d , are shown for sorption of neptunium onto unsieved synthetic hematite under a carbon-dioxide overpressure (to obtain a pH of ~ 7). The pretreatment period was 2 to 3 days; the sorption period was 3 to 4 days.

IV. Sorption and Sorption Modeling Studies

continued from page 96

rated in calcite, higher neptunium sorption coefficients could be used in the calculations if it could be established through laboratory experiments that such coefficients are appropriate. To date, most neptunium sorption coefficients have been obtained using samples from the unsaturated zone, many of which came from levels above the repository horizon. According to the mineralogic studies, calcite is more common at depths below the potential repository horizon than it is at the intermediate depths. Many of the samples used in sorption experiments to date have been obtained from intermediate depths.

Protactinium

Behavior in solutions representative of Yucca Mountain groundwaters.

In aqueous systems, protactinium appears to exist dominantly in the +5 oxidation state although the +4 state may occur in reducing environments (Brookins 1988). In both oxidation states, protactinium is strongly hydrolyzed and forms highly insoluble compounds (Cotton and Wilkinson 1988). This result implies that the +5 solution chemistry of protactinium is more akin to that of Nb(V) than to other actinides in +5 oxidation states, such as PuO_2^+ or NpO_2^+ . If this interpretation is correct, then the solution parameter of greatest importance to protactinium sorption behavior would be pH.

Qualitative evidence for behavior in the surficial environment.

Information on behavior of protactinium in the surficial environment is sparse. Because protactinium forms such insoluble compounds, it is generally assumed to be immobile in the surficial environment.

Data from laboratory sorption experiments.

Batch-sorption experiments with protactinium have yielded some interesting results. In dilute to intermediate ionic-strength solutions, Allard et al. (1982) report large values (10^4 mg/l) for the protactinium sorption coefficient on alumina and silica at pH values greater than 6 to 7 but much lower

values (90–500 ml/g) at pH values less than 7. Rundberg et al. (1985) report protactinium sorption coefficients in the range from 3.7 to 8.2 ml/g for a zeolitic tuff in contact with J-13 water spiked with 10^{-11} to 10^{-14} M protactinium at pH values of 6.3 to 6.7. Together, these data suggest that protactinium sorbs by a surface-complexation mechanism and that there is a rather steep sorption edge for protactinium as a function of pH at a pH value of approximately 7.

Conclusions regarding sorption behavior with respect to expected variations in groundwaters.

Batch-sorption data for protactinium suggest that sorption coefficients for this element will be large ($> 1,000$ ml/g) at a pH value greater than 7 and small (< 10 ml/g) at lower pH values. Because protactinium sorption experiments on rock samples from Yucca Mountain have only been carried out in the low pH range, it would be prudent to carry out several experiments using a Yucca Mountain water at several pH values from 7 to 9.

Selenium

Behavior in solutions representative of Yucca Mountain groundwaters.

Selenium will occur as anionic species in all water compositions expected at Yucca Mountain. Although the two oxidation states of +4 and +6 (Howard 1977) are found for selenium in surficial waters in contact with atmospheric oxygen, the +4 state predominates under the conditions expected for groundwaters at Yucca Mountain (Howard 1977; White et al. 1991). In that state, selenium is found as the SeO_3^{2-} and HSeO_3^- selenite ions. In the +6 oxidation state, selenium occurs as the SeO_4^{2-} and HSeO_4^- selenate ions.

Qualitative evidence for behavior in the surficial environment.

Selenium behavior in the surficial environment is very closely tied to the redox potential of different parts of the near-surface environment. Under reducing conditions, selenium is immobilized as FeSe_2 at low pH (< 5) and as native selenium at higher pH (Howard 1977). The stability range for

native selenium extends nearly to surface redox conditions. When in contact with atmospheric oxygen levels, selenium is apparently stabilized as the selenite ion (SeO_3^{2-}). At higher redox potentials, selenium is oxidized to the selenate ion (SeO_4^{2-}), which appears to be more mobile in the surficial environment than the selenite ion (Howard 1977).

Data from laboratory sorption experiments.

Because selenium occurs as anionic species in the surficial environment, its adsorption behavior is controlled primarily by surface-complexation reactions on oxide minerals including iron oxides and oxyhydroxides (Balistrieri and Chao 1987), manganese oxides and oxyhydroxides, clays (Bar-Yosef and Meek 1987), and other minerals with affinities for anionic species. These surface-complexation reactions are quite sensitive to pH. For example, adsorption on iron oxyhydroxides decreases for both selenite and selenate ions with increasing pH (Balistrieri and Chao 1987). Selenate ions appear to sorb dominantly in the outer layer of the electrical double layer present on oxide surfaces, whereas selenite tends to sorb in the inner layer (Hayes et al. 1987). Selenate ions are subject to ionic-strength effects as well as competitive effects with sulfate and other anions in solution, presumably because they sorb in the outer layer. Selenite ions are not subject to ionic-strength effects but may be subject to competition from other anions sorbing on inner-layer sites (Hingston et al. 1971).

Studies of selenite adsorption on soils in the pH range expected for Yucca Mountain groundwaters indicate relatively limited adsorption (< 30%) from 0.05 N chloride solutions containing 0.16 to 0.63 mg/l selenium (Neal et al. 1987). This limited sorption potential will likely be further decreased in natural waters containing high concentrations of competing anions.

Data for selenium sorption coefficients on Yucca Mountain rock samples in contact with J-13 water have been summarized by Thomas (1987). Most

measured values are less than 5 ml/g, and they do not appear to correlate with rock type. A puzzling feature of the data is that, for a given rock sample, sorption coefficients are larger in the higher pH experiments (pH of 8.8) compared to the lower pH experiments (pH of 6.0). This result is contrary to the pH dependence predicted on the basis of double-layer theories. Neal et al. (1987) noted a similar effect for selenium sorption on soils for a solution phase enriched in calcium. They suggested the effect may be due to the formation of a calcium-rich surface precipitate or, alternatively, a change in surface charge due to the adsorption of divalent calcium cations. Benjamin (1983) made similar observations involving other divalent cations. These data suggest that in groundwaters relatively enriched in calcium, and perhaps other divalent cations, selenium adsorption may be somewhat enhanced in the alkaline pH range.

Conclusions regarding sorption behavior with respect to expected variations in groundwaters.

Sorption coefficients for selenium on Yucca Mountain rock samples have only been measured in J-13 water. These experiments do not show the expected decrease in sorption coefficient with pH. Therefore, variations in pH over the range expected in Yucca Mountain groundwaters do not appear to be the most important groundwater compositional parameter in the sorption behavior of this element. Based on the data obtained in other studies, divalent cations may have a significant impact on the sorption behavior of this element in Yucca Mountain rock-water systems. Additional experiments with waters enriched in divalent cations (such as UE-25 p#1 water) may be productive and may enlarge the range of selenium sorption-coefficient values appropriate for use in performance-assessment calculations.

Uranium

Behavior in solutions representative of Yucca Mountain groundwaters.

Under the redox potentials expected in Yucca Mountain groundwaters, particularly in the unsaturated zone, uranium should be in the +6 oxidation

IV. Sorption and Sorption Modeling Studies

state. In this oxidation state, uranium will be present in solution in a variety of complexes including $(\text{UO}_2)_2\text{CO}_3(\text{OH})_3^-$, $\text{UO}_2(\text{CO}_3)_2^{2-}$, $\text{UO}_2(\text{CO}_3)_3^{4-}$, $\text{UO}_2(\text{OH})_2(\text{aq})$, $\text{UO}_2(\text{CO}_3)(\text{aq})$, and other minor species. Phosphate, fluoride, or sulfate species will not be significant within the concentration ranges for these anions and the pH range expected in Yucca Mountain groundwaters. In the high-silica groundwaters of Yucca Mountain, the solubility-controlling compound for uranium should be haiweeite ($\text{Ca}(\text{UO}_2)_2(\text{SiO}_2)_6(\text{H}_2\text{O})_5$), according to available thermodynamic data (Bruton 1990). Interestingly, leaching experiments on uranium-oxide pellets (Bates et al. 1990) at 90°C using J-13 water produced a variety of phases on reacted surfaces that did not include haiweeite.

Qualitative evidence for behavior in the surficial environment.

Data on the behavior of uranium in the surficial environment are available from various sources. Several types of uranium ore deposits have been studied as natural analogs to repository settings. Other sources of data include studies of uranium mill-tailings piles, waste-stream outfalls, and other uranium ore deposits. Only the natural analog studies will be discussed in this section.

The deposits that have been studied as natural analogs include the deposits at Oklo, Gabon, the Alligator Rivers region in Australia, Cigar Lake in Canada, Poços de Caldas in Brazil, and Peña Blanca in Mexico. Each of these deposits has been studied in considerable detail to define the geochemical behavior of uranium and its daughter products in the environments in which the ore deposits are found. Although none of the environments are completely analogous to the Yucca Mountain site, the Peña Blanca deposit is at least situated in Tertiary volcanic tuffs similar to those present at Yucca Mountain.

A critical aspect of any analog to potential uranium migration at the Yucca Mountain site is that the uranium source must be subject to redox potentials similar to those expected at Yucca Mountain, par-

ticularly in the unsaturated zone. This fact eliminates from detailed consideration data from the Cigar Lake and probably the Oklo deposits (Goodwin et al. 1989; Cramer and Sargent 1994; Brookins 1983).

The Alligator Rivers deposits are exposed to oxidizing conditions in a surficial environment (Gilbin and Snelling 1983). Uranium isotope-disequilibrium studies at this site indicate that uranium migration has occurred relatively recently (Snelling and Dickson 1979). However, evidence for recent transport does not by itself provide an estimate of the rate of transport and, more importantly, of the chemical controls on this rate. The latter type of information could be very useful to the Yucca Mountain Program.

At the Koongarra deposit, uranium migration is significantly retarded by the precipitation of uranyl phosphate minerals (Snelling 1980). Although phosphate concentrations in local groundwaters are not high (0.01–0.1 mg/l), significant phosphate concentrations are found in the country rocks in minerals such as apatite. The phosphate in the rocks is apparently redistributed locally by groundwater, resulting in the precipitation of uranyl phosphate minerals within the zone of weathering (Snelling 1980). This retardation mechanism is not expected to be important at Yucca Mountain, given the low phosphate concentrations found in Yucca Mountain rock units (Broxton et al. 1986).

Uranium in the zone of weathering at Alligator Rivers also appears to be associated with and is probably retarded by ferric-iron compounds (Payne et al. 1991 and others). Sorption experiments have been carried out involving uranium sorption on whole-rock samples and on pure mineral samples (Payne et al. 1991). The results of these experiments suggest that ferric hydroxides are strong sorbers of uranium in this system over a pH range of 5 to 9. This result is not particularly new as similar results on ferric oxyhydroxides have been reported by others (for example, Hsi and Langmuir 1985). A potentially important result from these studies

would be the derivation of some defensible estimate of the rate of transport of uranium in this system using the experimentally derived chemical constraints on uranium adsorption behavior and a valid groundwater flow model. Unfortunately, hydrologists who are knowledgeable about the site suggest the complicated nature of the flow system may preclude the development of defensible flow models (S. N. Davis, cited in Curtis and Fabryka-Martin 1988).

The Peña Blanca uranium deposits in Mexico provide a potentially more appropriate analog site in relation to Yucca Mountain. The primary uranium deposits at this site are hydrothermal in origin and were emplaced in structural features associated with Tertiary silicic volcanic tuffs that overlie Mesozoic calcareous basement (George-Aniel et al. 1991). In addition to the hydrothermal deposits, which contain sulfide minerals as well as uranium oxides, supergene deposits have formed locally through the leaching of uranium from the volcanic rocks and subsequent precipitation as uranyl silicate minerals, including uranophane (Murphy 1992). The supergene deposits are hosted by kaolinitized and silicified rhyolite and do not appear to contain sulfide minerals. The absence of sulfide minerals is important because sulfides, such as pyrite, oxidize readily in the surficial environment to produce acidic conditions unlike those expected within Yucca Mountain. The supergene deposits are thought to have formed in the surficial environment (George-Aniel et al. 1991), and their study may offer useful insight into the potential for migration of uranium from the proposed repository within Yucca Mountain. No data on the present-day sorption behavior or rate of migration of uranium in these deposits has been reported to date. However, several geochemical studies are currently underway to provide such data (Murphy 1992).

A qualitative study by Rosholt et al. (1971) established that uranium was leached from devitrified tuff samples but not from hydrated glassy samples obtained from a given geologic unit. This and other data presented suggest devitrification makes

the uranium in tuffs more mobile in the surficial environment. Zielinski et al. (1986) and Flexser and Wollenberg (1991) observed that uranium in Yucca Mountain devitrified tuffs was commonly associated with manganese oxides. This fact suggests that although uranium may be mobile in the unsaturated devitrified tuffs in Yucca Mountain, it could be retarded to the extent that there are manganese oxides present along the flow path with sufficient capacity to sorb the potential flux of uranium from the proposed repository horizon. Given the amount of uranium to be emplaced in the potential repository, it would seem the sorption capacity of the manganese oxides present in the mountain (Bish and Chipera 1989) would be rapidly saturated. Nonetheless, manganese oxides may significantly retard the movement of uranium in some of the fracture-flow scenarios.

Data from laboratory sorption experiments.

Data have been presented on the adsorption of uranium onto a variety of pure mineral phases in simple electrolytes. Among the solid phases investigated are goethite (for example, Hsi and Langmuir 1985), hematite (Ho and Miller 1986), silica gel (Zielinski 1980), clays (Tsunashima et al. 1981), and zeolites (Ames et al. 1983). The results reported are sometimes difficult to reconcile. For example, Hsi and Langmuir report that hematite sorbs very little of the uranium in solutions with 5×10^{-5} M uranium and 10^{-3} M total carbonate, whereas Ho and Miller report that hematite sorbs up to 100 per cent of the uranium in their experiments with similar uranium and bicarbonate solution concentrations. Both sets of experiments had similar hematite surface areas. The main difference was that the solution phase in the Hsi and Langmuir experiments also contained 0.1 M NaNO_3 . However, NaNO_3 is generally considered to be a nonreactive electrolyte, and nitrate does not form complexes with uranium in the pH range addressed in these experiments. Why there is a difference in these results is unclear. One possibility is that the surface characteristics of the solid phases used were not the same in the two sets of experiments.

IV. Sorption and Sorption Modeling Studies

Silica gel appears to have a clear affinity for uranium as established by the results of laboratory experiments and by observations on the association of uranium with opals in nature (Zielinski 1980). According to Maya (1982), the uranium is adsorbed to silica gel as the uranyl ion, free of carbonate ligands. Zielinski has shown that sorption of uranium onto silica gel is sensitive to the total carbonate concentration of the solution phase when this concentration is above 0.01 M. Interestingly, experiments carried out at elevated temperatures (65–80°C) resulted in somewhat higher sorption coefficients. Data regarding competitive effects on silica gel between uranium and other constituents in groundwaters at near-neutral pH have not been found in the literature.

Sorption of uranium by clays has been investigated in some detail. Borovec (1981) has presented data that indicate montmorillonite has a high selectivity for uranyl ions relative to divalent ions of zinc, manganese, calcium, magnesium, cobalt, cadmium, and nickel at a pH of 6 in chloride solutions. However, Tsunashima et al. (1981) found montmorillonite has a greater selectivity for calcium, magnesium, and barium ions than for uranyl ions in nitrate solutions over the pH range from 4.0 to 4.5. Montmorillonite was found to have a greater selectivity for the uranyl ion than for sodium and potassium ions in the same solutions. Ames et al. (1983) found that uranium was strongly sorbed to montmorillonite from 0.01 M NaCl solutions but weakly sorbed from 0.01 M NaHCO₃ solutions in the pH range from 8 to 9.

Because groundwaters in Yucca Mountain contain significant concentrations of bicarbonate, calcium, and magnesium ions, these data suggest overall that uranyl ions may not compete favorably for exchange sites on clay minerals in Yucca Mountain, although quantitative prediction of the extent of exchange would require more detailed analysis.

Data available on uranium sorption on zeolitic minerals are very limited. Ames et al. (1983)

report that clinoptilolite has a low affinity for trace levels of uranium in the pH range from 8 to 9 in 0.01 M NaHCO₃. Doi et al. (1975) found that uranium at concentrations of 1.0×10^{-6} g per g of solution was strongly sorbed onto clinoptilolite from perchlorate solutions in the pH range from 4 to 8.5.

Data on uranium sorption coefficients for Yucca Mountain rock-water systems were reported by Thomas (1987) and discussed by Meijer (1990, 1992). The affinity of the devitrified and vitric tuffs for trace levels of uranium is generally small ($K_d < 5$ mg/l) over the pH range from 6 to 9 in J-13 water. For zeolitic tuffs, the K_d is near zero at a pH of 9 but increases with decreasing pH to values of approximately 25 mg/l at a pH of 6 in J-13 water. This behavior suggests uranyl ions can exchange with the major cations in zeolites. In UE-25 p#1 water, uranium batch-sorption experiments were only carried out in the pH range from 8.3 to 9.3 with the result that the measured sorption coefficients were small (0–2.7 mg/l; Thomas 1988). The devitrified sample showed the largest sorption coefficient. In the pH range from 6 to 8, it is expected that the sorption coefficients for uranium in UE-25 p#1 water will increase with decreasing pH, but they will likely be smaller than the coefficients obtained for the same rock samples in J-13 water over this pH range. In H-3 groundwater, sorption coefficients were also low for zeolitic and devitrified rock types over the pH range from 9.2 to 9.3, presumably reflecting the elevated carbonate content of this water. However, data for a vitric sample showed values of 6.2 mg/l for the uranium sorption coefficient at a pH of 9. This relatively high value has not been explained.

We studied the sorption of U(VI) onto samples of the three types of tuff in J-13 water (under oxidizing conditions) at the two pH values (7 and 8.5). However, to identify the sorbing minerals in the tuffs, we also studied sorption onto the pure minerals hematite, clinoptilolite, albite, and quartz. We found that uranium in J-13 water does not sorb

onto devitrified and vitric tuffs, albite, and quartz (Table 18).

We used wet-sieved tuffs, albite, and quartz samples with particle sizes in the range from 75 to 500 μm . Initial uranium concentrations ranged from 8×10^{-8} to 1×10^{-4} M. The pretreatment period was 2 to 4 days, and the sorption period, 3 to 4 days. The negative values reported in Table 18 are the result of analytical error for the case of very little sorption (that is, a small number obtained as the difference of two large numbers). For the experimental conditions cited, uranium sorption onto zeolitic tuffs and clinoptilolite is nonlinear and can be fitted with Freundlich and Langmuir isotherms (Figs. 65 and 66).

For the clinoptilolite-rich zeolitic tuff sample G4-1510, the scatter in the data makes it impossible to conclude whether there is a significant difference between the experiments performed under a carbon-dioxide overpressure and a pH of 7 or at atmospheric conditions and a pH of 8.5 (Fig. 65). However, the experiments with pure clinoptilolite indicate that sorption increases with decreasing pH for U(VI) (Fig. 66), as is the case for Np(V). Because the major constituent of tuff sample G4-1510 is clinoptilolite, predictions of the K_a (K_d divided by the solid-phase surface area) were made for uranium sorption onto this tuff by assuming that clinoptilolite is the only sorbing phase. Inspection of Table 19 indicates that reasonable predictions are obtained with this assumption for a pH of 7 but not for a pH of 8.5. In all cases, predictions based on clinoptilolite sorption are conservative.

The sorption of uranium onto pure iron oxides (such as hematite) is very large (and large uncertainties in the K_d values result from measuring the small amounts of radionuclide left in solution after

Table 18. Uranium Sorption in J-13 Water under Oxidizing Conditions

Solid phase	pH	K_d (ml/g)*
G4-268, devitrified tuff	7	2×10^{-1}
	8.5	7×10^{-1}
GU3-1405, vitric tuff	7	-5×10^{-1}
	8.5	6×10^{-1}
Quartz	7	1×10^{-1}
	8.5	7×10^{-2}
Albite	7	-5×10^{-2}
	8.5	-1×10^{-1}

*The uncertainties in the data are ± 3

sorption). Although the measured sorption of uranium onto pure hematite is very large, sorption onto devitrified tuffs, which appear to have traces of hematite ($1\% \pm 1$), is essentially zero. This result could be due to differences in the surface of pure hematite compared to hematite in tuff. It could also be due to passivation of the hematite surfaces in the tuff by elements (such as the rare earths) that have a higher affinity for hematite than uranium and, thus, occupy the sorption sites.

Conclusions regarding sorption behavior with respect to expected variations in groundwaters. The dominant groundwater compositional controls on the sorption behavior of uranium on Yucca Mountain rock samples will likely be pH, carbonate content, and the concentrations of calcium and magnesium ions in solution. The pH and carbonate contents influence the sorption largely as a result

Table 19. Prediction of Uranium Sorption on Clinoptilolite-rich G4-1510 Tuff in J-13 Water

Initial concentration (M)	pH	Measured K_a (m)	Predicted K_a (m)*
2×10^{-7} to 4×10^{-7}	7	8×10^{-7}	8×10^{-7}
	8.5	8×10^{-7}	4×10^{-7}

*Assuming clinoptilolite is the only sorbing mineral in the tuff

IV. Sorption and Sorption Modeling Studies

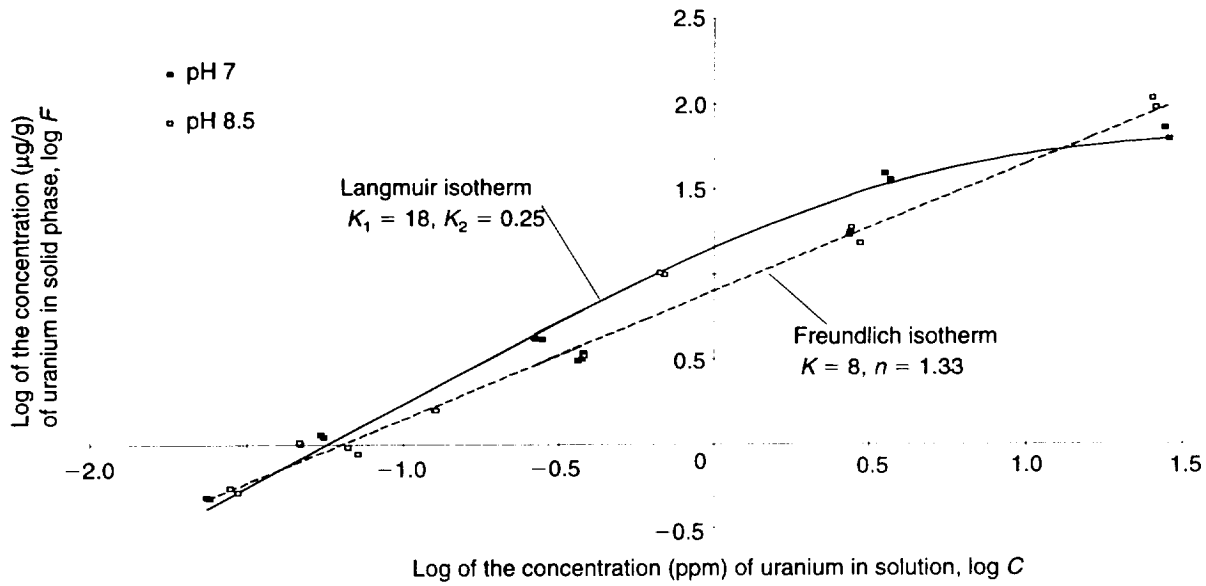


Figure 65. Uranium Sorption onto Clinoptilolite-rich Tuff. A log-log plot of the concentration of uranium in the solid phase, F , of the clinoptilolite-rich tuff G4-1510 versus the concentration of uranium in the solution phase, C , of J-13 well water. The tuff was wet-sieved to give particles that ranged in size from 75 to 500 μm . The period of pretreatment was 2 to 4 days; the period of sorption was 3 to 4 days. The data for a pH of 7 have been fitted with a Langmuir isotherm; the data for a pH of 8.5 have been fitted with a Freundlich isotherm.

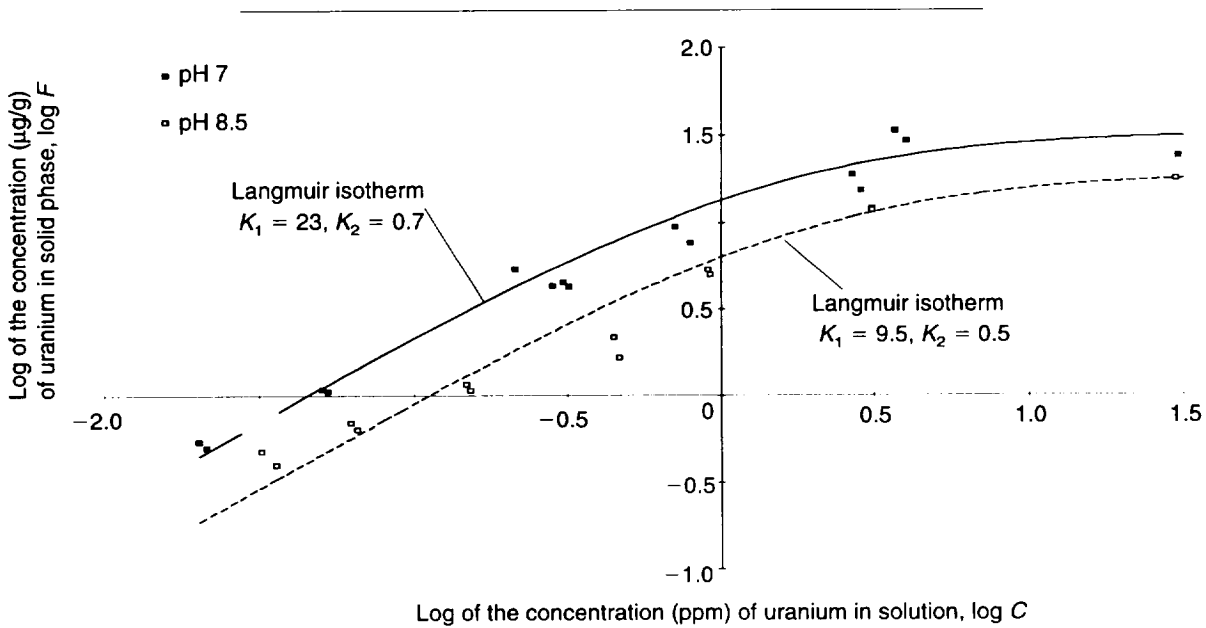


Figure 66. Uranium Sorption onto Clinoptilolite. A log-log plot of the concentration of uranium in the solid phase, F , of clinoptilolite versus the concentration of uranium in the solution phase, C , of J-13 water. The mineral was unsieved. The period of pretreatment was 2 to 4 days; the period of sorption was 3 to 4 days. The data for each pH (7 and 8.5) have been fitted with a Langmuir isotherm.

of the decrease in carbonate complexation of uranium with decreasing pH. These two parameters are therefore not entirely independent. However, different water compositions can have different carbonate contents at a given pH. The expectation is that waters with higher carbonate contents will be associated with lower sorption coefficients. This trend would apply to both ion-exchange and surface-complexation sorption mechanisms. However, decreasing pH will have different effects on uranium sorption behavior in zeolitic and clay-rich samples versus devitrified and vitric samples. In the former samples, the uranium sorption coefficient will likely increase with decreasing pH due to the increase in uranyl ion concentrations with decreasing pH. For a given rock-water system, the magnitude of this increase will depend on the concentrations of competing ions such as calcium and magnesium in the water. For high calcium and magnesium waters, the competition effects will be substantial. Because unsaturated-zone waters are relatively enriched in calcium and magnesium, uranium sorption coefficients in the unsaturated zone may be on the low end of the range reported to date (Thomas 1987, 1988) unless the low total carbonate concentrations in these waters balance the effect of the elevated calcium and magnesium concentrations.

It will be important to carry out experiments on representative rock samples using a high-calcium-and-magnesium, low-carbonate, unsaturated-zone water composition with pH controlled over a range from 6 to 9. Similar experiments should be carried out with a high-total-carbonate and high-calcium-and-magnesium water composition, such as UE-25 p#1 water, over the pH range from 6 to 8.

Carbon, Chlorine, Iodine, and Technetium

Because carbon, chlorine, iodine, and technetium are unlikely to have significant sorption affinity in the rock-water systems expected at Yucca Mountain, their sorption behavior will not be discussed in detail. For carbon, the most robust retardation mechanism will be isotopic exchange with

stable carbon isotopes in groundwater and on carbonate mineral surfaces (Meijer 1993).

Chloride and iodide ions will have no significant retardation in Yucca Mountain rock-water systems and may even have slightly enhanced migration rates due to anion-exclusion effects (Ogard and Vaniman 1985). If conditions were to become sufficiently oxidizing to convert iodide to iodate, some retardation of iodine might occur in the flow system. Although such conditions might occur locally, for example, due to radiolysis effects, it is considered unlikely that such conditions would be present over a significant volume of the flow system for an extended period of time.

Technetium appears to show nonzero, although minimal, retardation in Yucca Mountain rock-water systems (Ogard and Vaniman 1985; Rundberg et al. 1985; Thomas 1988). However, the cause of this retardation has not been identified, and it may simply be an experimental artifact. Because the minimal values obtained for technetium sorption coefficients to date will not result in significant retardation of technetium, it does not seem prudent to expend funds on the detailed investigation of potential sorption mechanisms for this element. More significantly, if sufficiently reducing conditions could be shown to exist in portions of the flow system down-gradient of the proposed repository, retardation of technetium by the precipitation and sorption of Tc^{4+} species might occur.

B. EFFECTS OF ORGANICS ON ACTINIDES

Introduction

Naturally occurring organic compounds generated during the transformation of plant and animal debris over time and as a result of the synthetic activities of microorganisms are ubiquitous in surface and subsurface environments. For example, pore water from a well-developed soil environment usually contains dissolved organic carbon in quantities greater than 20 mg/l in top soils and in quantities of about 5 mg/l in subsoils. Dissolved organic carbon concentrations in groundwaters typically depend on the environment and are usually below 2 mg/l (Drever 1988). The decrease in concentrations of organic materials with increasing depth is attributed to chemical and biological degradation as well as to sorption on mineral surfaces. Sorption of organic materials onto mineral surfaces is considered the dominant contributing factor to the removal of organics from solution during percolation through the subsurface.

The interaction between organic materials and mineral surfaces in the natural environment is important to mineral surface geochemistry. Sorption of organic material onto mineral surfaces affects not only the solubility and charge of the organic materials in solution but also the properties of the mineral surfaces, such as their charge and hydrophobicity, thereby altering the reactivity of the mineral toward metal ions. A clear understanding of the effects of the organic materials that frequently coat mineral surfaces in natural environments will lead to improvements in the sorption models used to predict the mobility of radionuclides in natural aquatic environments (Choppin 1992).

The objective of this section is to summarize the laboratory results for the effect of organic materials on the sorption of plutonium and neptunium on selected mineral oxides and tuff material.

Experimental Procedures

Preparation of tuff and oxide minerals

Three synthetic iron oxides (goethite, hematite, and ferrihydrite), one synthetic aluminum oxide (boehmite), and a natural crushed-tuff material from Yucca Mountain (USW G4-270, a devitrified tuff) served as model sorbents. Methods for preparing the oxides are described in the literature (Kung and McBride 1989a, 1989b, 1991).

In brief, iron oxide was synthesized by reacting ferric chloride with dilute sodium hydroxide under slightly acidic conditions and was then aged at raised temperature for several days. X-ray powder diffraction (XRD) analysis confirmed the oxide to be pure goethite. The surface area of the goethite, calculated from nitrogen adsorption by the three-point BET method, was about 89.5 m²/g.

The ferrihydrite preparation involved the overnight hydrolysis of ferric salt at low pH followed by raising the pH with dilute sodium hydroxide and, finally, aging the mixture for two weeks at raised temperature. The surface area of the freeze-dried material was 91.5 m²/g. XRD analysis indicated a poorly crystalline product containing ferrihydrite.

Hematite was prepared by aging ferric nitrate solution at raised temperature for 3 days. The surface area of the freeze-dried material was 39.4 m²/g. XRD analysis confirmed that this material was well-crystallized hematite.

Boehmite was prepared by fast hydrolysis of aqueous aluminum chloride with sodium hydroxide, followed by mixing and aging. The surface area of the freeze-dried material was 324 m²/g. XRD analysis confirmed that this aluminum oxide was poorly crystallized boehmite, an aluminum oxyhydroxide.

The metal oxides were stored either in a freeze-dried state or in suspensions containing 0.1 M KCl. For those in suspensions, the solid concentration of these oxide suspensions was less than 20 mg/ml.

XRD analysis of the crushed-tuff material (USW G4-270, a devitrified tuff), obtained from S. Chipera, indicated that it was about 30% silica and 69% feldspar, the remainder consisting of trace amounts of layer silicates and iron oxide. Part of the tuff material was treated with a 15% hydrogen peroxide solution to remove any natural organic material from the tuff surface.

Preparation of organics and radionuclides

Catechol, alanine, DOPA, and NAFA were used as model organic materials. Catechol is a phenolic compound that may chelate with metal ions and undergo redox reaction with the metal. Alanine is an amino acid that will complex with the hard-acid type of metal ions in solution. DOPA, a naturally occurring amino acid commonly found in plant seedlings, pods, and broad beans, was chosen because it contains well-defined organic functional groups such as carboxylic acid, amine, and phenols. The catechol, alanine, and DOPA, purchased from Fluca Chemical Company with purity greater than 99%, were used as received. The NAFA, obtained from the International Humic Substances Society (IHSS), is identified by IHSS as a reference fulvic acid with the code number 1R105F and is prepared and homogenized from a designated aquatic source by IHSS.

Neptunium-237 was obtained from Amersham International (product code NGZ-44). The plutonium-239 stock solution was prepared in the Pu(V) oxidation state (this concentrated stock solution was obtained from P. Parmer at Los Alamos). The desired concentrations of neptunium and plutonium were diluted and stored in 0.1 M KCl solutions. Under the experimental conditions used in this work, the plutonium and neptunium are expected to exist as the chemical species PuO_2^+ and NpO_2^+ , respectively.

Sorption Measurements

DOPA sorption

Sorption isotherms were obtained by mixing the desired sorbent suspension and sorbate in Teflon or

polycarbonate centrifuge tubes. The initial DOPA concentrations ranged from 20 to 100 μM . The pH was adjusted by adding 0.05 M NaOH or HCl immediately after mixing. The tubes were capped and shaken for at least 20 hours at $22 \pm 1^\circ\text{C}$. The solid phase was separated from suspension by centrifugation. The supernatant was analyzed for unadsorbed DOPA by ultraviolet spectrometry (Hewlett-Packard 8450A), and the amount of sorption was calculated by determining the difference between the initial and final concentrations. Potassium chloride was used as a background electrolyte to maintain an essentially constant ionic strength of 0.1 M.

Radionuclides sorption

A similar method was used to obtain plutonium and neptunium sorption isotherms. The amount of radionuclide in solution was determined by liquid scintillation counting (Packard 2550-TR/AB). The metal ions were introduced into the tubes after the pH in each suspension was adjusted. For the multisorbate systems, the organic sorbate was added before the radionuclide sorbate. Solution pH was measured after shaking. The carbon dioxide was not controlled in all the systems studied. For the initial sorption isotherms, about 0.03 to 0.5 μM plutonium solutions and about 0.1 to 4 μM neptunium solutions were used. Standard sorbate solutions (to which no sorbent was added and which were subjected to the same shaking treatment) were used to generate standard curves. No sorbate sorption onto the centrifuge tubes was detected.

Results and Discussion

Neptunium

Sorption as a function of tuff and oxide minerals.

The isotherms for neptunium sorption on different iron oxides are shown in Fig. 67. In this experiment, the three iron oxides were used as sorbents. Results show that, on a weight basis, hematite was the most adsorptive, whereas goethite was the least adsorptive. Thus, the sorption of neptunium on model iron oxides follows the order hematite > ferrihydrite > goethite.

Two things should be noted in this study. First, the surface areas of these iron oxides were different, and the sorptivity of neptunium was not compared on a unit surface-area basis. For ferrihydrite and goethite, the surface areas are around $90 \text{ m}^2/\text{g}$, whereas the surface area of hematite is about $40 \text{ m}^2/\text{g}$. Higher surface areas are expected to have higher sorptions. Secondly, the sorption experiments were not conducted at the same pH. Sorption on ferrihydrite was conducted at a pH of 6.2, whereas sorption on hematite and goethite were conducted at a pH of 6.9. The pH may affect the sorptivity of neptunium on iron oxides. The effect of pH on neptunium sorption will be presented in the next section.

The effect of oxide surface areas on neptunium sorption was replotted in Fig. 68. In this figure the amount of neptunium sorption was normalized on a unit surface-area basis (m^2). Results again showed that the sorption of neptunium on iron oxides follows the order hematite > ferrihydrite > goethite. Evidently, hematite has the highest sorptivity for neptunium on the basis of both weight and unit surface area.

Effect of pH on sorption.

To quantify organic sorption, it is required that we understand the effect of organics on radionuclide sorption. Experiments were conducted to study organic

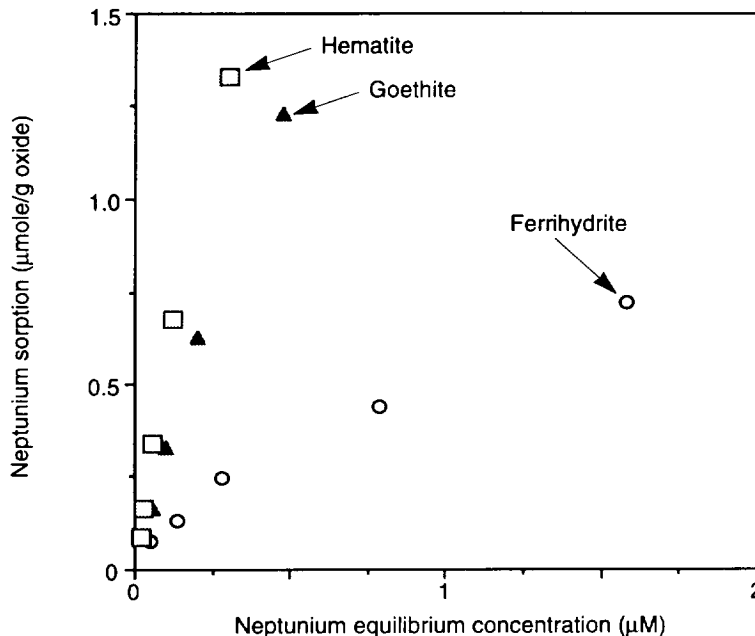


Figure 67. Neptunium Sorption per Unit Mass on Iron Oxides. The plot shows isotherms for the sorption of neptunium on three different iron oxides, calculated on the basis of unit mass.

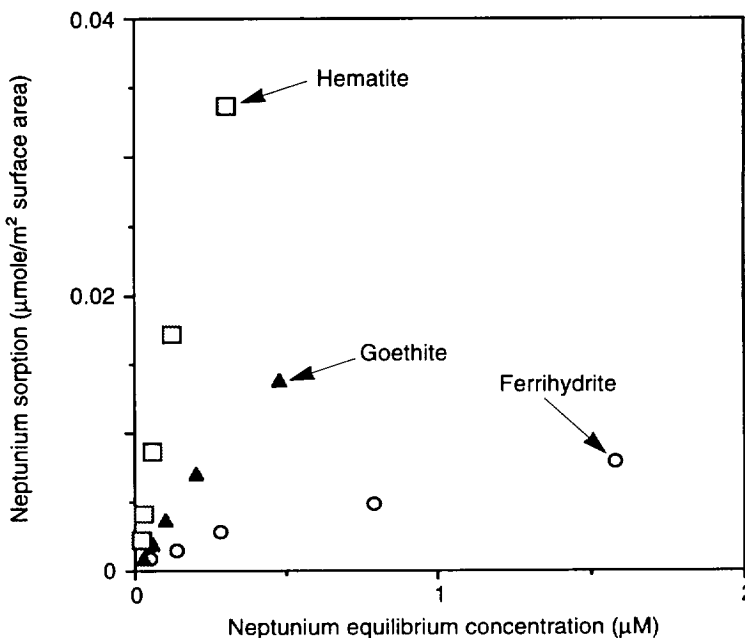


Figure 68. Neptunium Sorption per Unit Area on Iron Oxides. The plot shows isotherms for the sorption of neptunium on three different iron oxides, calculated on the basis of unit surface area.

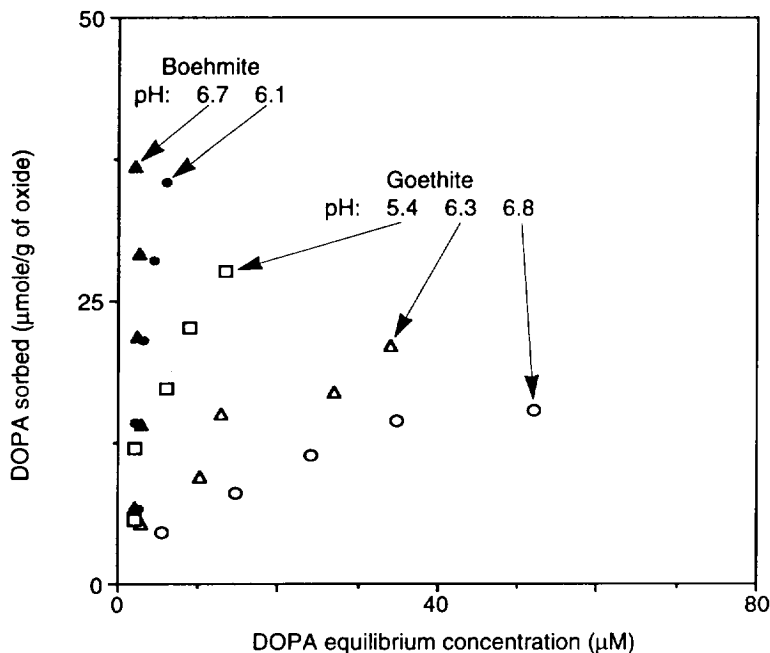


Figure 69. pH Dependence of DOPA Sorption on Oxides. This plot shows isotherms for the sorption of DOPA on goethite and on boehmite at different pH levels in the presence of 0.1 M KCl.

sorption, and the results are presented in this section. The isotherms for DOPA adsorption on goethite and boehmite at different pH levels are shown in Fig. 69. On a weight basis, boehmite was more adsorptive than goethite. The linear sorption curves for these oxides suggest a low degree of coverage of the surface reactive sites by the organic material in the presence of excess potassium chloride. This finding is consistent with the theoretical calculation of coverage, which suggests that the amount of DOPA sorption is much less than a monolayer, based on the BET surface area.

Increasing the solution pH resulted in a higher organic sorptivity for all oxides. Under neutral and slightly acidic conditions (pH values from 5.5 to 7), iron and aluminum oxides were expected to have positive surface charges (Sposito 1989). Although the sorption of DOPA is apparently not dependent on surface charge effects such as electrostatic attraction, it may be controlled by the deprotonation process of the organic material.

DOPA is expected to be dominated by neutral species under neutral and slightly acidic conditions, but raising the pH level will increase the concentration of deprotonated DOPA species, which are expected to have a stronger affinity for oxide surfaces in direct surface complexation. Therefore, it is reasonable to assume that DOPA forms direct surface bidentate complexes on the oxide surfaces.

The isotherms for neptunium sorption on goethite at different pH levels are shown in Fig. 70. Increasing the solution pH from 6.2 to 6.9 resulted in a higher neptunium sorptivity.

Effect of model organics on sorptive behavior.

We examined the effect of natural organics on radionuclide sorption onto natural tuff material that may have been pre-coated with natural organic material. The standard method for removing the natural organic material from mineral samples is to use hydrogen peroxide to oxidize the material (Kunze and Dixon 1986). We used a 15% hydrogen-peroxide solution when we removed organic material from crushed-tuff samples collected from Yucca Mountain. In the sorption experiments conducted to study the effect of the naturally presorbed organics on neptunium sorption, half of the tuff samples were treated with hydrogen peroxide, half were not.

Figure 71 shows the sorption isotherms of neptunium on both types of tuff samples. The results suggest that treatment with hydrogen peroxide had little or no effect on the sorption of neptunium onto the tuff material.

The lack of effect of hydrogen-peroxide treatment on neptunium sorption on tuff materials is attribut-

IV. Sorption and Sorption Modeling Studies

able to three factors. First, untreated tuff may contain very little or no organic material on its surface. Low organic content on the untreated tuff surface could be expected because crushed tuff material is generated from bedrock that may have little exposure to natural organic materials. New surfaces generated during the crushing process would not contain organic materials, in which case untreated tuff would be expected to behave essentially the same as tuff treated with hydrogen peroxide. Second, neptunium has intrinsically low sorptivity on tuff material. No observable difference in sorption on both treated and untreated tuff is attributed to the low sorption of neptunium on both sorbents. Any minute differences in sorption are likely to occur below the level of detection. Third, the sorption of neptunium may be unaffected by organic material, assuming that organic materials such as DOPA do not influence neptunium sorption on tuff, goethite, or boehmite.

To explore the possibility that the untreated tuff contained little organic material, 4 to 50 μM of DOPA was purposely added to both treated and untreated crushed tuff materials, and the sorption isotherms of neptunium on these systems were compared. As Figs. 72 and 73 illustrate, the addition of DOPA had no effect on neptunium sorption on either treated or untreated crushed-tuff materials. These data thus sup-

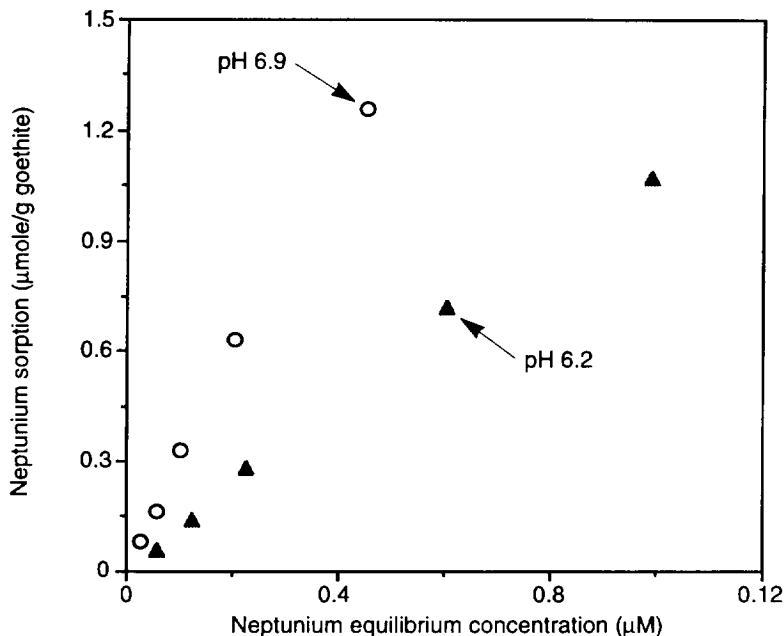


Figure 70. Neptunium Sorption on Goethite. This plot shows isotherms for the sorption of neptunium on goethite at a pH of 6.2 and 6.9.

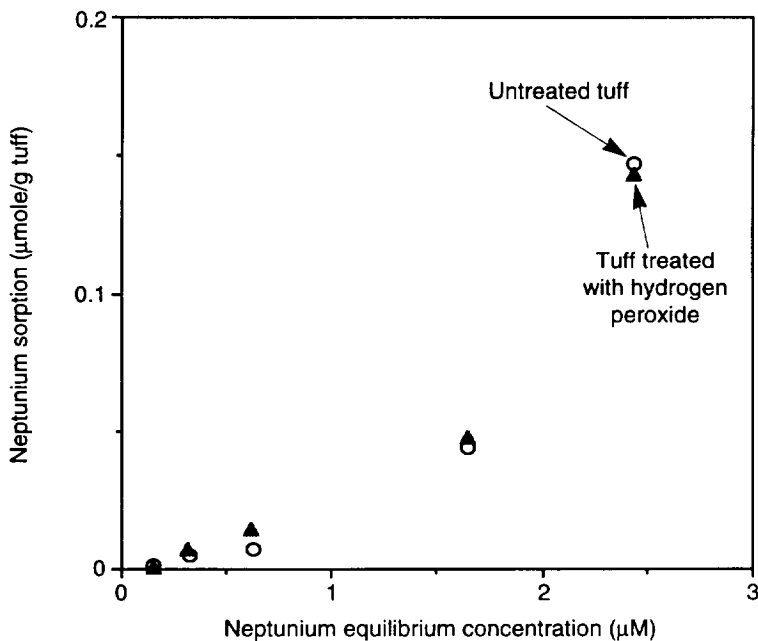


Figure 71. Neptunium Sorption on Treated and Untreated Tuff. This plot shows isotherms for the sorption of neptunium on devitrified tuff (G4-270) treated with hydrogen peroxide and untreated.

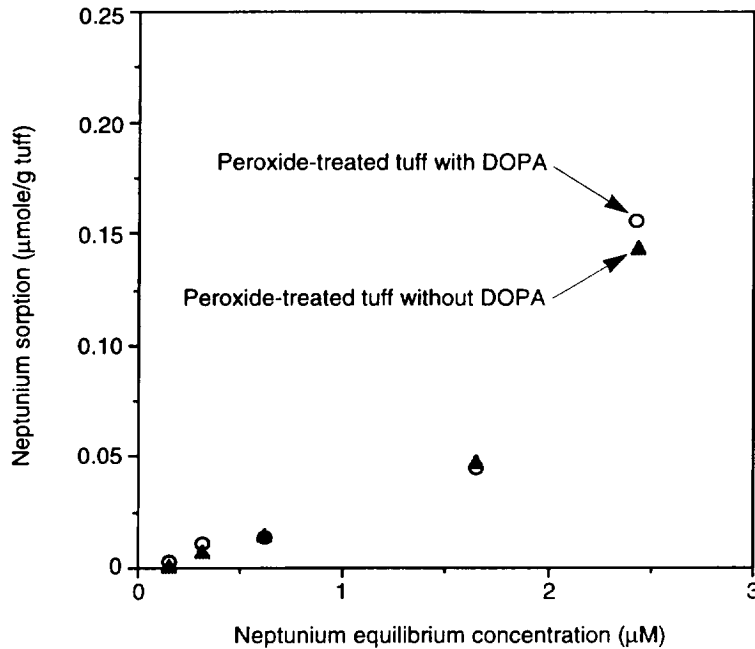


Figure 72. Sorption with and without DOPA on Treated Tuff. This plot shows isotherms for the sorption of neptunium on hydrogen-peroxide-treated tuff materials (G4-270) with and without DOPA.

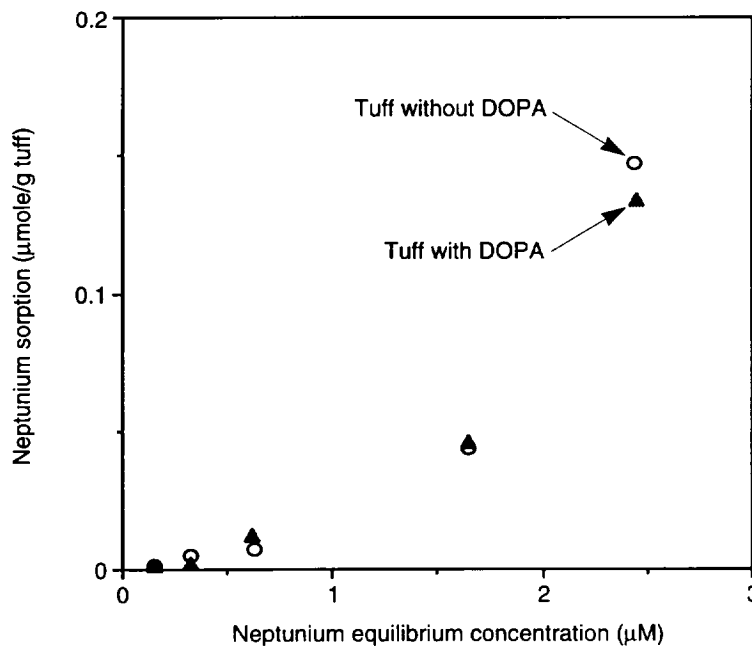


Figure 73. Sorption with and without DOPA on Untreated Tuff. This plot shows isotherms for the sorption of neptunium on untreated tuff samples (G4-270) with and without DOPA.

port the premise that the presence of organic material does not affect neptunium sorption on tuff materials.

Because this experiment did not rule out the possibility that the lack of an observable effect was a result of the intrinsically low sorptivity of tuff materials, the sorption of neptunium on iron and aluminum oxides in the absence and presence of DOPA was examined. The sorption of neptunium is expected to be much higher on iron and aluminum oxides than on tuff material. Thus, any effect of DOPA on neptunium sorption ought to appear in the oxide systems. To verify this assumption, sorption isotherms were measured for neptunium on iron and aluminum oxides and tuff material in the absence of organic materials with 0.1 M KCl at a pH of 6.2. The results (Fig. 74) indicate that the sorptivity of boehmite and goethite is approximately one and two orders of magnitude higher, respectively, than the sorptivity of tuff material. Thus, any effect of DOPA on neptunium sorption should be easily detectable in these oxide systems.

Neptunium sorption isotherms on iron and aluminum oxides in the presence of DOPA are shown in Figs. 75 and 76. In these experiments, 0.1 M KCl was used to maintain an essentially constant ionic strength, and the final pH of the suspensions was adjusted to a value of 6.2. The

IV. Sorption and Sorption Modeling Studies

initial neptunium concentration ranged from 0.2 to 2 μM , and the initial DOPA concentration ranged from 4 to 50 μM . The sorption isotherms of neptunium on aluminum and iron oxides suggest that DOPA does not significantly affect the sorption of neptunium. The relatively weak complexation of the pentavalent neptunium ion is a result of its relatively low effective charge on the cation (Choppin and Rao 1984). These results imply that there is no significant influence of DOPA on neptunium sorption on aluminum and iron oxides.

The occurrence of surface complexation between DOPA and oxide surfaces is supported by the observed sorption of catechol on metal oxide, which indicates that catechol chemisorbs on metal oxide by forming a bidentate complex with the surface metal atoms. DOPA is an organic with functional groups like catechol (phenols) and alanine (amino acids). Thus, the effect of simple organics such as catechol and alanine on the sorption of neptunium was studied. Both catechol and alanine are expected to complex with metal ions in solution. Besides the formation of metal-organic complexes, catechol readily undergoes redox reactions with some metal and metal oxides (McBride and Wesselink 1988). For example, catechol at high concentrations may undergo electron-transfer reactions with manganese and iron oxides.

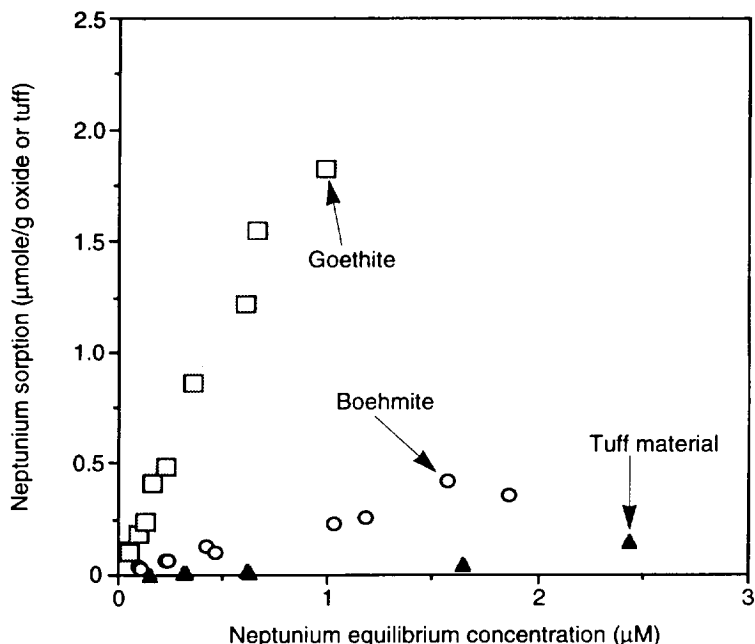


Figure 74. Neptunium Sorption on Oxides and Tuff. This plot shows isotherms for the sorption of neptunium on goethite, boehmite, and tuff material (G4-270).

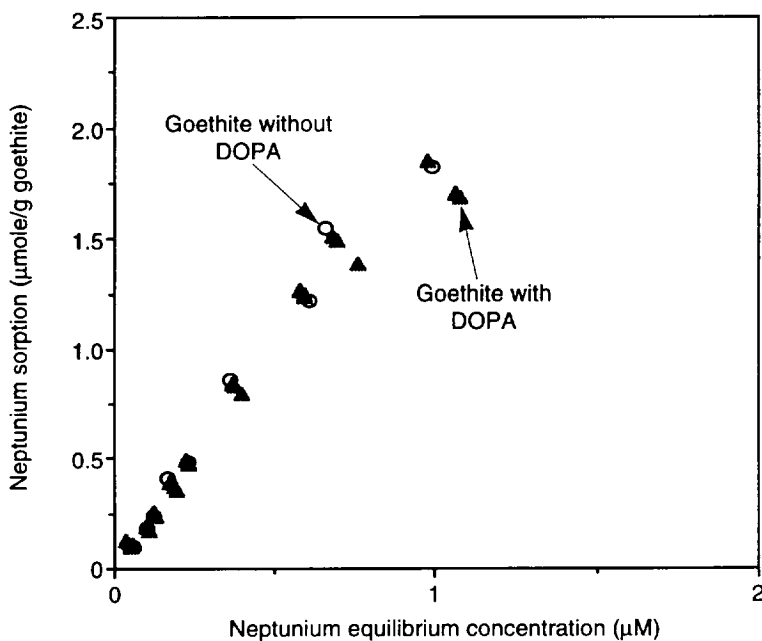


Figure 75. Sorption on Goethite with or without DOPA. This plot shows isotherms for the sorption of neptunium on goethite in the presence and absence of DOPA at a pH of 6.2.

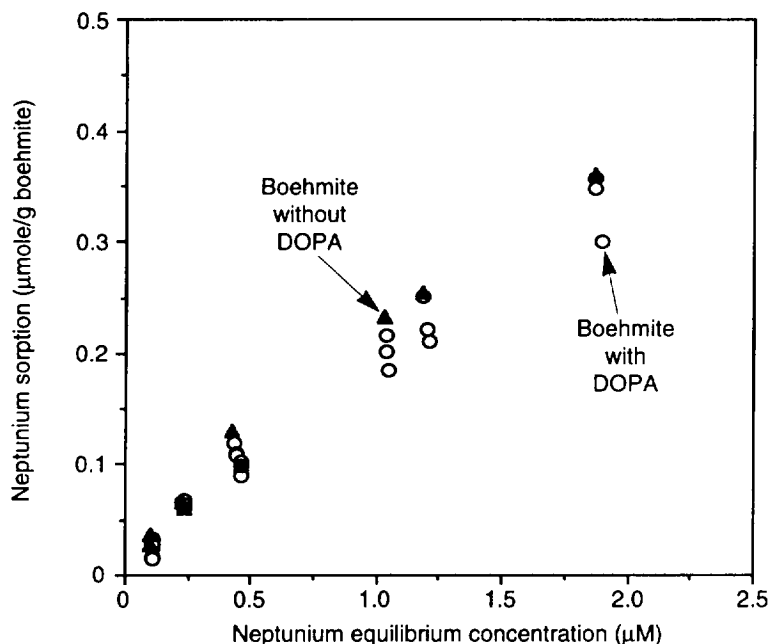


Figure 76. Sorption on Boehmite with or without DOPA. This plot shows isotherms for the sorption of neptunium on boehmite in the presence and absence of DOPA at a pH of 6.2.

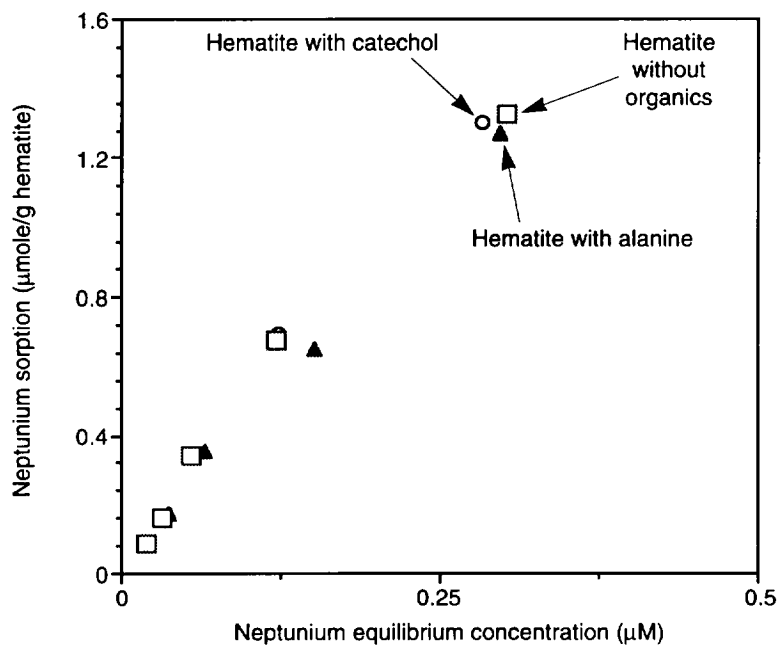


Figure 77. Sorption on Hematite with or without Organics. This plot shows isotherms for neptunium sorption on hematite in the presence and absence of catechol or alanine (1 μM) at a pH of 6.9.

We quantified the effect of catechol and alanine on neptunium sorption by measuring isotherms for sorption on hematite, ferrihydrite, and goethite in the presence and absence of catechol and alanine (Figs. 77 to 79). In these experiments, 0.1 M KCl was used to maintain an essentially constant ionic strength. The final pH of the suspensions was adjusted to 6.2 for ferrihydrite and to 6.9 for goethite and hematite. The initial neptunium concentration ranged from 0.2 to 2 μM, and the initial catechol and alanine concentrations were 1 μM. The sorption isotherms of neptunium on iron oxides suggest that catechol and alanine does not significantly affect the sorption of neptunium. The implication of these results is that there is no significant influence of catechol and alanine on neptunium sorption on different iron oxides.

Although both catechol and alanine may complex with neptunium in solution, the organic-metal complexes are apparently not strong enough to affect the neptunium sorption. These results are consistent with the data of Fig. 75 for the iron oxide, goethite, which indicate that DOPA has no effect on neptunium sorption.

In another set of experiments to study the effect of naturally occurring organic material on neptunium sorption, NAFA served as the model fulvic material. The isotherms for the sorp-

tion of neptunium on boehmite in the presence and the absence of NAFA are shown in Fig. 80 and for the sorption of neptunium on goethite in Fig. 81. Similar isotherms for the sorption of neptunium on treated tuff materials are shown in Fig. 82 and for untreated tuff materials in Fig. 83. In these experiments, 0.1 M KCl was used as the background electrolyte, and the final pH was adjusted to 6.2. Initial neptunium concentrations ranged from 0.2 to 3 μM , and the NAFA concentrations ranged from 0.1 to 0.4 ppm.

As shown in Figs. 80 to 83, the fulvic material NAFA had little effect on neptunium sorption in all systems. Thus, we concluded that organics do not affect the sorption of neptunium both in simple, low-molecular-weight organics and in naturally occurring fulvic organic material. The lack of detectable effects of organics on neptunium sorption is possibly attributable to the stable redox state of Np(V) in solution and to low complexation between neptunium ions and organic chemicals.

Plutonium

Sorption as a function of tuff and oxide minerals.

Plutonium sorption on different iron oxides is shown in Fig. 84. On a weight basis, hematite was the most adsorptive, whereas goethite was the least adsorptive. The sorption of plutonium on model iron oxides follows the order hematite > ferrihydrite >

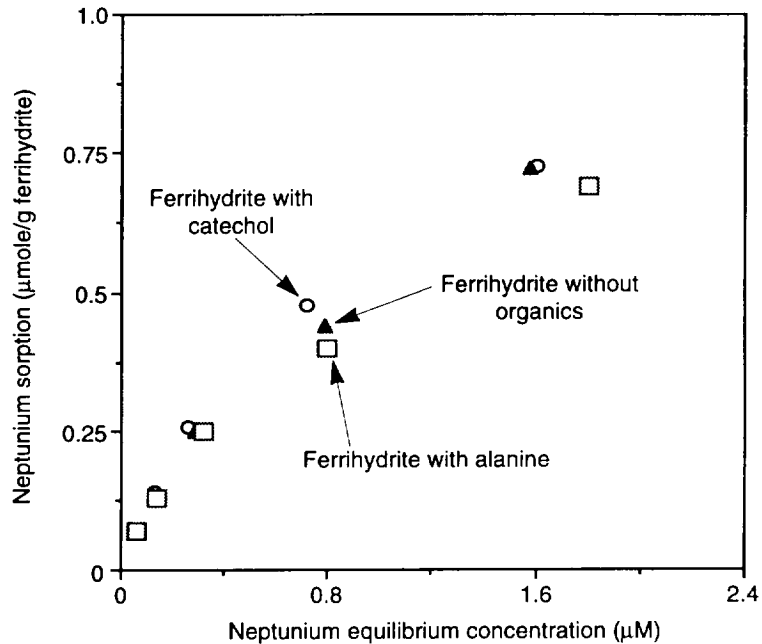


Figure 78. Sorption on Ferrihydrite with or without Organics. The plot shows isotherms for sorption of neptunium on ferrihydrite in the presence and absence of catechol or alanine (1 μM) at pH 6.2.

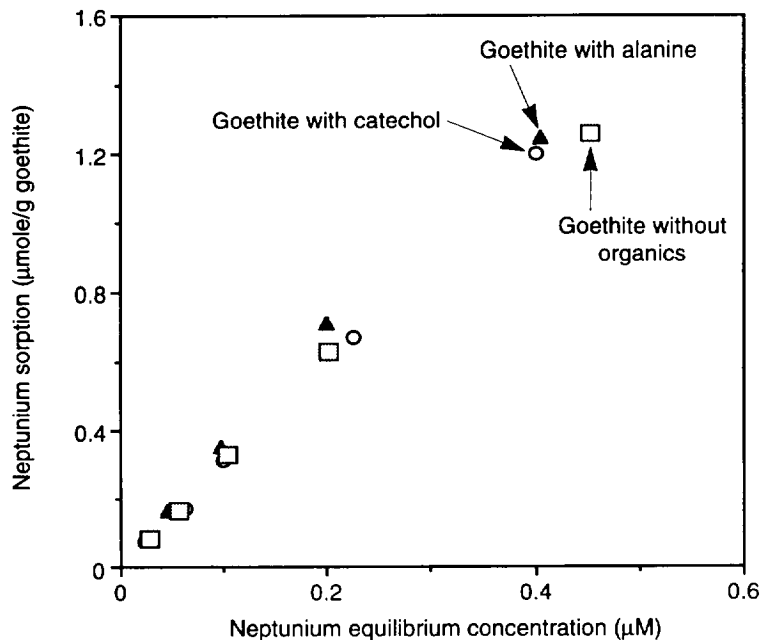


Figure 79. Sorption on Goethite with or without Organics. This plot shows isotherms for the sorption of neptunium on goethite in the presence and absence of catechol or alanine (1 μM) at a pH of 6.9.

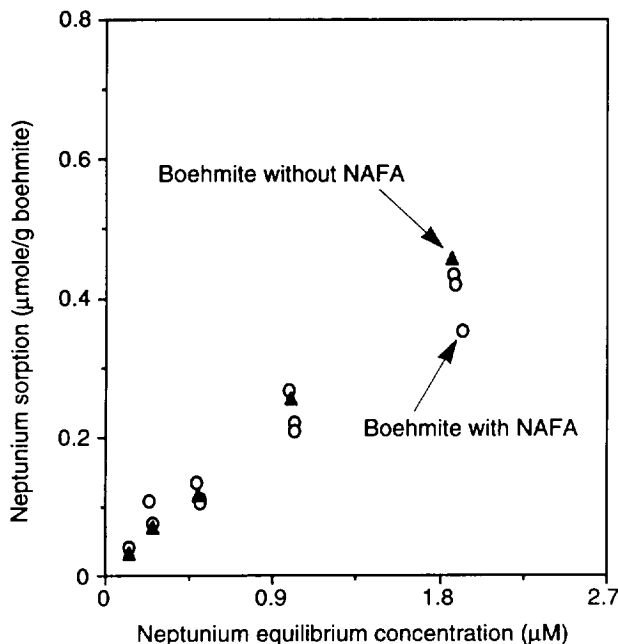


Figure 80. Boehmite with or without NAFA. This plot shows isotherms for the sorption of neptunium on boehmite with and without NAFA.

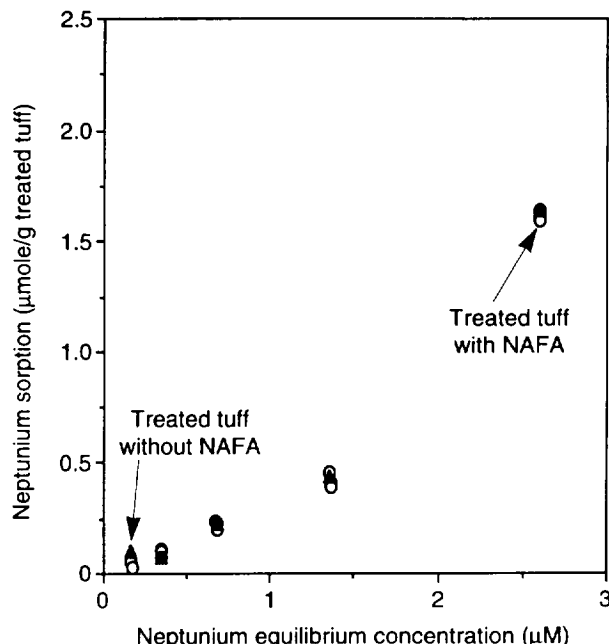


Figure 82. Treated tuff with or without NAFA. This plot shows isotherms for neptunium sorption on treated tuff (G4-270) with and without NAFA.

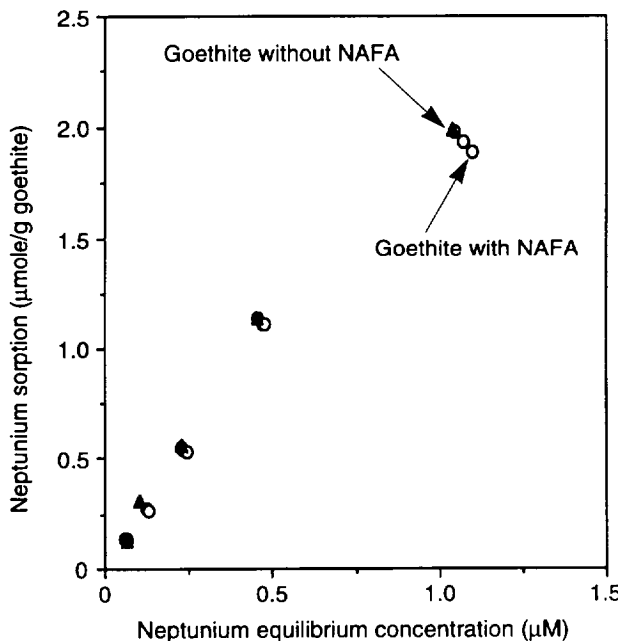


Figure 81. Goethite with or without NAFA. This plot shows isotherms for the sorption of neptunium on goethite with and without NAFA.

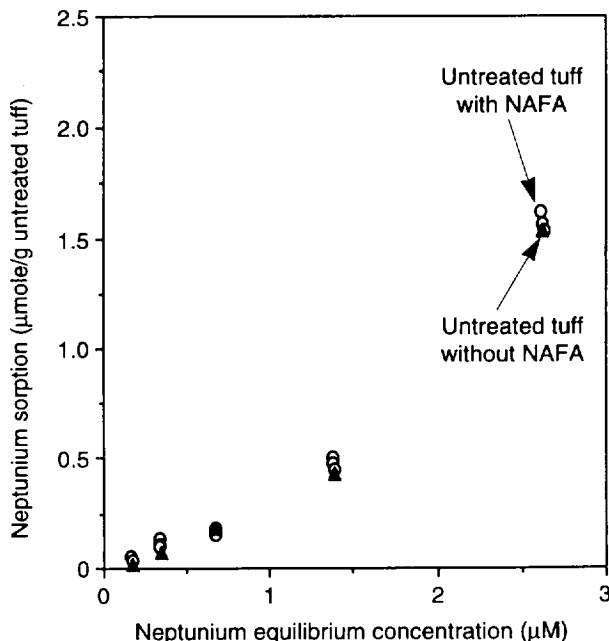


Figure 83. Untreated tuff with or without NAFA. This plot shows isotherms of neptunium sorption on untreated tuff (G4-270) with and without NAFA.

goethite. Thus, for both neptunium and plutonium, hematite is the most adsorptive, but goethite and ferrihydrite reverse order.

As was the case for neptunium, two things should be noted in this result for plutonium. First, the surface area of these iron oxides were not the same. For ferrihydrite and goethite, the surface areas are around 90 m²/g; for hematite, the surface area is about 40 m²/g. Second, the sorption experiments were not conducted at the same pH. The sorption on ferrihydrite was conducted at a pH of 6.1; the sorptions on hematite and goethite were conducted at a pH of 6.9.

The effect of oxide surface areas on plutonium sorption was replotted in Fig. 85, with the amount of plutonium sorption normalized to unit surface area (m²). Results again showed that the sorption of neptunium on model iron oxides follows the order hematite > ferrihydrite > goethite.

Effect of pH on sorption.

The isotherms for plutonium sorption on goethite at two different pH levels are shown in Fig. 86. Increasing the solution pH from 6.6 to 6.9 resulted in a higher plutonium sorptivity. It should be noted that the initial plutonium concentration was the same for both isotherms; however, the amount of goethite was different. The linear sorption curves suggest a low degree of coverage of the surface reactive

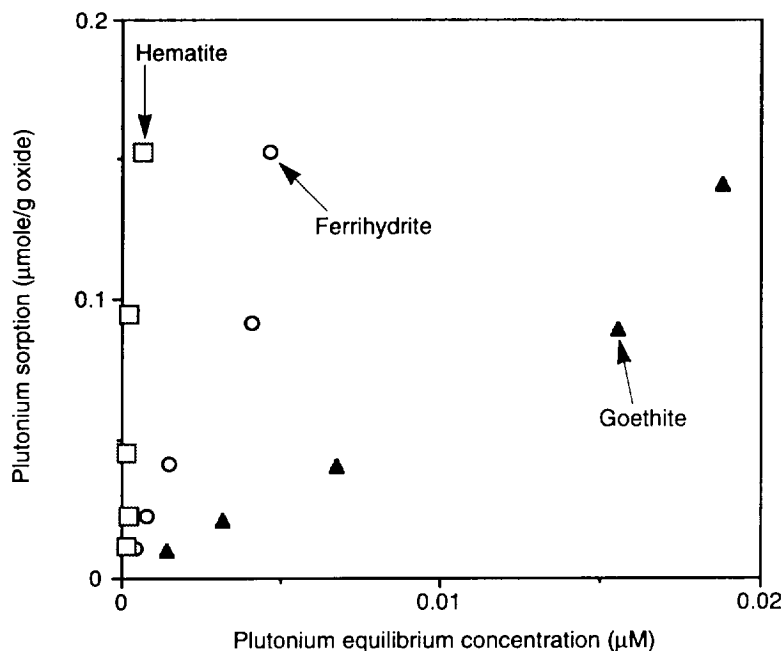


Figure 84. Plutonium Sorption per Unit Mass on Iron Oxides. This plot shows isotherms for the sorption of plutonium on three iron oxides, calculated on the basis of unit mass.

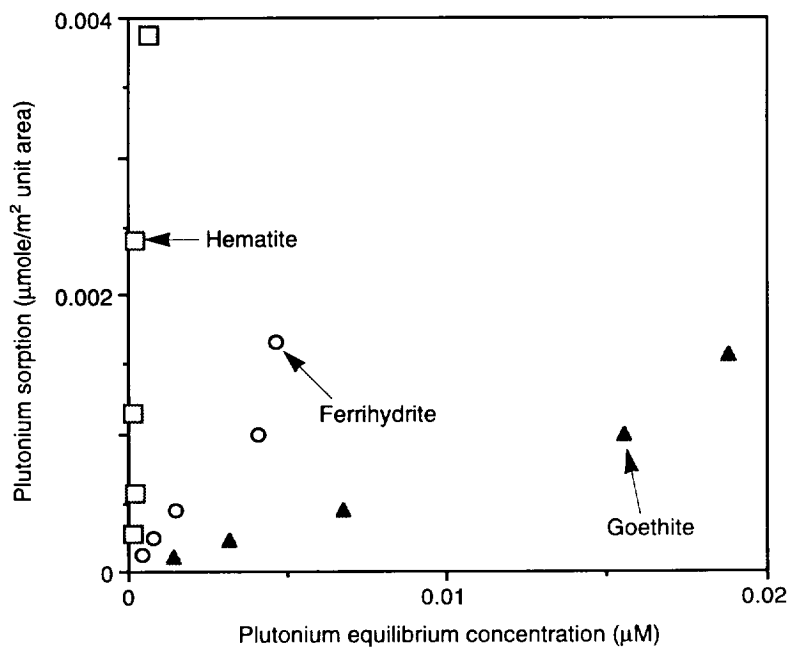


Figure 85. Plutonium Sorption per Unit Area on Iron Oxides. This plot shows isotherms for the sorption of plutonium on three different iron oxides, calculated on the basis of unit surface area.

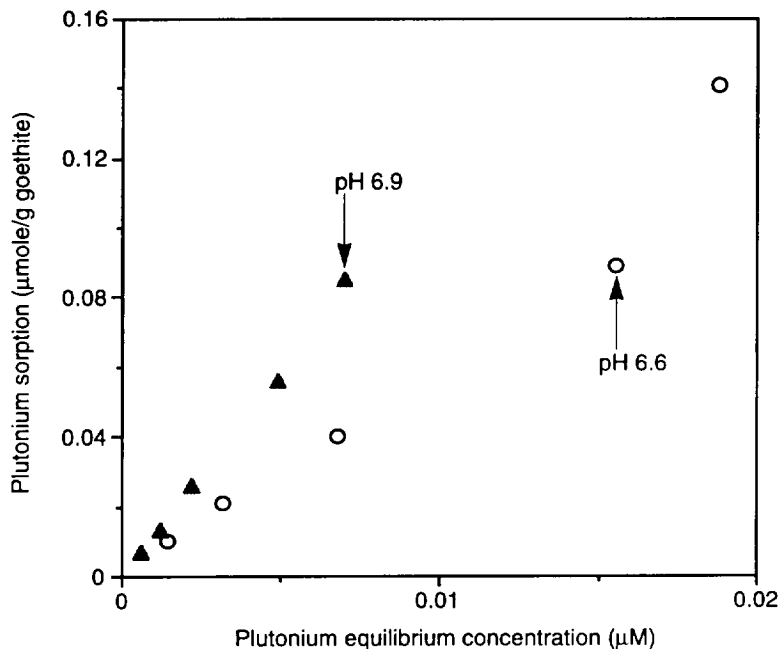


Figure 86. pH Dependence of Plutonium Sorption on Goethite. This plot shows isotherms for the sorption of plutonium on goethite at two different values of pH.

sites by plutonium ions in the presence of excess potassium chloride. This finding is consistent with the theoretical calculation of coverage, which suggests, based on BET surface areas, that the amount of plutonium sorption is much less than a monolayer.

Increasing the solution pH resulted in a higher plutonium sorptivity. Under neutral conditions (a pH of 7), goethite is expected to have positive surface charges. However, the sorption of plutonium on goethite was found to increase as solution pH increased. The sorption of plutonium is apparently not dependent on ion exchange because iron oxide should have no cation-exchange capacity. The sorption is believed to be controlled by a surface-complexation process because plutonium is expected to be dominated by the cationic species PuO_2^+ under neutral and slightly acidic conditions.

Effect of model organics on sorptive behavior. The isotherms for plutonium sorption on ferrihydrite in the presence of catechol and alanine are

shown in Fig. 87, and the isotherms for plutonium sorption on goethite and hematite in the presence of catechol and alanine are shown in Fig. 88. The isotherms clearly demonstrate that the sorption of plutonium onto goethite and ferrihydrite was affected by the presence of the organic materials.

The amount of plutonium sorption on goethite and ferrihydrite was lower in systems that contained alanine than in systems that contained no alanine. Apparently, the presence of alanine suppressed the plutonium sorption on the surface of these iron oxides, probably because of a lowering of the free plutonium-ion activity in solution by the formation of an alanine-plutonium complex.

Conversely, the amount of plutonium sorption on goethite and ferrihydrite was higher in the presence of catechol than it was in the absence of catechol. Evidently, catechol enhanced the sorption.

However, the effect of catechol and alanine on plutonium sorption was not found in the hematite system. The presence of these organic materials had little effect on the sorption of plutonium on hematite (Fig. 88). The lack of an observable effect in this case is probably a result of the intrinsically high sorptivity of plutonium on hematite. Any small enhancement or suppression of sorption that might be attributed to catechol and alanine under such a high sorptivity would not be detected.

Overall, the results of our study suggest that the model organic materials catechol and alanine do affect the sorption of plutonium on iron oxides.

The isotherms for sorption of plutonium on ferrihy-

drite and goethite in the absence of DOPA and in its presence at three concentration levels (1, 0.1, and 0.01 μM) clearly demonstrate (Figs. 89 and 90) that such sorption was affected by the presence of the organic material DOPA. Plutonium sorption was higher in systems that contained DOPA than in systems that contained no DOPA. Furthermore, sorptivity increased as the initial DOPA concentration increased from 0.01 to 1 μM . Evidently, the presence of DOPA enhanced the sorption of plutonium on goethite and ferrihydrite. This result is likely attributable to the formation of stable surface DOPA-plutonium ternary complexes and to a redox reaction between DOPA and plutonium. Reduction of Pu(V) to lower oxidation states will enhance the sorption/precipitation of the plutonium.

For neptunium, however, the effect of DOPA on sorption was not found in goethite (Fig. 75), boehmite (Fig. 76), and tuff material (Fig. 73). The presence of DOPA had little effect. It is possible that DOPA does not complex with neptunium in solution or that DOPA cannot reduce Np(V) to lower oxidation states. Such relatively weak complexation is possibly a result of the relatively low effective charge on the cation (Choppin and Rao 1984), consistent with the fact that neptunium complexed weakly with a natural humic material extracted from a groundwater (Kim and Sekine 1991).

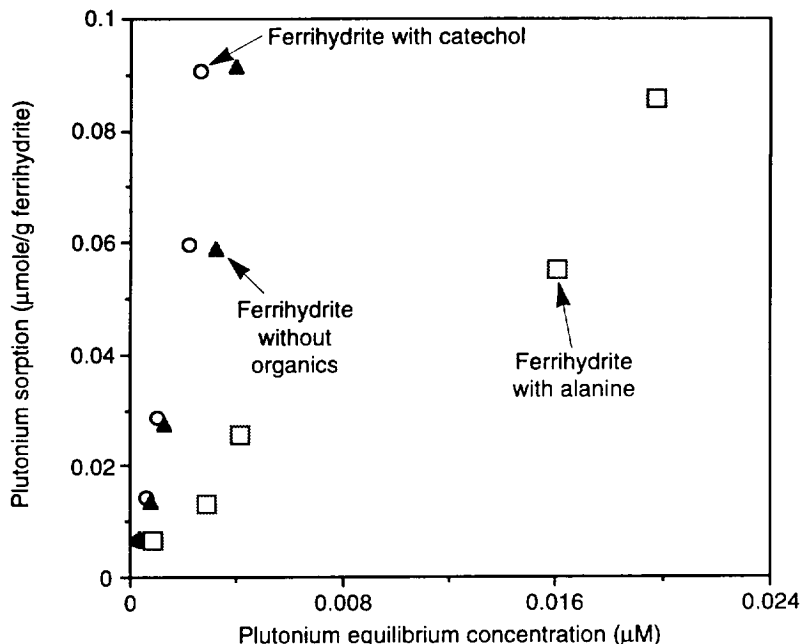


Figure 87. Sorption on Ferrihydrite with and without Organics. This plot shows isotherms for plutonium sorption on ferrihydrite with and without catechol or alanine (1 μM) at a pH of 6.2 in 0.1 M KCl.

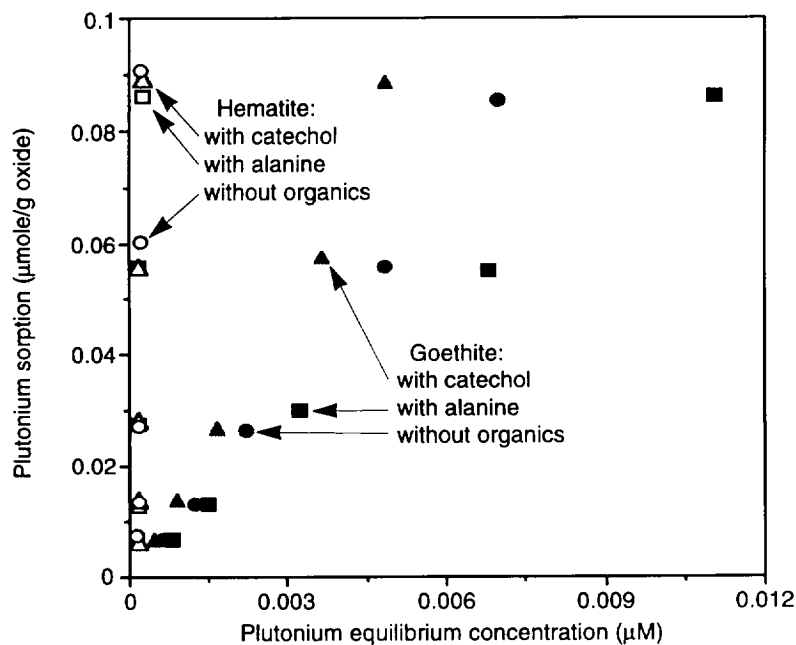


Figure 88. Sorption with and without Organics. This plot shows isotherms for the sorption of plutonium on hematite and goethite with and without catechol or alanine at a pH of 6.9 in 0.1 M KCl.

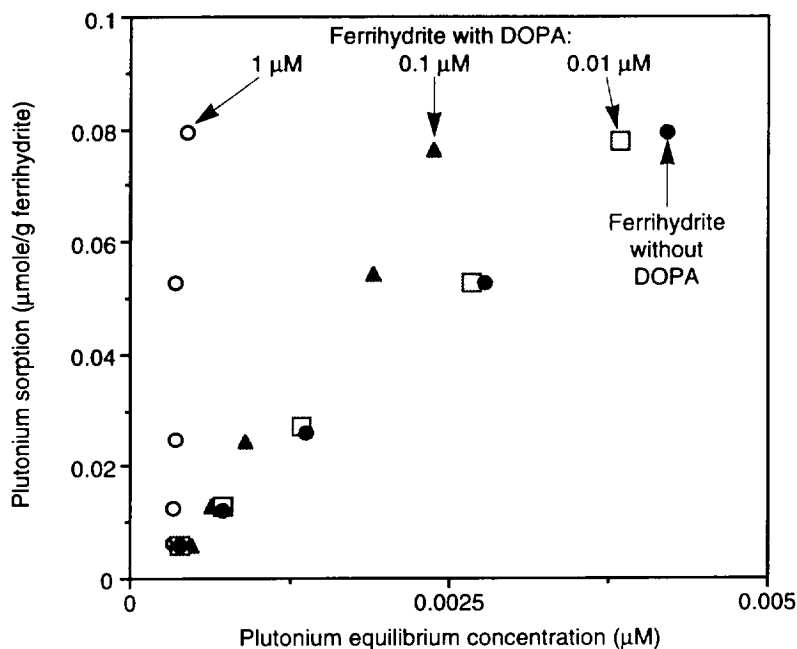


Figure 89. Sorption on Ferrihydrite with and without DOPA. This plot shows isotherms for the sorption of plutonium on ferrihydrite with and without DOPA at a pH of 6.2 in 0.1 M KCl.

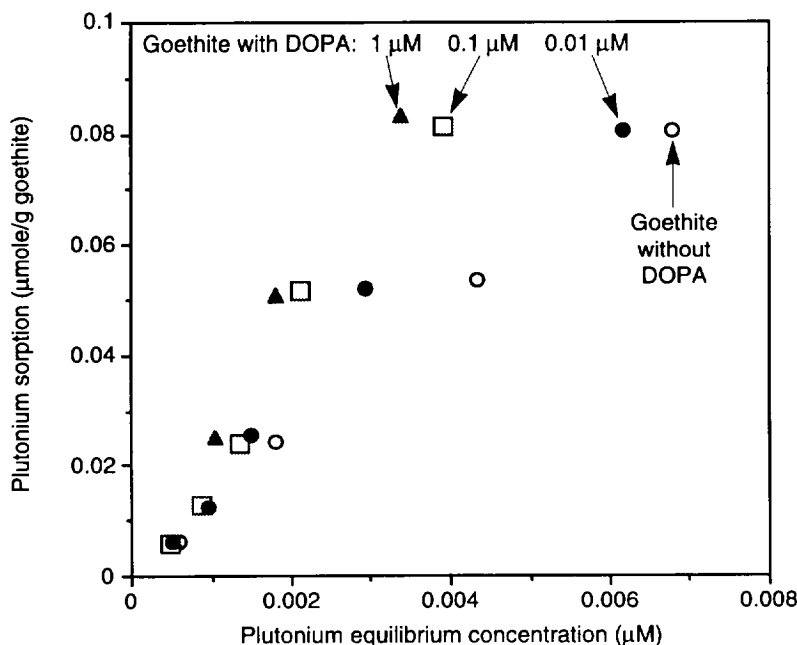


Figure 90. Sorption on Goethite with and without DOPA. This plot shows isotherms for the sorption of plutonium on goethite with and without DOPA at a pH of 6.9 in 0.1 M KCl.

Summary

From the sorption data, the following conclusions can be drawn concerning the effect of natural organic materials on the sorption of neptunium and plutonium by iron and aluminum oxides and by crushed-tuff material:

- The sorption of model organic material DOPA on oxide surfaces follows the order aluminum oxide > iron oxide. For a given sorbent, the higher the pH, the more DOPA is sorbed. Surface complexation is the most likely sorption mechanism.
- The sorption of plutonium on iron oxides generally follows the order hematite > ferrihydrite > goethite. The sorption of neptunium on iron oxide is higher than that on aluminum oxide. The sorption of neptunium on crushed-tuff material was much lower than that on oxide surfaces.
- The sorption of plutonium and neptunium on iron oxides increases as the solution pH is raised. The sorption of plutonium on hematite, goethite, and ferrihydrite is much higher than that of neptunium.
- The amount of neptunium sorption was not affected by any of the organic materials that were studied. The presence of the model organic materials of alanine, catechol,

IV. Sorption and Sorption Modeling Studies

DOPA, and NAFA did not influence the sorption of neptunium on tuff or on iron and aluminum oxides. This lack of an observable effect is presumably a result of the weak complexation between neptunium and the model organics.

- The sorption of plutonium was influenced by the presence of DOPA on goethite and ferrihydrite. Increasing the amount of DOPA resulted in higher sorption of plutonium on goethite and ferrihydrite. Alanine decreases the sorption of plutonium. However, in the system containing catechol, plutonium sorption was increased. The enhancement of plutonium sorption in the presence of catechol is probably due to the reduction of Pu(V) to Pu(IV) by the organic. The inhibition of plutonium sorption in the presence of alanine is probably caused by the lowering of the free plutonium-ion activity in solution by formation of an alanine-plutonium complex. No observable effect of organics on plutonium sorption was found in the hematite system, which is probably due to a relatively high sorptivity of plutonium on the hematite surface.

C. MODELS THAT CAN EXPLAIN THE SORPTION DATA

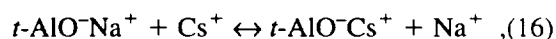
Radionuclides are known to be adsorbed by mineral surfaces in rocks and soils. The strongest interactions between aqueous species and mineral surfaces are the formation of electrostatic and covalent bonds. Ion-exchange reactions are primarily electrostatic interactions (outer electronic sphere and diffuse layer). Inner-sphere surface complexes form a chemical bond (to the mineral surface) that is more covalent. The electrostatic interaction does not have the same degree of selectivity between aqueous ions of like charge as does the more covalent inner-sphere surface complex. Stable inner-sphere complexes can be formed even when the mineral surface charge is the same as the aqueous ion. On the other hand, the adsorption of metal ions via cation exchange will only occur on surfaces of opposite charge and is affected by such common components of groundwater as sodium. Both of these processes can, in principle, be modeled using a triple-layer surface-complexation model. There are significant differences between the cation exchange in zeolites and clays and the formation of outer-sphere complexes on metal oxides. For this reason, cation exchange and surface complexation will be treated separately.

Cation Exchange

Description of the process

The cation-exchange capacity of aluminosilicates is often high. Zeolites, such as clinoptilolite and mordenite, and clays, such as montmorillonite, have enormous surface areas because of their channeled and layered structures, respectively. The surfaces are negatively charged because they are composed of tetrahedrally bound silica and alumina. Aluminum requires an additional electron in order to share electrons equally between four oxygen atoms in a tetrahedral structure. The excess negative charge is balanced by an alkali-metal or alkaline-earth cation. These cations can be exchanged for cationic radionuclides. The extent to which a radionuclide is adsorbed depends on the selectivity

for that cation. The equilibrium reaction can be represented, for example, as follows:



where $t\text{-AlO}^-$ represents a tetrahedrally bound aluminum site. The equilibrium expression for this reaction is

$$K = \frac{[\text{AlO}^- \text{Cs}^+][\text{Na}^+]}{[\text{AlO}^- \text{Na}^+][\text{Cs}^+]}, \quad (17)$$

where K is the selectivity coefficient. For a mineral with one type of cation exchange and a binary aqueous salt, this expression can be rewritten in terms of the solid-phase concentration, q , of one of the cations of interest (here, cesium). The result is

$$q = \frac{KQc}{(K-1)c} + c_0, \quad (18)$$

where, in this case, $q = [\text{AlO}^- \text{Cs}^+]$, c is the solution-phase concentration of the cation, $[\text{Cs}^+]$, c_0 is the total solution-phase cation concentration ($[\text{Cs}^+] + [\text{Na}^+]$), and Q is the cation-exchange capacity of the solid phase ($[\text{AlO}^- \text{Cs}^+] + [\text{AlO}^- \text{Na}^+]$). Equation 18 is nearly identical to the Langmuir isotherm (derived for the adsorption of gases on solids) and will be referred to as such in the remainder of this report.

Factors affecting cation exchange

There are many factors affecting cation exchange in natural systems, such as competition between multiple cation-exchange sites, selectivity between cations in groundwater and the radionuclide of interest, and aqueous speciation of the radionuclide, to name a few. Competition between multiple cation-exchange sites leads to nonlinear adsorption isotherms. The selectivity between cations depends on the geometry of the cation-exchange site and the relative degree of hydration of the aqueous cations. In clays and zeolites, the selectivity coefficient increases from more- to less-hydrated cations, so that the order for alkali metal cations is lithium < sodium < potassium < rubidium < cesium (see McBride 1994, for example). Aqueous speciation can change the charge and the net size of the ions. In addition, there are sites in

IV. Sorption and Sorption Modeling Studies

minerals, such as analcime, that can exclude larger ions, like cesium, entirely.

In principle, an equilibrium code, such as EQ3/EQ6 (Wolery 1983), could predict cation exchange if selectivity coefficients for all the significant cationic constituents of groundwater were known for each cation-exchange site in each mineral contained in tuff. In practice, few selectivity coefficients are known for single minerals, let alone individual exchange sites.

Experimental methods

The most useful experiment for determining sorption thermodynamic data is the adsorption isotherm. The adsorption isotherm is a measurement of the solid-phase concentration versus the aqueous-phase concentration at constant temperature. If the behavior of the isotherm is ideal, it can be described by a Langmuir isotherm (Eqn. 18), which can be the case only if there is one type of cation-exchange site and if outer-sphere surface complexation is not significant.

Pure cation exchange cannot be measured in a system also capable of surface complexation, whether that system is a whole rock or a clay mineral. By varying the pH and electrolyte concentration, either surface complexation or cation exchange can be enhanced, which allows information about both mechanisms to be extracted from the data. The Swiss nuclear waste program has made great progress in developing such methods (Baeyens and Bradbury 1995a, 1995b; Bradbury and Baeyens 1995).

Ion-exchange models

One approach that allows the determination of the free energy of exchange in even nonideal systems is that of Gaines and Thomas (1953). This approach requires that the adsorption isotherm be taken from one end member (for example, sodium saturated) to the other end member. In this case, the free energy of exchange, ΔG° , is related to the definite integral over the mole ratio of cations from one end member to the other as follows:

$$\Delta G^\circ = -\frac{RT}{Z_1 Z_2} \left[(Z_2 - Z_1) + \int_0^1 \ln K dA \right], \quad (19)$$

where Z_1 and Z_2 are the charges on the original and incoming cations, respectively, A is the mole ratio of the incoming cation, R is the gas constant, and T is absolute temperature. This approach cannot, in general, be used to calculate distribution coefficients because it cannot describe nonideal solid solutions.

Ion exchange arises from two distinctly different chemical structures on the surfaces of minerals. One is the incorporation of aluminum (with a valence of 3) in a tetrahedrally bonded silicate structure. The other is the amphoteric reaction of metal oxides with acids and bases. The former is a negatively charged surface of a fixed nature with the charge compensated by cations. The latter can be either negatively or positively charged depending on the pH of the aqueous phase. The exchange capacity of the former structure is fixed, whereas the exchange capacity of the latter depends on pH, ionic strength, and the concentration of specific inner-sphere complexing ligands. The adsorption of exchangeable ions on an activated metal-oxide surface is a form of outer-sphere surface complexation.

The selectivity in aluminosilicates for a given radionuclide over another has been shown to be not a simple binary-exchange process, even when the solution is a simple binary aqueous solution, because not all positions in aluminosilicate are equivalent with respect to crystallographic structure. For example, there can be differences due to steric crowding. These differences have been studied by deconvolving the ion-exchange isotherm.

The method of deconvolution has been shown to be effective in studying structural effects on ion selectivities in synthetic zeolites (Triay and Rundberg 1989a). In that study, the shape of the ion-exchange isotherm was shown to be due to differences in the crystallographic structure at the ion-exchange sites. This interpretation could not be made on the basis of the deconvolution of adsorption isotherms without spectroscopic data. How-

ever, the method of deconvolution does allow a quantitative correlation of the ion-exchange data with the spectroscopic data.

The method of analysis assumes ion exchange. The thermodynamics of ion exchange have been reviewed by Cremers (1977). The selectivity coefficient K for the hypothetical ion-exchange process in the reaction



is given by

$$K = \frac{q_2 a_1}{q_1 a_2}, \quad (21)$$

where a_1 and a_2 are the activities in solution of the cation to be exchanged and the entering cation, respectively, and q_1 and q_2 are the corresponding concentrations of these cations in the solid phase expressed as moles of cation per gram of the exchanger.

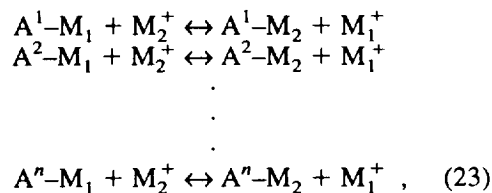
As a result of mass-balance considerations, Eqn. 21 can be rewritten as

$$q_2 = \frac{KQ\gamma_2 C_2}{C_o\gamma_1 + (K\gamma_2 - \gamma_1)C_2}, \quad (22)$$

where Q is the total moles of exchangeable sites per gram of exchanger ($Q = q_1 + q_2$), C_2 is the concentration of the entering cation in the liquid phase, C_o is the total concentration of cations in the liquid phase ($C_1 + C_2$), and γ_1 and γ_2 are the activity coefficients in the solution phase of the cation to be exchanged and the entering cation, respectively (that is, $a_1 = \gamma_1 C_1$ and $a_2 = \gamma_2 C_2$).

Equation 22 represents the dependence of the solid-phase concentration on the liquid-phase concentration. It has the mathematical form of the Langmuir isotherm. In general, adsorption isotherms do not follow the Langmuir isotherm. Many authors have successfully described cation exchange in terms of multiple sites (Barrer and Klinowksi 1972; Barrer and Munday 1971; Brouwer et al. 1983). The underlying assumption of the deconvolution method is that the nonideality

of the adsorption isotherm is due to adsorption at multiple sites. Consequently, one may consider a set of simultaneous equilibria



where $\text{A}^1, \text{A}^2, \dots, \text{A}^n$ represent different sites in the ion exchanger.

The solid-phase concentration of the cation M_2^+ in site i is given by

$$q_2^i = \frac{K^i Q^i \gamma_2 C_2}{C_o \gamma_1 + (K^i \gamma_2 - \gamma_1) C_2}, \quad (24)$$

and the total solid-phase concentration of M_2^+ is given by the sum

$$q_2 = \sum_n^{i=1} q_2^i = \sum_n^{i=1} \frac{K^i Q^i \gamma_2 C_2}{C_o \gamma_1 + (K^i \gamma_2 - \gamma_1) C_2}. \quad (25)$$

This approach is further generalized by replacing the sum in Eqn. 25 with the integral equation

$$q_2(C_2) = \int q_2(C_2, K) f(K) dK, \quad (26)$$

where $f(K)$ is a distribution function for the selectivity coefficient of the exchange.

The idea of expressing the heterogeneity of the exchanger in terms of a distribution function has been previously presented (Brouwer et al. 1983; Adamson 1982; Sposito 1979, 1980, 1984; Kinniburgh et al. 1983). Equation 26 is a Fredholm integral of the First Kind, and the methodology used here to solve for $f(K)$ has been described by the authors (Triay and Rundberg 1987, 1989b) and others (Butler et al. 1981; Britten et al. 1983). The computer code INVPOS has been written (Travis 1996) to solve Eqn. 26. INVPOS uses the method of Butler, Reeds, and Dawson (1981) to find an optimal solution using regularization with a positivity constraint.

Semiempirical adsorption isotherms, such as the Freundlich isotherm, are derived by evaluating the

integral (Eqn. 26) using closed-form approximations and assuming some arbitrary site energy distribution. These approaches are only valid for data interpolation because they do not provide insight into the actual mechanism of adsorption.

Description of cation-exchange sites in Yucca Mountain tuff

Detailed adsorption isotherms adequate for the analysis described above have not been done for the Yucca Mountain Project. Measurements of the mineralogy of Yucca Mountain tuff have shown an abundance of minerals known to have both pH-independent cation-exchange sites (that is, tetrahedral aluminum sites) and surface-complexation sites (for example, clay edge sites) for outer-sphere surface-complex formation. The most abundant minerals found in Yucca Mountain tuff (Bish et al. 1983; Daniels et al. 1982) with a high cation-exchange capacity are listed in Table 20.

In addition to the minerals listed in that table, feldspars may be important cation exchangers in the devitrified tuffs. Cation-exchange capacity for a feldspar is not an intrinsic property because only the external surfaces are available for exchange. Thus, the number of sites depends on the crystal size and morphology.

State of knowledge of cation exchange with respect to Yucca Mountain

As early as 1983 (Daniels et al. 1982), it was shown that the sorption distribution coefficient, K_d , for the adsorption of cesium onto Yucca Mountain tuff could be predicted to within a factor of three using literature data for the cation exchange on the minerals in Table 20 with the addition of analcime. These predictions only considered competition with sodium. This simplification was made because there were no data for the cation exchange of the other alkali metals and alkaline earths present in J-13 well water. Some of the observed scatter could possibly be reduced with these additional data. Unfortunately, over the years since then, the situation has not changed. Thus, there is no predictive model based on mineralogy for cation

exchange for radionuclides other than cesium.

We determined the relative contribution of cation exchange to the adsorption of neptunyl onto the zeolitic tuff sample G4-1506 from a sodium-bicarbonate solution. The experiment was based partly on the method of Baeyens and Bradbury. Crushed tuff G4-1506 was equilibrated with 1 M sodium perchlorate to remove alkali metals and alkaline earths by mass action. Solutions containing 0.0022 M sodium bicarbonate (as a pH buffer) were prepared with sodium perchlorate added to provide sodium concentrations that varied from 0.0022 M to 0.22 M. Distribution coefficients for neptunium were determined using the standard procedure (Fig. 91).

The surface complexation of neptunyl has been shown to be inner sphere and noncharging. Therefore, the surface complexation of neptunium is expected to be largely independent of sodium-ion concentration. The results show a linear decrease in K_d with sodium concentration at low sodium concentrations that is consistent with cation exchange (see Eqn. 21). At high sodium concentrations, the K_d asymptotically approaches 2.5 ml/g, consistent with surface complexation. The ion-exchange component is larger than the surface-complexation component, which corresponds to a K_d of about 10 in 0.0022 M sodium bicarbonate. The relatively low K_d for neptunyl in a zeolitic tuff is likely due to the large ion size and high hydration number. The K_d in pure sodium bicarbonate solution is larger than

Table 20. Minerals in Yucca Mountain Tuff with High Cation-exchange Capacities

Mineral	Maximum abundance	Capacity (meq/g)
Clinoptilolite	90 %	2.3
Mordenite	60 %	2.3
Montmorillonite	40 %	0.8–1.5
Illite	20 %	0.13–0.42

that observed in J-13 water; this effect is due to competition with the additional cations in J-13 water of calcium, magnesium, and potassium. A model that describes these data and predicts neptunium sorption in the zeolitic tuff of Calico Hills will be described in the next section.

Surface Complexation

Description of surface-complexation process

The model that we will use to interpret the results of our experiments is the triple-layer surface-complexation model (Davis et al. 1978). The most important difference between this model and conventional chemical equilibria is the effect of surface charge on the activity of ions in the triple layer. This effect is calculated by multiplying the bulk-solution concentration, $[M^+]_{\text{bulk}}$, by a Boltzmann factor

$$[M^+] = [M^+]_{\text{bulk}} e^{-\left(\frac{e\psi_0}{kT}\right)}, \quad (27)$$

where k is the boltzmann constant, T is the absolute

temperature, e is electronic charge, and ψ_0 is the potential of the ion in the inner Helmholtz layer.

The charge on the metal-oxide surface is produced by the amphoteric reaction of the metal-oxide surface with acids and bases. The basic charge-producing reactions are with Brönsted acids and bases:



for which the equilibrium constants are:

$$K_{a_1}^{\text{int}} = \frac{[\text{MOH}][\text{H}_3\text{O}^+]}{[\text{MOH}_2^+]} e^{-\left(\frac{e\psi_0}{kT}\right)} \quad \text{and} \quad (30)$$

$$K_{a_2}^{\text{int}} = \frac{[\text{MO}^-][\text{H}_3\text{O}^+]}{[\text{MOH}]} e^{-\left(\frac{e\psi_0}{kT}\right)}. \quad (31)$$

Cations and anions can interact with the electric field near the metal-oxide surface by forming outer-sphere complexes. Ions can also be repelled from the aqueous phase near the metal-oxide surface, as illustrated by Eqn. 16, which can lead to what appears to be a negative sorption distribution

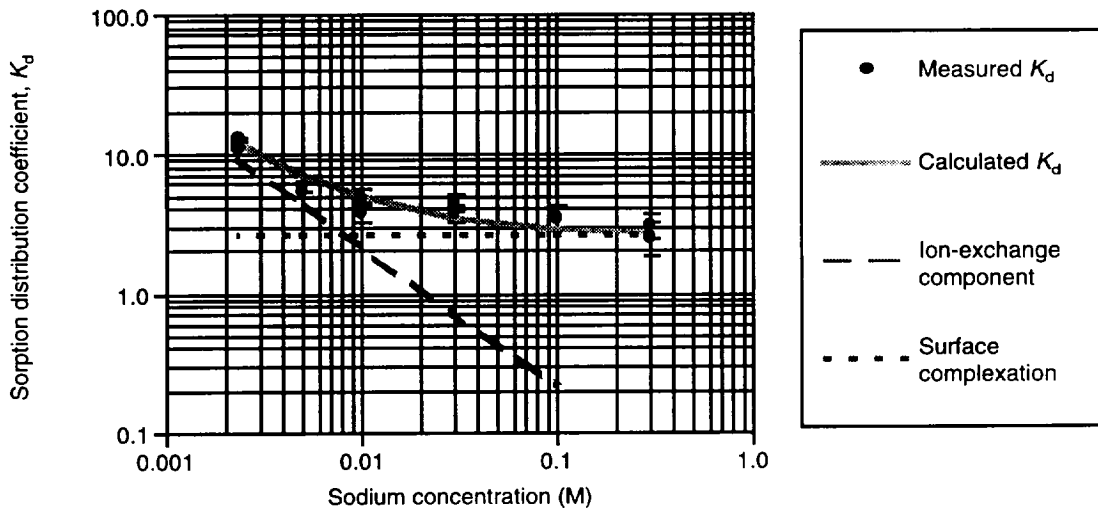


Figure 91. Modeling of Neptunium Sorption. The plot shows data points for the sorption distribution coefficient of neptunium on the zeolitic tuff sample G4-1506 at a pH of 8.4 as a function of sodium ion concentration. Surface complexation should not vary with sodium concentration, so the horizontal dashed asymptote at high concentrations is a measure of surface complexation, and the dashed linear slope at low concentrations is a measure of the ion-exchange component of the sorption.

coefficient. This phenomenon is a result of the increase in tracer concentration in the bulk solution due to repulsion of ions from the solution within the double layer. This effect is always small, $K_d > -1$ ml/g. The strict definition of K_d does not allow for negative values because that would imply a negative concentration (which is meaningless). The negative K_d arises because, experimentally, it is impossible to separate the solid phase without including the thin layer of water close to its surface.

Negative K_d values can be used in the same way as positive K_d values and lead to the correct prediction of more rapid migration of excluded tracer with respect to tritiated water, that is, retardation factors less than 1. This phenomenon has been used by van den Hul and Lykelma (1968) to measure the specific surface area of suspended materials. Outer-sphere surface complexation can account for this phenomenon and is represented by the following equations:



where An^- is the anion, Cat^+ is the cation. The equilibrium constants corresponding to these equations are

$$K_{\text{an}}^{\text{int}} = \frac{[\text{MOH}_2^+ \text{An}^-]}{[\text{MOH}_2^+][\text{An}^-]} e^{-\left(\frac{e\psi_\beta}{kT}\right)} \quad \text{and} \quad (34)$$

$$K_{\text{cat}}^{\text{int}} = \frac{[\text{MO}^- \text{Cat}^+]}{[\text{MO}^-][\text{Cat}^+]} e^{\left(\frac{e\psi_\beta}{kT}\right)} \quad . \quad (35)$$

where ψ_β is the potential of the ion in the outer Helmholtz layer. The ions adsorbed in the outer layer can be exchanged for other ions. The ion-exchange process would be expected to have selectivity differences due to factors such as ion size.

Factors affecting surface complexation

Surface-complexation models are equilibrium models and, therefore, account for speciation reactions explicitly. It is inherently difficult to characterize whole rock, however. This difficulty arises from the very surface nature of the reactions

described. The number of available sites depends on the crystal size and morphology. The identity of available sites depends on the availability of mineral surfaces to the pore water and can be changed by weathering. Given these inherent difficulties, we will attempt to develop a simplified model of surface complexation, including cation exchange.

HSAB (hard-soft acid-base) theory

The surface-complexation coefficients for monodentate surface complexes have been shown to be proportional to the first hydrolysis constant of the aqueous metal ion. This relationship is the natural consequence of the Lewis acid-base theory. The Lewis definition of an acid is an electron-pair acceptor and of a base, an electron donor. The hydrolysis of metal ions in aqueous solution proceeds by reacting with a water molecule displacing a hydrogen ion (an Arrhenius acid) yielding a monohydroxide:



This reaction is analogous to the formation of a monodentate surface complex on a metal oxide, for example, alumina:



The principal difference between these reactions is that the hydroxide ion is the Lewis base in the aqueous hydrolysis reaction (Eqn. 36) and the surface oxygen is the Lewis base in the surface-complexation reaction (Eqn. 37). The strength of the Lewis acid M^{n+} in both reactions is related to the first hydrolysis constant, K_{11} . The basicity of the surface oxygen is related to the second acid-dissociation constant, K_{a2} , of the metal oxide. This relationship can be tested by comparing the sum of the logarithms of the surface-complexation constant and the second acid-dissociation constant against the logarithm of the first hydrolysis constant of the metal ion. The $\log K_a$ values for the first and second acid-dissociation constants of metal oxides expected to be found in Yucca Mountain tuff are listed in Table 21, along with the point of zero charge (the pH at which surface in equilibrium with that solution has no net charge). The compar-

ison of literature values (Dzombak and Morel 1990; Kinniburgh et al. 1976; Huang and Stumm 1973; Schindler 1985) for surface complexation ($\log K_s + \log K_a$), of metal ions on alumina, silica, and iron oxide are shown in Fig. 92.

The results of this comparison demonstrate that the surface-complexation constant can be estimated to within an order of magnitude, for most metals, given the first hydrolysis constant. A similar comparison for bidentate attachment has yet to be developed, primarily because of the lack of reliable data for bidentate surface complexes.

Description of surface-complexation sites in Yucca Mountain tuff

Although surface complexation has just begun to be studied on Yucca Mountain tuff, there are a number of mineral surfaces having known surface-complexation sites. These are hematite and related iron oxides, silica, and the edge sites of clays. The clay edge sites have been studied and found to be

Table 21. Intrinsic Constants for Metal Oxides

Metal oxide	$\log K_a$	$\log K_a$	Point of zero charge
SiO ₂	-0.5	-8.2	4.3
Al ₂ O ₃	-7.8	-11.3	9.3
FeOOH	-7.6	-11.4	8.5

most similar to octahedral alumina (Wieland 1988; Stumm 1992). Although there is no supporting data to determine the relative abundance of these sites, the HSAB approach described above allows one to predict the surface-complexation mechanisms in terms both of stoichiometry and of equilibrium constants.

Modeling of Yucca Mountain tuff

A surface-complexation model for neptunium adsorption onto the zeolitic tuff sample G4-1506

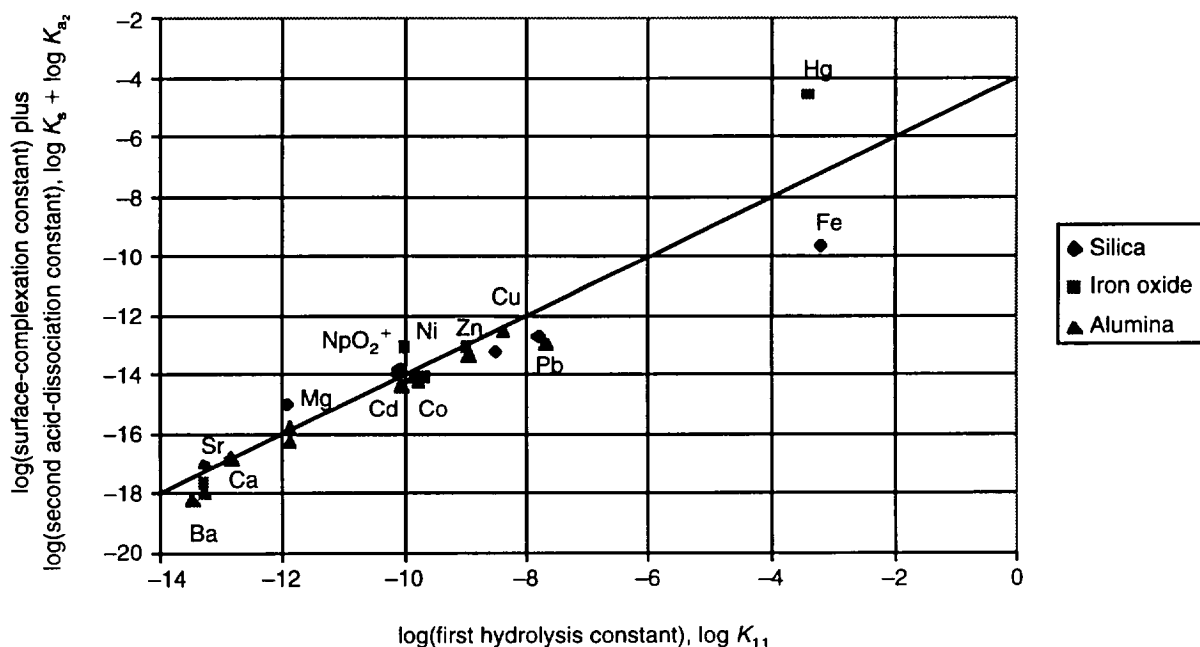


Figure 92. Surface Complexation versus Hydrolysis. This plot compares surface complexation ($\log K_s + \log K_a$) for monodentate attachment of metal ions with hydrolysis ($\log K_{11}$) based on the HSAB (hard-soft acid-base) theory.

was developed to fit the sodium-concentration dependence. The model considered a simple ion-exchange mechanism:



and the formation of an inner-sphere surface complex with octahedral alumina (edge sites) or hematite:



The number of cation-exchange sites available to neptunium (Table 22) was based on the apparent saturation of sites observed in a neptunium adsorption isotherm measured for tuff sample G4-1608 in a carbon-dioxide atmosphere (Thomas 1987). The neptunium-exchange capacity is four orders of magnitude smaller than the cation-exchange capacity of clinoptilolite (Table 20). This difference can

be explained by the large size of the hydrated neptunyl ion. If no sorption occurs in the intracrystalline channels of the clinoptilolite, the maximum exchange capacity will be on the order of a μmole per gram, assuming a 3- μm crystal diameter. The selectivity for neptunium was used as an adjustable parameter, and the model was fit to the results of the sodium-ion dependence of neptunium adsorption onto tuff sample G4-1506.

The inner-sphere surface complexation of neptunium was modeled assuming that surface complexation occurs primarily on clay edge sites or iron-oxide surfaces. The constant for inner-surface complexation of neptunium onto iron oxide was used because the analogous constant for alumina is expected to be nearly equal on the basis of the HSAB theory shown above. Thus, the second

Table 22. Equations and Parameters Used to Model Neptunium Adsorption onto Zeolitic Tuff

Type of reaction	Equilibrium reactions	log K	
Aqueous reactions:	$\text{NpO}_2^+ + \text{H}_2\text{O} \leftrightarrow \text{NpO}_2\text{OH}(\text{aq}) + \text{H}^+$	-10.8	
	$\text{NpO}_2^+ + 2\text{H}_2\text{O} \leftrightarrow \text{NpO}_2(\text{OH})_2^- + 2\text{H}^+$	-23.5	
	$\text{NpO}_2^+ + \text{CO}_3^{2-} \leftrightarrow \text{NpO}_2\text{CO}_3^-$	4.13	
	$\text{HCO}_3^- \leftrightarrow \text{CO}_3^{2-} + \text{H}^+$	-10.25	
	$\text{CO}_2(\text{g}) + \text{H}_2\text{O} \leftrightarrow \text{H}_2\text{CO}_3 \leftrightarrow \text{HCO}_3^- + \text{H}^+$	-7.8	
Metal-oxide surface protolysis:	$\text{MOH} + \text{H}^+ \leftrightarrow \text{MOH}_2^+$	7.6	
	$\text{MOH}_2^+ + \text{ClO}_4^- \leftrightarrow \text{MOH}_2^+\text{ClO}_4^-$	2.0	
	$\text{MOH} \leftrightarrow \text{MO}^- + \text{H}^+$	-11.4	
	$\text{MO}^- + \text{Na}^+ \leftrightarrow \text{MO}^- \text{Na}^+$	1.2	
Neptunyl adsorption reactions:	$t\text{-Al}^- \text{Na}^+ + \text{NpO}_2^+ \leftrightarrow t\text{-Al}^- \text{NpO}_2^+ + \text{Na}^+$	2.1	
	$\text{MOH} + \text{NpO}_2^+ \leftrightarrow \text{MONpO}_2 + \text{H}^+$	-2.2	
Extension to groundwater:	$2t\text{-Al}^- \text{Na}^+ + \text{Ca}^{2+} \leftrightarrow t\text{-Al}_2^{2-} \text{Ca}^{2+} + 2\text{Na}^+$	5.0	
	$\text{MOH} + \text{Ca}^{2+} \leftrightarrow \text{MOCa}^+ + \text{H}^+$	-5.85	
	$\text{MOCa}^+ + \text{Cl}^- \leftrightarrow \text{MOCa}^+ \text{Cl}^-$	2.0	
Parameters			
Type of site	Site density (eq/kg)	Layer	Capacitance (F/m ²)
Tetrahedral (t) aluminum	2×10^{-4}	Inner Helmholtz	1.1
Octahedral aluminum (edge)	3×10^{-6}	Outer Helmholtz	0.2

adjustable parameter was the edge-site density.

To extend this model to the empirical measurements done under the project's geochemistry program, additional assumptions were made. The competition of cations in groundwater for cation-exchange sites was based on the selectivities derived from measurements on the mineral tobermorite (Tsuji and Komarneni 1993). This approach was the result of the argument explaining the reduced cation-exchange capacity for neptunium. If exchange occurs only on the exterior of the zeolite crystal, then steric effects must be avoided. Tobermorite offers an open structure that could be expected to have less steric effects than a zeolite. Furthermore, that work showed little difference between magnesium and calcium so that both magnesium and calcium were treated as one competitor. There were no data for potassium, so competition with potassium was not considered.

The surface-complexation constant for calcium was taken from the HSAB theory. Thus, there were no additional adjustable constants. The concentrations used for J-13 and UE-25 p#1 well water are shown in Table 23. The calculations were made using the FITEQL equilibrium code in the forward mode only, that is, no fitting. The results of the modeling are shown in Figs. 93 and 94. The agreement between the model calculations and the measured results were in general excellent. The correct pH dependence was predicted for the dry-sieved samples; the wet-sieved samples agreed better with a calculation that had no surface-complexation sites. The implications of these results are not yet fully understood. Two possibilities are that either the clay particles are washed out, reducing the available edge sites, or that a trace component of J-13 water is forming a strong surface complex that competes with neptunium. The model also predicted the observed reduction in the sorption distribution coefficient, K_d , due to the components of UE-25 p#1 water. In this water, the higher carbonate concentration eliminates the contribution of surface complexation observed in J-13 water at pH values above 7.

Table 23. Groundwater Compositions Used for Neptunium Sorption Modeling

Constituent	Concentration (mg/l)		
	J-13 water	UZ water	UE-25 p#1 water
Sodium	45	26–70	171
Potassium	5.3	5–16	13.4
Magnesium	1.8	5–21	31.9
Calcium	11.5	27–127	87.8
Silicon	30	72–100	30
Fluoride	2.1	–	3.5
Chloride	6.4	34–106	37
Sulfate	18.1	39–174	129
Bicarbonate	143	–	698
pH	6.9	6.5–7.5	6.7

A model was also developed for pH dependence of uranium adsorption onto crushed devitrified tuff. This treatment was similar to that used to model neptunium adsorption except that 1) the cation-exchange capacity for uranium was not known (that is, there was no adsorption isotherm) and 2) a cation exchange with the monohydroxy-uranyl complex was included. The parameters used are listed in Table 24. The number of sites used to model these data was much greater than for the zeolitic tuff. The possible reason for this is the exposure of fresh surfaces of feldspar and quartz combined with the lack of exposure to a complex groundwater.

The results of this exercise are shown in Fig. 95 and are in excellent agreement with the results of Leckie and his students (Davis et al. 1978). The equilibrium concentration of uranium at pH values of 9 and above are above the solubility limit for uranium hydroxide. The effect of precipitation was evident in the experimental data. The solubility product was not included in this model.

State of knowledge of surface complexation with respect to Yucca Mountain

Surface-complexation reactions with Yucca Moun-

IV. Sorption and Sorption Modeling Studies

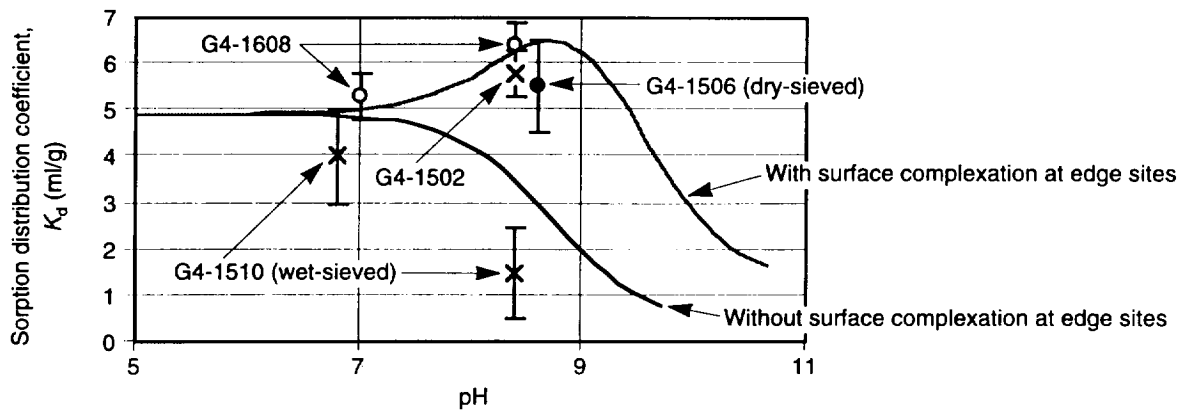


Figure 93. Neptunium Sorption in J-13 Water. This plot compares sorption data (points) with the predictions of the FITEQL code for the pH dependence of neptunium sorption on zeolitic tuff from J-13 water with and without surface complexation at edge sites (curves). The sorption data for samples G4-1608 and G4-1502 are from Thomas (1987).

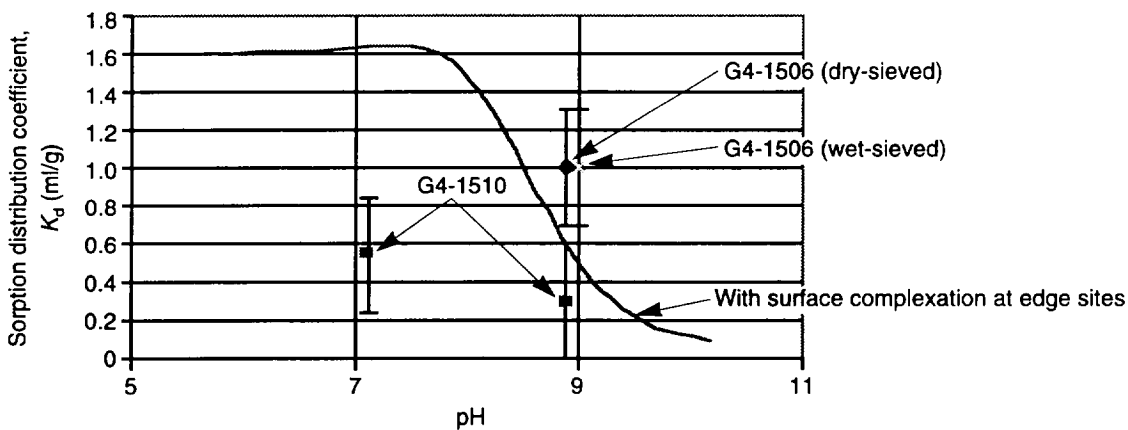


Figure 94. Neptunium Sorption in UE-25 p#1 Water. This plot compares sorption data (points) with the predictions of the FITEQL code for the pH dependence of neptunium sorption on zeolitic tuff from UE-25 p#1 water with surface complexation at edge sites (curve).

tain tuff have just begun to be studied. The pH dependence of actinide adsorption can be readily explained with a combined surface-complexation and ion-exchange model. The effect of changing groundwater composition on neptunium adsorption has also been successfully modeled using a surface-complexation model. There are significant gaps in the knowledge base, however. From a fundamental standpoint, an HSAB model for bidentate inner-sphere complexes needs to be developed. The consequences of a bidentate attachment mech-

anism, as was included in the uranium adsorption model, is an increased sensitivity to competition with metal ions favoring monodentate attachment (for example, calcium). From an experimental standpoint, the effects of wet-sieving needs to be better understood. If wet-sieving removes all of the clay minerals, the resulting distribution coefficients may be too low (overly conservative). On the other hand, if a trace component of groundwater is responsible for the decrease in surface complexation, it must be identified and measured in

Table 24. Additional Equations and Parameters Used to Model Uranium Adsorption onto Devitrified Tuff

Type of reaction	Equilibrium reactions	log K
Aqueous reactions:	$UO_2^{2+} + H_2O \leftrightarrow UO_2OH^+ + H^+$	-5.8
	$UO_2^{2+} + 2H_2O \leftrightarrow UO_2(OH)_2 + 2H^+$	-12.5
	$2UO_2^{2+} + 2H_2O \leftrightarrow (UO_2)_2(OH)_2^{2+} + 2H^+$	-5.62
	$3UO_2^{2+} + 5H_2O \leftrightarrow (UO_2)_3(OH)_5^+ + 5H^+$	-15.63
Uranyl adsorption reactions:	$2t-Al^-Na^+ + UO_2^{2+} \leftrightarrow (t-Al^-)_2UO_2^{2+} + 2Na^+$	1.8
	$t-Al^-Na^+ + UO_2^{2+} + H_2O \leftrightarrow t-Al^-UO_2OH^+ + Na^+ + H^+$	-1.5
	$MOH + UO_2^{2+} \leftrightarrow MOUO_2^+ + H^+$	0.60
	$MOH + UO_2^{2+} + Cl^- \leftrightarrow MOUO_2^+Cl^- + H^+$	2.8
	$2MOH + UO_2^{2+} \leftrightarrow (MO)_2UO_2 + 2H^+$	-2.8
Parameters:	Type of site	Site density (eq/kg)
	Tetrahedral (t) aluminum	2×10^{-2}
	Octahedral aluminum (edge)	2×10^{-3}

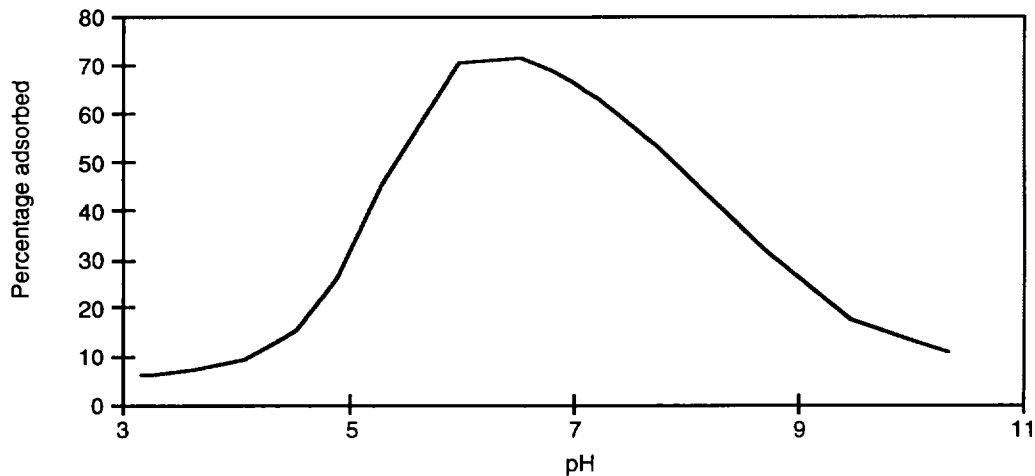


Figure 95. Uranium Adsorption. The curve above shows the predictions of the FITEQL code for the adsorption of uranium onto crushed devitrified tuff from an 0.1 M sodium-chloride solution in a controlled atmosphere with an initial uranium concentration of 1×10^{-6} M.

groundwaters and in pore waters.

The modeling of actinide sorption shows that high carbonate concentrations will severely reduce the ability to form surface complexes on tuff. The ion exchange of actinides appears to dominate under

normal conditions over surface complexation.

Furthermore, divalent cations are found to be strong competitors for cation-exchange sites found in Yucca Mountain tuff.

D. SORPTION DATA RECOMMENDED FOR PERFORMANCE ASSESSMENT

Sorption is a function of water chemistry and the type of tuff at Yucca Mountain. The water chemistry at Yucca Mountain was reviewed by Meijer (1992) and is discussed in "Yucca Mountain Waters" (Section I.C) and "Groundwater Chemistry Model" (Chapter II) of this report. The concentration of the major cations and anions in unsaturated-zone (UZ) groundwaters appears to be intermediate between the saturated-zone tuffaceous waters (for example, from Well J-13) and waters from the Paleozoic carbonate aquifer (from Well UE-25 p#1). Consequently, the first assumption made for the performance-assessment recommendations was that the waters from Wells J-13 and UE-25 p#1 bound the chemistry of the groundwaters at Yucca Mountain.

The second assumption made dealt with grouping all strata on the basis of rock type (the stratigraphy considered from the repository horizon to the accessible environment is outlined in Table 4, page 17). This assumption reduced the number of sorption-coefficient distributions elicited to four per radionuclide: iron oxides, devitrified tuff, vitric tuff, and zeolitic tuff. The basis for this grouping is the fact that sorption of radionuclides is the result of a chemical reaction between the radionuclide in the groundwater and the minerals in the tuff. The mineralogy of the different strata of the same rock group is very similar, and the sorption coefficients can be grouped in terms of these rock types (Thomas 1987).

The containers to be used in the repository were added to the list after consideration of whether the corrosion by-products of the massive multi-purpose container could become a substrate for sorption. Actinides are sorbed strongly by iron oxides. However, although hematite is found in the tuffs at Yucca Mountain, the iron-oxide minerals in the tuffs appear to be "passivated"—that is, all of the sorption sites could be occupied by other metals (Triay et al. 1993b)—and the sorption of the

radionuclides onto tuff (containing iron oxides as trace minerals) is not as large as predicted on the basis of the sorption of radionuclides onto synthetic pure iron oxides. Because the sorption sites on the degraded container material would not necessarily be occupied by other metals, the experts agreed to add iron oxides to the list of "rock" types.

The effect of temperature on sorption coefficients was reviewed by Meijer (1990). Measured sorption coefficients onto tuffs were higher at elevated temperatures for all elements studied: americium, barium, cerium, cesium, europium, plutonium, strontium, and uranium. Consequently, the third assumption made was that sorption coefficients measured at ambient temperatures should be applicable and generally conservative when applied to describing aqueous transport from a hot repository. (This assumption is meaningful provided that the high temperatures that will be sustained for long time periods due to potential high thermal loads do not result in changes in the mineralogy and the water chemistry at Yucca Mountain that are not predictable by short-term laboratory and field experiments.)

Tables 25 shows the parameters for the sorption-coefficient-probability models recommended for performance assessment for the unsaturated-zone units, and Table 26 shows the same parameters for saturated-zone units. We now discuss the source of these values for each of the elements separately.

Americium

Americium sorbs strongly to most materials (Triay et al. 1991b). The potential mechanisms for actinide sorption onto mineral surfaces has been reviewed by Meijer (1992). The sorption-coefficient distributions for americium in Yucca Mountain tuffs and iron oxides given in Tables 25 and 26 were inferred from the data presented by Thomas (1987), Triay et al. (1991b), and Meijer (1992).

Plutonium

One of the problems of interpreting sorption data for plutonium is that this element can exist in multiple oxidation states under oxidizing conditions at near-neutral pH values (Nitsche et al. 1993a). Plutonium can also exist as a polymer (Triay et al. 1991a). The lack of information on the speciation of plutonium in the groundwaters at Yucca Mountain makes it difficult to assess the sorption mechanism for this element. However, the empirical data obtained in Yucca Mountain tuffs indicate that plutonium sorbs strongly. The sorption-coefficient distributions for plutonium in Yucca Mountain tuffs given in Tables 25 and 26 were inferred from the data presented by Thomas (1987) and Meijer (1992).

Uranium

No additional data for uranium has been collected for Yucca Mountain tuffs since the 1991 total-system performance-assessment effort (TSPA-1991). Consequently, no change was made for the sorption-coefficient distributions used for this element. As previously discussed (Meijer 1992), uranium sorbs strongly to synthetic iron oxides.

Thorium

The information elicited for americium was also used for thorium. This approach is due both to the lack of sorption information available for thorium and to the similarities exhibited by the sorption behavior of these two elements (Thomas 1987).

Radium

Barium has been used as an analog for radium in the experiments performed at Los Alamos (Thomas, 1987). These elements sorb to Yucca Mountain tuffs via an ion-exchange mechanism and surface-adsorption reactions (Meijer 1992). The sorption-coefficient distributions for radium in Yucca Mountain tuffs and iron oxides given in Tables 25 and 26 were inferred from the data pre-

sented by Thomas (1987), Meijer (1992), and Triay et al. (1991c).

Lead

Lead tends to complex with fulvics in the groundwaters and sorbs as a complex. The sorption-coefficient distributions for lead in Yucca Mountain tuffs and iron oxides given in Tables 25 and 26 were inferred from the data presented by Meijer (1990).

Neptunium

Sorption-coefficient distributions for neptunium in tuff are the same as those used in TSPA-1991. Recently obtained data (Triay et al. 1993b) agrees with previous observations. Neptunium is a poorly sorbing radionuclide in tuff even when the tuffs are known to have iron oxides, because the iron oxides in the tuff appear to be passivated. The neptunium sorption-coefficient distribution for sorption onto iron oxides given in Tables 25 and 26 was inferred from data presented by Meijer (1992) and Triay et al. (1993b) for sorption onto synthetic iron oxides.

Protactinium

Very little information exists for protactinium sorption onto tuffs (Thomas 1987), so the experts decided to use for this element the same sorption coefficients elicited for neptunium.

Tin

There is very little information for the sorption of tin onto tuffs (Thomas 1987). Based on the data available, Meijer (1992) suggested that tin exhibited large values of K_d in the devitrified tuffs (larger than 1000 ml/g). The sorption-coefficient distributions given in Tables 25 and 26 were inferred from the work by Andersson (1988); the uniform distributions chosen was the result of the expert's uncertainty about the sorption of tin.

IV. Sorption and Sorption Modeling Studies

Table 25. Sorption-coefficient Distributions for Unsaturated-zone Units

Element	Rock type	Min K_d (ml/g)	Max K_d (ml/g)	$E[x]$	COV*	Distribution type
Americium	Devitrified	100	2000			Uniform
	Vitric	100	1000	400	0.20	Beta
	Zeolitic	100	1000			Uniform
	Iron oxide	1000	5000			Uniform
Plutonium	Devitrified	20	200	100	0.25	Beta
	Vitric	50	200	100	0.25	Beta
	Zeolitic	30	200	100	0.25	Beta
	Iron oxide	1000	5000			Uniform
Uranium	Devitrified	0	4.0	2.0	0.3	Beta
	Vitric	0	3.0	1.0	0.3	Beta
	Zeolitic	0	30.0	7.0	1.0	Beta(exp)
	Iron oxide	100	1000			Uniform
Neptunium	Devitrified	0	6.0	1.0	0.3	Beta
	Vitric	0	15.0	1.0	1.0	Beta(exp)
	Zeolitic	0	3.0	0.5	0.25	Beta
	Iron oxide	500	1000			Uniform
Radium	Devitrified	100	500			Uniform
	Vitric	50	100			Uniform
	Zeolitic	1000	5000			Uniform
	Iron oxide	0	500	30	1.0	Beta(exp)
Cesium	Devitrified	20	1000			Uniform
	Vitric	10	100			Uniform
	Zeolitic	500	5000			Uniform
	Iron oxide	0	500	30	1.0	Beta(exp)
Strontium	Devitrified	10	50			Uniform
	Vitric	0	20			Uniform
	Zeolitic	500	2000			Uniform
	Iron oxide	0	30	10	0.25	Beta
Nickel	Devitrified	0	500	100	0.33	Beta
	Vitric	0	100	50	0.33	Beta
	Zeolitic	0	500	100	0.33	Beta
	Iron oxide	0	1000			Uniform
Lead	Devitrified	100	500			Uniform
	Vitric	100	500			Uniform
	Zeolitic	100	500			Uniform
	Iron oxide	100	1000			Uniform
Tin	Devitrified	20	200			Uniform
	Vitric	20	200			Uniform
	Zeolitic	100	300			Uniform
	Iron oxide	0	5000			Uniform
Protactinium	Devitrified	0	100			Uniform
	Vitric	0	100			Uniform
	Zeolitic	0	100			Uniform
	Iron oxide	500	1000			Uniform
Selenium	Devitrified	0	30	3	1.0	Beta(exp)
	Vitric	0	20	3	1.0	Beta(exp)
	Zeolitic	0	15	2	1.0	Beta(exp)
	Iron oxide	0	500	30	1.0	Beta(exp)
Carbon	Iron oxide	10	100			Uniform

Actinium, Niobium, Samarium, Thorium, Zirconium: see Americium

Chlorine, Technetium, Iodine 0 0

*Coefficient of variation: $COV = \sigma[x]/E[x]$

Table 26. Sorption-coefficient Distributions for Saturated-zone Units

Element	Rock type	Min K_d (ml/g)	Max K_d (ml/g)	$E[x]$	COV*	Distribution type
Americium	Devitrified	100	2000			Uniform
	Vitric	100	1000	400	0.20	Beta
	Zeolitic	100	1000			Uniform
	Iron oxide	1000	5000			Uniform
Plutonium	Devitrified	50	300	100	0.15	Beta
	Vitric	50	300	100	0.15	Beta
	Zeolitic	30	300	100	0.15	Beta
	Iron oxide	1000	5000			Uniform
Uranium	Devitrified	0	5.0	2.0	0.3	Uniform
	Vitric	0	4.0	1.0	0.3	Uniform
	Zeolitic	5	20.0	7.0	0.3	Beta
	Iron oxide	100	1000			Uniform
Neptunium	Devitrified	0	10.0	3.0	0.3	Beta
	Vitric	0	15.0	1.5	1.0	Beta(exp)
	Zeolitic	0	12.0	4.0	0.25	Beta
	Iron oxide	500	1000			Uniform
Radium	Devitrified	100	500			Uniform
	Vitric	100	500			Uniform
	Zeolitic	1000	5000			Uniform
	Iron oxide	0	1500	30	1.0	Beta(exp)
Cesium	Devitrified	20	1000			Uniform
	Vitric	10	100			Uniform
	Zeolitic	500	5000			Uniform
	Iron oxide	0	500	30	1.0	Beta(exp)
Strontium	Devitrified	10	200			Uniform
	Vitric	20	50			Uniform
	Zeolitic	2000	5000			Log uniform
	Iron oxide	0	30	10	0.25	Beta
Nickel	Devitrified	0	500	100	0.33	Beta
	Vitric	0	200	100	0.33	Beta
	Zeolitic	0	500	100	0.33	Beta
	Iron oxide	0	1000			Uniform
Lead	Devitrified	100	500			Uniform
	Vitric	100	500			Uniform
	Zeolitic	100	500			Uniform
	Iron oxide	100	1000			Uniform
Tin	Devitrified	20	200			Uniform
	Vitric	20	200			Uniform
	Zeolitic	100	300			Uniform
	Iron oxide	0	5000			Uniform
Protactinium	Devitrified	0	100			Uniform
	Vitric	0	100			Uniform
	Zeolitic	0	100			Uniform
	Iron oxide	500	1000			Uniform
Selenium	Devitrified	0	30	3	1.0	Beta(exp)
	Vitric	0	20	3	1.0	Beta(exp)
	Zeolitic	0	15	2	1.0	Beta(exp)
	Iron oxide	0	500	30	1.0	Beta(exp)
Carbon	Iron oxide	10	100			Uniform

Actinium, Niobium, Samarium, Thorium, Zirconium: see Americium

Chlorine, Technetium, Iodine 0 0

*Coefficient of variation: $COV = \sigma[x]/E[x]$

IV. Sorption and Sorption Modeling Studies

Nickel

For devitrified, vitric, and zeolitic tuffs, the nickel sorption-coefficient distributions given in Tables 25 and 26 were inferred from data presented by Meijer (1992). For iron oxides, the nickel sorption-coefficient distribution was inferred from the data presented by Siegel et al. (1992 and 1993).

Cesium

Cesium sorption-coefficient distributions for tuff and iron oxides were inferred from the data presented by Thomas (1987), Meijer (1992), and Triay et al. (1991c). Cesium has one of the highest selectivity coefficients for zeolites among all chemical elements (Meijer 1992). Cesium sorption onto devitrified and vitric samples could be the result of ion exchange onto clays or feldspars in the tuff samples or surface-adsorption reactions (Meijer 1992).

Strontium

Strontium sorption-coefficient distributions for tuff and iron oxides were inferred from the data presented by Thomas (1987) and Triay et al. (1991c). Strontium sorbs strongly onto zeolites by ion exchange. This element's sorption onto other types of tuff may be dominated by the amount of clay in the tuff units. The values given in Tables 25 and 26 are generally conservative.

Selenium

There are limited data on tuff for selenium sorption (Thomas 1987), so the experts decided to use the same sorption-coefficient distributions for selenium as the ones elicited for uranium. This decision is a conservative one because uranium can be oxidized much more readily than selenium in Yucca Mountain groundwaters.

Carbon

Carbon is a special case because transport is

expected to occur primarily in the gaseous phase as carbon dioxide. The major retardation mechanism is exchange of carbon-14 with the carbon in the carbon dioxide dissolved in the groundwater.

Actinium, Samarium, Niobium, and Zirconium

All these elements are strongly sorbing (Meijer 1992). The experts advised using for these elements the same sorption-coefficient distributions as those elicited for americium.

Iodine, Technetium, and Chlorine

Iodine and chlorine have anions that do not sorb onto tuffs. Technetium exists as pertechnetate under oxidizing conditions and does not sorb either (Triay et al. 1993a).